# Redesigning of Soil Landscape Models Within the Rangitikei District for the Inclusion of Groundwater Information (e.g., Nitrogen and Phosphorus)

A thesis presented in partial fulfilment of the requirements for the degree of

## Master of Science in Earth Science

At Massey University, Manawatu, New Zealand

Courtney Sarah Durham

2024

To Nigel and Grandad

# Abstract

Soil models used within the agricultural and sustainable land use sectors rarely address groundwater nutrient influences, particularly the interaction with soil profiles and the role of soils in nutrient mitigation. This study redevelops soil landscape models to include nutrient information from groundwater analysis. A Rangitikei farm in the Manawatu-Whanganui region was identified to have 14 soil types (~95% of these soils being Brown and Pallic) influenced by 6 geological members. The geological and soil information resulted in 3 soil landscape models being created, each with specific landscape, geological, and soil features. LRI and LUC maps were created identifying 10 LRI units and 6 LUC units each with different management procedures across the study area, including individual maps of each LRI component. The instillation of 6 piezometers across the study area at locations that intersected drainage zones with distinctive landform features and geologies, allowed for an overview of the drainage across the study area, with the aim to provide supportive evidence of the denitrifying properties of the soil system in terms of groundwater nitrogen. Groundwater samples from the piezometers were analysed for dissolved reactive phosphorus (DRP), dissolved oxygen (DO), pH, oxidation-reduction potential (ORP) and N-$NO_3$. The majority of the DRP results from the piezometers and surface waters were above accepted levels, while the majority of the N-$NO_3$ results were below accepted levels. The DO results primarily showed the support of N reduction within the subsurface system, while N reduction was not supported from the ORP results seen from the piezometers. Piezometer water levels showed a primary response to rainfall prior to sampling. LiDAR data at 1m resolution was utilised for the creating of a landform element map that identified valleys, ridges, spurs, and hollows across the study area.

# Acknowledgments

The master's process has been a long and sometimes difficult, particularly when dealing with COVID interruptions, but throughout it all I have been privileged to have a number of people who have been by my side throughout this process.

Firstly, I would like to acknowledge the support from Horizons Regional Council for granting me the Sustainable Land Use Initiative (SLUI) Scholarship and Massey University for granting me the George Mason Sustainable Land Use Scholarship. These two scholarships allowed be to complete the study necessary by buying equipment and taking final pressure off throughout these years.

I would like to thank my supervisors Alan Palmer, Ranvir Singh and Matthew Irwin who have provided help and guidance in their respective field throughout my Masters journey. A special thanks to Matthew Irwin, you kindly listened to my ranting and ravings in your office when things got stressful or tough for me and provided the help I needed that has got me through to the end where I now have a complete thesis.

If it was not for Richard Lambert and having is permission and interest in the work being completed on his farm. His enthusiasm towards the future and science surrounding farm processes filled me with the energy needed to get through the long days of field work, especially when carrying an extra 20kg when completing my water sampling. Thank you for letting me help out in the wool shed when I was rained out during my fieldwork days, it showed me another side to farm life.

A special thank you to Ian Furket and David Feek for their behind-the-scenes help. Thank you, David, for your help and knowledge surrounding the creating of piezometers, and for allowing me to follow along on one of your sampling runs to learn the infield processes for collecting groundwater samples. Thank you, Ian, for your help within the lab to show me how to analyse my groundwater samples.

Most importantly, I would like to thank my family. Mum, Dad, Klynton, you have had your fair share of my blood, sweat and tears land on your shoulders throughout this process. You have all been my rock through the thick and thin of it all. I know I would not have got through all this without your support and guidance. I am sorry to you all for not telling you how hard it was to complete my sampling when you came into the field to see what I talked about each month. Thank you Klynton for driving me out to Hunterville and for the use of your ute the few times it was needed. I can now say that my thesis is completed so we made it.

# Table of Contents

# List of Figures

# List of Tables

# Chapter 1 – Introduction

The government's implementation of the Essential Freshwater package as part of several amendments to the Resource Management Act 1991 requires the integration of freshwater farm plans. The introduction of freshwater farm plans aims to be phased in from the beginning of 2022 with the intentions of being fully implemented across New Zealand by 2025 with the intention to develop solutions that are tailored to individual farms and the surrounding areas (with regulations requiring freshwater farm plans to be certified and audited) that are aimed to steadily improve waterway health (Ministry for the Environment and Ministry for Primary Industries, 2021). Intensive agricultural activities, such as increased fertiliser applications and farm effluent spreading, have generally been associated with an increase in nutrients, primarily nitrogen (N) and phosphorus (P), leaching from soil profiles into surface and groundwaters. Elevated levels of nutrients entering into water bodies have been shown to lead to excessive growth of plants and algae, that can result in algal blooms, oxygen deficiency and loss of habitat, ecosystem function and biodiversity (Collins, et al., 2017). Sampling of both surface water and ground water is easy for analysing elevated levels of nitrogen, phosphorus, pathogens and to observe the results (via algal blooms) but the source of these pollutants from a soil landscape is hard to precisely identify (although some critical source areas can be identified). In addition, exact locations where mitigation is occurring (that may be enhanced by intervention or from different on-farm practices) is again hard to identify. Soil landscape models have been an import factor within the agricultural and sustainable land use sectors of science, particularly surrounding the protection of waterways and mitigating erosion, while maintaining land use efficiency and profitability. However, existing soil models do not address nutrient cycling throughout the soil profile. Sustainable Land Use Initiative (SLUI) and Land Resource Inventory/Land Use Capability (LRI/LUC) are current examples that do not address soil nutrient cycles and does not possess the predictive capability of landscape models to model groundwater or sediment movement; properly applied soil mapping using landscape models do have the predictive power. The Horizons Regional Council in 2004 started SLUI with a focus on reducing erosion across hill country with the aim of improving water ways (Reid, 2014), but there is limited knowledge on the nutrients transported within the soils entering into these water ways. Previous studies on soil landscape modelling have been completed, addressing different spatial modelling techniques (Schmidt, Tonkin, & Hewitt, 2005). Soil landscape models are primarily developed during routine soil surveys and focus on soil drainage, structure, texture, colour, and other important soil factors. Topography, land use, rainfall, soil texture and underlying geology all have an effect on the transport and transformation of nutrients within a catchment (Elwan, Singh, Horne, Roygard, & Clothier, 2015), therefore the addition of catchment characteristics to soil landscape models will further

advance soil landscape modelling and incorporate nutrient cycling information. The establishment of existing published studies, identifying the lacking understanding and reporting of the relationship between nutrient reduction capability within soils and groundwater nutrient levels will be addressed within this thesis.

The Rangitikei catchment dominates 18% of the 22,000km$^2$ of the Manawatu-Whanganui Region located in the lower North Island, New Zealand (Singh, et al., 2017). The Porewa[1] stream drainages a 170km$^2$ catchment that begins in the steep hill country approximately 20km north of Hunterville, along with discharge from the Hunterville Waste Water Treatment Plant (discharge contributes more than 90% of the streams flow during summer when stream flow is low (Waterclean, 2011)) and drains out to the Rangitikei River (Rangitikei River flow rate as of 21$^{st}$ November 2023 was 48.747m$^3$/s (LAWA - Land Air Water Aotearoa, (n.d. b))), influencing the degree of nutrients entering into major river ways and the degree of dilution of nutrients, pathogens and sediments entering into waterways. Agriculture landuse accounts for 90% of the Rangitikei District (Rees C. , Palmer, Palmer, & Singh, 2019).

An understanding of the geology of the Rangitikei is paramount for the understanding of the soils identified across the Rangitikei in particular for this study covering a ~450ha Hunterville hill country, sheep, and beef farm. This study identifies and investigates soils across the study area to recognise relationships between the soil, sediment sources, and groundwater and surface water systems. Soil analysis and understanding allowed for the presentation of improved LRI/LUC maps and along with an understanding of the geology allowed for the creation of soil landscape models. The presented landscape models are typical for a sheep and beef farm of the Rangitikei hill country and steepland, that can therefore be applied to surrounding farms with similar landscapes. The applications of these soil landscape models can be applied to form the basis of a farm plan in regard to new regulations. Piezometer installation across the study area is the first for the hill and steepland of the region and provides access to ground water for nutrient analysis. This study presents results for ground water and surface water dissolved reactive phosphorus (DRP) and N-$NO_3$ and ground water dissolved oxygen (DO) and oxidation-reduction potential (ORP). The distribution of spurs/hollows and ridges/valleys using LiDAR information processed through ArcGIS Pro are presented. The culmination of data presented within this thesis helps to understand how freshwater is affected by farming.

[1] The stream of Porewa is not officially spelt Pourewa and is not officially spelt Porewa. However, the location of Porewa north-east of Marton is officially Porewa (Toitū Te Whenua - New Zealand Land Information, 2013). The use of Porewa for both location and stream will be used within this thesis.

# Chapter 2 – Literature Review

## 2.1. Early Development of the Soil-landscape Modelling and Mapping Concepts and Definitions.

It was hypothesised by Huggett (1975) that "the soil landscape is constructed of a three-dimensional open system whose boundaries are defined as drainage divides, the surface of the land and the weathering front at the base of the soil profile". Conacher and Dalrymple (1977) defined the term soil as being "a three-dimensional body developed on the Earth consisting of horizons of mineral and organic material whose morphological, physical, chemical and biological properties differ from those of the original parent material".

Identifying elements of a fully developed hillslope is fundamental to identifying personal location in the field and to help with soil and sediment property indications downslope (Hammond, 1997). Within a low order drainage basin, the hillslope elements identified include divide, interfluve, side-slope, head-slope, and nose slope. The head and side-slopes can be further subdivided into different slope profile components that include summit, shoulder, backslope, footslope and toe slope (Figure 1).

Rhue and Walker (1968) and Walker and Rhue (1968) (both as cited by (Hammond, 1997)) developed two models for hillslope landscape systems based on the identified hillslope elements. The two hillslope models recognised are open system and close system models; open systems occur in drainage basins that are part of a more extensive drainage network, and closed systems occur where drainage is trapped in a closed basin (Figure 2).

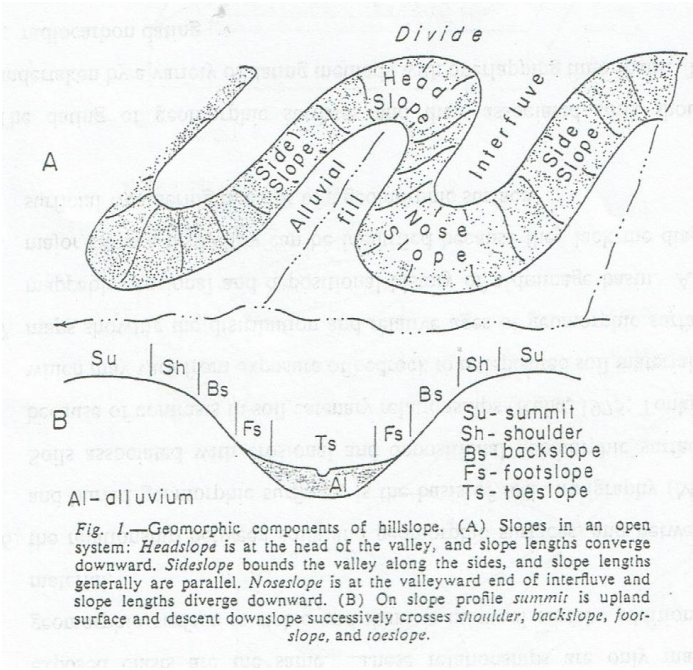


*Fig. 1.*—Geomorphic components of hillslope. (A) Slopes in an open system: *Headslope* is at the head of the valley, and slope lengths converge downward. *Sideslope* bounds the valley along the sides, and slope lengths generally are parallel. *Noseslope* is at the valleyward end of interfluve and slope lengths diverge downward. (B) On slope profile *summit* is upland surface and descent downslope successively crosses *shoulder*, *backslope*, *footslope*, and *toeslope*.

*Figure 1: Hillslope elements of an open hillslope model. Originally reproduced from Rhue and Walker (1968, as cited by and retrieved from (Hammond, 1997)).*

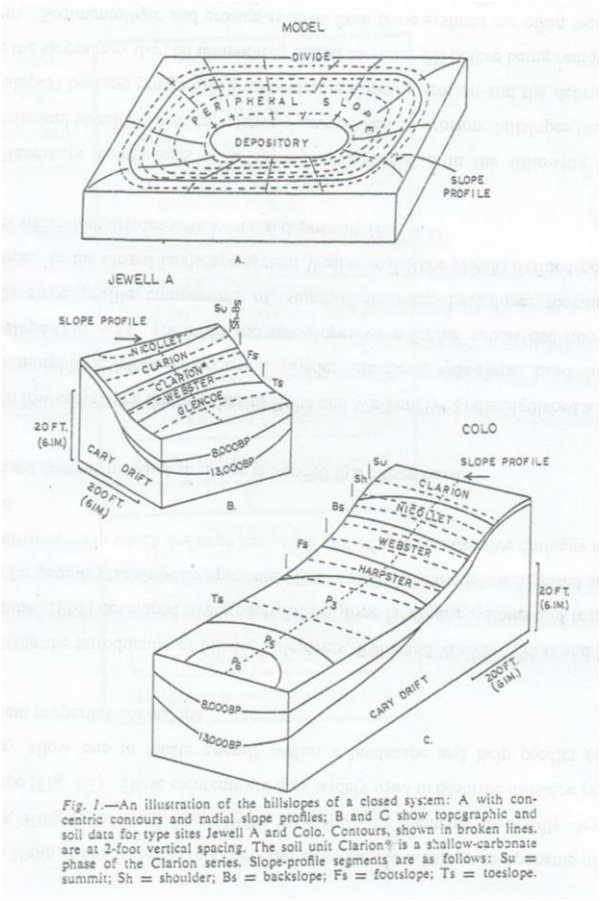


*Fig. 1.*—An illustration of the hillslopes of a closed system: A with concentric contours and radial slope profiles; B and C show topographic and soil data for type sites Jewell A and Colo. Contours, shown in broken lines, are at 2-foot vertical spacing. The soil unit Clarion* is a shallow-carbonate phase of the Clarion series. Slope-profile segments are as follows: Su = summit; Sh = shoulder; Bs = backslope; Fs = footslope; Ts = toeslope.

*Figure 2: Hillslope components of a closed hillslope model along with illustrating the restricted drainage of a closed system. Originally reproduced from Walker and Rhue (1968, as cited by and retrieved from (Hammond, 1997)).*

Early development of soil-landscape models presented by Huggett (1975) shows early models were divided into two approaches; the first approach, traditionally used by pedologists, observed changes that can be described by relatively simple equations (such equations are models of the soils system, but are limited to the micro scale and are applied strictly to a small part of the whole soil system) and are termed isomorphic models. The second approach determined that due to the complexity of the soil system it is impractical, if not impossible to use the isomorphic models. Therefore, the term homomorphs was used for the second model that utilises a many-to-one relationship approach which aims to predict the behaviour of the system as a whole (Huggett, 1975).
These approaches, led to the modifying of Jenny's (1941) concept that 5 soil forming functions (climate, organisms, relief, parent material, & time) define the soil system, producing a more workable model of soil development, by stating that soil formation is a function of organic matter production, the amount of water available for leaching and time. Jenny soon established that the soil is a three-dimensional body resulting in existing models to become irrelevant. Kellogg (as cited by (Huggett, 1975)) pointed out that soils have shape and area, breadth, and width, as well as depth and is all a part of the three-dimensional landscape. The describing of three-dimensional soil bodies had been attempted; however, actual functioning of the soil landscape had received little consideration, especially when considering the notion that the vertical movements of materials are far more important in soil profile development than movements tangential to the surface (Huggett, 1975).

The geomorphic surface concept was developed as a means for analysing late Quaternary erosional and depositional soil-landscape histories of an area. Rhue (1969 as cited by (Hammond, 1997)) defined a geomorphic surface as "a portion of the land surface comprising both erosional and depositional elements, having continuity in space and a common time of origin; it may occupy an appreciable part of the landscape and may include many landforms". The definition for geomorphic surfaces was to link nicely to the K-cycle (discussed in chapter 2.2.1.1) by the inclusion of erosional and depositional parts having a continuity in space and a common time of origin as established by Tonkin (1994). Hammond (1997) and Tonkin (1994) both considered the work of Rhue and recognised a spatial and chronological continuity within the erosional and depositional elements of a geomorphic surface. Recognised spatial continuity can be identified as buried and exhumed geomorphic surfaces; these surfaces can either be destroyed or buried through degradational or aggregational phases forming intermediate elements prior to a new geomorphic surface being formed (Hammond, 1997). The common time origin component of the geomorphic surface definition established by Rhue, can be expanded to describe that a geomorphic surface has a common 'time' of origin and not a common instant of origin, which in essence means that formation

may have taken place over a period of time that could include a number of erosion and deposition events. Differentiation of soil patterns is all depended on whether a geomorphic surface is diachronous (either erosional geomorphic surfaces, where patterns are determined by lithological variations; or depositional geomorphic surfaces, where patterns are determined by mode and regularity of sediment transfer and deposition; or synchronous, where relative contribution of controlling factors changes with time (Tonkin, 1994) (Figure 3).

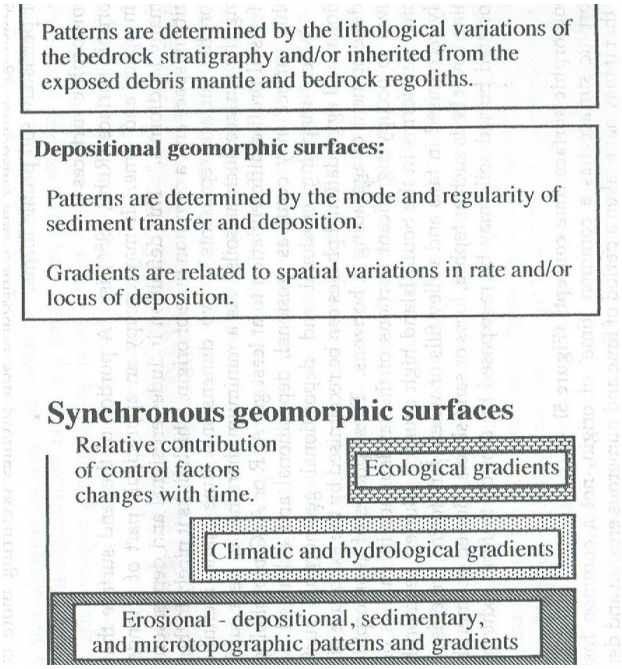


*Figure 3: Categories of geomorphic surfaces – Diachronous and synchronous. Retrieved from (Tonkin, 1994).*

## 2.2. Soil Landscape Modelling & Mapping

New Zealand provides a unique laboratory for the study and development of models for soil-landscape relationships (Tonkin, 1994). Quaternary scientists are constructing models that link climate, vegetation change, and tectonic events, with landform evolution, which has been provided extensive opportunities to document throughout New Zealand (Tonkin, 1994).

### 2.2.1. Mapping

Soil mapping, classification and pedologic modelling have been important drivers in the advancement of our understanding of soils from the earliest days of the scientific study of soils. Early soil maps typically used outline maps of political boundaries but eventually developed to being surficial geology maps during the 19th century (Brevik, et al., 2016). Boundaries between landform units are based toward convenience and ease of defining boundaries in the landscape when completing terrain modelling and land mapping (Tonkin, 1994). Brevik et al (2016) identified that soil surveying received a large amount of attention and significant funding through the latter parts of the 20th century, however, funding, and surveying activity declined in many parts of the world starting in

the late 1980's. The following sections address' existing published literature surrounding soil mapping.

#### *2.2.1.1. Soil Catena and K-Cycle Definitions and Applications*

The soil catena concept was developed by Milne in the 1930's (as cited by (Hammond, 1997) to map and classify soil patterns observed on hillslopes. A catena is described as a sequence of soils along a slope having different characteristics due to variations in relief, elevation, and drainage, as well as the influence of slope processes on sediment removal and delivery (Figure 4) (Gerrard, 1993; Schaetzl, 2013). This definition can be further enhanced by Rhue (1975, as cited by (Hammond, 1997)) who describes a soil catena as "a physiographic complex of soils between the crest of hills and the floors of adjacent depressions or drainage ways whose profiles change from point to point in the traverse, depending on the conditions of drainage and past history of the land surface". A soil catena integrates geomorphic processes (erosion, transport, and deposition) and hydrological processes (throughflow and solute transport) with pedological processes (Hammond, 1997). Soil catenary is more evident when a drainage basin is in its residence time, influencing zonation within a catena. The recognition and definition of these zones changes with time and soil development, along with having a hydrological influence on sediment and solute transformations. Tonkin (1994) describes these zones as either being zones of eluviation (a zone of net loss), transfer (where substances are moving through the slope often by through-flow or overland flow), or illuvial (a zone of net gain) (Figure 5). Milne considered there to be two types of catena; the first is where parent rock is uniform, the resulting differences in soils in a catena are a result in differences of drainage and differences in lateral movement of materials both at the surface and subsurface. The second is where there is more than one type of parent rock that influences soil genesis (as cited by (Hall, 1983)). Hammond (1997) established that the soil catena can be divided into two; open systems are those where drainage results in sediments and solutes being able to leave the area, while closed systems are those where sediments and solutes are trapped, commonly in closed depressions. Catena modelling has been used widely to predict soil distribution across hillslopes and, therefore, is central to soil mapping. However, it is found that soil distribution is dependent on hillslope land use management especially in areas of agricultural practices (such as intensive cropping, tile drainage, fertilisers, tillage, and erosion) (Richter & Burras, 2017). The catena concept has a great influence on soil survey work due to the repetition of a sequence of soil properties in association with certain topography (Conacher & Dalrymple, 1977). Hammond (1997) established that the catena model by Milne evolved into the toposequence model. The toposequence model is defined as a hydrosequence where soil profile colours are used as indicators of water table elevation. However,

water movement, particularly lateral movement and the properties related to movement of minerals in solution and suspension have been a limiting factor for this model.

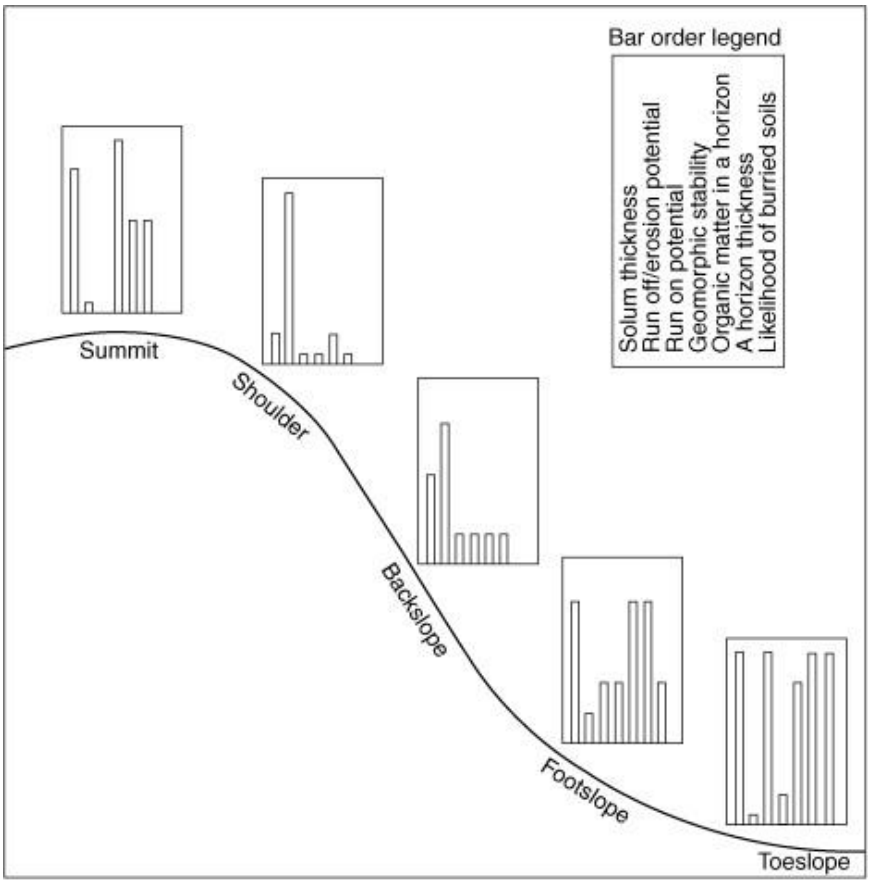


*Figure 4: The effects of hillslope position on soil properties in a catena in a humid climate. Retrieved from (Dixon, 2015).*

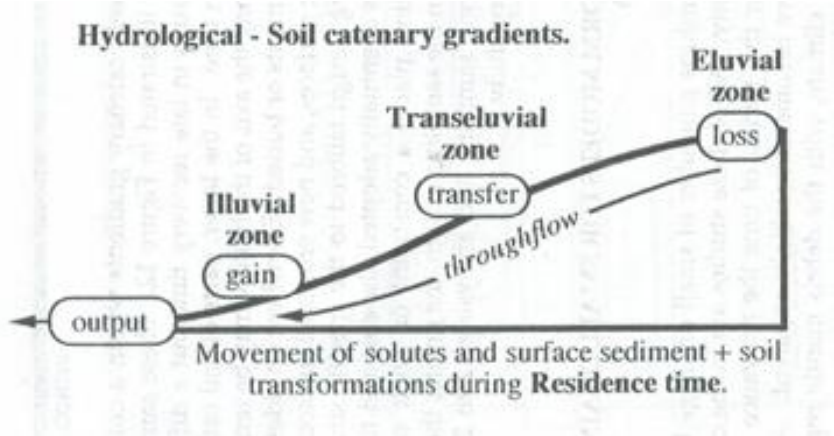


*Figure 5: The illustration of zonation within a catenary system, along with showing hydrological influence. Retrieved from (Tonkin, 1994).*

Another widely named soil-geomorphic model for hilly terrain is the K-cycle model developed by Butler (1959, as cited by (Hammond, 1997)). The K-cycle has similar features to the catena model developed by Milne; however, this model is showing the formation of soil-landforms related to episodic periods of erosion and deposition and environmental conditions. Butler termed a K-cycle as a complete erosion-deposition cycle, along with the soils which form. He states that a subsequent period of instability and soil formation would result in the initiation of a second K-cycle. Hammond (1997) demonstrated that hillslopes comprise of 4 zones within the K-cycle model; A persistent zone (occurs on those parts unaffected by erosional or depositional slope process), a sloughing or erosion zone (located on the steeper parts of the slope where erosion or periods of instability occur), an alternating zone (occurs in a location where erosion is less effective resulting in exhumed, truncated, cumulative and polygenetic profiles), and an accretionary or depositional zone (located where erosion is void and periods of accretion occur) (Figure 6).

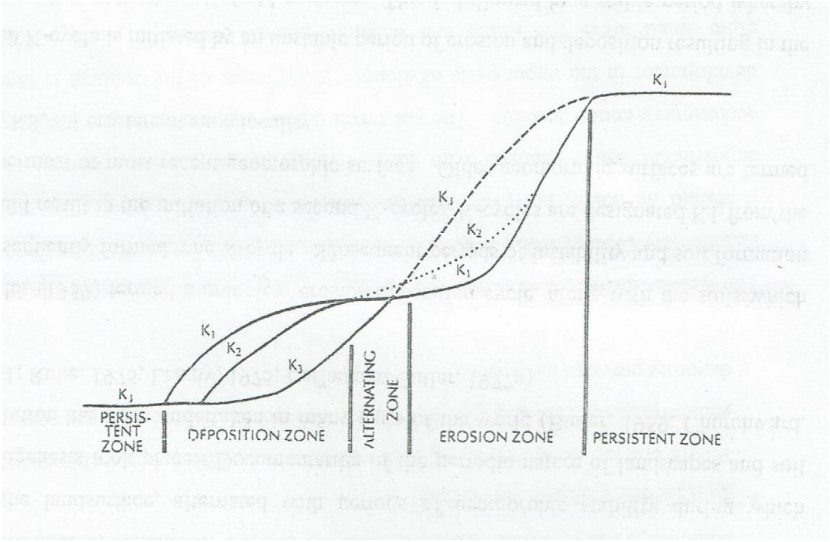


*Figure 6: A diagram of the different hillslope zones and individual K-cycles (K1, K2, K3) within the K-cycle model by Butler 1959. Retrieved from (Hammond, 1997).*

### *2.2.1.2. Soil Mapping Scales and Mapping Coverage*

Soil map sets at a variety of scales, with patchy distribution, has been the result of soil surveying in New Zealand from 1939 to 2001. Limitations included incomplete coverage, especially national coverage, inconsistencies at the regional scale, the generation of new soil series and the scarcity of directly useful information for land management (Hewitt & Dymond, 2013).

The national soil database (NSD) contains the descriptions of about 1500 New Zealand soil profiles along with the chemical, physical, and mineralogical descriptions of the profiles. Hewitt, Lynn, Manderson, Wilde & Willoughby (2008) showed that within the Manawatu-Wanganui region there are 236 soil series recognised at 1:63 360.

The stability of the inherent soil properties allows soils to be reliably mapped for conventional soil maps (Hewitt & Dymond, 2013). The NZLRI, a spatial database and a series of map worksheets that describes the Land Resource Inventory (LRI) and Land Use Capability (LUC) (Lilburne, Lynn, & Webb, 2016), consists of fifteen soil-property maps known collectively as fundamental soil layers (FSL). Each FSL contains spatial information for 16 key attributes. According to Manaaki Whenua, FSL predates S-map despite there not yet being national coverage for S-map therefore FSL are still referred to (Fundamental Soil Layers, n.d.).

The availability of data and the coverage of data varies regionally. The Horizons district is one example of where LIDAR is used but does not have complete coverage. McLeod, Rijikse & Dymond (1995) completed a soil-landscape model for the Gisborne-East Cape area, specifically in close jointed mudstone hill and steep land country. They state existing spatial soil information was restricted to broad scale data set information from the General Survey of the Soils of North Island, New Zealand (1:253 440 scale (Lilburne, Hewitt, & Webb, 2012)). The New Zealand Land Resource Inventory (NZLRI) was utilised in this study, to include soil data based on enhancements from the addition of the Fundamental Soil Layers (FSL). However, survey polygons with more-detail required simplification, done by finding boundaries are generally more reliable when the map units are larger.

The NZLRI presented soil and land resources at a national scale addressing 5 key physical soil and land resource factors that drive land use capability (Vogeler, Cichota, & Beautrais, 2016). Soil information scale and reliability are limiting factors for farm scale mapping and management purposes in New Zealand. Limited availability for the farming community in New Zealand can be attributed to this community not being the targeted customer, with well-resourced organisations being an illustration of a targeted customer (Manderson & Palmer, 2006). The NZLRI is nominally scaled at 1: 50 000 (New Zealand Land Resource Inventory - Soil, n.d.). At this scale the level of detail is constrained and consequently the detail provided is insufficient for farming. Tonkin (1994) addressed the importance of the scales used for the study of soil-landscapes by stating that the scales used determines what is seen due to being conditioned by how close landscapes are viewed. To obtain sufficient detail for within-paddock soil patterns, ‘farm scale’ is preferred. Scales range between 1: 5 000 for dairy farming and 1:25 000 for more extensive hill country, with most hill and steep land sheep and beef farms being 1: 10 000. Minimum specifications for data sets in Whole Farm Plans (WFP) include LRI data at scales between 1:5 000 – 1:15 000 (AgResearch Grasslands, 2007). Comprehensive WFPs are done at on-farm scale with paddock-scale assessments, containing physical parameters such as soil type, vegetation, erosion, and land use capability (LandVision, 2017). LandVision Ltd include soil maps, nutrient budgeting and management, analysis of current production systems, LUC mapping, analysis of physical and environmental attributes within their

comprehensive WFPs. Carrick, Hainsworth, Lilburne & Fraser (2014) stated that the level of detail needed to resolve the soil pattern in areas with significant risk of leaching or runoff depends upon the nature of soil variability. One consequence surrounding the utilisation of different scales providing different degrees of detail is the increase in cost related to increased detail of information. The greater the detail the higher the cost, ultimately the key reason for why soil information is rarely available at scales suitable for farming (Manderson & Palmer, 2006).

#### 2.1.1.3. Geographic Information Systems (GIS) Use in Mapping

The geospatial revolution has introduced tools and technologies such as geographic positioning systems (GPS), geographic information systems (GIS), remote sensing, GIS-linked proximal sensing, and spatial statistics; with these technologies soil mapping throughout the 21$^{st}$ century has greatly changed (Brevik, et al., 2016). With the advent of (GIS), the greater accessibility of high resolution remotely sensed data (LIDAR, hyper-spectral/spatial imagery), and the development of spatial statistical techniques, it is now possible to integrate a variety of environmental factors that when correlated with soil properties greatly improves the ability to predict their spatial distribution (Maynard & Johnson, 2014). The wide availability of digital elevation models (DEMs) provides the basis for many landscape analyses based on surface topography. Numerous studies have demonstrated the importance of terrain attributes for predicting landscape-scale soil variability, demonstrating the considerable uncertainty that exists as to the scale-dependency of Light Detection And Ranging (LiDAR) derived terrain attributes on the accuracy of soil-landscape model predictions (Maynard & Johnson, 2014). It is due to these finding that Maynard & Johnson (2014) compiled a study that provides a robust framework for investigating pedomorphological processes on a landscape through examination of the scale dependency of modelled terrain attributes in quantitative soil-landscape modelling. The authors commented that soil properties were used as predictor variables in ordinary least square (OLS) regression models, as dependent variables, and terrain attributes. These were calculated from LiDAR derived DEMs of various grid resolutions (ranging from 5-50m) and neighbourhood extents (ranging from 15-350m). The increasing availability of LiDAR data is in part due to a generalised assumption that fine scale topographic data will produce more accurate predictions of landscape attributes. This may be true for certain landscape attributes, Maynard & Johnson (2014) comment that their results show that it remains unclear whether the high horizontal resolution achievable with LiDAR is sufficiently beneficial in soil-landscape modelling, specifically given the high cost and high computational requirements associated with its use.

Ground penetrating radar (GPR) is a rapidly growing field that has been significantly progressing over the past 15-20 years. The diversity of GPR applications encompasses a variety of areas including in

the field of groundwater contamination (Jol, 2008). GPR uses radio waves to probe 'the ground' (any low loss dielectric material). The most common form of measurements deploys a transmitter and a receiver in a fixed geometry, which is moved over the surface to detect reflection from subsurface features (Annan, 2008). GPR systems specifically designed for soil reconnaissance can chart the depth and extent of diagnostic subsurface horizons. The full-wave inversion method has been applied to a broad spectrum of soil surveys including soil descriptions, soil moisture estimation, organic matter thickness and description, and the description of ground vegetation. The use of multi-offset data and inverse modelling has been shown to have the advantage of the simultaneous determination of all subsurface properties without the need to know at least some of them in advance (Zajícová & Chuman, 2019). Doolittle (1987) addresses some limitations that occur with the usage of GPR for soil surveying and states that performance amongst different soils varies. The author discusses how generally probing depths are 5-25m in coarse textured soils, 2-5m in moderately coarse-textured soils, 1-2m in moderately fine-textured soils and <0.5 to 1.5m in fine textured soils. They state that GPR is site specific. Zajícová & Chuman (2019) support this by stating that one disadvantage of GPR is the surveys of fine-textured soils were often unsuccessful due to the lower signals being disguised and inferred by stronger reflections near the soil.
Upscaling efforts to date using landscape analysis have been based on individual hillslopes or experimental catchments. This carries inherent risks that representation of the overall catchment or the larger scale may still present inaccuracies (Blume & Van Meerveld, 2014).

#### *2.2.1.4. Erosion Mapping Driving Erosion Modelling*

Early classification of the soil system includes the notion that the erosion drainage basin is one factor forming the boundary of the soil system. This introduced the notion that the solid, colloidal, and soluble material of the soil system exists in a continuum, in terms of particle size and stability and hence mobility, when in transit through denuded systems. Meaning at one end of the continuum there are the relatively large, stable, and immobile particles of the soil skeleton, while at the other extreme of the continuum is the very mobile, unstable soil solution (Huggett, 1975). When simplified, it show that within an erosion drainage basin the stability of the soil system is in a continuum and has the ability to transport material out of the system, whether it is in the form of erosion or drainage.

In 2004 the Manawatu-Wanganui Regional Council launched the Sustainable Land Use Initiative (SLUI) which primarily focuses on assisting farmers of highly erodible hill country to implement on-farm practices that aim for a reduction of erosion, improvements in regional river water qualities and improve on-farm soil management (Manderson, Mackay, Lambie, & Roygard, 2013; Reid, 2014). The prediction of erosion-prone land at regional scale is accomplished by estimating the extent and

magnitude of the prementioned land at catchment level using a number of models including the NZLRI. It has been ascertained by Manderson, Mackay, Lambie & Roygard (2013) that the models used at the regional scale may not be well rendered for erosion at the farm scale. The conservation planting effectiveness model developed by Douglas et al (2008, as cited by (Manderson, Mackay, Lambie, & Roygard, 2013)) is used along with the New Zealand Empirical Erosion Model (NZeem®) developed by Dymond, Betts, & Schierlitz (2010) to represent a 'worst case' for sediment run off, resulting in the estimating accumulative effectiveness of SLUI. Manderson, Mackay, Lambie & Roygard (2013) have recommended that for it to be possible to model the potential erosion reduction rates from mixed land uses, the model could be modified from projecting over longer time frames to include harvestable species. In addition, enhancement of the model has been identified to include further study into the mechanisms involved. Real-world water quality monitoring and further measurements are included which aim to improve water quality by sediment reduction. The use of SedNet could be incorporated for further understanding of spatial distribution of sediment loss. The creation of WFPs are central to SLUI, where they are implemented to help reduce erosion (Manderson, Mackay, Lambie, & Roygard, 2013). Reid (2014) stated that the mapping completed within a WFP is completed according to the characteristics of the land resources, along with the current and potential levels of pasture productivity. Where upon the land resource information is presented using a LUC classification. The LUC classification categorises land units into 8 classes according to the long-term capability to sustain one or more productive uses (Figure 7) (Lynn, et al., 2009). Todd (2018) shows examples of real-world applications and highlights the difference farm scale makes compared to regional scale and showing how the differences in scales affect the outcome to sediment loss predictions and modelling.

| LUC Class | Arable Cropping Suitability | Pastoral Grasing Suitability | Production Forestry Sutability | General Suitability |
|---|---|---|---|---|
| 1 | High ↓ Low | High ↓ Low | High ↓ Low | Multiple use land |
| 2 | | | | |
| 3 | | | | |
| 4 | | | | |
| 5 | Unsuitable | | | Pastoral or forestry land |
| 6 | | | | |
| 7 | | | | |
| 8 | | Unsuitable | Unsuitable | Conservation land |

*Figure 7: Increasing limitations to use and decreasing versatility of use for the different LUC classes. Retrieved from (Lynn, et al., 2009)*

#### *2.2.1.5. Soil Mapping Presentation Driven by Modelling*

S-map is a digital product that has been initiated to bring together soil information in a multi-layer soil database with national coverage (Lilburne L. , Hewitt, Webb, & Carrick, 2004). S-map has three levels within the development of the tool. These levels consist of the underlying data (that includes spatial soil data & morphology attributes, soil processes & management research, and lab measured analytical data), information inference engine (also referred to the model stage and the generation of information) and delivery/presentation. At the modelling and information generation stage a new national model has been released (in August 2020). The new model now has improved data representation allowing for better portrayal of data specifically for soil siblings and the depiction of data for soil water retention information (the presentation of the soil water retention information can be found online at S-map). The model used is based around the research presented in the study by McNeill, Lilburne, Carrick, Webb & Cuthill (2018) which utilises pedotransfer functions for the soil water characteristics of New Zealand soils. The beta regression model, when applied at the extrapolation phase, reduced the number of soil siblings that could not have key properties predicted for Overseer, because extrapolation was too unreliable, from 424 to only 4 resulting in a more stable model and a reliable extrapolation phase. However, the development of the S-map model, to include the discussed improvements, are limited to the national approach. Further research is being completed on a prototype S-map farm test that will be able to apply S-map science at a farm scale (Manaaki Whenua - Landcare Research, 2020). It is suggested by Carrick, Hainsworth, Lilburne & Fraser (2014) that a national protocol needs to be tailored to different landscape environments for farm soil information. This recognises that soil information and mapping scale for hill country would be quite different to those required for lowlands. The lack of soil landscape models and soil description information in S-map within the developmental stages restricts the degree of information available for users. Basic soil property data like depth and stoniness along with more complex data like nitrogen leaching risk and water holding capacity are presented within S-Map (Manaaki Whenua - Landcare Research, 2023); however, information from soil landscape models and soil descriptions are the two main forms of data that people would want to access.

The aspect of hill slopes have an impact on the exposure the soils have to natural elements and how they respond to changes over time, for instance net radiation has been shown to be greater for north facing aspects (for periods encompassing the autumn and spring equinoxes and the winter solstice) and when combined with wind speed values being higher on north facing aspects evapotranspiration values are impacted. Bretherton (2012) briefly illustrated the effect of hills slope aspect on evapotranspiration and soil moisture conditions through the use of water balance on a hill slope. Water balancing in a simplified expression takes into the equation rainfall, drainage, soil water

storage, and evapotranspiration. Radcliffe (1968) and Gillingham (1973) found that that top 75mm of soils on north facing slopes had considerably lower soil moisture content levels than soils on south facing slopes. Evapotranspiration has been shown to be higher on north facing aspects than south facing aspects for slopes on the foothills of the Southern Ruahine Ranges due to the proportions of net radiation utilised for evapotranspiration (Lambert & Roberts, 1976). Increased evapotranspiration rates in combination with lower rainfall exposure and lower soil moisture content increases the prospect for the genesis of Pallic Soils, related to the increased occurrence of wetting-drying cycles creating desiccation shrinkage. Lower evapotranspiration rates in combination with increased rainfall and higher soil moisture content increases the prospect for the genesis of Brown Soils.

### 2.2.2. Modelling

Due to the varying nature of soil, sampling the soil as a finite number of places or points in time yields incomplete pictures, therefore, the need for predicting sampling points is often required. The need to predict ahead in time to compare the effects of different scenarios or management practices was identified by Heuvelink & Webster (2001). Soil landscape models, usually developed during routine soil surveys, are empirical rules relating landforms to soil properties or soil classes and provide a detailed description of soil-landscape relationships (McLeod, Rijikse, & Dymond, 1995). The creating of models has the intention of being able to reduce the time, effort and money that is expended during the analysis of different factors, such as soil-landforms and hydrology as analysed throughout this chapter.

#### *2.1.2.1. Modelling of Soil-Landform*

Hammond (1997) established that Tonkin and his students, using the fluvial systems model (Figure 8) developed by Schumm (1977) viewed the interrelationships of soils to landforms within drainage basins, valley floors, terraces, and fans of the South Island New Zealand. The use of this model allows for the description of movement or transfer of materials through various reaches of the fluvial system and relates to the landforms seen; allowing for the recognition of a number of spatially linked cascading subsystems, each of which may impact on the evolution of another linked subsystem (Tonkin, 1994); also allowing for the recognition of landforms providing the foundation from which the regolith, soils and soil patterns evolve. The fluvial system model employs the principles of soil stratigraphy, the K-cycle, soil chronosequence and soil geomorphic surface concepts when considering the temporal and spatial organisation of landforms and their associated soils (Hammond, 1997). Tonkin established the first step in the fluvial system model to be subdividing the landscape into consistently recognisable soil landforms. Followed by determining the factors that

have influenced the development and distribution of soils of each soil-landform. The identification of these landforms provides the foundation upon which the regolith, soils and soil patterns are evolving (Tonkin, 1994). Tonkin (1994) defines the drainage basin subsystem as being a "sediment production zone with the transfer of sediment to the valley floor and beyond". The evolution of a drainage basin system is determined by a period of sediment accumulation followed by a period of sediment residence, during which soil catenary gradients evolve and is succeeded by a period of evacuation (Figure 9). An example of catenary soil landform models for small drainage basins in residence time is the work completed by Schmidt, Tonkin & Hewitt (2005) on the Haldon and Hurunui soil sets (modelling approaches are presented later in this section).

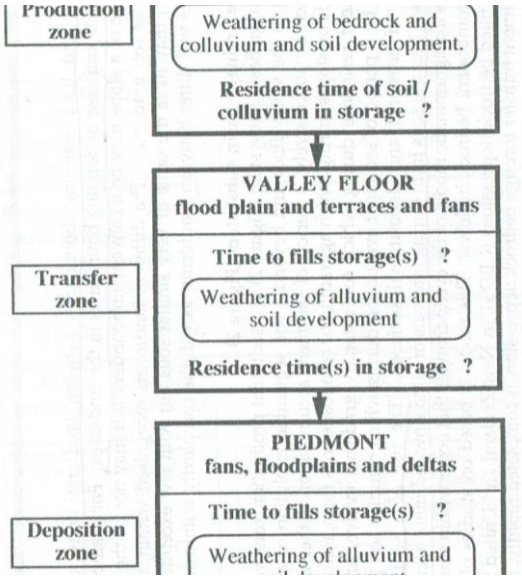


*Figure 8: Fluvial system model developed by Schumm (1979), showing the relationships between each of the different zones (Production, transfer, and deposition) and the influence on the transfer/transformation of materials. Retrieved from (Hammond, 1997).*

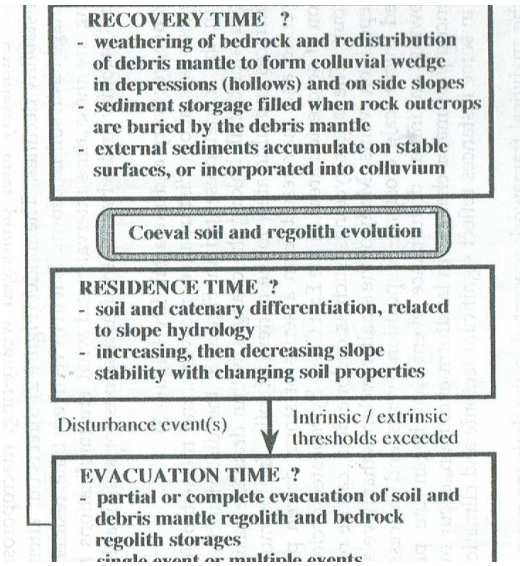


*Figure 9: The drainage basin subsystem within the fluvial system model. Retrieved from (Tonkin, 1994).*

The manual interpretation of aerial photography in combination with field surveying is the foundation of fundamental mapping techniques. Nowadays, digital terrain models (DTMs) and satellite imagery have been the source for increasingly detailed digital land surface information for the application of soil-landscape modelling (Schmidt, Tonkin, & Hewitt, 2005). The surveyor developed a mental conceptual model of soil-landscape relationships and subsequently developed a spatial representation of this mental model by representing soils as map units. The subjective technique of aerial imagery is unlikely to be reproduceable, even with the images displaying many features of complex landscapes (including landform, surface roughness, vegetation, and stream networks). Schmidt & Hewitt (2004) state that the advantage of calculating land elements from DTMs is the maps produced can be used to measure the uncertainty in a classification and not only just produces a landform classification. This method is simple with respect to computational and parameter requirements and is therefore easy to apply.

Schmidt, Tonkin, Hewitt (2005) present a study for the Haldon and Hurunui soil sets in New Zealand that present quantitative soil landscape models that details different spatial modelling techniques applied, including terrain analysis and fuzzy classifications. This study illustrates how conceptual soil-landscape approaches can be quantified and expressed as soil maps. The authors address previous studies completed on the study soils and discuss how these studies are integral as 'a priori' which are transferred into terrain analysis techniques that result in derivation of landform components. Schmidt, Tonkin & Hewitt (2005) utilised and discussed three different approaches towards soil-landscape modelling (Figure 10) that included conceptual landscape models, quantitative landscape models, and soil taxonomic models (soil properties for landscape units). Conceptual landscape models are the initial phase used in a conceptual soil-landscape model to describe soil variation in relation to the pattern of land components in the land system. Succeeding this the conceptual patterns were modelled using a quantitative landscape model (including the usage of fuzzy classifications) based on spatial analysis techniques in a GIS framework. The final phase, completing the quantitative soil landscape modelling, included the use of a soil taxonomic model statistically related to soil profiles and soil properties of landscape units (that used pedotransfer functions). The authors stated that the accuracy of the developed landscape model relates to the question of how well the quantitative model represents the conceptual mode and the contributions of errors in the original data and model inadequacies to errors in the final results. Field mapping landform elements and soil profiles were applied for the testing of the accuracy of the quantitative spatial model. The result of this testing shows that the modelled land elements generally conformed well with observed landform structure, however, they also highlighted that due to the methodology being a fixed-scale technology, small-scale features cannot be resolved causing many small hollows to be missed in

analysis. They finally state that you cannot fully replace all fieldwork by spatial models, but an intensive interaction with in-field surveyors (therefore completing extensive field work) is required within the development of conceptual soil-landscape models.

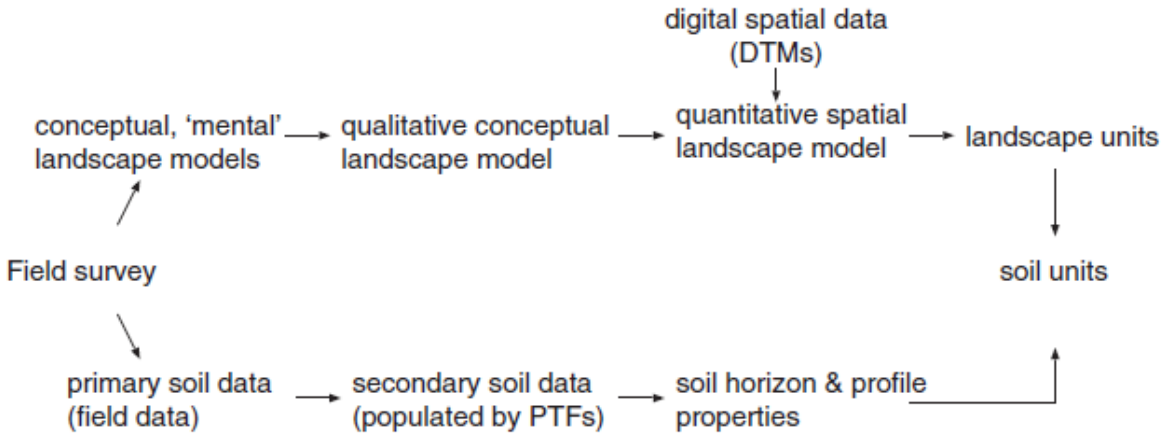


*Figure 10: Fundamental concept and methodology for soil-landscape modelling used by Schmidt, Tonkin & Hewitt (2005). The results produce landscape unit maps. Retrieved from (Schmidt, Tonkin, & Hewitt, 2005).*

Schmidt & Hewitt (2004) presented a study that uses the term 'fuzzy' to describe the inherent uncertainty within classifications. They state that a unique, non-ambiguous classification into land elements will not be possible. This is a result of the high degree of uncertainty inherent in the description of land elements and the descriptor variables used. They provide an example for this by stating that it is unclear what a hillslope is in semantic terms, because if a hill slope is simply defined as a high gradient area, there is still the uncertainty present as to what is considered 'high gradient' in quantitative terms. Therefore, the authors state that there are no clearly defined spatial boundaries and identify land elements as 'fuzzy objects'. Schmidt & Hewitt (2004) after defining 'fuzzy/fuzziness' present the fuzzy classification and the position it has within soil-landscape modelling. They show that the fuzziness surrounding 'flat' or 'sloped' in terms of specific slope thresholds can be differently drawn by mappers, especially with terrain characteristic differences. Therefore, the authors state it is appropriate to substitute the hard classification threshold used for form classification with fuzzy boundaries, leading to a fuzzy classification of landforms. Ultimately showing that the rules defining a form element can be implemented on the basis of the semantic import of models by applying a fuzzy classification model, for example by replacing the usage of 'AND/OR' to 'Minimum/'maximum' within the classifier. Schmidt & Hewitt (2004) discuss the advantages and disadvantages of the different approaches available for modelling land elements to

give spatial estimates of soil properties, encompassing statistical and heuristic models (Figure 11)

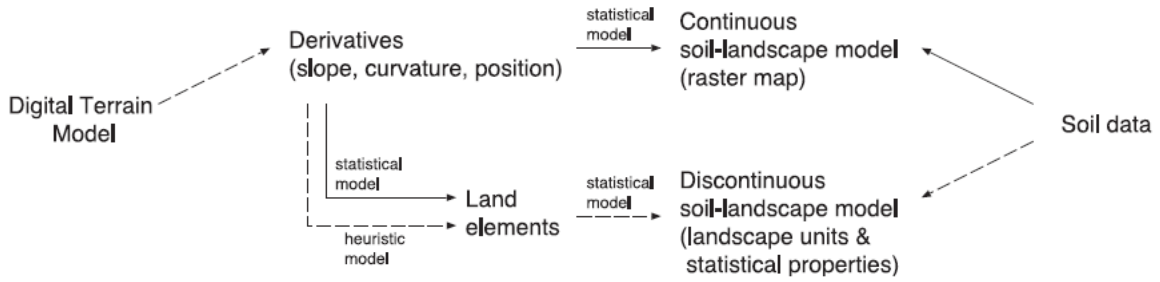


*Figure 11: Different methodologies in soil-landscape modelling. Dashed lines show the approach used by Schmidt & Hewitt (2004). Retrieved from (Schmidt & Hewitt, 2004).*

### *2.1.2.2. Hillslope Erosion Modelling*

Bathurst (2011) stated that human activity is the greatest single influence on erosion and sediment yields; however, climate and geology are dominant at larger spatial scales (Basher, et al., 2020). Basher et al (2020) further expanded on this by discussing that rainfall amount and intensity specifically are the main triggers for different forms of erosion and are important factors that are directly or indirectly involved in most erosion models.

The clearing of indigenous forest for pastoral agriculture following the settlement of Europeans after 1840, deforestation in New Zealand has led to an increase in soil erosion and sediment loads in rivers, ultimately causing adverse effects to aquatic ecosystems. The presence of tree roots in hill country soils are important for stabilising slopes consequently the increase in deforestation increases sediment loss from the loss of root stability (Dymond & Vale, 2018). Phillips, Marden & Basher (2018) outline how geomorphological understanding has underpinned forest management in New Zealand's erodible steep land. The authors state that the most pressing concerns are the incidence of post-harvest, storm-initiated landslides, and debris flows (especially during rainstorms, which can deliver large quantities of logging slash, such as branches to whole trees, and sediment into waterways). There are three areas where geomorphological information and understanding are required to support forestry development; the development of an improved national erosional susceptibility classification to support a new national standard for forestry planting and understanding of post-harvest shallow landslide-debris flows, including their prediction and management (Phillips, Marden, & Basher, 2018). Phillips, Marden & Basher (2018) illustrate how in recent years attention has changed to centre on determining sediment yield during or following forest harvesting, determining mining slope wash during post-harvesting, post-harvest landscape response and policies relating to harvesting, reforestation, and catchment protection. The studies analysed by the authors suggest that the most important hillslope processes generating and

delivering sediment to streams is storm-initiated landslides; the degree of soil disturbance from harvesting operations and the amount of surface erosion in the first year are strongly correlated; the amount of sediment produced on site can be greater than that leaving the catchment as sediment yield; forest sediment yield at harvest time can increase 5 times over pre-harvest rates with rates declining back within 2-3 years after replanting; in exotic forests, post-harvesting sediment yields vary from 10s to 100s of t $km^{-2}$/ year across a range of geologies; at small catchment and storm-event scales, forested catchments yield significantly less sediment than pasture catchments by 50-80%.

The mitigation of excess sedimentation into rivers at catchment wide approaches is required. This ,however, can be an expensive taking due to usually requiring a combination of land use change, erosion control tree planting, riparian management and drain works (Dymond & Vale, 2018). Dymond & Vale (2018) state that due to the expensive nature of soil conservation, conservation should be guided by predictive models that explicitly link erosion and sedimentation with land use and land management. The authors develop an event-based model for soil erosion and sediment transport, with storms being the event for the model drivers due to having peak discharge in tributaries. They found that the spatiotemporal model within their study will be useful in several contexts that include assessing impacts of climate change, land use change and temporal assessment of conservation. The event-based model of Dymond & Vale's (2018) maintains moderate complexity, similar to that of the SedNet model but more closely mirrors the physical drivers of sediment production.

The hillslope erosion model (HEM) was developed by scientists at the USDA-ARS Southwest Research Watershed Centre to describe erosion and sediment yields on rangelands. Cogle, Lane, & Basher (2003) use this model to simulate erosion and sediment yield as a function of position on a hillslope and to simulate the influence of spatial variability in hillslope properties. The aim of this is to assess the application of the model developed in the United States to India, New Zealand, and Australia. The model was applied to four experimental plots near Auckland with results showing the model over predicted the mean sediment yield on the bare plots by 1-13% and under predicted on the pasture plots by 65%, while explaining about 80% and 60% of the variance in observed sediment data, respectively. From these results the authors summarise that the model's application in New Zealand will require calibration with observed data.

Wilkinson, Prosser, Rustomji, & Read (2009) developed SedNet, a spatially distributed budget model of fine sediment for Australia with the driving processes in the hills being hillslope soil erosion, riverbank, and gully erosion. Ausseil & Dymond (2008) identify SedNet as a catchment-scale model of long-term averages of erosion, sediment yield and sediment storage calculated at the sub

catchment level. They also state that SedNet can estimate sediment yield but does not predict sediment concentration. Dymond et al (2016) described a similar model to SedNet that was adapted for New Zealand erosion processes and implemented in the Manawatu catchment. The studies by Dymond et al (2016), Schierlitz, Dymond & Shepherd (2006), and Ausseil & Dymond (2008) all have applications to the Manawatu district using SedNet and its application to WFP or to estimate spatial distribution of sediment concentrations in the Manawatu River.

The results presented by Dymond et al (2016) showed the relationship between measured and estimated suspended sediment loads were moderately agreeable ($R^2$=0.85 after log transformation), considering large uncertainties were associated with the measurements. Schierlitz, Dymond & Shepherd (2006) presented various scenarios that revealed in a realistic scenario of 500 farm plans in the highest priority farms category, a reduction of approximately 50% of mean sediment discharge in the Manawatu River was seen. While in the scenario where half of the 500 farm plans in the highest priority farms category were targeted there was a reduction of 80% in comparison to the original scenario of 500 farm plans in the highest priority farm. Ausseil & Dymond (2008) present results that were comparable with the results of Dymond et al (2016); stating that the predicted sediment concentrations from their model presented acceptable consistency, however, they also stated that further measurement sites are required to fully confirm the accuracy and compatibility of the model. They also discuss that their model is rapid and simple in predicting sediment concentration changes in response to land use change or the implementation of WFP in the Manawatu catchment. The model's flexibility to reconfigure quickly allows for prioritisation of land use change and implementation of farm plans. Wilkinson, Prosser, Rustomji & Read (2009) produce the results of predicting a variety of sediment sources within hill country using SedNet allowing for increased focus on these high-risk locations. SedNet results show the vulnerability of steep land and the prioritization needed within WFP to help reduce soil erosion and the loss of nutrients from the soil system.

The New Zealand Empirical Erosion Model (NZeem®) was used by Dymond, Betts, & Schierlitz (2010) to evaluate regional land use scenarios, specifically in the Motueka catchment and the Manawatu catchment. Dymond, Betts, & Schierlitz (2010) state that the model describes long-term erosion rates and the resulting long-term mean sediment discharge. The NZeem® partitioned landscapes according to the factors controlling erosion such as rock type, landform (e.g., slope and angle), rainfall, and landcover (Dymond, Betts, & Schierlitz, 2010; Envirolink, 2012). The results of the model showed that the accuracy has presented an $R^2$ value of 0.65 and a residual standard error of 0.91 when comparing the predicted specific sediment discharge with measurements at 80 sites. Fernandez & Daigneault (2017) adapted the NZeem® to estimate mass-movement erosion, the

major contributor of fine sediment loads to waterways, with the NZeem® estimates being used for highly erodible land. Following the use of the NZeem® in Dymond, Betts, & Schierlitz (2010) to assess the effectiveness of reducing sediment loads by the implementation of farm plans in the Manawatu catchment, Dymond et al (2016) repeated the study of the Manawatu catchment using SedNet as previously discussed. Basher et al (2020) further developed estimating the effect of erosion control on reducing sediment loads which has been addressed above earlier in this section.

## 2.3. Nitrification Identification & Modelling

### 2.3.1. Soil Redox

Over the past three decades there has been an increased rate of nitrogen (N) use within agriculture allowing for increased stocking rates and changes in land use (particularly seen with 515,000 ha of sheep and beef farms converted to dairying and a 17% increase in stocking rates). Increased stocking rates (resulting in increased cow urine patches) and effluent land application are all potential sources of nitrogen leaching from the soil profile over large areas (Collins, et al., 2017). The understanding of attenuation was assessed within the lower Rangitikei catchment of New Zealand by Collins et al (2017) through the use of existing bores. The authors sampled the groundwater according to the National Protocol for State of the Environment Groundwater Sampling in New Zealand with an array of different monitoring parameters (including dissolved oxygen (DO), specific electrical conductivity, oxidation-reduction potential (ORP), and temperature). Shallow groundwater monitoring was completed using the above-mentioned parameters along with various sites having push-pull tests completed. The authors recognised that the results revealed a mostly reducing groundwater environment in the lower parts of the Rangitikei catchment, with the results being augmented with the results of shallow piezometers and push pull tests. In addition to the push-pull tests, groundwater analysis of well sites were carried out using in-field analysis equipment with further in-lab experiments. The in-field analysis used a multiparameter YSI® water quality meter with a flow cell.

Low DO levels and nitrate concentrations within the subsurface environment in the Manawatu River catchment were found where soil and rock types have poor drainage characteristics in the study by Rivas et al (2017). The authors cited the use of McMahon and Chapelle's (2008) method, along with using redox indicator species and electron donor parameters. They concluded that groundwater under nitrate reducing conditions have DO levels below 1 mg $L^{-1}$ with an ORP value below 150 mv while groundwater conditions under non-reducing conditions have DO values greater than 1 mg $L^{-1}$ with an OPR value above 150 mv. Rivas et al (2017) concluded that oxidised environments which are unsuitable for subsurface denitrification were influenced by different hydrogeological factors such as

soil texture and aquifer materials; allowing for faster movement of percolated water or groundwater throughout the subsurface, increasing the levels of DO in the subsurface. The redox parameter observations within the Manawatu River catchment provided supplementary material to the statement that other factors aside from land use affect the variability in groundwater quality (Rivas, et al., 2017). However, throughout this study the travel time of water throughout the hydrological system was not investigated and further research was suggested for the determination of the location of denitrification (e.g., within the soil profile, ground water, riparian zone etc).

Regulatory approaches to nutrient management is often proceeded by establishing environmental objectives and is followed by defining the nutrient concentration criteria that achieves the intended results (Snelder, Whitehead, Fraser, Larned, & Schallenberg, 2020). Snelder, Whitehead, Fraser, Larned & Schallenberg (2020) stated that at the time of their publication there had been limited effort to quantify the scale of nitrogen issues nationally, despite concern about elevated nitrogen concentrations in New Zealand waters. The author's study linked current nitrogen concentrations and loads to minimum acceptable environmental objects. This established that in some locations relatively large load reductions were required to achieve the objectives. Their study not only shows that there are receiving environments with high nitrogen concentration, but it also provides further insight into the spatial distribution of excess nitrogen concentrations. Snelder, Whitehead, Fraser, Larned & Schallenberg (2020) made clear that through their study it is shown that land and water management decisions need to be spatially specific.

### 2.3.2. Electron Donors

Rivas et al (2017) employed charge balance error (CBE) to determine groundwater quality by considering $Na^+$, $K^+$, $Mg^{2+}$, $Ca^{2+}$, $Fe^{2+}$, $Cl^-$, $HCO_3^-$, $SO_4^{2-}$ and $NO_3^-$. The data for each parameter was assessed for normality using a selection of different tests, any data that was not displaying a normal distribution was transformed. This data was then analysed using IBM SPSS Statistics 22.0 to determine the correlations between groundwater quality parameters and their differences among different hydrogeological factors (Rivas, et al., 2017). The study of electron donors and the use of them in the identification of redox environments, is based on criteria by McMahon & Chapelle (2008) that utilises the natural succession of electron donors to identify the state of redox within subsurface waters (Figure 12). Denitrification requires suitable electron donors that can be classed as either organic or inorganic electron donors (Korom, 1992). Inorganic electron donors include $Mn^{2+}$, $Fe^{2+}$ and sulphates. Organic electron donors include organic carbon, i.e., shell material ($CaCO_3$) which illustrated by Trudell, Gillham & Cherry (1986) is where $CaCO_3$ is consumed during the denitrification process. The requirement of electron donors is the result of a series of redox

reactions that occur within the subsurface and are addressed by (Close, et al., 2016; Collins, et al., 2017; Jha, Singh, & McMillan, 2018; Korom, 1992; Rivas, et al., 2017). Shell bed deposits within subsurface environments have the potential to alter soil nutrient concentrations, soil pH and soil development (Smith & McGrath, 2011) (for instance interactions between soil type and $Ca^{2+}$ revealed the importance of polyvalent cations in aggregate stability of soils (Wuddivira & Camps-Roach, 2007)).

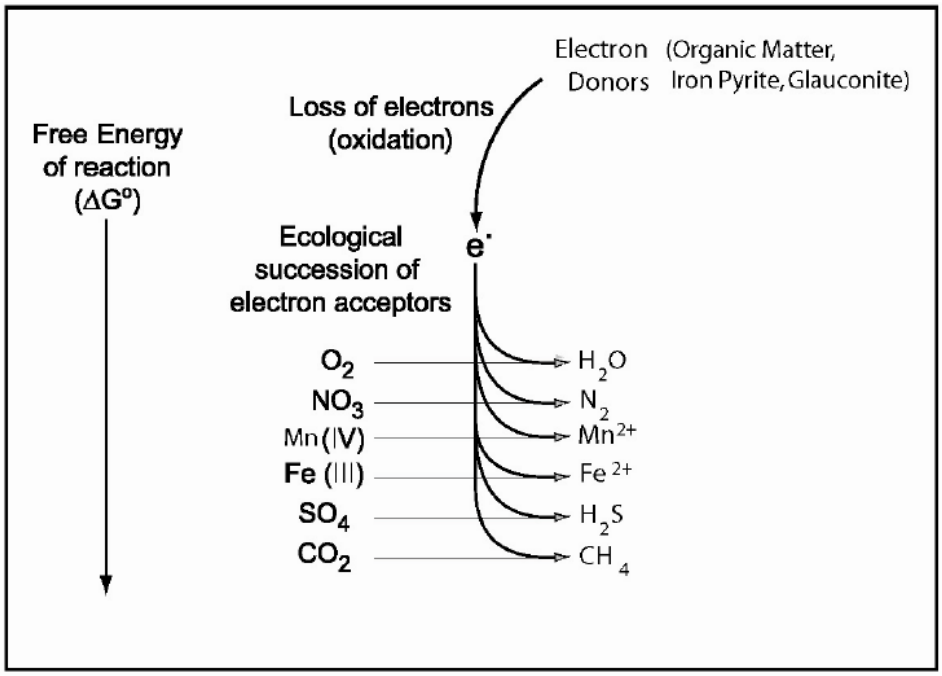


*Figure 12: Ecological succession of electron accepting donors (utilised in the identification of redox conditions) and sequential production of final products in groundwater. Retrieved from (Rissmann, 2011).*

Attenuation within the soil profile and groundwater systems can be assessed by identifying the abundance of denitrifier genes (*nos*Z, *nir*S and *nir*K) alongside DO and varying electron donors (Jha, Singh, & McMillan, 2018). The preliminary results presented by the authors show that the oxidising shallow groundwater (DO >1 mg $L^{-1}$) across different sites across the Manawatu and Rangitikei catchments had lower *nos*Z gene abundance compared to the reducing shallow groundwater zones (DO <1 mg $L^{-1}$). It is suggested that further observations and analysis is needed for comprehensive understanding of denitrification attenuation, using denitrification genes in shallow groundwaters across a contrast of New Zealand sites.

### 2.3.3. Attenuation Factor

Elwan, Singh, Horne, Roygard, & Clothier (2015) through their research (utilising linear regression analysis) into previous studies identified that there was a lack of research into the relationship between the nitrogen attenuation factor ($AF_n$) and catchment characteristics (e.g., land use,

topography, rainfall, soil type and underlying geology). Previous definition of the attenuation factor by Roygard & Clark (2012) allowed for the defining and quantifying of the nitrogen attenuation capacity as the $AF_n$ while presenting an equation. The results from this study concluded that sub-catchments with higher attenuation capacity are dominated by groundwater showing reducing conditions within the subsurface. Sub-catchments with lower attenuation capacity are dominated by groundwater with oxidising conditions. The authors analysis showed that the relationship between $AF_n$ and fine textured soils is a positive relationship, whereas the relationship between $AF_n$ and well-drained soils is a negative relationship. These suggest that sub-surfaces classed with well-drained soils and high permeability of underlying geology result in larger and faster movements of water, reducing the time and increasing the flow of groundwater within the sub-surface, ultimately decreasing denitrification and increased loss of nitrogen from the subsurface. Sub-surfaces with contrasting conditions (e.g., fine textured soils and low permeability of underlying geology) present smaller and slower movements of water resulting in increased time and ultimately denitrification within the subsurface (Elwan, Singh, Horne, Roygard, & Clothier, 2015). However, under different soil settings these rules can be redundant (i.e., if iron and organic matter are present soils can also be under reducing conditions).

Singh, Elwan, Horne, Manderson & Patterson (2017) analysed the research completed by Elwan, Singh, Horne, Roygard & Clothier (2015) by investigating the effects of soil and rock types on land-based nitrogen loads in the Rangitikei. The approach of this study was to adapt a basic nitrogen attenuation factor model to account for different catchment characteristics (e.g., rock type, soil type), with information being provided from either FSL and/or Qmap layers. The modelled nitrogen loads were compared with measured nitrogen loads. The comparisons showing significant differences between the modelled values and the measured values. The models that included any of the catchment characteristics (e.g., rock type, soil type) have the effect of improving the predictions and accounting for nitrogen loading and potential attenuation, however, with a combination of multiple factors the prediction for nitrogen loading was increased significantly.

A Soil Denitrification Potential (SDP) rating was completed on agricultural soils and geology of Southland, with the given values separated into three categories ranging from low through to high (Beyer, et al., 2016). The three categories of SDP for soils in Southland are based on the following factors: waterlogging (based on the criteria set out in S-map), aeration (level of aeration impedance) and New Zealand Soil Classification Order (NZSC, as defined in S-map). For example, soils with severe waterlogging had high SDP whereas soils with slight or nil water logging had low SDP. The degree of soil nitrogen attenuation is seasonally dependent, influencing soil moisture water logging and water table rise and fall. Anaerobic conditions occur during short term waterlogging for periods up to one

week as opposed to long term waterlogging that are sustained for greater than one week due to high water table levels or a perched water table (Manaaki Whenua - Landcare Research, n.d.). Soils with very severe aeration had low SDP, soils with minimal aeration had high SDP. Of the soil classes identified within Southland, Gley Soils provided a high SDP summary while Brown Soils presented low SDP summaries. This report expressed the importance of different soil reduction zones when predicting redox conditions in surface and groundwater.

To derive a model that predicts subsurface redox status across a region requires a wide range of parameters, which for Close et al (2016) included parameters from geology, land use, topography, and soil. From these categories 10 of the best parameters were selected for discriminating redox states. This includes: QMAP main_rock and sub_rock (the main rock type present and the secondary rock type(s) present (Westerhoff, Tschritter, & Rawlinson, 2019)), geological formation age, land use, NZ soil order, NZ soil drainage class, minimum soil carbon status, maximum soil carbon status, elevation, and slope. Close et al (2016) at regional scale, covering Canterbury and Waikato regions, shows that the environments in the Canterbury region, which were formed on alluvial gravels deposited by several large flowing rivers, have high hydraulic gradients and high rainfall environments, specifically in the mountains. However, when combined with inert greywacke parent materials this leads to low carbon environments, resulting in oxic conditions. In contrast to the Canterbury region the Waikato region is dominated by volcanic material, reworked by alluvial processes, while particularly in the Hauraki Plains the flat, peaty, and partly swampy land results in predominantly reduced or mixed redox conditions (Close, et al., 2016). The authors concluded that the predicted redox states were consistent with the geological processes identified in the Canterbury and Waikato regions, improving the spatial prediction of reduced groundwater zones, and ultimately improving estimates of denitrification for catchments and regions.

Collins et al (2017) stated that within catchment characteristics soil type, underlying geology and subsurface geochemistry may further affect the transport and transformation of nitrogen along pathways within the subsurface. Rees, Palmer, Palmer, & Singh (2019) stated that glauconite and illite (a clay mineral) can facilitate the reduction of nitrate in the subsurface due to containing structural and exchangeable $Fe2^{+}$.

### 2.3.4. Nutrient Modelling

A discriminant analysis seeks to statistically distinguish between two or more groups of cases with the use of a set of discriminating variables that measure characteristics (Close, et al., 2016). Close et al (2016) utilised linear discriminant analysis (run through SYSTAT 1.3) to analyse redox conditions in the Canterbury and Waikato regions. The same approach was also used, along with utilising SYSTAT,

within the report to predict groundwater redox status in the Southland region by Wilson, Close & Abraham (2016), where the results were entered into a GIS framework to extrapolate the results to each study region within Southland.

Overseer® is a nutrient budget model used to help agricultural management, specifically nutrient management (Selbie, Watkins, Wheeler, & Shepherd, 2013). Collins et al (2017) use Overseer® to obtain spatial nutrient modelling for estimating root-zone nitrogen leaching (leaching from the top 60cm within a soil profile) under different land uses. The data obtained for use within the Overseer® model was obtained from AgriBase. Leachate predictions using the Overseer® model were completed by Carrick, Fraser, Dennis, Knight, & Tabley (2013) to monitor alluvial sediment leachate with results suggesting that further data on historical leaching is needed. The authors make it clear that on-farm leaching measurements are necessary to validate the prediction of models. Overseer® mostly accounts for nutrients within the farm boundary and predicts nutrients from the root zone, however, other influences such as catchment characteristics and surface geochemistry may further affect the transport and transformation of nitrogen (Singh, et al., 2017). They state that Overseer ® does not account for the effects of catchment characteristics (e.g., underlying geology and subsurface geochemistry) within estimations based on transport and transformation of nutrients.

## 2.4. Hydrological Modelling

Early investigations into the relationships between soil systems and hydrology were addressed by Huggett (1975) where the study of flowlines of a topographic body (initiated by the concept that the soil body was a three-dimensional form) influenced infiltration patterns on a slope. Huggett (1975) determined that the greater part of percolating water flows down the hillside within the soil layer as through flow, ultimately contributing to stream flow, and is related to the finding that throughflow is of much greater importance in transmitting rainfall to streams than overland flow. The concept that each horizon of the soil body has its own hydraulic conductivity, depending upon factors including size and arrangement of particles, directed analysis towards identifying zones of convergence and divergence from infiltrating water over an area of land. Ultimately this results in Huggett (1975) stating that topographic concave contours down slope lead to convergent flowline whereas topographic convex contours down slope lead to divergent flow lines (Figure 13). This formed the theory that convex slopes lead to divergent infiltration and concave slopes lead to convergent infiltration, where flow tends to converge into slope hollows and diverge over slope noses.

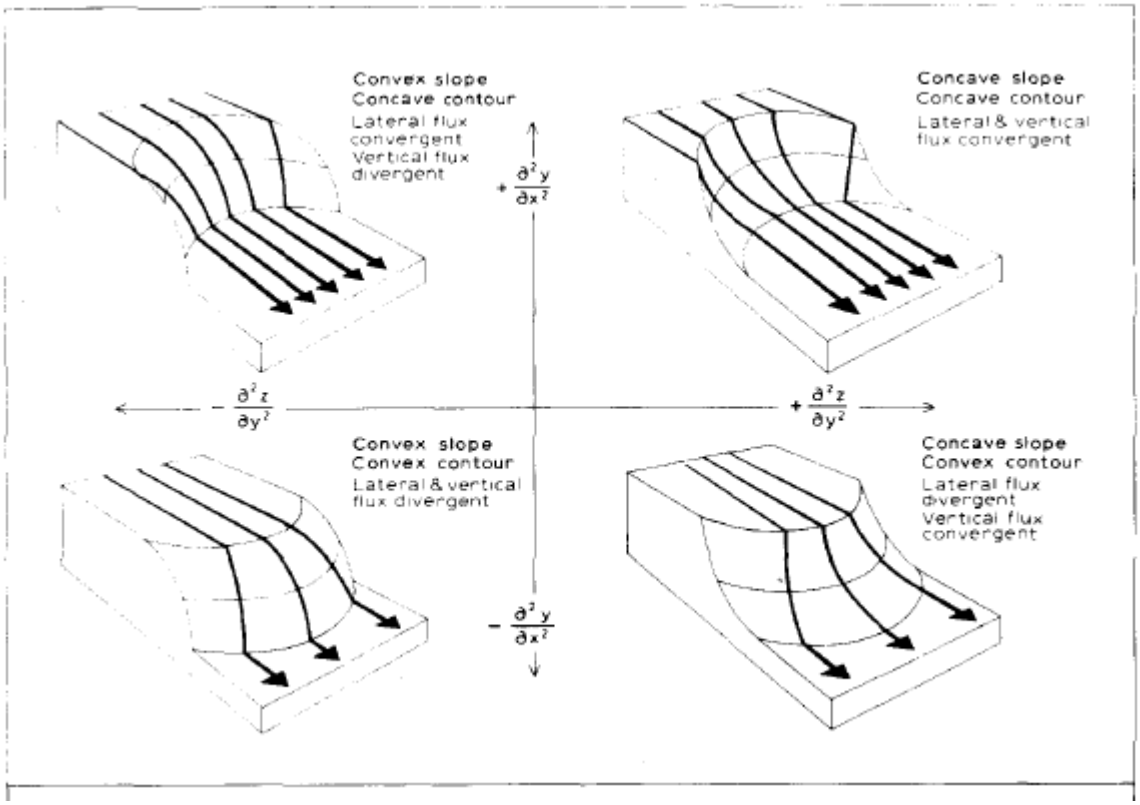


*Figure 13: The fundamental pattern of flow lines arising from various topographic combinations (variations of slope curvature and contour curvature). Retrieved from (Huggett, 1975).*

### 2.4.1 Hillslope Hydraulic Connectivity and Response

Subsurface hillslope-stream connectivity occurs when hillslopes become hydraulically connected to the stream by subsurface flow. The extent and establishment of subsurface connectivity is controlled by physical structure (e.g., soil type, layering and preferential flow path networks), catchment state (antecedent wetness conditions) and driving forces (rainfall and snow melt). Further influences in connectivity include soil and bedrock permeability, surface and subsurface topography, and artificial drains (e.g., pipe and/or mole drains) in agricultural areas and other anthropogenic features. The investigation into hillslope connectivity is completed by studying how, when and where water moves through a hillslope, by measuring either the amount of subsurface flow in trenches, or directly and/or indirectly measuring groundwater levels, or moisture content. However, it is assumed that saturation is an indication of subsurface flow and hill slope connectivity, especially when considering the distributed groundwater level approach (Blume & Van Meerveld, 2014). Mapping and assessment of dominant hydrological processes including connectivity, can be achieved by combining a field-based decision scheme with maps of topography, soil type, geology, and land use according to Blume & Van Meerveld (2014).

Blume & Van Meerveld (2014) stated that inter-site comparisons have been shown to prove useful information on commonalities and differences in the factors that control connectivity. However, different experimental approaches are preferred when studying subsurface connectivity. Numerical simulations and virtual experiments have been assessed for their application in modelling. The authors identified that the advantages of numerical simulations include analysis of hydrological responses that do not require a large number of observations. With numerical simulations, models can be used to interpret and visualize field data and study situations that have not been encountered within the field. Numerical experiments, driven by a collective field intelligence, are described by Blume & Van Meerveld (2014) as being virtual experiments and are a tool used to understand observed phenomena and test hypotheses. Virtual experiments allow for the study of the effects of hillslope characteristics, initial conditions, and input variables particularly on hillslope hydrological responses. They do not fully describe or model a particular system or field site, at the same time they allow for individual study that contain generalizations of findings. One application of virtual experiments is with the combination of hillslope-scale hydrological modelling (Blume & Van Meerveld, 2014).

Blume & Van Meerveld (2014) expressed that implementing connectivity and threshold-dominated response into catchment scale models is not a simple task. However, an example was given utilising TOPMODEL, Vertical Equilibrium Model (VEM), and Catchment Connectivity Model (CCM) all the while presenting advantages and disadvantages. The authors followed this with commenting that models that approach larger scales can be based on a GIS analysis which incorporates dominant runoff generation processes, including subsurface flow process such as macropore flow and interflow. Stieglitz et al (2003) also utilised TOPMODEL, a conceptual rainfall-runoff model that accounts for the impacts of topography, to explore how hydraulic connectivity potentially affects nutrient transport. The export of organic matter and nutrients from the land surface is mostly under the control of hydraulic processes. The authors present simulations that suggest that for much of the year water draining through a catchment is spatially isolated in consequence it is only during storm events that highlands and lowlands are hydrologically connected within a catchment. They also provide preliminary evidence that seasonal timing of hydrologic connectivity may affect a range of ecological processes, which includes downslope nutrient transport, C/N cycling and biological productivity along the toposequence. Stieglitz et al (2003) states that a better understanding of hydraulic connectivity will be necessary for the understanding of local processes as well as material export from land to water at regional and global scales.

Stenger et al (2012) investigated the assimilative capacity of groundwater stating that it is the second major attenuation process at the catchment scale. The dilution of high nitrogen

concentrated waters can occur when mixed with clean groundwater or from water sources such as conservation land or other low nitrogen leaching water sources. Along with dilution, dispersion and diffusion can occur along groundwater flow lines and any location where mixing of water can occur. The authors made it clear that the assimilative capacity of groundwater only reduces the nitrate concentration within the system whereas denitrification reduces the nitrate mass.

Groundwater is a larger component in water storage than what soil moisture is. McMillan & Srinivasan (2015) established that the spatial standard deviation of both soil moisture and groundwater is larger in winter than summer with peaks occurring during rainfall events. The authors identified that aspect and distance from the stream are the most important controls on spatial variability in storage. Modelling, measurement, and predictions for hydrogeology have far reaching implications from the high variability of soil and groundwater. The work of Lana-Renault et al (2014, as cited by (McMillan & Srinivasan, 2015)) illustrates that not only topography but also soil properties and previous agricultural land use influenced a Mediterranean catchment's near surface saturation and transient water table patterns. The topography of the Mediterranean catchment would have had the influence of how water percolate into and through the soil profile (e.g., the location of where water flow lines converged and diverged and whether the topography was in an open or closed drainage system). Soil properties such as clay plans, micro- and macro-pore distribution will have an influential response on the near surface saturation and transient water table patterns. In contrast to this increased saturation near the surface and transient water table patterns can decrease soil strength (which in addition to agricultural land use, such as the use of tillage or the existence of livestock on excessively wet soil causing pugging damage, will increase the loss of porosity and strength within the soil profile), increasing the potential for sediment loss from the system and reducing the storage capability of the soil system. Machinery tillage of the soil profile is a component of agricultural land use that has an influential role in soil hydrology. For example, tillage of soil surfaces aims to increase total porosity by decreasing bulk density, however, the soils below the tilled layer can experience the opposite effect where porosity is destroyed, increasing bulk density from the stresses applied by tillage machinery (Klute, 1982). The authors (McMillan & Srinivasan (2015)) referred to the results from three Nordic catchments that showed a negative relationship between soil moisture content and depth to water table. Ground water recharge variability has been described as another factor controlling groundwater responses. The study of the Langs Gully catchment by McMillan & Srinivasan (2015) analysed soil moisture variability and groundwater in a head catchment. Results showed seasonal variability, in particular winter wet up, has been shown to be a critical event in terms of flow prediction and spatial variation, showing the complexity of winter wet up due to different hill slope aspects having different responses. Strong

seasonal cycles in catchment wetness are characteristics for temporal variability with cycling being driven by potential evapotranspiration rather than rainfall depth.

### 2.4.2. Hydraulic Conductivity

Hydraulic conductivity is a fundamental property used to determine groundwater flow and contaminant transport (Rees C. , Palmer, Palmer, & Singh, 2020). Air permeameter usage to estimate in situ $K_s$ (saturated hydraulic conductivity) was completed, giving the results that individual hydrostratigraphic units have variations in permeability and hydraulic conductivity. These variations are identified due to changes in grain size, porosity, fabric, and level of cementation. Rees, Palmer, Palmer & Singh (2020) stated that creating high permeability zones that promote horizontal subsurface flow in a down dip direction, is due to bedding plane orientation influencing hydraulic attributes. This study shows that lithologies with coarser grain sizes have higher $K_s$ while finer grain sizes have a smaller $K_s$ as expected, but sorting is also very important. Poorly sorted sediments having lower $K_s$, compared to soils with well sorted lithologies that have higher $K_s$. 18 subsoils from across New Zealand were analysed for hydraulic conductivity by Gradwell (1979) with results of downward water movement after initial drainage varying between negligible to appreciable depending on the hydraulic conductivity of soils. Soils with the greatest conductivities were described as soils with low density from volcanic ash or soils on loess being well drained; in contrast soils with low hydraulic conductivities have heavy sticky clays or dense fragipans that usually permit only a slow water flow when wet (Gradwell, 1979).

Hydraulic conductivity was measured using a falling head permeameter for different samples taken from the Porewa Stream catchment in the lower North Island of New Zealand by Rees, Palmer, Palmer, & Singh (2019). The results from the hydraulic conductivity analysis were used as a component to determine aquifers and aquitards, along with porosity, grainsize and bulk density where values were given to each geological unit. The completion of a hydrostratigraphic map highlighted two important factors that influenced the hydraulic properties of the lithologies of the Porewa Stream catchment (Rees C. , Palmer, Palmer, & Singh, 2019). The two factors were the age of sedimentary units and differences in depositional setting within the hydrostratigraphic units. The evidence presented in this study establishes the information presented within Rees, Palmer, Palmer, & Singh (2020) showing the variations in $K_s$ amongst different lithologies. Along with the variations in grain size being an important influence on hydraulic conductivity Rees, Palmer, Palmer, & Singh (2019) has stated that grain size follows the fine tail fraction in importance. One example shows that a lithology with moderate to high fine content, with a larger grain size, has a lower hydraulic conductivity compared to a differing lithology with a smaller grain size. Rees, Palmer, Palmer, &

Singh (2019) found that the difference in hydraulic conductivity could be attributed to the different measures of fines which act to fill the spaces between pores, but sorting is also shown from this to be another important factor. The presence of several springs within the study area were related to paleo-channels and it is suggested that the paleo channels contain coarse gravels with high hydraulic conductivity and is likely to be the pathways for water with high nitrogen content that has not been denitrified. This results in the funnelling of shallow groundwater along flow paths of least resistance in the landscape (Rees C. , Palmer, Palmer, & Singh, 2019).

The drainage characteristic of a soil profile is one of the key properties ultimately determining land suitability for agricultural production, water infiltration and movement, and transport of nutrients and contaminants. Vogeler, Carrick, Cichota, & Lilburne (2019) stated that drainage conditions are determined by observations of water tables, soil wetness, landscape position and soil morphology. It is reported that in New Zealand poorly drained soils are estimated to have annual periods of three to six months wetter than field capacity in contrast to one to two months for soils with imperfect drainage. Vogeler, Carrick, Cichota, & Lilburne (2019) used the two-domain model SWIM3 for hydraulic conductivity as part of the simulator model APSIM (Agricultural Productions System sIMulator). This experimental study was completed on a poorly drained soil in the Otago region and the results emphasized the value that inverse modelling can have for the determination of the soil hydraulic conductivity, particularly for slowly permeable subsoil horizons. It was recommended for the upscaling of hydraulic properties to larger areas, that small-scale core measurements with inverse modelling be used for identifying likely ranges of hydraulic values (Vogeler, Carrick, Cichota, & Lilburne, 2019). For slowly permeable horizons the unsaturated conductivity function was highlighted as of critical importance for modelling soil hydraulic behaviour and that hydraulic conductivity on its own is not sufficient as an input parameter when representing a bimodal pore system. However, hydraulic conductivity at field capacity ($K_{FC}$) has been concluded to have a significant influence on modelling hydraulic behaviour. Therefore, the authors recommended that $K_{FC}$ should not be set as a constant value for slowly permeable horizons. A further recommendation that soil information systems such as S-map provide the values for $K_{FC}$ alongside hydraulic conductivity at saturation.

Further analysis into not only the sources but also flow pathways and the direction of leached nitrogen and transport mechanisms of nitrogen flow to receiving waterways was addressed by Collins et al (2017). To assess groundwater flow directions, a piezometric survey of existing bores was completed, where groundwater heights of the bores were measured, analysed, and then presented in a visualisation using Surfer® version 13. Interactions between groundwater and rivers were measured through a series of river flow gauging's using the SonTek River Surveyor® m9. The

results presented by Collins et al (2017) showed that depending on the direction of groundwater flow and river interactions, leached nitrogen from root zones, could resurface at sensitive receiving surface waters. Within this study it shows that groundwater level contours for shallow strata show a clear groundwater flow component towards the river in the lower Rangitikei catchment. The river flow gauging survey revealed a dynamic relationship between the Rangitikei River and the aquifer beneath it. Other results from the river flow gauging surveys show that the river loses water to groundwater (groundwater recharge) and that most groundwater discharge occurs near Bulls which coincides with the gradient lines for the shallow groundwater flow.

### 2.4.3. Statistical Hydrological Modelling

Rivas et al (2017) utilises Principal Component Analysis (PCA), a multivariate statistical tool, to identify the main processes responsible for the hydrochemistry in groundwater for the Manawatu Catchment area. The study of major constituents and the ratios in groundwaters enables different water type identification (Zarour, 2018). Groundwater constituents are classified based on 4 classes ranging from major (1-1,000 mg/L) to trace (<0.001 mg/L). Groundwater quality parameters used by Horizons are assessed based on 7 classes which include physiochemical field measurements, major cations, major anions, nutrients, bacterial contamination indicator etc. Twenty-six chemical and physical parameters were measured for 56 groundwater samples. Results showed there were five different types of groundwater across the study area with there being no clear evidence of influence of depth on ground water types especially for shallower wells (Rivas, et al., 2017). Various reviews of previously used hydrogeochemical assessments were completed by Zarour (2018) highlighting the currently preferred method; geographical methods – ion ratios and hydrogeochemical facies plots. They described the evolution of Piper and Durov diagrams, resulting in the evolved Durov plot. Main characteristics and interpretations of the groundwater facies (groundwater types) in the lower Manawatu catchment were summarised using the Expanded Durov Diagram.

### 2.4.4. Ground Penetrating Radar (GPR) and Electromagnetic Induction (EMI) Use in Hydrological Modelling

Ground penetrating radar (GPR) and electromagnetic induction (EMI) have been most widely used in soil surveys (Chapter 2.2.1.5), however, these two methods differ in the physical properties they measure. GPR measures soil dielectric permittivity, EMI detects changes in soil electrical conductivity (Zajícová & Chuman, 2019). The principal factors that influence the conductivity of soils are the moisture content, the amount and type of salts in solution, and the amount and type of clays present. Moisture content is shown to be the primary determiner of conductivity (Doolittle, 1987). Zajícová & Chuman (2019) state that soil moisture estimation is the most frequently used application

of GPR. Weihermüller, Huisman, Lambot, Herbst, & Vereecken (2007) used two GPR techniques to estimate the shallow soil water content at the field scale. The aim of this study was to test the applicability of the ground wave method and the off-ground inverse modelling approach at the field scale for a soil with a silt loam texture. The authors state that due to the strong attenuation of the GPR signal related to the silt loam texture at the test site the results for the ground wave technique were difficult to interpret. As a result of this they state that laboratory experiments should be conducted, and the results should be implemented into modelling approaches. Weihermüller, Huisman, Lambot, Herbst, & Vereecken (2007) commented that remote sensing provides an effective methodology for mapping soil water content over large areas, however, the disadvantage of most remote sensing techniques is the low temporal resolution and masks the underlying heterogeneity observed at the land surface. They highlighted that the even more important disadvantage of remote sensing is the shallow measurement depth and the inability to observe the soil water content when dense vegetation is present. The surveying of soil water content especially of the shallow upper layer is relevant for flood control, soil erosion protection, $CO_2$ production and plant water availability (Weihermüller, Huisman, Lambot, Herbst, & Vereecken, 2007).

Sherlock & McDonnell (2003) utilised two EMI meters, EM31 and EM38, to establish a relationship between apparent and predicted water-table depth (ɗ) and volumetric soil moisture content (θ). Apparent ɗ was obtained through established shallow piezometer clusters at the time of each EMI survey. Spatially distributed apparent θ was obtained through a network of tensiometer nests, while field-determined moisture-release curves from measurements of matric potential (ɦ) were also used to obtain θ. The results presented by the authors showed that a very strong relationship was found between the EM31 $EC_v$ (vertical orientation) and $EC_h$ (horizontal orientation) measurements and ɗ with EM31 $EC_v$ being used to predict ɗ with a slightly greater certainty than $EC_h$. The same results were found for EM38 data. The results presented showed a shift in linear regression trend lines over time, which can be accounted for the differences between survey dates, increasing accuracy of predictions can be achieved by repeat surveys. The authors stated that the results indicated that the EM31 and EM38 meters are potentially useful tools for the mapping of ɗ and θ and in-spite of bedrock depth variability and the relatively contaminated hillslope (by solute concentrations found surrounding environments), strong relations emerged between EM31 EC measurements and ɗ, and EM38 EC measurements and θ. Sherlock and McDonnell (2003) addresses areas of future research which discusses the development of an instrument capable of logging several EMI frequencies simultaneously, which may reveal subsurface properties that have not been identified by a single-frequency instrument.

# Chapter 3 – Study Area

New Zealand is a narrow mountainous country located on the continental plate of Zealandia in the Southern Hemisphere, along the 40$^{th}$ parallel south and along the 175$^{th}$ line of longitude. It is the nearest body of land to Australia by some 1600 km (Chappell, 2015). The New Zealand continent (Zealandia) extends over a large area (~2,000,000 km$^2$) with the majority of this being submerged (Sutherland, 1999). New Zealand is astride the Indo-Australian and the Pacific plates, constructing a complex tectonic setting. Subduction of the Pacific plate beneath the Indo-Australian plate occurs at the Hikurangi trough and Kermadec trench, the opposite setting can be seen in the South Island where the Australian Plate is subducting below the Indo-Australian plate. The transformation from the Pacific plate subducting under the Indo-Australian to the Indo-Australian subducting under the Pacific is connected and transformed by a dextral strike-slip fault extending throughout most of the South Island (Figure 14) (Ristau, 2008). Early Palaeozoic terranes of the Western Province and Late Palaeozoic-Mesozoic Eastern province terranes are separated by a suite of Carboniferous-Cretaceous arc-related igneous rocks (MTZ – Median Tectonic Zone) and is the basement geology of New Zealand (Sutherland, 1999). The subduction zone between the Indo-Australian and the Pacific plate is where convergence formed the axial ranges between the Taupo Volcanic Zone (TVZ) and the Wanganui Basin (WB) (Rees C. , Palmer, Palmer, & Singh, 2020).

The WB is a partially inverted, late Miocene-Quaternary marine basin that forms a portion of the western lower North Island (Rees, Palmer, & Palmer, 2020). Uplift of 0.3-0.5m ka$^{-1}$ and 1-3m ka$^{-1}$ of the WB occur in the locations of the modern coastline and adjacent to the axial ranges, respectively. In relation with tectonic activity, downcutting in the Late Quaternary has resulted in exposures of gently dipping marine successions within deeply incised northeast-southwest oriented river valleys (Rees, Palmer, & Palmer, 2020). Regional tilting of Neogene strata in the WB is considered to be a response to southward migration of the depocenter and coeval uplift towards the north. The northern and eastern margins of the basin are now uplifted, and marine strata are gently dipping at 2-15$^o$ (Naish & Kamp, 1995). The field of study for this thesis is located off of SH1 outside of Hunterville in the Rangitikei region. Naish & Kamp (1995) completed a study of the WB that covers the Rangitikei region and their studies identified that between Mangaweka and Vinegar Hill, a ~1100 m thick, southward dipping (4-9$^o$), late Pliocene (2.6-1.7Ma) marine cyclothemic succession is spectacularly exposed in the cliff of the Rangitikei River. The WB succession contains numerous cycles, where each cycle is represented by a couplet consisting of a coarse-grained, conglomeratic to heterolithic transgressive system tract and a fine-grained siltstone to sandy mudstone highstand system tract (Rees C. , Palmer, Palmer, & Singh, 2020). Naish & Kamp (1995) identified 20 sedimentary cycles or cyclotherms within the succession. The authors observed that each of the 20

cycles contain coarse grained (sandstone and coquina) and fine-grained (siltstone) units. Diagnostic molluscan and foraminiferal fauna are situated within the fine-grained lithologies. This establishes that deposition is predominantly mid-shelf environment (~50-100m water depth), whereas it is indicated that coarse-grained lithologies accumulated in a range of nearshore-inner shelf environments (~0-50m water depths). Of these 20 cycles identified, 19 of these cycles are reassigned to the Rangitikei group, with six new formations being defined within the Rangitikei group and their distribution within the Ohingaiti region are presented within the study completed by Naish and Kamp (1995). The findings by Naish and Kamp (1995) were present in a new 1:50,000 geological map. New detailed stratigraphic logs are presented for the Rangitikei River section and a 200m deep stratigraphic drill hole site in the Simpsons Reserve is also presented. The work by Naish & Kamp (1995) was reflected in the work completed by Rees (2020) who created a 1:25,000 geological map with composite stratigraphic log, covering the Hunterville study area of this thesis (Figure 16). Naish & Kamp (1995) and Rees (2020) both identified within the Rangitikei district, more specifically within the research field for this thesis, the following geological formations: Orangipongo formation (Or), of Early Pleistocene age and Mangaonoho formation (Mo), of Marahauan age – including the Mangamako Shellbed (Mm) of Marahauan age (Figure 38) (Naish & Kamp, 1995).

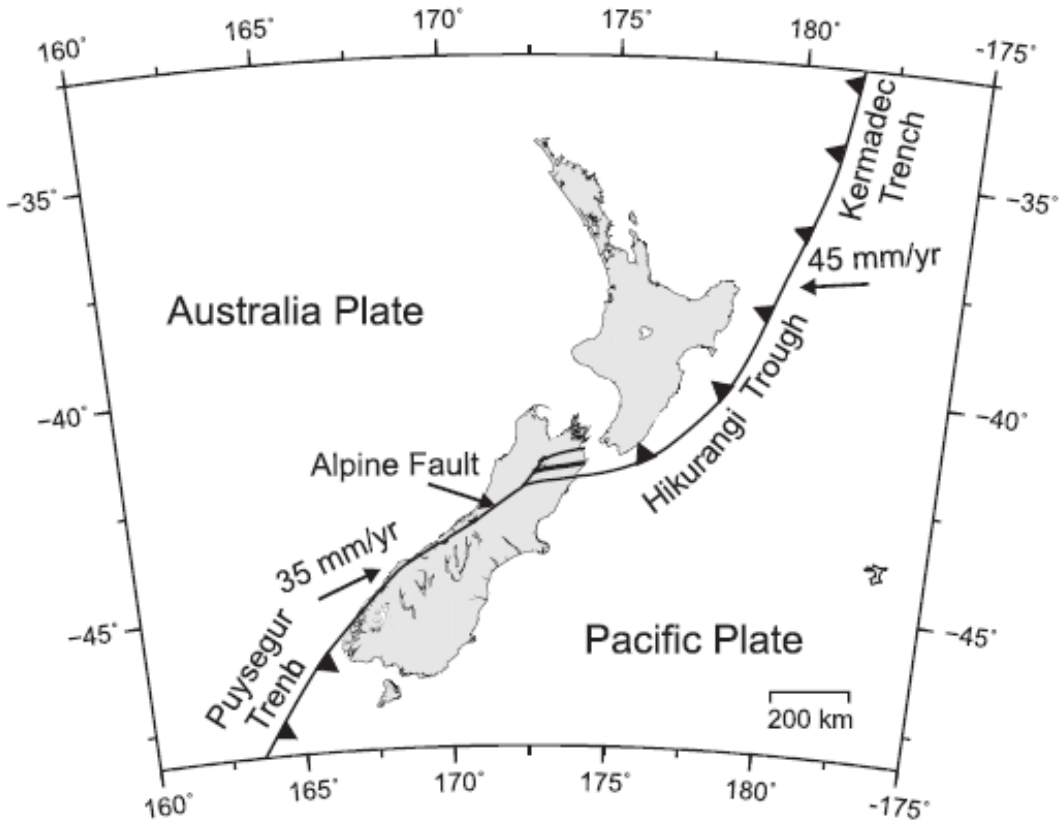


*Figure 14: An overview of the tectonic setting within New Zealand, adapted from (Ristau, 2008).*

**Orangipongo Formation (Or)**

The Orangipongo Formation (Or) is a formation established by Naish & Kamp (1995) that is applied to all cyclothemic strata between the base of the Ohingaiti Sand and the base of the Managamako Shellbed. This formation is 170m thick and is dated to be of the Nukumaruan age (2.08 – 1.63 Ma (Abbott, Naish, Carter, & Pillans, 2005)) within the Early Pleistocene epoch (Figure 15). The Or cyclothemic strata comprises of 7 lithologically similar siliciclastic sandstone members, 5 lithologically similar siliciclastic siltstone members, 5 coquina shellbed members and a tephra member (Naish & Kamp, 1995) (Figure 16). The Ohingaiti Ash member is a 1.5m thick grey, rhyolitic tephra located approximately 90m above the base of the Ohingaiti Sand. The tephra is moderately lithified, bioturbated horizontally bedded, glassy, and reworked, volcaniclastic silty fine sand (from the 4$^{th}$ siliciclastic sandstone member) (Naish & Kamp, 1995). The upper half of the tephra includes a significant amalgamation of terrigenous silty fine sand of sedimentary origin along with inner shelf benthic forminifera (Naish T. , et al., 1996). The tephra layer sharply overlies bioturbated grey siliciclastic sandy siltstone and passes gradationally upsection into brownish-grey thick bedded siliclastic silty fine sandstone (Naish & Kamp, 1995; Naish T. , et al., 1996). The depositional environment show that the siliciclastic sandstone members were deposited in transitional inner shelf to shoreface environments; the coquina members that accumulated during transgression are attributed a shoreface to shelfal depositional environment; the siltstone members accumulated during episodes of sea-level highstand aggradation and show an upsection-shoaling from mid to inner shelf depositional environment (Naish & Kamp, 1995). The sedimentary structures and foraminiferal faunas of the lithofacies enclosing the tephra indicates an accumulation on the inner shelf in water depths <50m. Further evidence implies a paleoshelfal setting in water depths shallower than the contemporary storm wave base (Naish T. , et al., 1996).

**Mangaonoho Formation (Mo)**

The Mangaonoho Formation (Mo) is a formation established by Naish & Kamp (1995) that is applied to all strata between the base of the Mangamako shellbed and a prominent fossiliferous sandstone member that marks the base of the Vinegar Hill Formation. This formation is calculated to be 135m thick and is dated to be of the Marahauan age (a substage of the Nukumaruan stage (Boreham, 1963) – Figure 15). The Mo formation is lithologically similar to that of the Or formation with similar cyclic signatures and is comprised of a shellbed member (the Mangamako Shellbed), 2 coquina members, 2 siliciclastic sandstone members and 4 siliciclastic siltstone members (Figure 16). The depositional environment for all 4 coquina members represents stratigraphic condensation during a period of marine transgression, while shallow-water foreshore-shoreface fauna is present within the

lower part of coquina member 4 and fauna preserved in coquina member 2 and 3 are similar to many older coquina members which show an open marine shelf deposition environment; the siltstone members shelfal deposition is indicated by the presence of molluscan fauna; the sandstone members are indicating as being accumulated in transitional inner shelf to shoreface environments (Naish & Kamp, 1995). The Mangamako Shellbed depositional environment will be discussed within the section on the Mangamako Shellbed.

**Mangamako Shellbed (Mm)**

The Mangamako Shellbed member (Mm), coquina member 1 and sandstone member 1 (Figure 16), is approximately 15m thick and comprised of a lower 1m thick siliciclastic fine sandy silt supported shellbed, which unconformably overlies the Orangipongo formation. This member is a part of the Mo formation that is aged to be within the Marahauan period. The upper section is a densely packed, reworked (at the base), trough cross-stratified, pebbly shell conglomerate that is scoured into underlying mollusc-rich silty sands. A siliciclastic fine sandstone supports abundant in-situ or near-situ molluscan fauna and passes upwards into less fossiliferous, horizontally bedded sandy siltstone within the upper portion of the shellbed. Truncation at an incredibly low angle of the underlying beds in this section is the mark of the lower contact. Ophiomorphic burrows penetrate prominent sharp discontinuities within the upper half of the coquina member (Naish & Kamp, 1995). A 20cm thick reworked megascopic tephra was observed within this shellbed member in a drill core from Simpsons Reserve, however, the tephra does not appear to be present at the sampling location presented in the paper by Naish & Kamp (1995). The depositional environment is interpreted to be within the shore-connected sand prism in a position further shoreward than older coquina members.

| ERA | PERIOD | TIME million years | NZ SERIES | NZ STAGE | SUB STAGE | SYMBOL | EPOCH |
|---|---|---|---|---|---|---|---|
| | QUATERNARY | 0.00117 | HAWERA | | Aranuaian | Quor | HOLOCENE |
| | | 0.128 | | | Otiran | Quti | PLEISTOCENE |
| | | 0.25 | | Haweran | Oturian | Qutu | |
| | | 0.34 | WHANGANUI | Castlecliffian | Putikian | Wu Wc | |
| | | 0.78 | | | Okehuan | Wk | |
| | | 1.63 | | Nukumaruan | Marahauan | Wa Wn | |
| | | 2.4 | | | Hautawan | Wh | |
| | | 2.58 | | Mangapanian | | Wm | PLIOCENE |
| | | 3.00 | | Waipipian | | Wp | |
| | | 3.70 | | | | | |

*Figure 15: Geological time scale including New Zealand series and stages. Adapted from (Ballance, 2009)*

**Upper Kakariki (Q1k1) and Lower Kakariki (Q1k2) Terrace Deposits**

The Kakariki deposits are deposits related to the Kakariki river terraces (Milne, 1972), with Kakariki Terrace 1 being the upper Kakariki Terrace which floods every 20-30 years while Kakariki Terrace 2 is the lower Kakariki Terrace which floods every year and is the lowest degradation surface closest to the river (Palmer, 2023). These deposits are some of the youngest identified on Ngatiapa due to the frequency new material is added to the deposits (Figure 16). Clement & Fuller (2007) have shown that 7 different terrace groups have been identified within the Rangitikei, with the youngest terrace group, 12ka to present, including the Kakariki terraces. Aggradation gravels, forming river terraces, are seen within the region in outcrops near Mt Curl, Manawatu-Whanganui, with the Kakariki conglomerate closely resembling these gravels (Palmer, Begg, Townsend, & Wilson, 2006). Both terrace deposits have been identified on Ngatiapa within the north-west reach of the study area, on the closest reaches to the Porewa stream.

**Swamp Deposits (Q1a)**

Swamp deposits are comprised of silt and clay sediments with vegetation matter deposited in environments that have extensive saturation or filled with water (National Geographic Society, 2022). The swamp deposits identified on this farm are primarily located in valley depressions and areas of low relief. Material eroded from the surrounding slopes transported to these depressions, zones of extended saturation or filled with water for an extended period of time, resulted in the formation of these swamp deposits. These deposits are also some of the youngest deposits identified on Ngatiapa (Figure 16)

**Undifferentiated Quaternary Landslides (UQl)**

Various quaternary landslides have occurred within the landscape, that overtime have become indistinguishable within deposit environments. These deposits are classified as one unit due to the indistinguishability of individual landslide units within the landscape. These deposits have formed within recent times and are therefore identified with the above deposits as being some of the youngest on Ngatiapa (Figure 16)

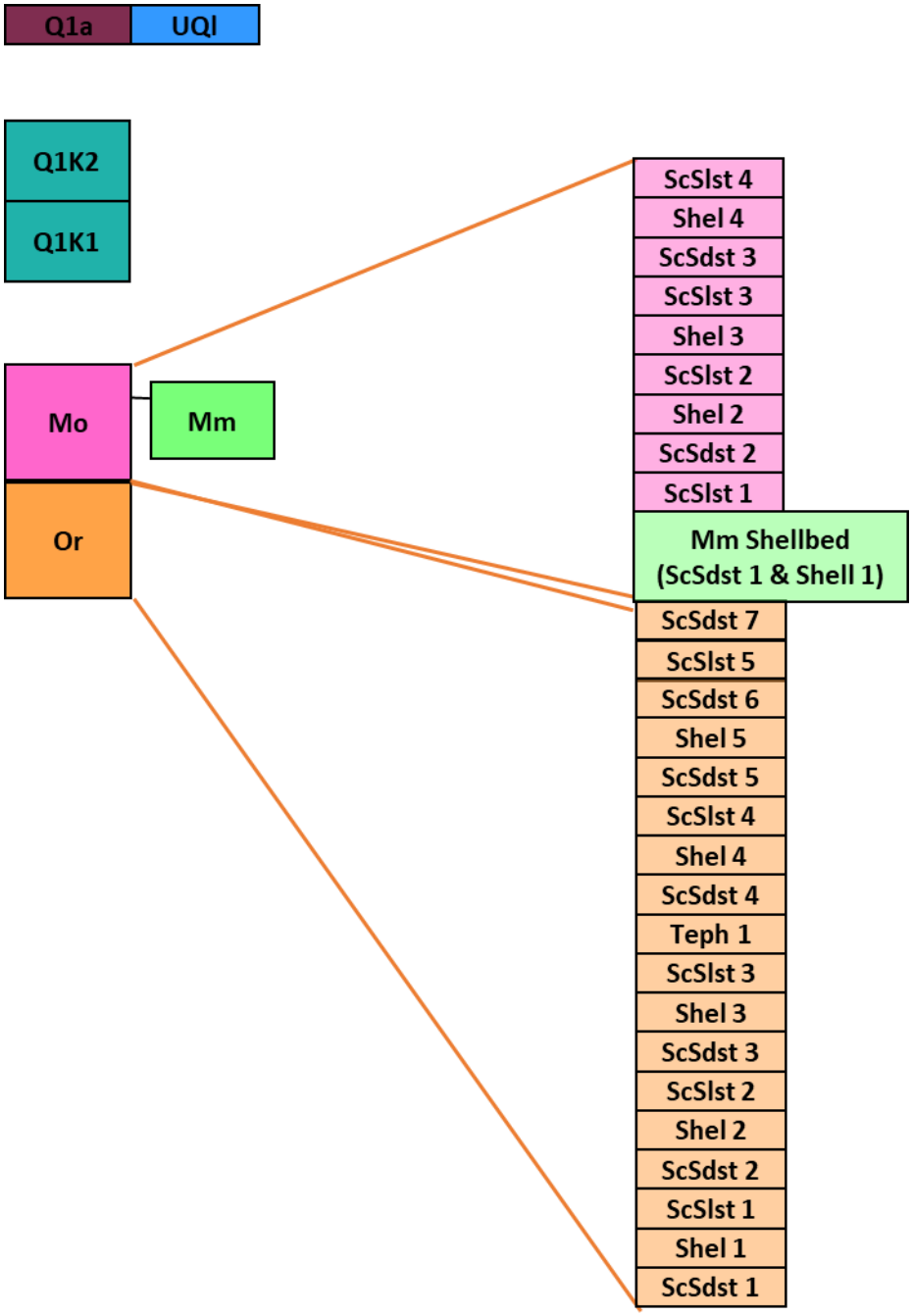


*Figure 16: Stratigraphic log of the geology located on Ngatiapa. ScSlst = Siliciclastic siltstone member; ScSdst = Siliciclastic sandstone member; Shel = shellbed/coquina member; Teph = Tephra member. Stratigraphic log not to scale. Adapted from (Naish & Kamp, 1995; Rees, 2020).*

The Manawatu-Wanganui (M-W) region is located within the North Island of New Zealand with three main catchments; the Wanganui, Manawatu, and Rangitikei catchments (Figure 17) (Basher, et al., 2020).

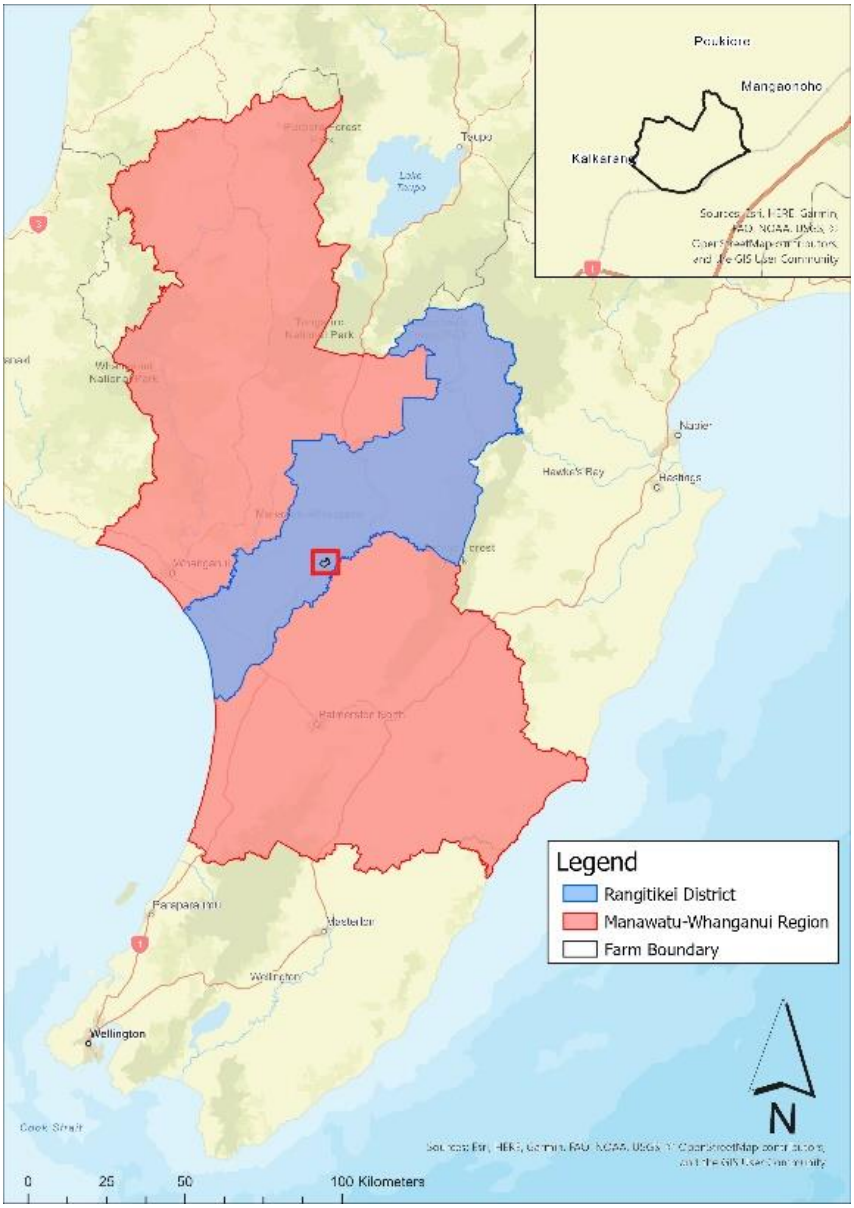


*Figure 17: The Manawatu-Wanganui (Red) region location within New Zealand in conjunction with the Rangitikei (Blue) district identification within the Manawatu-Wanganui. The inset shows the location of Ngatiapa (the study farm).*

Steep hill country and hilly steep lands within the M-W region (subdued to steep slopes (20 – 40°), with a dominant south-southwest aspect (Rees, Palmer, & Palmer, 2020)) comprises 58% of the region with erodible Tertiary-aged soft sandstone, siltstone and mudstone underlying the region (Basher, et al., 2020). Slope morphology of the Cenozoic sedimentary rock of the WB is varied including concave, convex, and rectilinear profiles, with ridges being narrow, sharp, and fluted. The

Rangitikei landscape particularly ridges, ledge, slopes, and waterfalls reflect the changes in the WB fill (Rees, Palmer, & Palmer, 2020).

The Rangitikei catchment dominates 18% (approximately 3887 $km^2$ (Singh, et al., 2017)) of the approximate 22,000 $km^2$ of the M-W Region and is fringed by Mesozoic greywacke-argillite rock of the Kaimanawa mountains and the Ruahine Ranges (Rees, Palmer, & Palmer, 2020). The primary rock types that dominate the Rangitikei catchment are sandstone, limestone, gravel, and mudstone; covering 32, 23, 22 and 12% respectively (Singh, et al., 2017). The lower Rangitikei, on the west coast, consist of two primary landscapes: sand country, and river flats and terraces (Collins, et al., 2017).

The soils of the lower Rangitikei region have developed into two primary landscapes; soils of the sand country and the soils of the river flats and terraces (Collins, et al., 2017). Reworked material brought down by rivers and reworked from sand dunes during times of floods form the soils of river flats. Old sediments that are sufficiently above river level to be relieved from flooding and the accumulation of fresh material form the soils of terraces. River terrace soils frequently have additions of loess, with layers being thicker on the east coast and thinning out towards the west (Collins, et al., 2017). Te Punga 1952 (as cited in (Rees C. , Palmer, Palmer, & Singh, 2019)) recognised seven episodes of terrace formation within the Rangitikei. Milne 1973 (as cited in (Rees C. , Palmer, Palmer, & Singh, 2019)) mapped aggregation and degradational terraces within the Rangitikei and recognised nine major terrace sets (Table 1).

| **TERRACE** | **AGE** |
|---|---|
| OHAKEA | 10 – 30 ka |
| RATA | 30 – 50 ka |
| POREWA | 70 – 80 ka |
| CLIFF | 90 – 100 ka |
| GREATFORD | 110 – 120 ka |
| MARTON | 140 – 170 ka |
| BURNAND | 250 – 280 ka |
| ALDWORTH | 350 – 350 ka |
| WAITUNA | 360 – 370 ka |

*Table 1:Major aggregation terraces in the Rangitikei. Retrieved from (Rees C. , Palmer, Palmer, & Singh, 2019).*

Pre-Māori New Zealand was a forested country with vegetation development up until the 14th century, in complete isolation without human presence and more significantly without grazing and browsing animals (Cumberland, 1941). Before the 19th century the forest, in large parts, had been

replaced by extensive communities of manuka (*Leptospermum scoparium*), bracken fern (*Pteridium esculentum*), and tussock steppe. North Island bush, including the inner Wanganui area, was mixed podocarp-dicotyledonous forest (including certain podocarps, rimu, totara, matai, miro, kahikatea, tawa, kamahi, and rata), while areas of high altitude, including the Ruahines, consisted of one or more species of *Nothofagus*. *Vegetation* at the time of European settlement in the Manawatu was comprised of scrub, fern, forest, and swamp communities, with most of this vegetation since being cleared for the sowing of pasture (Cowie & Rijkse, 1977). Cumberland (1941) addressed the comments made by Cowie & Rijkse (1977) first by discussing the change in vegetation within the Manawatu following European settlement. He states the transformation of a forest-clad New Zealand to a pastoral-biased New Zealand occurred in five clearly defined periods of cultural activity, characterised by European occupancy. Cumberland (1941) identified that there was a subtle change-over from sheep farming and 'extensive' wheat production to the development of a new industry, dairying. This leading to further modifications in vegetation cover and to a further increase in the already large acreage of cultural vegetation. More specifically in the Manawatu swamps and swamp forests suffered a similar fate as the rest of the past vegetation; subsequetly swamps and swamp forests were cleared, drained, consolidated and reclaimed for dairying. Simpsons scenic reserve in Hunterville is an example of what the past vegetation of the region was like and is open to the public. Human malpractice, misuse, or inattention in the 1940s initiated grassland deteriorated with evidence of sheet and slip erosion being present, specifically in the Wanganui area where slip-scarred slopes occur with silt and stump-strewn thalwegs; the remaining thin soils are being covered with manuka, ferns and second growth (Cumberland, 1941). As of 2018 forest, shrubland, and grassland dominated the Rangitikei district with 19%, 11% and 67% respectively and cropland occupying 1% of landcover (Table 2) (LAWA - Land Air Water Aotearoa, n.d.). Major land use of the Rangitikei region consists chiefly of sheep/beef/dairy at ~50% and non-farming blocks at ~42%. Dairy farming land and arable farming land cover approximately 18,000 and 1,100 ha respectively and is dispersed within the lower parts of the catchment (Horizons Regional Council, 2019; Singh, et al., 2017). Highly erodible land occupies ~7% of the Rangitikei region with 12% of the region being occupied by versatile soils. ~1,800 ha of wetland and ~6,000ha of bush is known to be remaining with the Rangitikei region (Horizons Regional Council, 2019)

Hunterville, located within the Rangitikei District, is a small town halfway between Taupo and Wellington that is the home to Ngatiapa (Figure 17 – inset), a 457-ha sheep and beef farm (70% sheep, 30% cattle), on the hill country off SH 1. Sheep are set for stocking all year round with varying rates depending on the time of the year; cattle are shuffle grazed before sheep to improve

grass grazing levels. Upon the farm superphosphate fertiliser and sulphur fertiliser are applied throughout the year (Lambert R. , 2022).

| Land Cover Class | Area % |
|---|---|
| **Forest** | **19%** |
| Indigenous forest | 16% |
| Exotic forest | 3% |
| **Scrub / Shrubland** | **11%** |
| Indigenous scrub / shrubland | 11% |
| Exotic scrub / shrubland | <1% |
| **Grassland / other herbaceous vegetation** | **67%** |
| Tussock grassland | 11% |
| Exotic grassland | 55% |
| Other herbaceous vegetation | <1% |
| **Cropland** | **1%** |
| Cropping / horticulture | 1% |
| **Urban / bare / lightly-vegetated surfaces** | **1%** |
| Natural bare / lightly vegetated surfaces | 1% |
| Artificial bare surfaces | <1% |
| Urban area | <1% |
| **Water bodies** | **1%** |
| Water bodies | 1% |

*Table 2: Land cover for the Rangitikei District as of 2018. Adapted from (LAWA - Land Air Water Aotearoa, n.d.)*

New Zealand precipitation patterns are influenced strongly by topographic features, which as a result the west side of topographic features receives higher precipitation than the lee side (Tommaso, 2015). The central North Island is sheltered by high country and is consequently less windy than many other parts of New Zealand. Summers are characterised by warm, dry, and settled weather, with winter being cool with generally more unsettled weather. The south-west areas of the North Island are often exposed to wind resulting in weather systems from the Tasman Sea, ensuring in settled, warm weather during the summers and relatively mild but unsettled winters. The eastern North Island, sheltered by the high-country, experiences dry sunny climates with warm settled summers; heavy rainfall can occur from the east or southeast. (Tommaso, 2015).

The Rangitikei region has warm summers (15-22°C) and mild winters (1-10°C) (Figure 18) with a reliable, even distribution of rainfall throughout the year (mean annual rainfall ranges from 800mm near the coast to over 2000mm in the ranges (Horizons Regional Council, 2019)) (Figure 19) (Radcliffe, 1976; Rees C. , Palmer, Palmer, & Singh, 2019) more specifically the Porewa catchment at Tututotara just south of Hunterville recorded 1297.5mm of rainfall over a 12 month period as of November 2022 (LAWA - Land Air Water Aotearoa, 2022) and Poukiore recording an average annual rainfall of 1044mm from January 1995 to April 2020 (Lambert R. , 2022). Evapotranspiration and transpiration follow seasonal patterns and are greater during the summer. Soils not affected by a

high-water table, dry out for two to three months in summer, with soil moisture deficits occurring on average for 10-15 days in January and February and commonly in March and April. Irrigation is used to offset these differences (Cowie & Rijkse, 1977; Rees C. , Palmer, Palmer, & Singh, 2019).
30-50 % of the time the Rangitikei district is exposed to prevailing winds from the west to northwest (Rees C. , Palmer, Palmer, & Singh, 2019). Exposure to the moisture laden westerly winds limits the susceptibility of the M-W to drought. A significant drought during the summer and early autumn of 2012-2013 with the hardest hit areas being within the eastern reaches. This included the Rangitikei district with severe soil moisture deficit periods (more than 130 mm of deficit) being observed (Chappell, 2015).

Major water bodies in the Rangitikei include the Rangitikei River (major river running through Hunterville), Porewa and Hautapu Rivers, Lake Moawhango, and coastal lakes. The study of groundwater quality has found that the predominant type is reducing (Collins, et al., 2017) (Chapter 2), with 31% of bore sites surveyed for groundwater level have declining levels and 19% with increasing water levels. Water use, excluding hydroelectricity, is dominated by agricultural and horticultural uses at 82% of consented water use within the region (Horizons Regional Council, 2019).

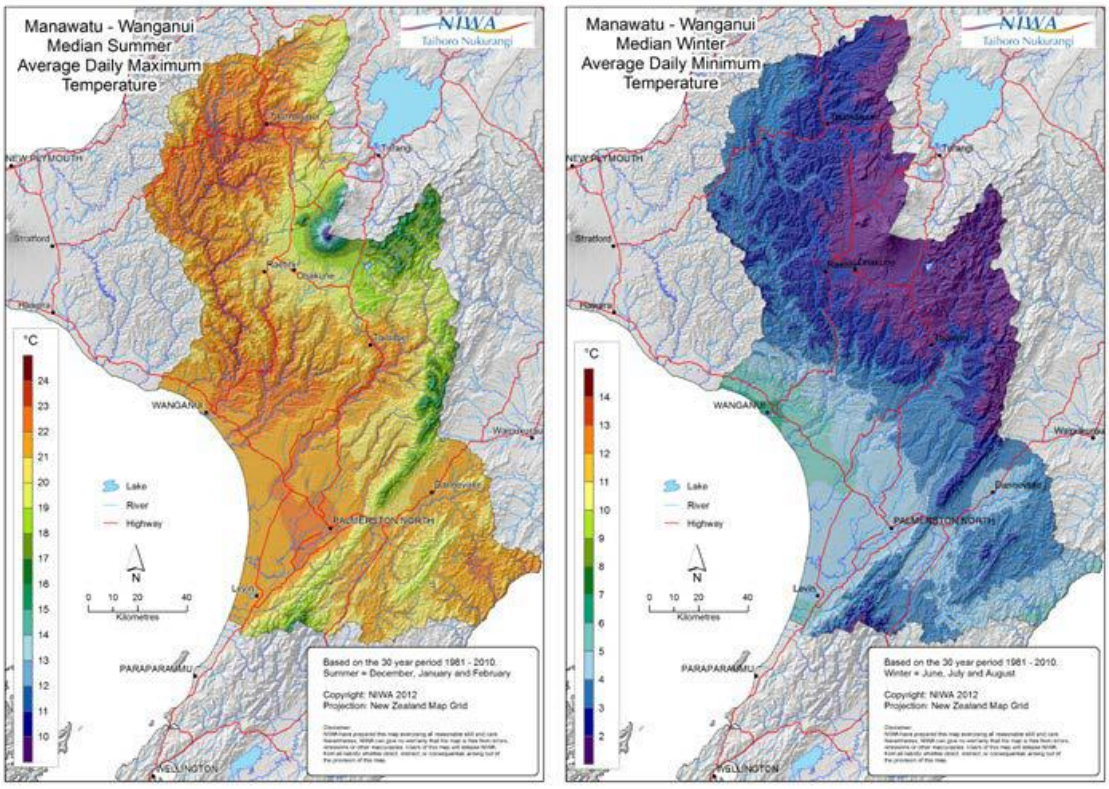


*Figure 18: Manawatu-Wanganui median summer (left) and winter (right) average daily temperatures from 1981-2010. Retrieved from (Chappell, 2015).*

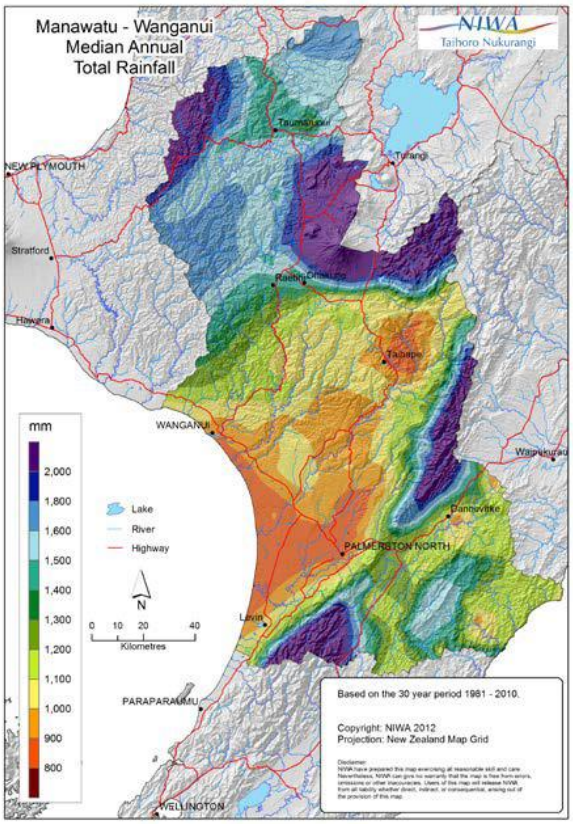


*Figure 19: Manawatu-Wanganui median annual total rainfall from 1981-2010. Retrieved from (Chappell, 2015).*

# Chapter 4 – Methodology

## 4.1. Field study

### *4.1.1. Soil Mapping*

Steepland and hill country terrains are complex systems reflecting the differing variables involved such as climate, geology, soil, slope, vegetation, and morphology. Altitude and aspect of a slope have been shown to be highly influential on many topsoil characteristics, particularly on those likely to be related to soil moisture status, leaching and weathering (McIntosh, Lynn, & Johnstone, 2000). The evolution of landforms and changes to soils and slopes involve gradual, continuous, and sequential adjustments (Gerrard, 1993), increasing the complexity of steepland and hill country and influencing the difficulty of being able to accurately map and represent these landforms and soils. Soil surveying of steepland and hill country does not come with the chance of there being zero bias involved; inaccessibility to locations, involved expenses along with natural geomorphology complexes are examples that increase the chance of bias occurring within surveying. Surveying approaches such as the ones identified within this section by Tonkin (1994) aim to remove the bias that occurs.

The characterisation of soil profiles is pivotal for the understanding of soil properties and processes. Due to the vast variety of rock types making up New Zealand, along with the varied conditions under which the rocks have been transformed into soil, the resulting soil patterns of New Zealand are complex (New Zealand Soil Bureau, 1968). Soil surveying is the process of recognising different soils and the determination of their important characteristics, the classification of defined soil units, and the plotting of their boundaries on soil maps (Tayor & Pohlen, 1962). The approach taken for identifying soil survey profile sites across a landscape was adapted from the method used by Tonkin (1994). Tonkin (1994) noted that soil surveying can be based on either a random approach, grid approach, or stratified observation points approach. The random approach is as it is described, a random distribution, alignment and number of samples taken within a designated search field. The grid approach utilises a grid layout to the survey area with samples being collected at either line transects or within the grid (Figure 20). The selection of a transect or grid approach is dependent on the design requirements of the specific study (Pennock, Yates, & Braidek, 2008). The stratified observation point approach is practical when dealing with a likely catenary gradient within a colluvial filled bedrock hollow or small drainage basin. This approach utilises the natural lie of the landscape and determines positions for sampling based on this. There are two techniques: the six sampling profiles technique; and the 10 sampling profiles technique (Figure 21). These techniques look at the distribution of soil in a potential catena within a sloped landscape and applies the theory that soils along a slope will be different depending on the location e.g., soils on the nose of a slope will be

different from those within the hollow or on the side slope, stemming from the concept of hydrological flow and interconnectedness of groundwater (addressed in chapter 2). The sampling approaches utilised within the surveying of this thesis included both the random and stratified observation points approaches. The combining of the random and stratified observation points (both six and 10 sampling profiles) was the best technique to apply to the landscape of the study farm. When looking at the landscape from an elevated position in the field, to get a comprehension of the landscape, photos were taken that were edited to show the selected location of potential soil sampling sites (Figure 22). The main approach is the stratified sampling approach using the 6 sampling profiles technique. The chosen sample sites across the farm were selected based on their location along the slope face e.g., along a nose, in a hollow at the valley floor, based on the aspect of the slope etc.

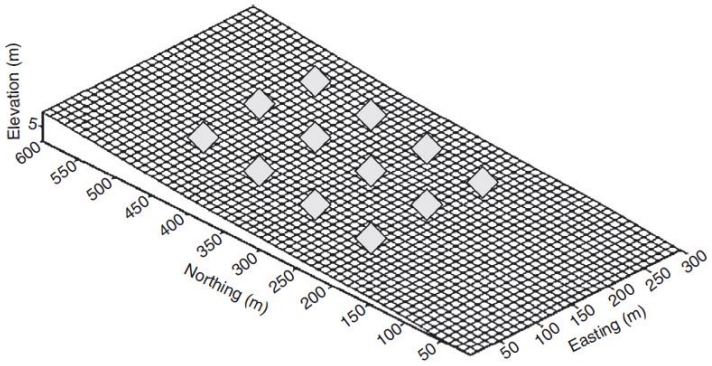


*Figure 20: A simplified example of the application of the grid sampling approach with samples being taken at each diamond point. Retrieved from (Pennock, Yates, & Braidek, 2008).*

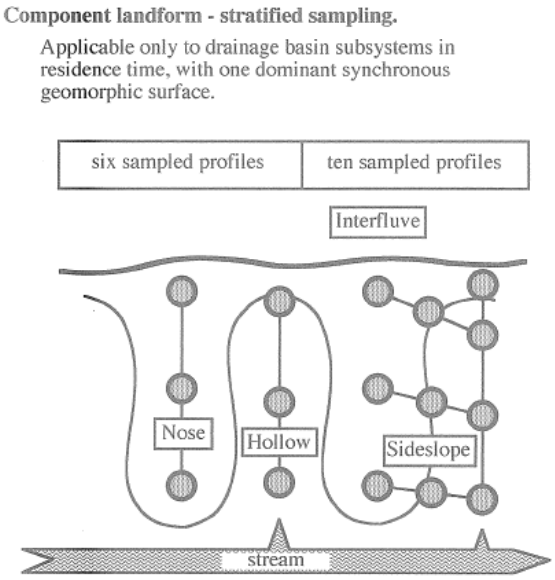


*Figure 21: The six and ten sampling profiles approaches under the stratified sampling approach. This shows the use of the natural landscape for the finding of sampling locations. Retrieved from (Tonkin, 1994).*


*Figure 22: Photos (A and B) from the field showing the application of the stratified sampling and random methods towards soil sampling. Red triangles are potential sampling locations.*

Following the selection of the sampling sites, soil descriptions were collected using the design and details set out by Hodgson (1974) and Milne, Clayden, Singleton & Wilson (1995). Taylor & Pohlen (1962) stated that each kind of soil is a three-dimensional body of which the internal attributes that characterise its profile has certain attributes mostly external that may be regarded as characterising its site. It is at the external characteristics that the soil description process starts. The location (usually measured by GPS point) was recorded along with the parent material, climate, organisms (e.g., cattle, sheep, deer etc), topography (e.g., slope and aspect), vegetation, current land use, drainage, and erosion. The effects of the external attributes of the soil reflect the morphology of the

soil profile seen throughout the vertical sections (horizons) (Tayor & Pohlen, 1962), therefore a detailed description of the soil profile is required. Once the external characteristics of the soil description were taken then the internal characteristics were recorded following the digging of a hole to 1m deep (or 60cm with an auger hole to 1m depth). The identification and naming of soil horizons is the fundamental step in the describing of a soil profile. Massey University utilises the horizon nomenclature adapted from the FAO soil horizon designation system (Food and Agriculture Organization, 2006). Soil profile description variables are described in depth by Hodgson (1974) and Taylor & Pohlen (1962) but they include information on the depth and thickness of horizons, soil colour (describe using the Munsell soil colour chart book (Munsell Color, 2009)), mottling, organisms, stones, roots, soil structure and texture, degree of soil development, consistence and plasticity, strength (McLaren & Cameron, 1996) and boundary description between horizons.

### *4.1.2. Water Sampling*

#### *4.1.2.1 Field Equipment Instillation*

Groundwater sampling methods vary depending on what the study is testing for. In this thesis piezometers were used to measure groundwater levels and help aid in the sampling of groundwater for dissolved nutrient concentrations. Piezometers are primarily stand tubes that are inserted into the saturated zone at or below the water table, with a screened opening at the lower end that allows water filtration into the tube (Bleam, 2016). Six piezometers were created using 28mm internal diameter PVC pipes. Three PVC pipes were cut down from 6m to 3m with each 3m section having holes drilled in the lower 1m. Nylon plugs were inserted into the base of the pipes, with a 25mm PVC pressure end cap, with a hole drilled in it to relieve internal pressure, inserted on the top of the pipe. The lower 1m with the drilled holes was covered with a synthetic mesh to prevent sediment entry into the pipes. The 6 piezometers were installed using a one-piece Dutch auger to dig a hole down to the bedrock, below groundwater level (Figure 23). The piezometers were inserted into the auger holes and back filled using washed fine garden sand up to 150mm from the soil surface (Figure 24), the remaining space was filled with bentonite clay along with a mound around the piezometer at the soil surface (Figure 25). The sand allows for water percolation into the piezometer while the clay prevents surface water percolating down through the soil profile into the groundwater (Figure 27). Before the clay was added around the piezometer installed, the PVC pipes were cut down to an appropriate height (approximately 30cm above ground surface) to prevent damage from livestock. Each cut off was measured to calculate the total length of the piezometer with the height above ground level being used to calculate the height of the piezometer below ground level. Pink spray paint was sprayed onto the piezometer caps for clear identification within the field. Each piezometer set up was allocated a pasture exclusion cage (to protect from cattle) that

was set over the PVC pipe above ground level to further prevent damage from livestock activities (Figure 26). The lengths for the piezometers installed are presented in table 3.

*Figure 23: An auger hole for piezometer instillation using a one-piece Dutch auger.*

*Figure 24: Back filling of an auge hole around the installed piezometer with fine sand around the installed piezometer.*

*Figure 25: Infilling around the installed piezometer with bentonite clay around the top section of piezometer at surface level.*

*Figure 26: The instillation of a pasture exclusion cage around a piezometer (piezometer sprayed pink for identification within the field).*

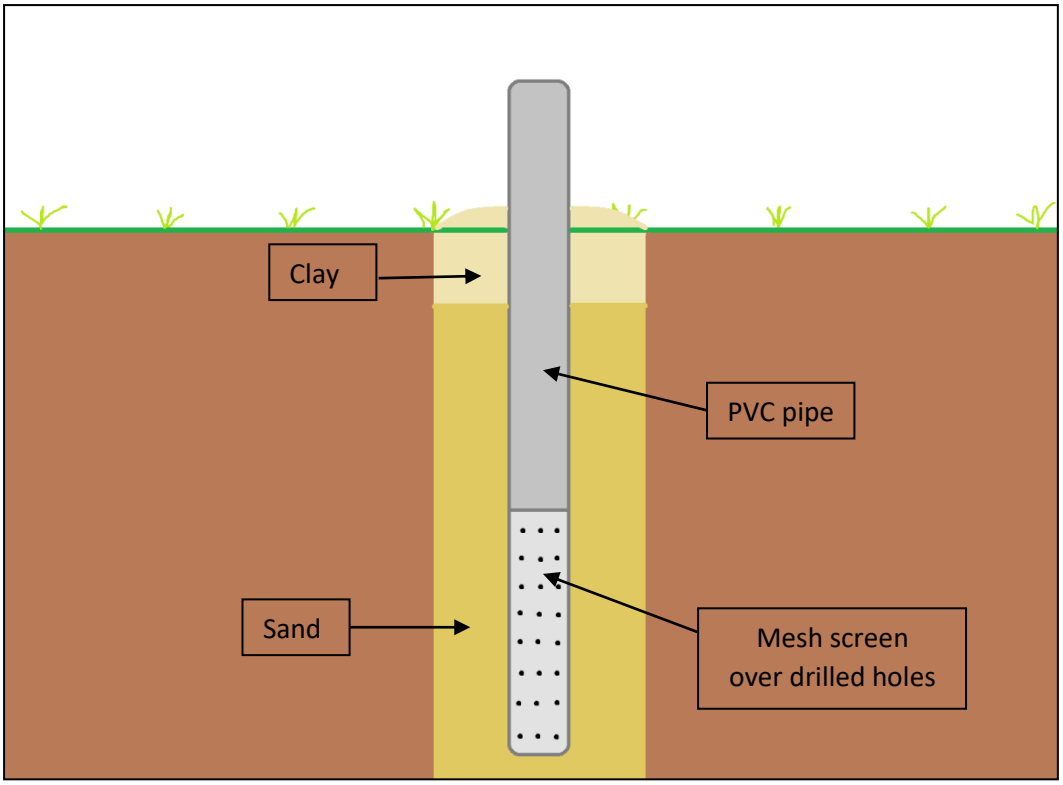


*Figure 27: A schematic drawing of the different installation components (including clay, PVC pipe, sand, and mesh screen over drilled holes) of a piezometer within the soil profile.*

**Piezometer Measurements**

| Piezometer Number | Above Ground Measurement (cm) | In Ground Measurement (cm) | Screen Length (cm) | Piezometer Location |
|---|---|---|---|---|
| **1** | 28 | 174.5 | 100 | 175.619146 E<br>-39.89499 S |
| **2** | 27 | 146 | 100 | 175.62184 E<br>-39.894204 S |
| **3** | 39 | 134 | 75 | 175.6241 E<br>-39.89544 S |
| **4** | 23.6 | 175.9 | 100 | 175.622873 E<br>-39.898338 S |
| **5** | 32.7 | 181 | 100 | 175.615454 E<br>-39.889898 S |
| **6** | 56 | 160 | 100 | 175.62968 E<br>-39.887828 S |

*Table 3: A table of measurements for the 6 installed piezometers.*

Most of the drainage from the southern and northwestern parts of Ngatiapa is to the west towards the Porewa Stream (Figure 28). The Porewa Stream occupies the Porewa valley and flows south along the western margin of Ngatiapa (Figure 29a) through Hunterville (approx. 7km southwest of Ngatiapa) and eventually to its confluence with the Rangitikei River (approx. 21km southwest of Hunterville). The streams across Ngatiapa are identified as ephemeral (Figure 29b) with dams connecting drainage pathways across the study area. The five piezometers were located in the main E-W valley north of the Ngatiapa woolshed, with each piezometer collecting data from different sub-catchments and the 6th piezometer was situated on the northern reach of the study area (Figure 30). The 5 valley piezometers were situated in a siltstone geology (according to the information provided by S-map at the time of piezometer instillations – all following references to geology will be based on information provided by Rees (2020)). The 6th piezometer was situated in one of the gullies in the northern reach of the study area in sandstone designed to get contrasting groundwater between sandstone and siltstone.

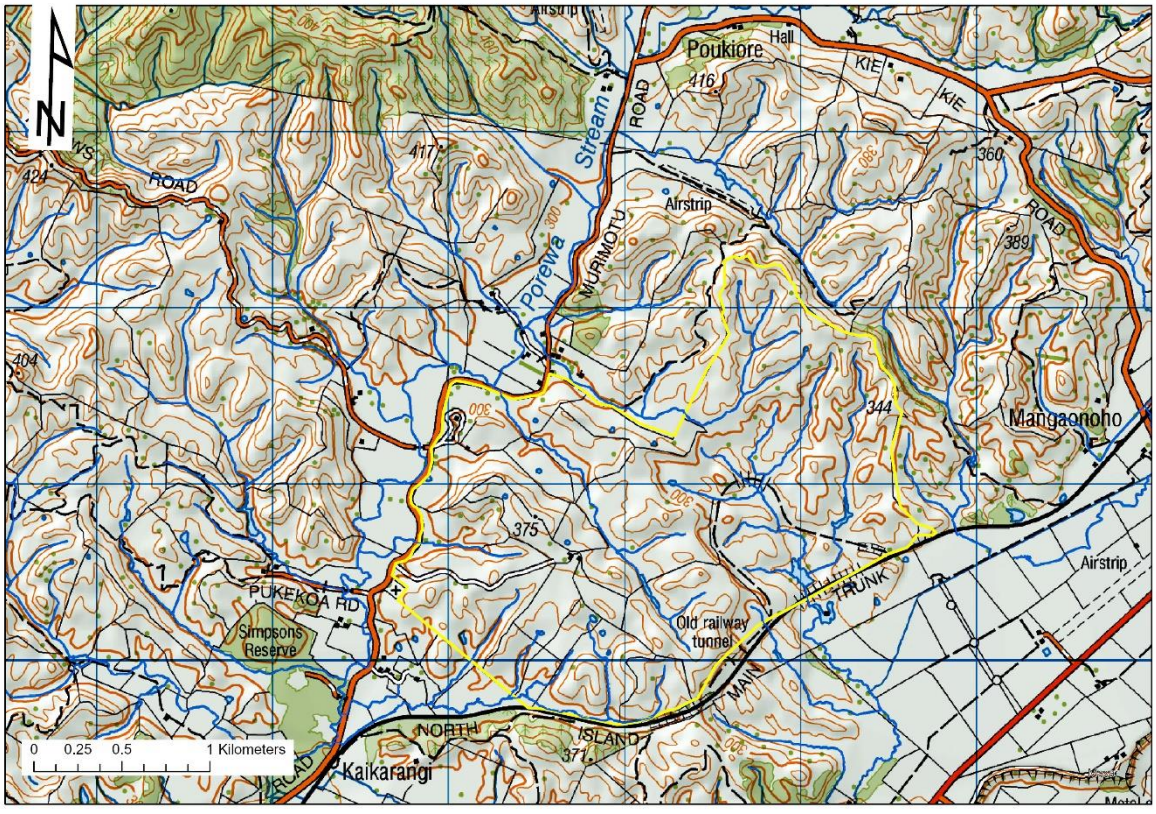


*Figure 28: The Porewa Stream in relation to Ngatiapa (Yellow boundary) shown on a 1: 50,000 topographic map downloaded from [www.topomap.co.nz](http://www.topomap.co.nz).*

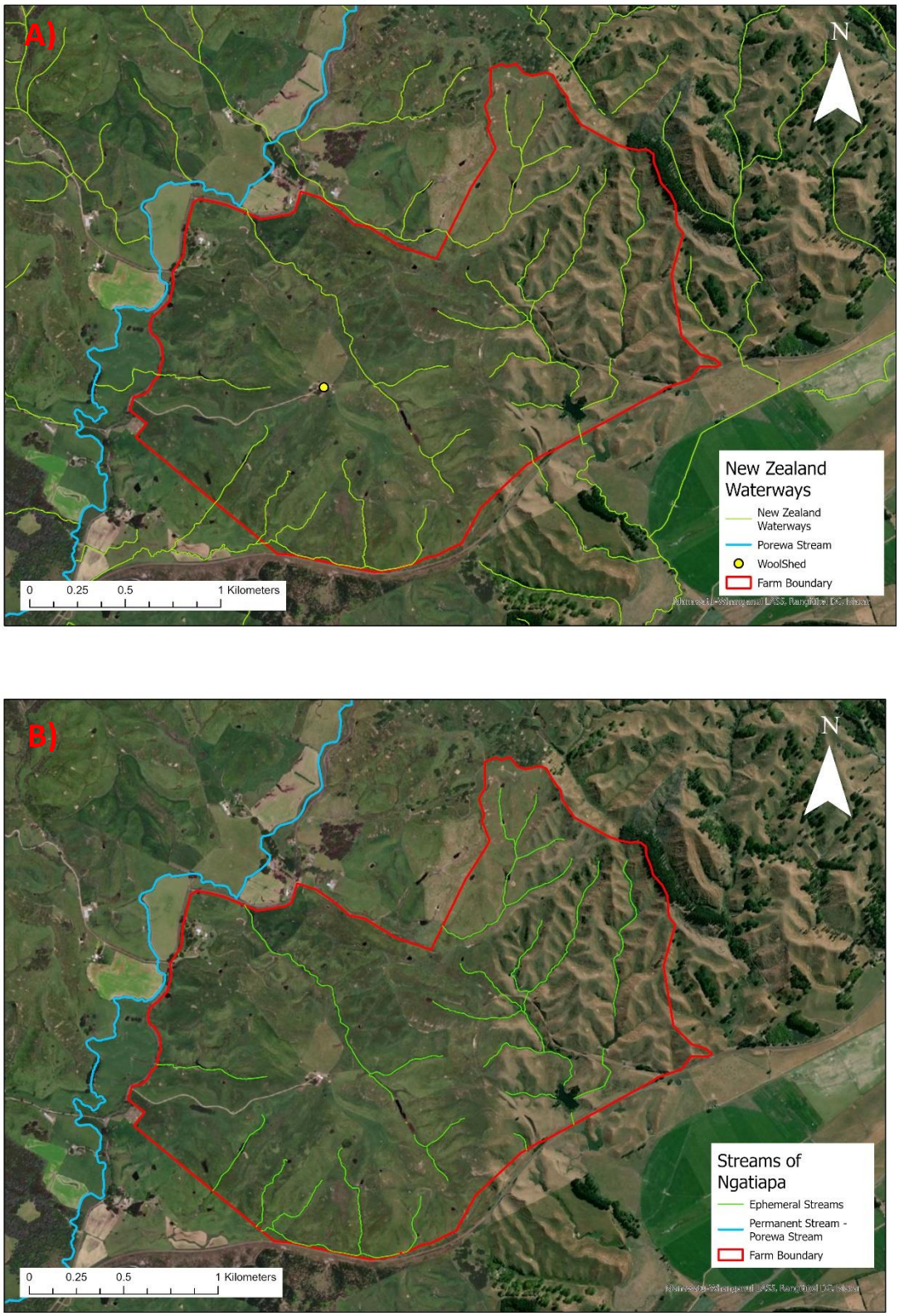


*Figure 29: The Porewa Stream (Blue line) with branches of the stream (Green lines) running through the southern reaches of Ngatiapa (Red boundary line). A) Identifies waterways of New Zealand surrounding Ngatiapa and the location of the Porewa stream. B) The identification of ephemeral and permanent waterways (the Porewa stream) in relation to Ngatiapa.*

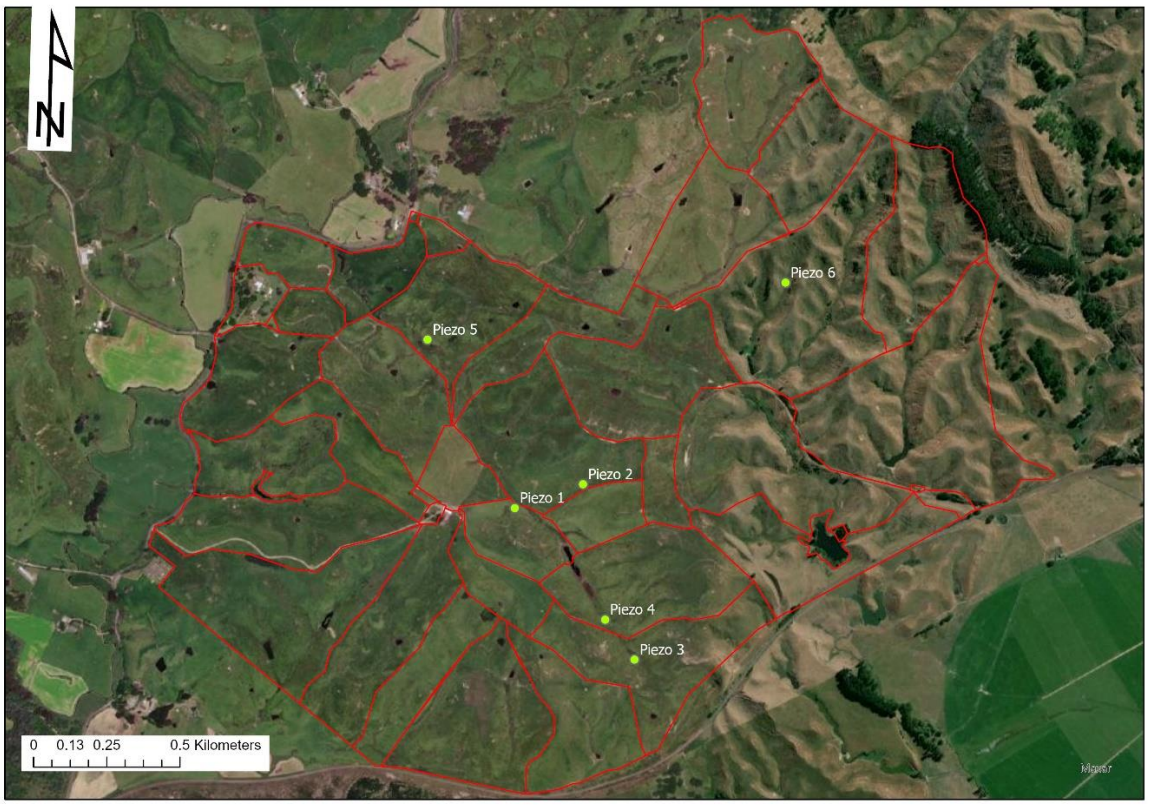


*Figure 30: The location of the 6 installed piezometers across the study area.*

### *4.1.2.2. Data collecting using flow cell meter and surface water sampling*.

Following the instillation of the 6 piezometers, sampling was completed on a monthly basis. Measuring of the groundwater levels was completed prior to the removal of water out of the piezometer system. This was achieved by using an EC Dipper Pro (here on referred to as dipper) to measure the depth of the ground water in each piezometer. The measuring tape of the dipper was lowered into the piezometer until the detector sounds, the height reading is measured at this point with respect to the top of the piezometer pipe. The heights of each recorded water level was subtracted from the total piezometer height (above ground and below ground combined) to find the groundwater level. The sampling of the groundwater involved the pumping of water using a Solinst Peristaltic Pump (Figure 31). This pump was attached to a YSI Flowcell sensor (Figure 31). This sensor continuously monitors a variety of factors described by Collins et al (2017). Continuous pumping of the groundwater, completed by inserting a tube down to the bottom of the piezometer and pulling back the tube approximately 3 cm from the base of the piezometer and pumping water out using pump level 2, was directed through the flow cell with live updates being displayed on a cell phone app (Figure 32). A recording was taken of the live readings during the sampling while 1 litre samples were collected in plastic bottles for further lab analysis. Before the collection of the 1 litre samples,

the water was 'cleaned' to ensure only groundwater was collected. The 'cleaning' process was completed by pumping water through the sensor until the live updates stabilised (remained within the same range for a period of time) with sampling collection beginning following the stabilisation. Samples were stored within chilli bins with ice packs in the field and during transport and later transferred to a fridge (average temperature of 5$^{o}$c) to remain chilled until analysed.

Sampling of surface waters near the installed piezometers were completed alongside the sampling of groundwater (Figure 33). These samples were taken by filling 2 sterilised 70ml pink top specimen containers with running surface waters. These samples were stored the same as the groundwater samples in chilli bins and fridges until analysis was completed.


*Figure 31: The equipment used for the sampling of groundwater. Top right - YSI Flowcell Sensor with sample collection bottle to the left. Bottom left - pipes in the piezometer and connected to the pump for the removal of water. Bottom right - Solinst Peristaltc Pump attached to battery with cell phone on top displaying live updates from the YSI Flowcell Sensor.*

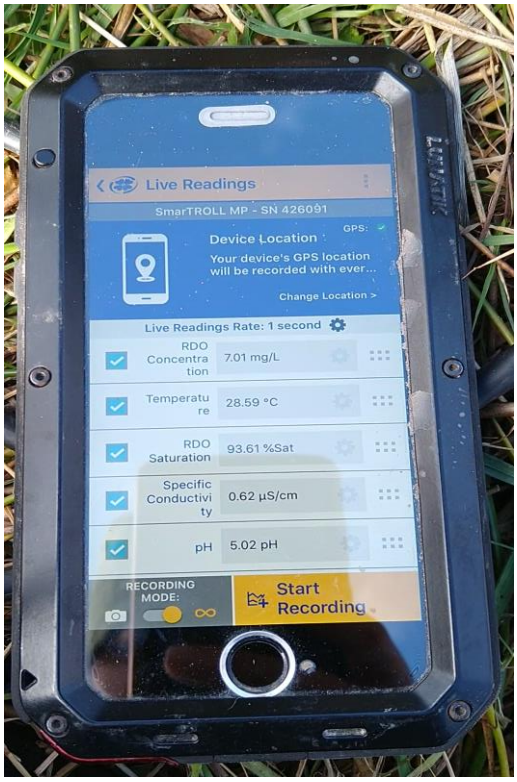


*Figure 32: The live display showing the variables analysed during the sampling of groundwater.*

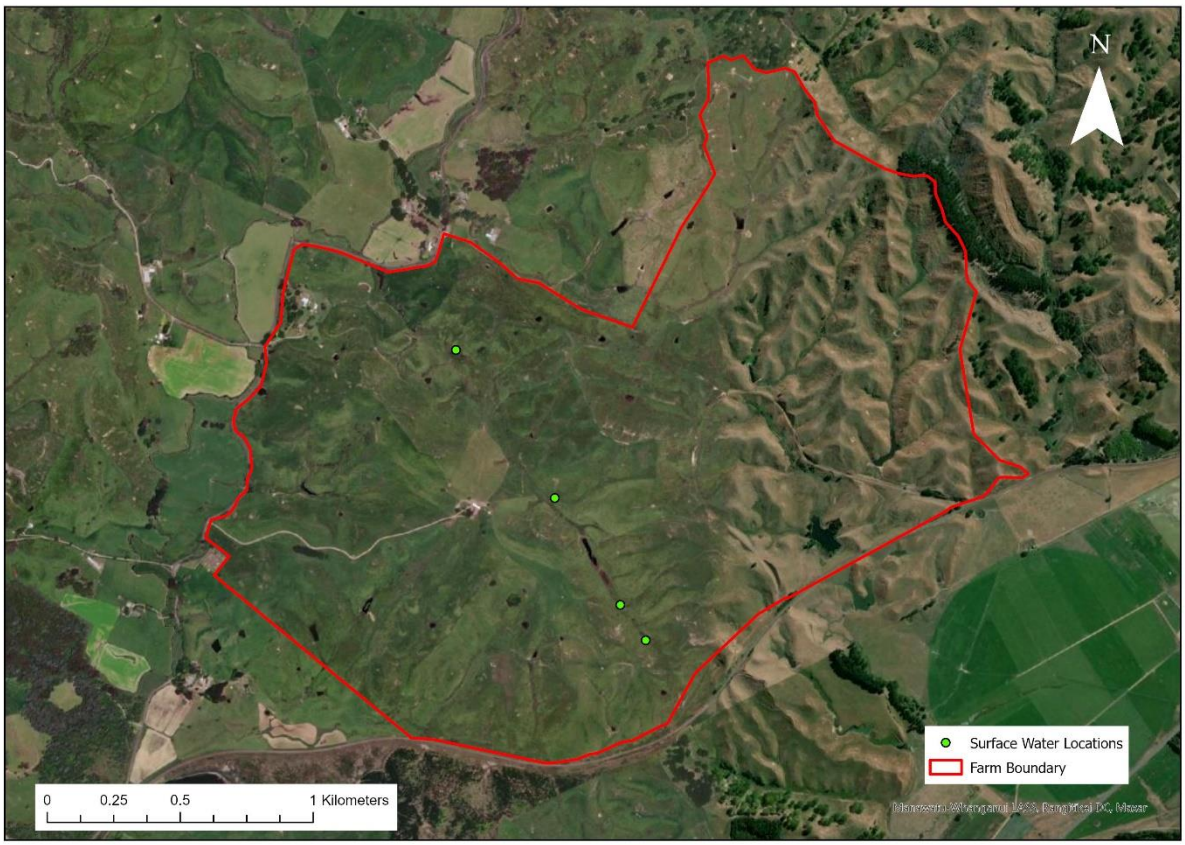


*Figure 33: The 4 surface water sampling locations across Ngatiapa.*

## 4.2. Laboratory study

### *4.2.1 Water analysis*

#### *4.2.1.1. Nitrogen*

Following the sampling of groundwaters and surface waters within the field, samples were brought to the lab to be analysed for nitrogen. A NICO immersion sensor from TriOS Optical Sensors was used to analyses the water samples specifically for nitrate ($N\text{-}NO_3$). A number of samples were diluted at a 1:1 ratio with RO (reverse osmosis) water and are identified within chapter 9 – appendix 3.

#### *4.2.1.2. Phosphorus*

Prior to analysis for dissolved reactive phosphorus (DRP) samples were filtered through 0.45µm Millipore filter paper using the vacuum filtration method (Figure 34). Following this 30ml aliquots of sample were pipetted into 50ml volumetric flasks. In addition to the samples 10mls of Murphy-Riley reagent were added with the remainder of the flask being filled with RO water, mixing all of the flask contents well. The Murphy-Riley reagent was made in a 250ml volumetric flask and was comprised of 100ml $4NH_2SO_4$, 30ml ammonium molybdate, 20ml ascorbic acid and 10ml potassium antimony tartarate with the remainder of the flask being filled with RO water. It is important when making up the Murphy-Riley reagent that each component is added in the order written and that the contents are mixed thoroughly after the addition of each component. Once the Murphy-Riley reagent was added to the samples and the volumetric flask was filled and mixed the solution was left to develop for 20 minutes. After this time, a small volume of the solution was put into a 4mm quartz curvet that got inserted into a Jenway 7315 Advanced UV/Visible Spectrophotometer and analysed at an absorption peak of 712nm (Figure 35).


*Figure 34: The vacuum filtration set up used to filter the water samples.*


*Figure 35: The screen of the Jenway 7315 Spectrophotometer with the 712nm absorbance peak used for analysing water samples for DRP.*

The produced absorbance values using the Jenway 7315 Spectrophotometer were then converted into DRP $mg^{L-1}$. Standard curve concentrations were attained by completing combining known concentrations of DRP solution with the Murphy-Riley reagent. The known concentrations were 0 $mg^{L-1}$, 0.2 $mg^{L-1}$, 0.4 $mg^{L-1}$, 0.6 $mg^{L-1}$, and 0.8 $mg^{L-1}$, with the known concentrations created by diluting a solution of 1$mg^{L-1}$ with RO water to the correct concentrations. The absorbance values of each of the known concentration solutions were analysed using the Jenway 7315 Spectrophotometer. The known concentrations and the analysed absorbance values were then used to create an XY scatter graph where a trend line was applied, including the associated trendline equation. It is the trendline equation $x = \frac{y-0.001}{1{\cdot}569}$. Once the concentrations ($mg^{L-1}$) were identified the concentration of the total flask volume ($\mu g^{ml-1}$) is calculated by multiplying the concentration by 50 (the flask volume). The concentration for the flask volume was then divided by 30 to calculate the concentration of the sample taken ($mg^{L-1}$), with these results being presented within chapter 5. The comparison of using a given standard curve and absorbance values with a created standard curve with retrieved absorbance values for the purpose of this thesis was completed with the results showing that for the purpose of this thesis the most appropriate approach, that provided more accurate and reliable results, was the use of the created standard curve and retrieved absorbance values. The comparison of original absorbance values (collected within a week of sampling) with reanalysed absorbance values collected at the end of August 2023 was completed. The results of this analysis showed that the original absorbance values were the more accurate and reliable absorbance values for this thesis (The delay between collection in the field and analysing the samples in August 2023 is likely to have had an influence on phosphorus concentration levels due to storage of water samples in refrigeration is only suitable for short-term storage – days to months, freezing of water samples would've been more appropriate for long-term storage – years (Maher & Woo, 1998))

### *4.2.2. Rainfall Data*

Rainfall data for the Hunterville area was retrieved from Weather Underground for a period from the 1st of July 2021 to 31st January 2022 covering the sampling days completed in the field. The weather station selected for the use in retrieving the rainfall data was weather station IMWTMANG2 located south of Hunterville (Figure 36). The data was typed into excel, to create graphs which are presented in chapter 5 (Appendix 2 - original rainfall data).

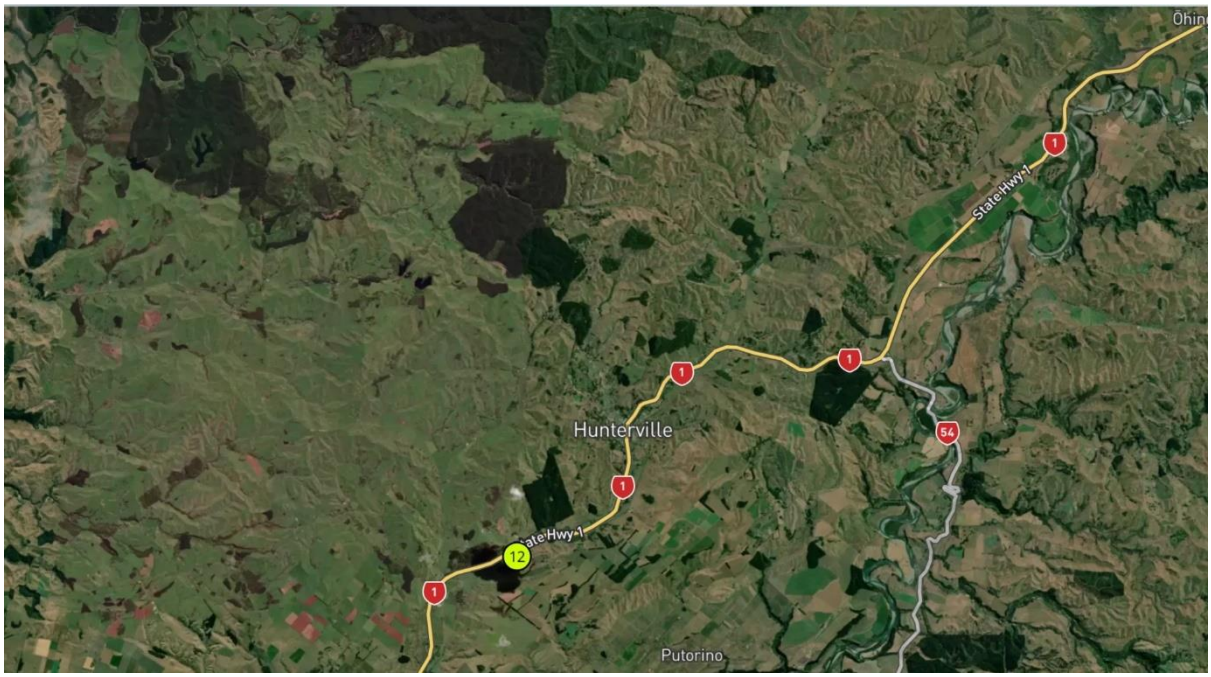


*Figure 36: The location of the weather station IMWTMANG2 (green circle with 12) in relation to Hunterville, used for the purpose of providing rainfall data. Retrieved from Weather Underground.*

## 4.3. Geographic Information Systems (GIS) Study

### *4.3.1. Slope, aspect, landform elements.*

The geographic information systems (GIS) figures and maps created for this thesis were completed using the computer software ArcGIS Pro (here on referred to as ArcGIS) by Esri. The data used for creating the slope, aspect, landform element and rivers figures was retrieved from LINZ data service (https://data.linz.govt.nz/).

The farm boundary layer along with the paddocks layer were created from maps that were provided from the landowner. These maps were inserted into ArcGIS where the farm boundary and paddocks were digitised by creating a new geodatabase (within the catalogue tab), within which a new feature class was created, allowing for a feature to be created (within the edit menu). GPS data collected in the field was inserted into ArcGIS and were displayed as points at the location of each GPS unit point. The digitising of the soil, LRI, LUC and geology (adapted from the geology data provided by Rees (2020)) was completed by creating polygons using the same method as described for the creating of the farm boundary and paddocks.

The soil landscape model figures created were based off an elevation profile developed in ArcGIS. The creating of the elevation profile started with digitising a line in the required location/s (again using the same approach as the digitising of the farm boundary and paddocks). Using the digitised line, the exploratory 3D analysis tool (under the analysis tab – exploratory 3D analysis – elevation

profile) was used to display an interactive elevation profile. The individual selection of each profile line displayed an elevation profile that was exported as a .jpg to be used to create soil landscape model base.

The M-W LiDAR 1m DEM (2015-2016) layer was downloaded for use in the creating of the slope, aspect, and landform element figures. The NZ River Centrelines (Topo, 1:50k) layer was downloaded and clipped to the farm boundary for use in identifying waterways on the study farm.
The M-W LiDAR 1m DEM (2015-2016) layer, once downloaded, was clipped to the farm boundary (using "extract by mask") for further processing (referred to as 1m farm DEM from here on). The slope data was created from the 1m farm DEM that was inserted into the "slope" tool (under the spatial analysis tools – surface), while the 1m farm DEM was inserted into the "aspect" tool (under the spatial analysis tools – surface) both using the default settings to create the aspect and slope figures of the study area.
The landform element layer, showing the distribution of valleys and ridges across the farm, was created from the base layer, the 1m farm DEM. The DEM was inserted into the "surface parameters" tool (spatial analysis tools – surface), with the parameter type set to profile (normal slope line) curvature (PC) (Figure 37), for working out ridges/valleys, and tangential (normal contour) curvature (tangential) (Figure 38), for working out spurs/hollows, with the neighbourhood distance set to 35m. The symbology for the PC and tangential layers were adjusted to manual interval (with 3 classes). The PC symbology classes were set between -0.24 – -0.011, -0.01 – 00012, and 0.013 – 0.255. The tangential symbology classes were set between -0.245 – -0.007, -0.006 – 0.016, and 0.017 – 0.264. The three manual interval classes were the base groups use for the reclassing of the PC and tangential. The reclass groups for the PC layer became 0 (rest of the space) from -0.01 – 0.012, 10 (ridges) from 0.013 – 0.255, and 20 (valleys) from -0.24 – -0.011. The reclass groups for the tangential layer became 0 (rest of the space) from -0.006 – 0.016, 1 (spurs) from 0.017 – 0.264, and 2 (hollows) from -0.245 – -0.007. The clean-up of these two layers followed the reclassing used the majority filter (under the spatial analysis tools – generalisation). The PC and tangential layers got combined together through the PLUS tool (image analysis tools – math – trigonometric). By combining the two layers the ridges/valleys and spurs/hollows were displayed in one layer. Three further clean ups of the layers were completed to remove additional visual noise from the figures and any remaining 'noise' with a "shape_area" below 200 was removed to further clean the figures.

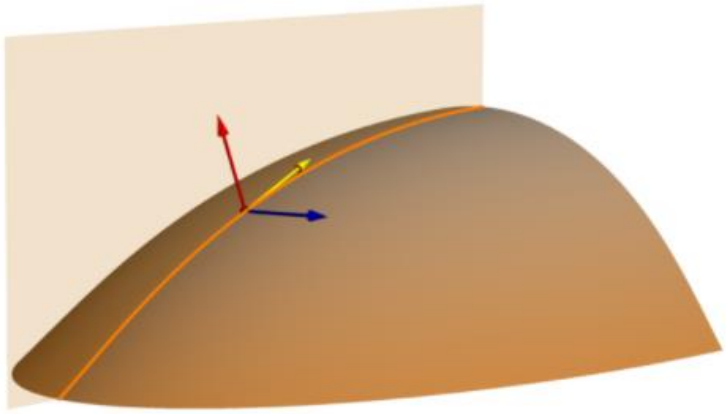

*Figure 37: A diagram of the profile (normal contour) curvature (PC) parameter for surface parameters, showing the application to a curvature, allowing for ridges/valleys to be identified. Retrieved from (ESRI, n.d.).*

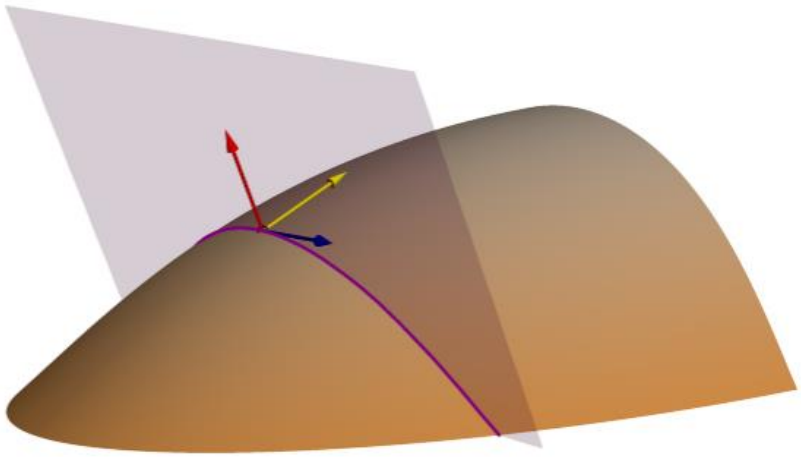

*Figure 38: A diagram of the tangential (normal contour) curvature (tangential) parameter for surface parameters, showing the application to a curvature, allowing for spurs/hollows to be identified. Retrieved from (ESRI, n.d.).*

# Chapter 5 – Results

## 5.1. Field Results

### 5.1.1 Geology

The geological map presented (Figure 39) are the result of adaptations from (Rees, 2020), using additional observations made during field mapping, providing a geological map that address the study area. The results showed that there were 6 geological units identified across Ngatiapa. These 6 classes include the Orangipongo formation (Or), the Mangaonoho formation (Mo), the Mangamako shell bed member (Mm), swamp deposits (Q1a), Upper and Lower Kakariki (Q1k1/Q1k2) and undifferentiated Quaternary landslide (UQl) (Chapter 3). The formations Or, Mo and Mm dominate the study area along with approximately 90% of the study area being under these three classifications (Table 4). The Or classification dominates the largest area with UQl classifying the smallest area (Table 4).

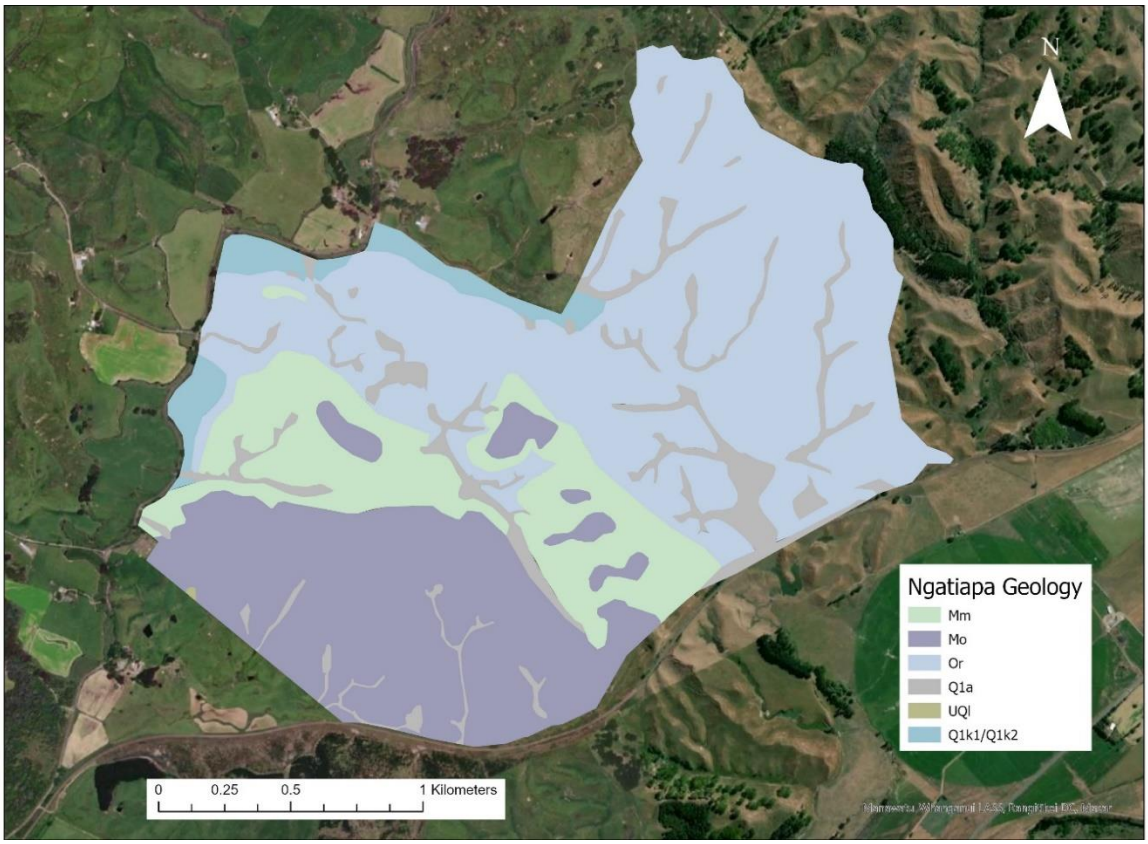


*Figure 39: The geological map of Ngatiapa adapted from (Rees, 2020). Mm – Mangamako Shellbed; Mo – Mangaonoho Formation; Or – Orangipongo Formation; Q1a – Swamp Deposits; UQl – Undifferentiated Quaternary Landslides; Q1k1 – Upper Kakariki Terrace Deposits; Q1k2 – Lower Kakariki Terrace Deposits.*

| Geological Code | Area (Ha) | Area % |
|---|---|---|
| Or | 210.8171 | 46.09 |
| Mo | 116.1797 | 26.40 |
| Mm | 70.7335 | 15.46 |
| Q1a | 68.6915 | 15.01 |
| Q1k2 | 15.9659 | 3.49 |
| No Data | 1.8815 | 0.41 |
| UQl | 0.1308 | 0.03 |

*Table 4: Geologies of Ngatiapa with area (ha) and area percentages. Total area is based off area provided by landowner (457.40ha).*

### 5.1.2. Soil Mapping

A total of 32 soil descriptions were completed during the development of the soil map (Figure 40). The 32 soil descriptions were comprised of 19 being collected during field sampling for the use in the soil map development, 7 being collected for test locations for piezometer instillation and an additional 6 soil descriptions being completed by Massey University student Stanley Oa (during a separate mapping exercise) that was provided for use as supplementary material (Chapter 9 – Appendix 4). All 32 soil descriptions were utilised in the creating of the soil maps.

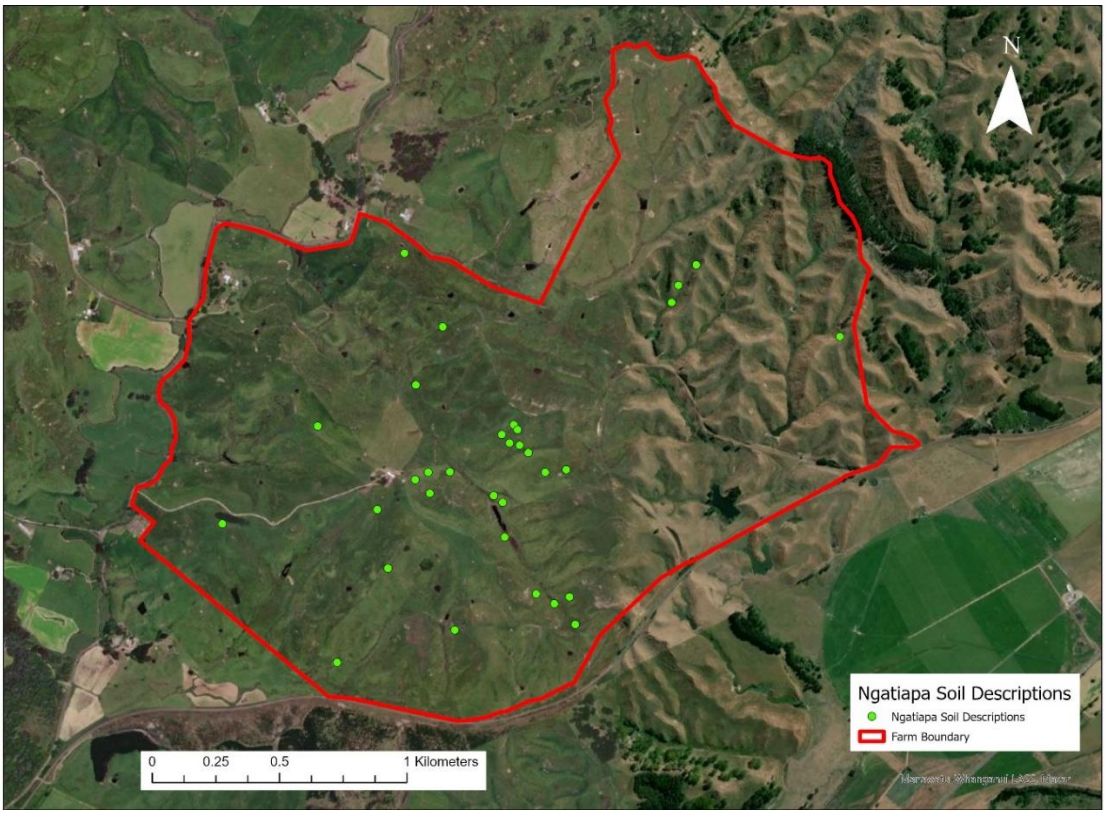


*Figure 40: Location of the 32 soil descriptions (green dots) across Ngatiapa (red boundary line).*

From the mapping completed 15 different varieties of soils were found (Figure 41). 9 soils were given names from the *Extended Legend of Soil Map of Rangitikei County, North Island New Zealand* (refered to as 'extended legend' from here on) (Campbell, 1978) where the soils identified across the study area were of a similar match to the soils identified in this resource (Table 5). The 6 remaining soils were give names from surrounding location names (Table 5, Figure 44). These 6 soils are informally named for the purpose of this study and are inevatibly new soils that are not described in exisitng smaller scale surveys.

The 9 soils named from the extended legend cover 251.0773ha (54.89% area percentage) with the soils named from surrounding locations covering 200.589ha (43.85% area percentage). These 9 soils from the extended legend include the Kairanga deep silt loam on clay (K (a)), Ohakea heavy silt loam (Oh (a)), Raumai hill soil with the Tidal_5a.1 sibiling name (RaH-T), Hunterville hill soil (HvH), Kairanga deep silt loam on sand (K (b)), Ohakea silt loam (Oh (b)), Whangaehu steepland soil (WhS), Pohangina steepland soil (PhS), and Raumai hill soil with the Heretaunga_28a.1 sibling name (RaH-H) (Table 5). The soil RaH-T has companion soils (RaH-T (a), RaH-T (b), RaH-T (c)) which display different variations from the dominating soil class. RaH-T companions vary from RaH-T based on variations in slope and aspect features.

Soil coverage results (for the soils with pre-existing soil names) showed approximately 40% of the study area was classed as PhS, WhS, RaH-T, with PhS dominating with the most coverage and Oh with the lowest coverage (Table 6).

The 6 soils given names from surrounding location names include the Murimotu silt loam (MmS), Simpsons soil (SpS), Pukiore soil (PkS), Manganonoho soil (MoS), Kaikarangi soil (KkS), and Rangitaira soil (RgS) (Table 5). Soil MmS has companion soils, MmS (a) and MmS (b), that have North, West and South aspect variations. The soil coverage results (for the soils with introduced names) showed that approximately 20% of the study area was classified as RgS and PkS, with RgS dominating. The smallest soil area classification was identified to be MmS (b) (Table 6).

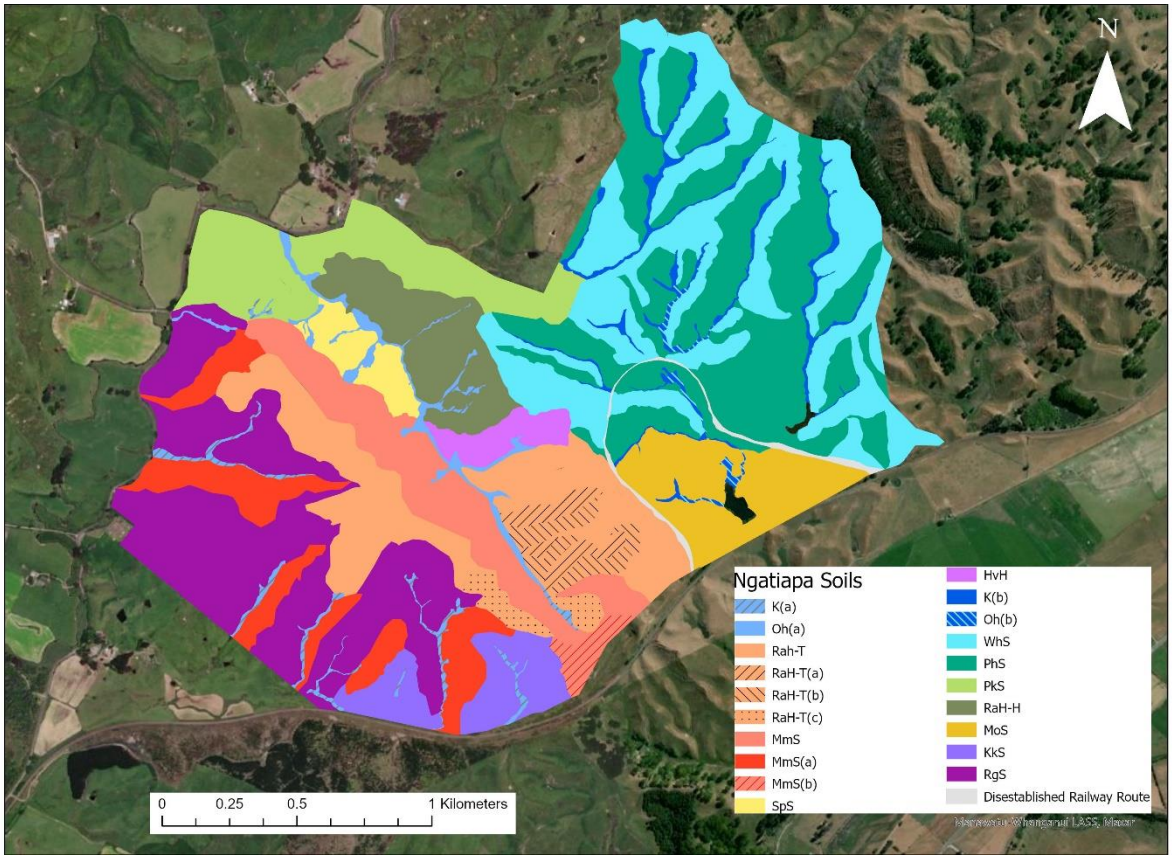


*Figure 41: Soil map of Ngatiapa. K (a) – Kairanga deep silt loam on clay; Oh (a) – Ohakea heavy silt loam; RaH-T – Raumai hill soil; MmS – Murimotu silt loam; SpS – Simpsons soil; HvH – Hunterville hill soil; K (b) – Kairanga deep silt loam on sand; Oh (b) – Ohakea silt loam; WhS – Whangaehu steepland soil; PhS – Pohangina steepland soil; PkS – Pukiore soil; RaH-H – Raumai hill soil; MoS – Mangaonoho soil; KkS – Kaikarangi soil; RgS – Rangitira soil.*

| Soil Name | Soil Sibling Name* | Soil Code |
|---|---|---|
| Kairanga deep silt loam on clay | Flaxton_61a.1 | K (a) |
| Ohakea heavy silt loam | Hastings_70a.1 | Oh (a) |
| Raumai hill soil | Tidal_5a.1 | RaH-T |
| | | RaH-T (a) |
| | | RaH-T (b) |
| | | RaH-T (c) |
| Murimotu silt loam** | | MmS |
| | | MmS (a) |
| | | MmS (b) |
| Simpsons soil** | | SpS |
| Hunterville hill soil | Heretaunga_27a.1 | HvH |
| Kairanga deep silt loam on sand | Hastings_30a.1 | K (b) |
| Ohakea silt loam | Hastings_57a.1 | Oh (b) |
| Whangaehu steepland soil | Duke_1b.1 | WhS |
| Pohangina steepland soil | Waikuku_30a.1 | PhS |
| Pukiore Soil** | | PkS |
| Raumai hill soil | Heretaunga_28a.1 | RaH-H |
| Mangaonoho soil** | | MoS |
| Kaikarangi soil | | KkS |
| Rangitira soil** | | RgS |

*Table 5: Soils of Ngatiapa with the soil names, soil sibling names and soil codes. Names with * retrieved from S-Map factsheets (Manaaki Whenua - Landcare Research, 2023) and are presented with respective soil sibling names. Names with ** are named after surrounding locations, with soil codes being created after soil names.*

| Soil Code | Area (Ha) | Area % |
|---|---|---|
| PhS | 76.3640 | 16.70 |
| WhS | 71.0124 | 15.53 |
| RgS | 67.3952 | 14.73 |
| RaH-T | 39.2573 | 8.58 |
| PkS | 30.6591 | 6.70 |
| MmS | 27.1354 | 5.93 |
| MmS(a) | 25.7970 | 5.64 |
| MoS | 22.7551 | 4.97 |
| RaH -H | 21.3958 | 4.68 |
| KkS | 15.3278 | 3.35 |
| MmS | 13.6506 | 2.98 |
| K (b) | 8.5589 | 1.87 |
| SpS | 7.5746 | 1.66 |
| No Data | 6.2869 | 1.37 |
| HvH | 6.1234 | 1.34 |
| RaH-T (b) | 6.0243 | 1.32 |
| Oh (a) | 5.6292 | 1.23 |
| K (a) | 5.2522 | 1.15 |
| RaH-T (a) | 4.9289 | 1.08 |
| RaH-T (c) | 4.7955 | 1.05 |
| MmS (b) | 3.9448 | 0.74 |
| Oh (b) | 1.7354 | 0.38 |

*Table 6: Soil area (ha) and soil area percentage (%) for the soils of Ngatiapa. Total farm area is based off area provided by landowner (457.40 ha).*

From the 15 soils identified across Ngatiapa, 3 soil orders were identified (Figure 42). These 3 soil orders include Brown, Gley and Pallic. Brown and Pallic Soils have been identified to dominate the study area with approximately 94% of coverage (Table 7). Table 8 shows each soil identied across Ngatiapa and the associated soil orders with associated S-Map soil subgroups (Manaaki Whenua - Landcare Research, 2023). The soils with names created from surrounding locations have no associated S-Map classifications and are identifies with a *.

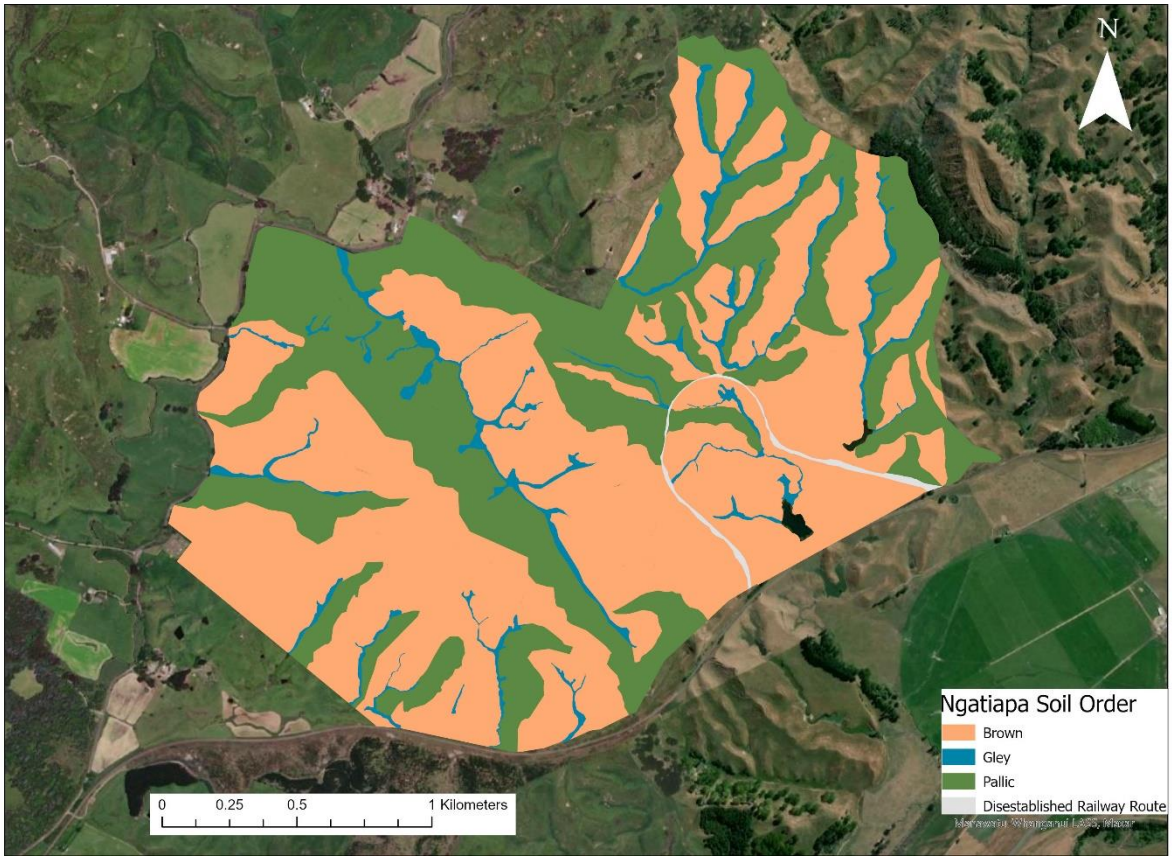


*Figure 42: The soil orders of the 15 Ngatiapa soils. These orders include Brown, Gley and Pallic.*

| Soil Orders | Area (Ha) | Area % |
|---|---|---|
| Brown | 261.8059 | 57.25 |
| Pallic | 168.1315 | 36.76 |
| Gley | 21.1757 | 4.63 |
| No Data | 6.2869 | 1.37 |

*Table 7: The soil order of the 14 identified soils of Ngatiapa with the results for area (ha) and area percentage (%).*

| Soil Code | Soil Orders | Soil Subgroup (S-Map) |
|---|---|---|
| K (a) | Gley | Typic orthic gley |
| Oh (a) | Gley | Typic orthic gley |
| RaH-T | Brown | Mottled orthic brown |
| RaH-T (a) | Brown | Mottled orthic brown |
| RaH-T (b) | Brown | Mottled orthic brown |
| RaH-T (c) | Brown | Mottled orthic brown |
| MmS* | Pallic | |
| MmS (a)* | Pallic | |
| MmS (b)* | Pallic | |
| SpS* | Pallic | |
| HvH | Brown | Pallic orthic brown |
| K (b) | Gley | Typic orthic gley |
| Oh (b) | Gley | Typic orthic gley |
| WhS | Pallic | Mottled immature pallic |
| PhS | Brown | Typic sandy brown |
| PkS* | Pallic | |
| RaH -H | Brown | Pallic orthic brown |
| MoS* | Pallic | |
| KkS* | Pallic | |
| RgS* | Pallic | |

*Table 8: The 15 soils of Ngatiapa with the associated soil orders and soil subgroup given on S-Map factsheets (Manaaki Whenua - Landcare Research, 2023). The soils with * are the soils with names given from surrounding locations.*

The drainage classes of each of the 15 soils identified across Ngatiapa are presented in Figure 43. The drainage classes include well drained, moderately drained, imperfectly drained, poorly drained and NFD. The classification of Needs Further Data (NFD) has been applied to a selected number of soils. The soils identified as well drainged are split into 2 sub classes that include well drained and well drained**. The soils identified as well drained** are soils that have been given names from surrounding locations and don't have the additional supporting data from the S-Map factsheets (Manaaki Whenua - Landcare Research, 2023) that the soils identified as well drained have. This same concept is applied to the soils of imperfectly drained and imperfectly drained** where the soils of imperfectly drained have the additional supporting data from the S-Map factsheets (Manaaki Whenua - Landcare Research, 2023). The soils classified as NFD did not have enough data to apply a drainage classification to the soils, due to the limited information provided in the soils classifications

by Oa, S (Appendix 9).

Imperfectly drained, well drained and imperfectly drained ** classes have been identified to have the highest coverage of the study area with approximately 70%, with imperfectly and well drained soils have an approximate 50% coverage of the study area. Poorly drained soils have been identified to have the lowest coverage of the study area (Table 9).

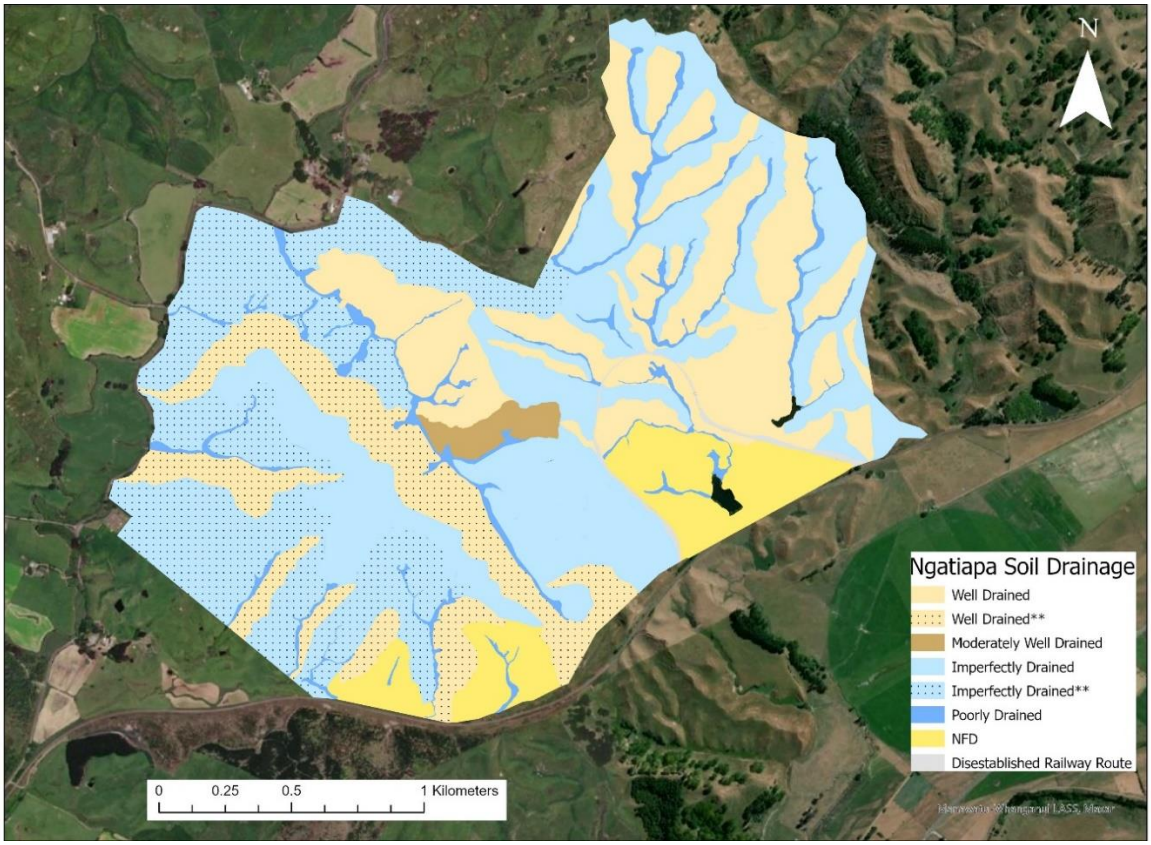


*Figure 43: The soil drainage of the soils of Ngatiapa. The drainage classes with ** are the classes that do not have supporting data from S-Map factsheets due to having been named from surrounding locations.*

| Drainage Classes | Area (ha) | Area % |
|---|---|---|
| Imperfectly Drained | 126.0184 | 27.55 |
| Imperfectly Drained** | 98.0543 | 21.44 |
| Well Drained | 97.7598 | 21.37 |
| Well Drained** | 63.8986 | 13.96 |
| Poorly Drained | 21.1757 | 4.63 |
| Needs Further Data (NFD) | 38.0829 | 3.23 |
| No Data | 6.2869 | 1.37 |
| Moderately Well Drained | 6.1234 | 1.34 |

*Table 9: The drainage classes of the soils of Ngatiapa with the results showing area (ha) and area percentages. Drainage classes with ** are the soils without additional supporting data from S-Map factsheets.*


*Figure 44: The identifying of the surrounding locations where the names were used for the soils of Ngatiapa. The red outline is the farm boundary location. The yellow circles highlight the names used for the labelling of 6 soils.*

The information collected during soil sampling allowed for the collection of LRI and LUC data. The LRI data resulted in 10 distinguishable units (Figure 45). The four LRI units, units 7, 10, 2 and 6, cover approximately 58% of the study area, with the remaining LRI units having area percentages lower than 7% (Table 10).

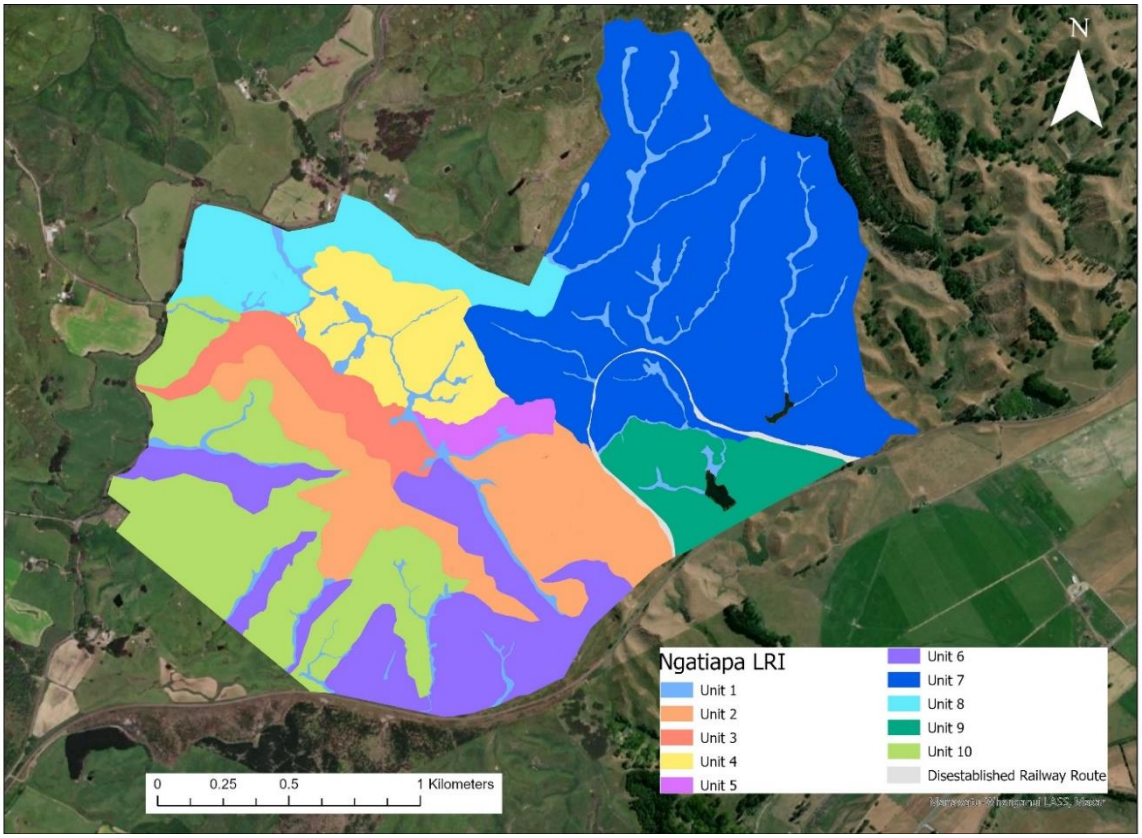


*Figure 45: The LRI distribution map of Ngatiapa farm.*

| LRI Unit Number | LRI Code | Area (ha) | Area % |
|---|---|---|---|
| Unit 7 | Code 1 | 147.3764 | 32.22 |
| Unit 10 | Code 2 | 67.3952 | 14.73 |
| Unit 2 | Code 3 | 55.0060 | 12.03 |
| Unit 6 | Code 4 | 54.0564 | 11.82 |
| Unit 8 | Code 5 | 30.6591 | 6.70 |
| Unit 4 | Code 6 | 28.9704 | 6.33 |
| Unit 9 | Code 7 | 22.7551 | 4.97 |
| Unit 1 | Code 8 | 21.1757 | 4.63 |
| Unit 3 | Code 9 | 17.5954 | 3.85 |
| | No Data | 6.2869 | 1.37 |
| Unit 5 | Code 10 | 6.1234 | 1.34 |

*Table 10: The LRI codes (full codes are in appendix 1) for Ngatiapa with the results for area (ha) and area percentage (%). Total area is based off area provided by landowner (457.40ha).*

The LRI units are comprised of several factors including erosion with 6 different erosion classes being identified across Ngatiapa (Figure 46). The 6 erosion classes include stream bank erosion, sheet erosion, soil slip with a shallow depth, and track erosion each with severity ranging from negligible to 2 combined with soil slip. The steep slopes of the northern reaches of Ngatiapa are dominated by soil slip with a level 1 severity. The western slopes are dominated by shallow soil slip with low sheet erosion (Table 11).

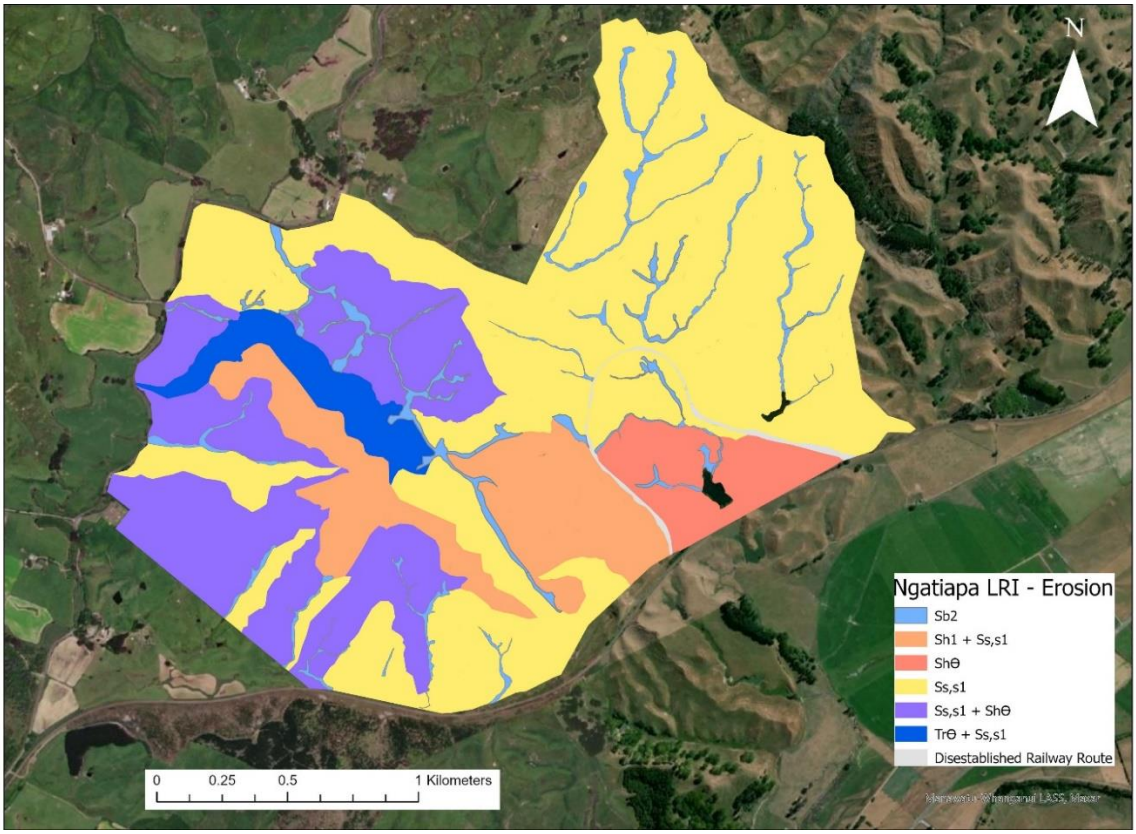


*Figure 46: The map of the erosion factors of the LRI distribution across Ngatiapa. Sb2 – Stream bank erosion with a level 2 severity; Sh2 + SS,s1 – Sheet erosion with a level 2 severity combined with soil slip with a shallow depth and a level 1 severity; ShΘ – Sheet erosion with a negligible severity; SS,s1 – Soils slip with a shallow depth and a level 1 severity; SS,s1 + ShΘ - Soil slip with a shallow depth and a severity of 1 combined with sheet erosion with a negligible severity; TrΘ + SS,s1 – Track erosion with a negligible severity combined with soil slip with a shallow depth and level 1 severity.*

| Erosion Code | Area (ha) | Area % |
|---|---|---|
| SS,s1 | 237.7529 | 51.98 |
| SS,s1 + ShΘ | 96.3656 | 21.07 |
| Sh2 + SS,s1 | 55.0060 | 12.03 |
| ShΘ | 22.7551 | 4.97 |
| Sb2 | 21.6381 | 4.73 |
| TrΘ + SS,s1 | 17.5956 | 3.85 |
| No Data | 6.2869 | 1.37 |

*Table 11: The 6 classes of erosion identified within the LRI classification of Ngatiapa. Erosion code (Sb2 – Stream bank erosion with a level 2 severity; Sh2 + SS,s1 – Sheet erosion with a level 2 severity combined with soil slip with a shallow depth and a level 1 severity; ShΘ – Sheet erosion with a negligible severity; SS,s1 – Soils slip with a shallow depth and a level 1 severity; SS,s1 + ShΘ - Soil slip with a shallow depth and a severity of 1 combined with sheet erosion with a negligible severity; TrΘ + SS,s1 – Track erosion with a negligible severity combined with soil slip with a shallow depth and level 1 severity), area (ha) and area percentage (%) are presented. Total area is based off area provided by landowner (457.40ha).*

The LRI codes are comprised of several factors including vegetation which is comprised of 4 different vegetation classes (Figure 47). The 4 vegetation classes include improved pasture (gI); improved pasture combined with short tussock grassland (gIgT); improved pasture combined with scattered short tussock grassland (gIgT*); rushes, sedges combined with scattered wetland vegetation (hRhW*). The dominating vegetation classes covering approximately 88% of the study area are gIgT* and gIgT (Table 12).

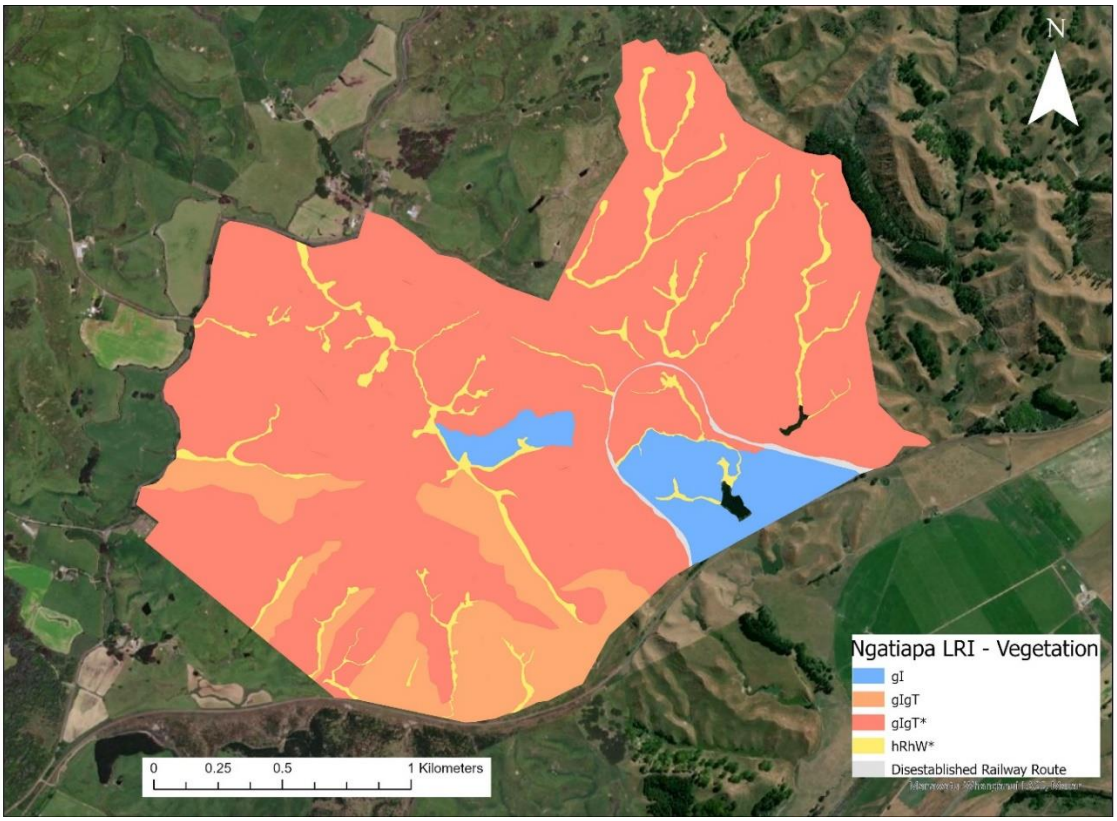


*Figure 47 : The map of the vegetation factors of the LRI distribution across Ngatiapa. gI – Improved pasture; gIgT – Improved pasture combined with short tussock grassland; gIgT* – Improved pasture combined with scattered short tussock grassland; hRhW* – Rushes, sedges combined with scattered wetland vegetation.*

| Vegetation Code | Area (ha) | Area % |
|---|---|---|
| gIgT* | 347.0025 | 75.86 |
| gIgT | 54.0564 | 11.82 |
| gI | 28.8785 | 6.31 |
| hRhW* | 21.1757 | 4.63 |
| No Data | 6.2869 | 1.37 |

*Table 12: The 4 classes of vegetation identified within the LRI classification of Ngatiapa. Vegetation code (gI – Improved pasture; gIgT – Improved pasture combined with short tussock grassland; gIgT* – Improved pasture combined with scattered short tussock grassland; hRhW* – Rushes, sedges combined with scattered wetland vegetation), area (ha) and area percentage (%) are presented. Total area is based off area provided by landowner (457.40ha).*

Slope and aspect information utilised in the completion of the LRI and LUC is addressed in association with GIS results in chapter 5.3.1.

6 LUC classes were identified based on the information provided during the completion of the LRI map (Figure 46) which include 4w1, 5e10, 5e7, 6e4, 6e9 and 6e13 (Full definitions can be located in Land Use Capability Survey Handbook by Lynn, et al (2009) . Approximately 64% of the study area is identified as classes 6e13 and 5e10 (Table 13).

The different LRI classes provides an assessment about the physical factors that are critical for long-term land use and management. The LRI information presented is used as the foundation for LUC classifications (an interpretation of the land based on the facts presented in an LRI classification (Hewitt, Lynn, Manderson, Wilde, & Willoughby, 2008)) to classify land according to its long-term capability to sustain one or more productive uses. 6 LUC classes were identified giving 6 areas of different capabilities (Lynn, et al., 2009).

The LUC class 4 was identified as 4w1. LUC class 4 is identified as being the worst of the arable land due to severe physical limitations to arable use (Figure 7) (Lynn, et al., 2009). The limitations identified, which is denotioned with 'w', is excessive wetness after drainage. LUC class 4 units have been identified to have a severe suceptability specifically to sheet, rill and gully The Gley soils have anoxic conditions due to extended wetness throughout the profile and presents clearly the wetness limitations seen throughout LUC class 4, with streambank erosion being the main limitation. erosion when cultivated (Lynn, et al., 2009).

The LUC class 5 was identified as 5e3 and 5w3. LUC class 5 is identified as being high-producing land (landscapes with slopes between 0-25$^{o}$ (Lynn, et al., 2009)) with physical limitations that make it unsuitable for arable cropping although has only negligible to slight limitations to pastoral, vineyard, tree crop or production forestry use (Figure 7) (Lynn, et al., 2009). The physical restrictions identified, which are notioned with 'e' and 'w', is erosion risk when cultivated and excessive wetness after drainage with slight stoniness respectively. The soils under LUC 5e3 (RgS, RaH-T, RaH-T (a), RaH-T (b), RaH-T (c), and MoS- Figure 41) exhibit the possibility of erosion risk primarily due to the slopes present across the landscape (moderately steep slopes – 21-25$^{O}$ (Lynn, et al., 2009) – Figure 81). The soils under LUC 5w3 (SpS and PkS) exhibits extensive wetness particularly during the wetter months where surface flooding occurs.

The LUC class 6 was identified as 6e9 and 6e13. LUC class 6 is identified as being unsuitable for arable use, and has slight to moderate physical limitations and hazards under perennial vegetation cover (Figure 7). The physical constraints identified, which is notioned with 'e', is moderate erosion hazard under prerennial vegetation with steep and very steep slopes (including land with a slope greater than 26$^{o}$). The soils under the LUC 6e9 (KuH and RaH-H – Figure 41) exhibit moderate

erosion hazards with evidence of previous large erosion events. These soils are on steep slopes that enhance erosion and soil depth for these locations. This class can be suited to grazing, tree crops and/or forestry provided erosion is controlled by appropriate conservation and pasture management (e.g. space-planted trees, conservation fencing, appropriate winter cattle management etc) (Figure 7) (Lynn, et al., 2009).

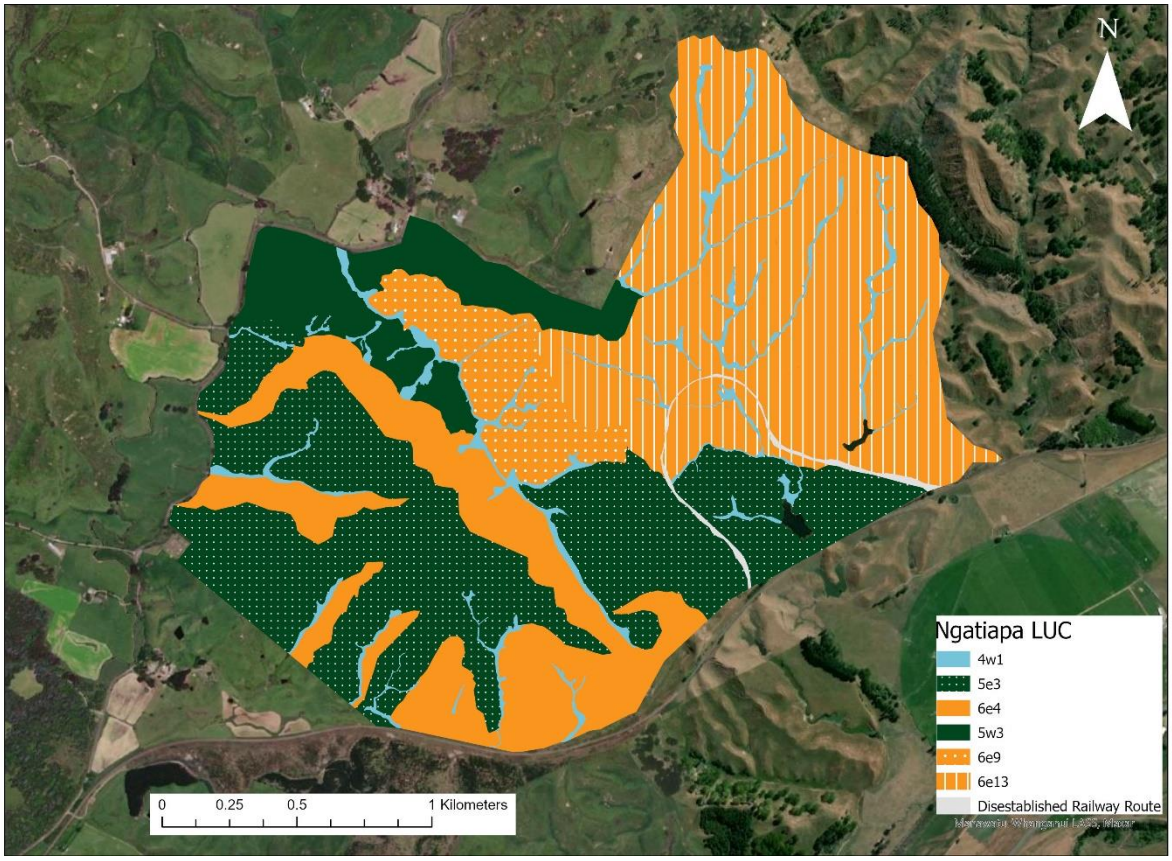


*Figure 48: The map of the LUC distribution across Ngatiapa.*

| LUC Code | Area (ha) | Area % |
|---|---|---|
| 6e13 | 147.3764 | 32.22 |
| 5e10 | 145.1563 | 31.74 |
| 6e4 | 71.6518 | 15.67 |
| 5e7 | 38.2337 | 8.56 |
| 6e9 | 21.5192 | 6.02 |
| 4w1 | 21.1757 | 4.63 |
| No Data | 6.2869 | 1.37 |

*Table 13: The 6 LUC classifications of Ngatiapa. Area (ha) and area percentage (%) are presented. Total area is based off area provided by landowner (457.40ha).*

Three transects have been drawn to show the relationship between soil, landscape, and geology resulting in three soil landscape models. Figures 49, 50 and 51 are the resulting images for the soil landscape models (Figure 52 – Legend). Figure 49 shows the result for location 1 (Figure 53) and is set in a north to south orientation measuring a distance of 728m covering 3 soil units and 2 geological units. Figure 50 shows the results for location 2 (Figure 53) and is set in a north to south orientation measuring a distance of 985m covering 8 soil units and 4 geological units. Figure 51 shows the results for location 3 (Figure 53) and is set in a north to south orientation measuring a distance of 495m covering 4 soil units and 2 geological units. The soils that location 1 cover include PhS, K (b), and WhS. The geologies that location 1 cover are Or and Q1a. The soils that location 2 cover include PkS, RaH-H, Oh (a), SpS, MmS, RaH-T, RgS and HvH (b). The geologies that location 2 cover are Or, Mm, Q1a, and Mo. The soils that location 3 cover include RaH-T, K (a), HvH (b) and KkS. The geologies that location 3 cover are Mo and Q1a.

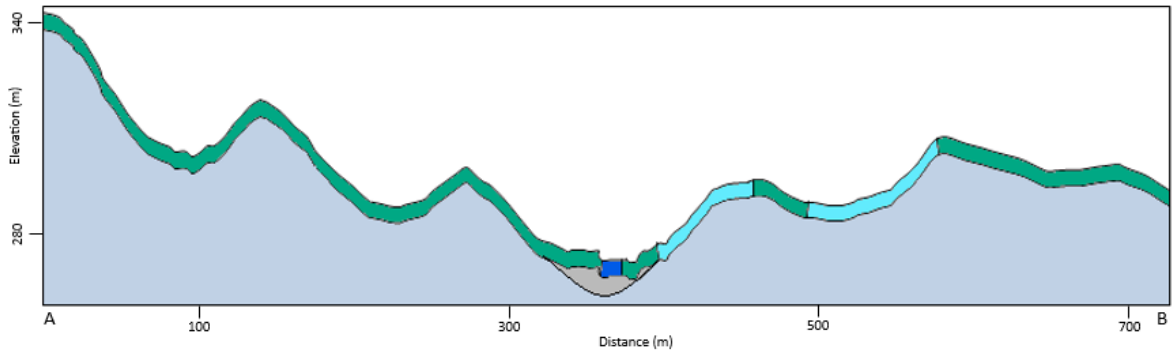


*Figure 49: The soil landscape model for location 1 with a north/south orientation covering 3 soil units and 2 geological units across 728m.*

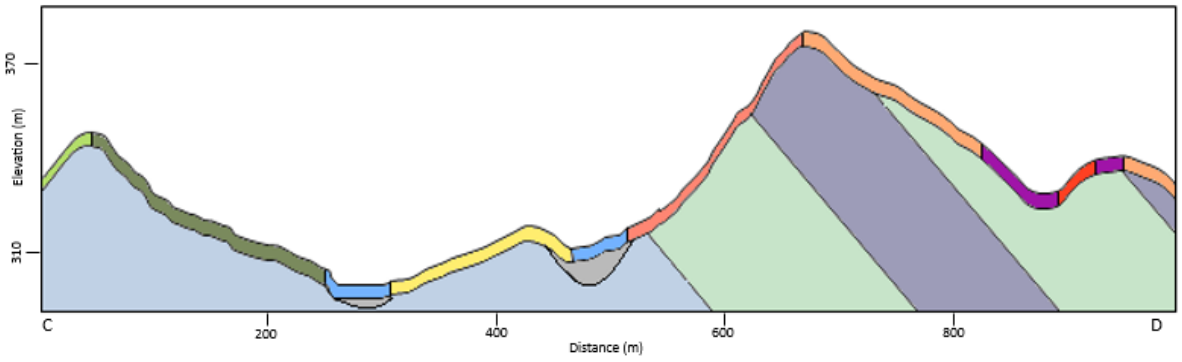


*Figure 50: The soil landscape model for location 2 with a north/south orientation covering 8 soil units and 4 geological units across 985m.*

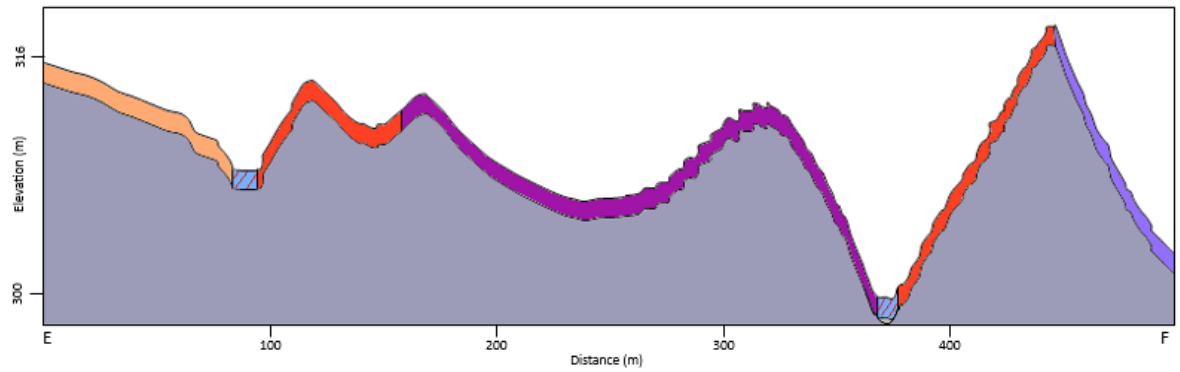


*Figure 51: The soil landscape model for location 3 with a north/south orientation covering 4 soil units and 2 geology units across 495m.*

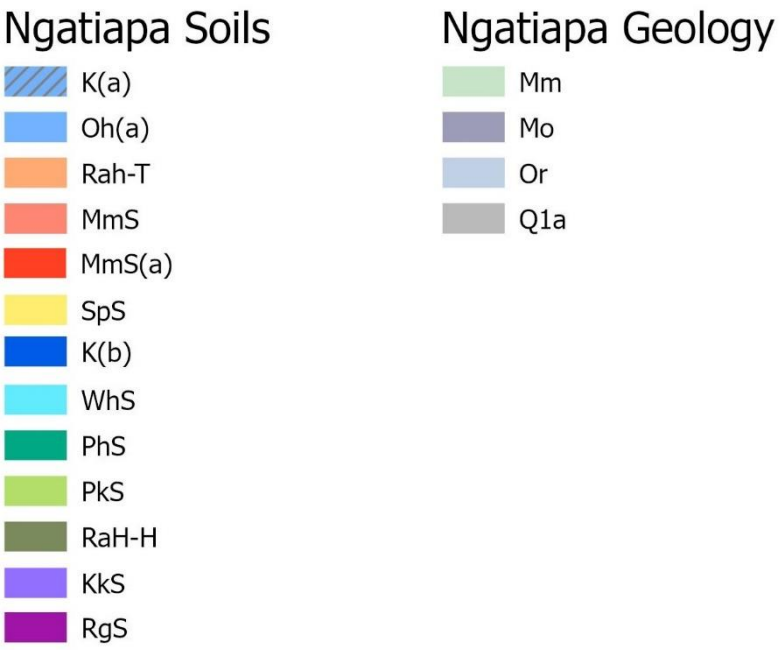


*Figure 52: Legend for the soil landscape models created for location 1, location 2, and location 3. K (a) – Kairanga deep silt loam on clay; Oh (a) – Ohakea heavy silt loam; RaH-T – Raumai hill soil; MmS – Murimotu silt loam; SpS – Simpsons soil; HvH – Hunterville hill soil; K (b) – Kairanga deep silt loam on sand; Oh (b) – Ohakea silt loam; WhS – Whangaehu steepland soil; PhS – Pohangina steepland soil; PkS – Pukiore soil; RaH-H – Raumai hill soil; MoS – Mangaonoho soil; KkS – Kaikarangi soil; RgS – Rangitira soil; Mm – Mangamako Shellbed; Mo – Mangaonoho Formation; Or – Orangipongo Formation; Q1a – Swamp Deposits; UQl – Undifferentiated Quaternary Landslides; Q1k1 – Upper Kakariki Terrace Deposits; Q1k2 – Lower Kakariki Terrace Deposits.*

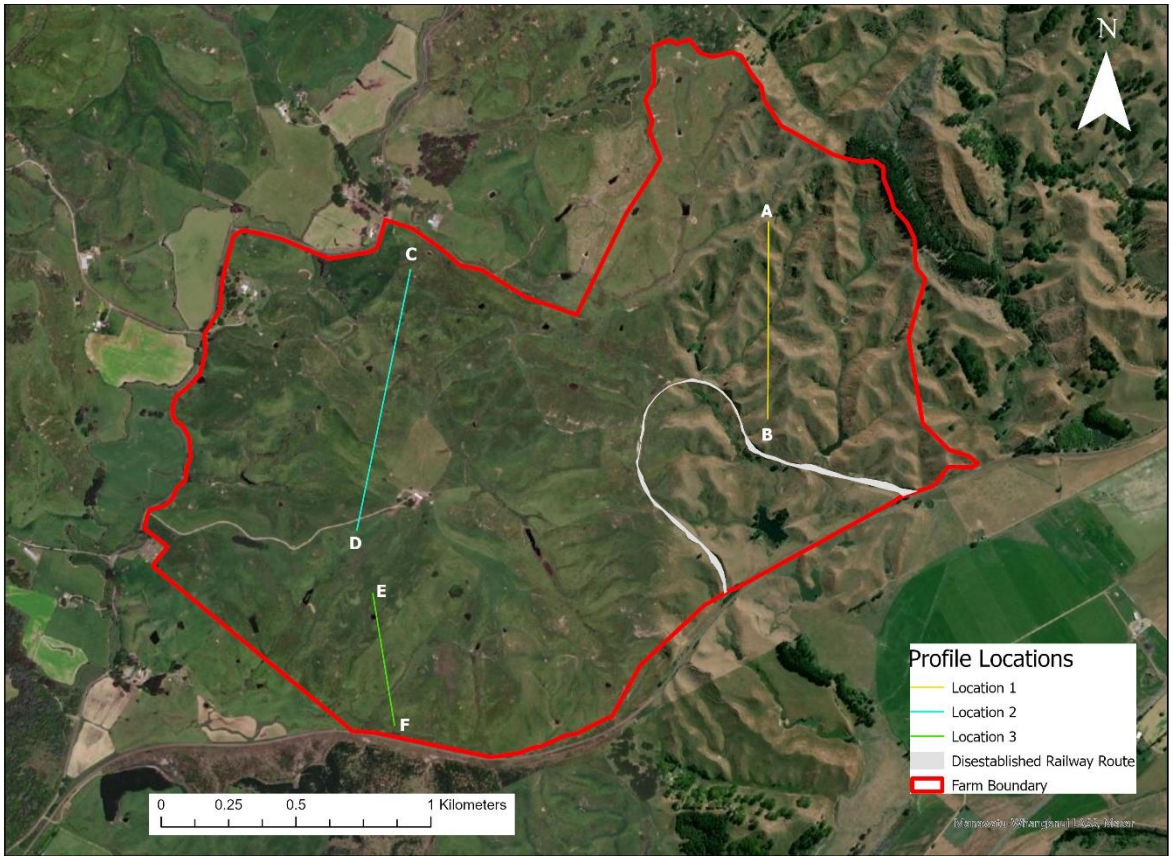


*Figure 53: The location of the 3 soil landscape model profiles.*

### 5.1.2. Water Level Results

Piezometers 1, 2, 5 and 6 show a slight increase in water level in June 2021. Piezometers 2, 4, 5 and 6 show a decrease in water level in November 2021 along with all piezometers showing a larger decrease in water level in January 2022. Piezometers 1 through to 5 all show a stable water level pattern until the decrease in November 2021. The decreases in water level occurs within the summer periods of the year (Figure 54, appendix 3).

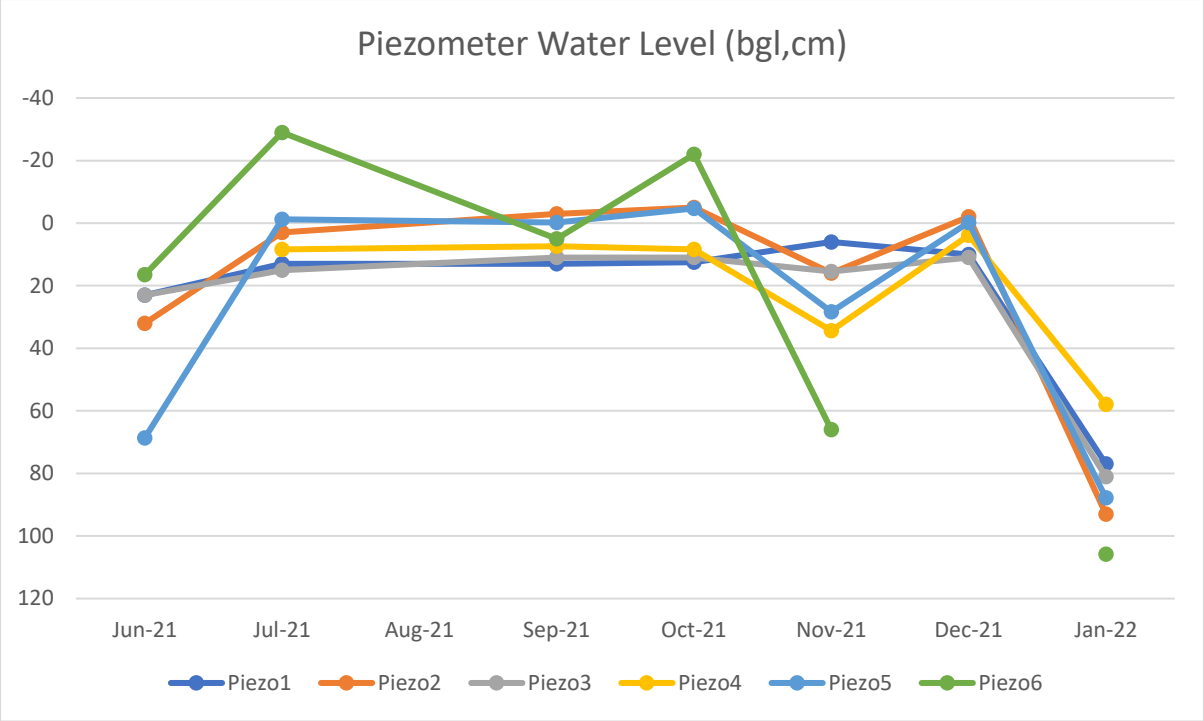


*Figure 54: Groundwater levels for all piezometers across the sampling months. The black outlined dot indicates the dry piezometer at the time of sampling.*

The sampling days on the 22nd and 23rd of June 2021 occurred following rainfall events between the 15th and 22nd which aligns with the shallow groundwater levels (Figure 55). These rainfall events had values ranging between 1.27mm to 10.67mm (Appendix 2 – table 18).

The sampling days on the 28th and 30th of July 2021 occurred following an extended period of rainfall between the 19th and 30th which aligns with the shallowing of groundwater levels (Figure 4). These rainfall events had values ranging between 0.25mm to 32.26mm. Following the sampling days in June there was a heavy rainfall day on the 28th with 28.45mm. This rainfall event along with the events experienced before the sampling in July all contribute to the groundwater levels measured in the piezometers (Appendix 2 – table 18).

The sampling days on the 22nd and 27th of September 2021 occurred following a period of rainfall events between the 7th and 17th (Figure 57). These rainfall events had values ranging between 0.20mm to 31.5mm. Low levels of rainfall across the month of August with the 6 days of no rainfall at the beginning of September align with the lower groundwater levels at the time of sampling (Appendix 2 – table 18, figure 89).

The sampling days on the 19th and 20th of October 2021 occurred following a period of rainfall events between the 4th and 19th (Figure 58) which aligns with the shallowing of groundwater levels. These rainfall events had values ranging between 4.06mm to 25.65mm. Following the sampling days in September there were heavy rainfall days on the 28th and 29th with both having values of 31.5mm.

These rainfall days along with the events experienced before the October samplings all contribute to the groundwater levels measured in the piezometers (Appendix 2 – table 19).

The sampling days on the 30th of November and the 1st of December 2021 occurred following a month of limited rainfall events with one identifiable period occurring between the 13th and 18th of November which aligns with the deepening of groundwater levels and the increased evapotranspiration during summer (Figure 59). These rainfall events had values ranging between 7.87mm to 39.37mm. Following the sampling in October there were heavy rainfall days on the 28th and 29th with 25.65mm and 25.91mm, respectively. These rainfall days along with the events experienced before the November samplings all contribute to the groundwater levels measured in the piezometers (Appendix 2 – table 19).

The sampling of piezometers on the 21st of December 2021 occurred following a period of heavy rainfall events between the 1st and 18th (Figure 60) this aligns with the very shallow groundwater levels. These rainfall events had values ranging between 0.25mm and 52.83mm (Appendix 2 – table 19).

The sampling of piezometers on the 24th of January 2022 occurred following a month of limited rainfall events with one small identifiable period occurring on the 20th and 21st of January (Figure 61) this aligns with the significant deepening of groundwater levels. These two rainfall events both had values of 7.37mm. Following the sampling days in December 2021 there were heavy rainfall days on the 28th and 29th with 13.72mm and 14.22mm, respectively. These rainfall days along with the events experienced before the January samplings all contribute to the groundwater levels measured in the piezometers (Appendix 2 – table 19).

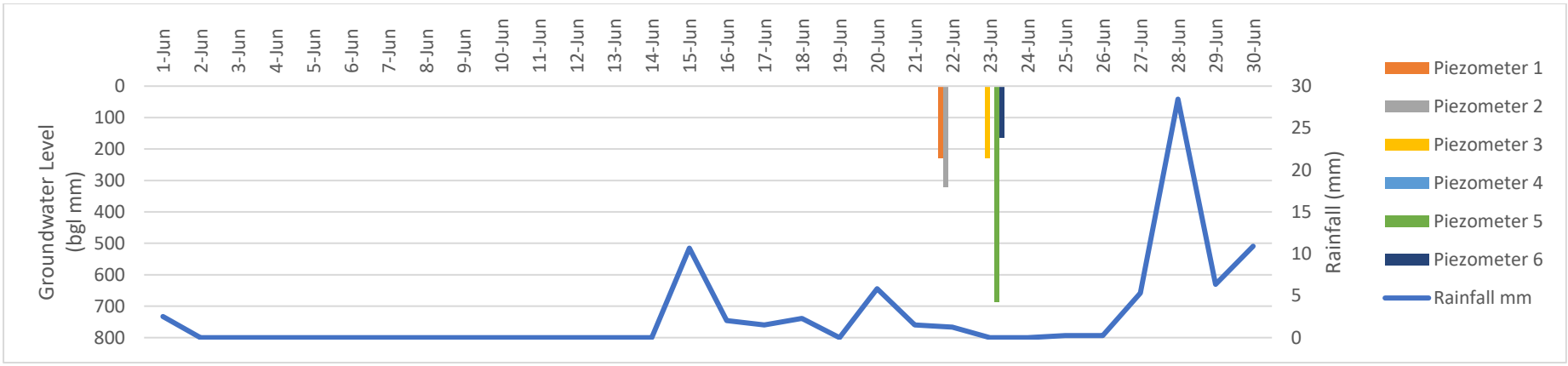


*Figure 55: Rainfall (blue line) vs piezometer groundwater levels (coloured bars) across the month of June 2021.*

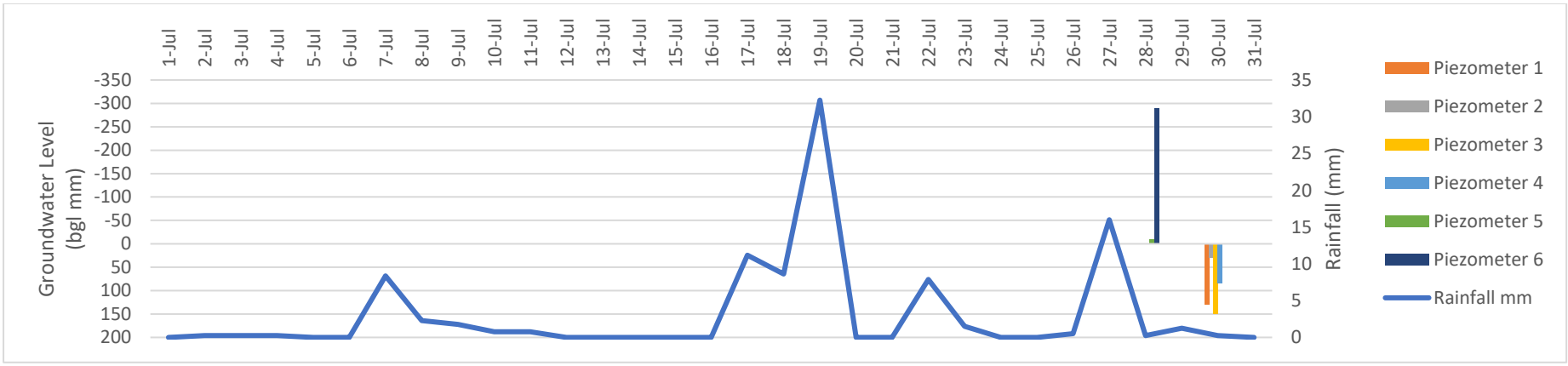


*Figure 56: Rainfall (blue line) vs piezometer groundwater levels (coloured bars) across the month of July 2021. The negative groundwater levels accounts for water being in the standpipe above ground level at the time of sampling.*

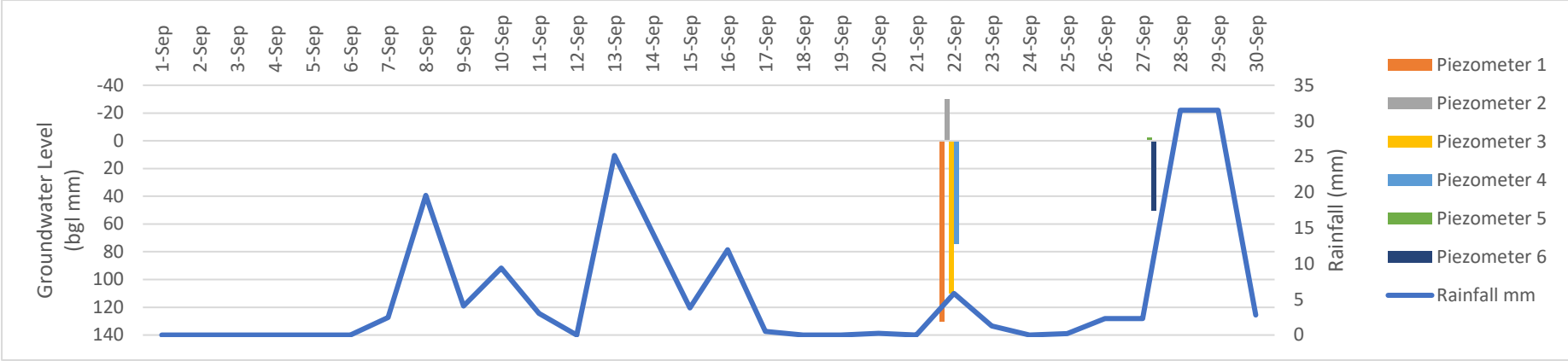


*Figure 57: Rainfall (blue line) vs piezometer groundwater levels (colour bars) across the month of September 2021. The negative groundwater levels accounts for water being in the standpipe above ground level at the time of sampling*

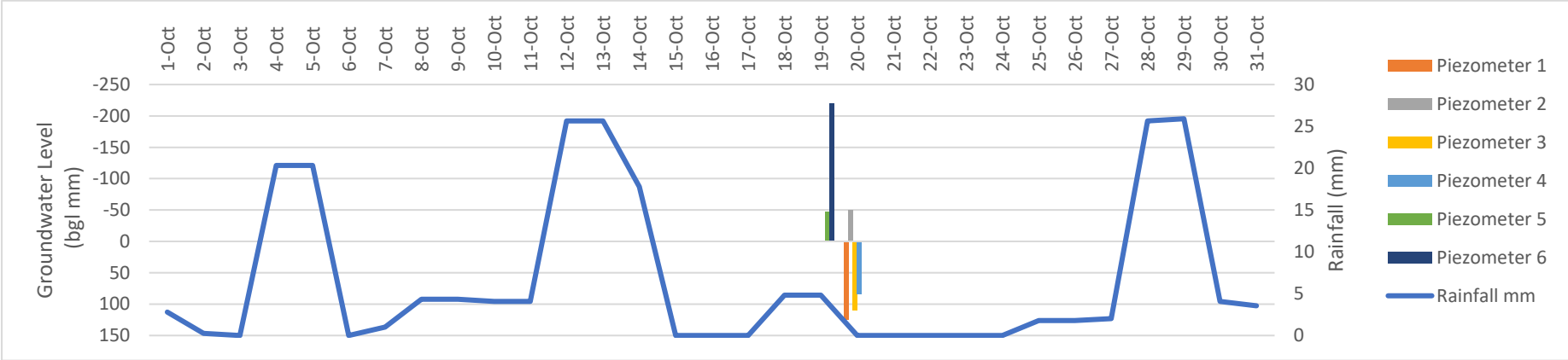


*Figure 58: Rainfall (blue lines) vs piezometer groundwater levels (colour bars) across the month of October 2021. The negative groundwater levels accounts for water being in the standpipe above ground level at the time of sampling*

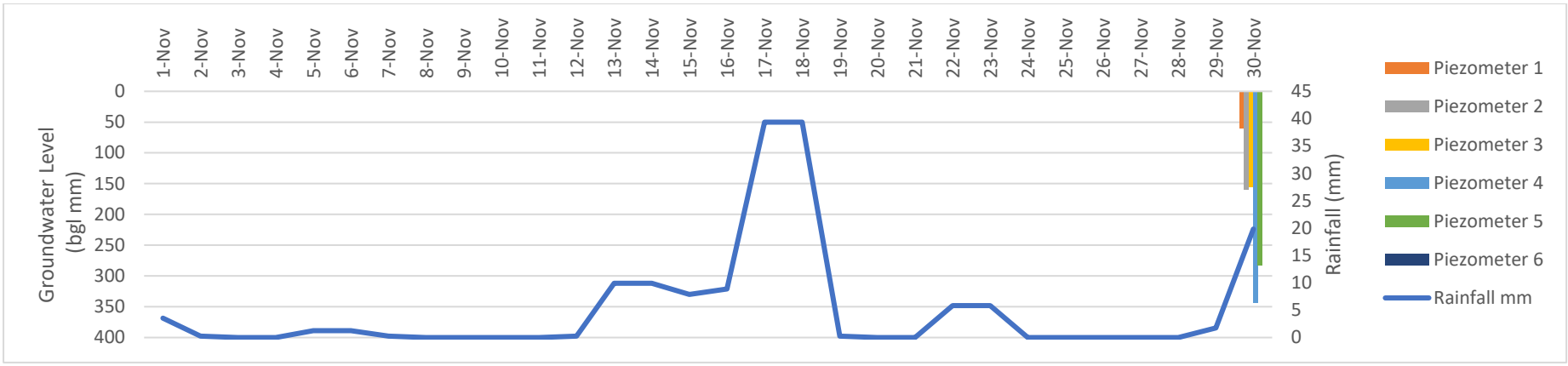


*Figure 59: Rainfall (blue line) vs piezometer groundwater levels (coloured bars) across the month of November 2021.*

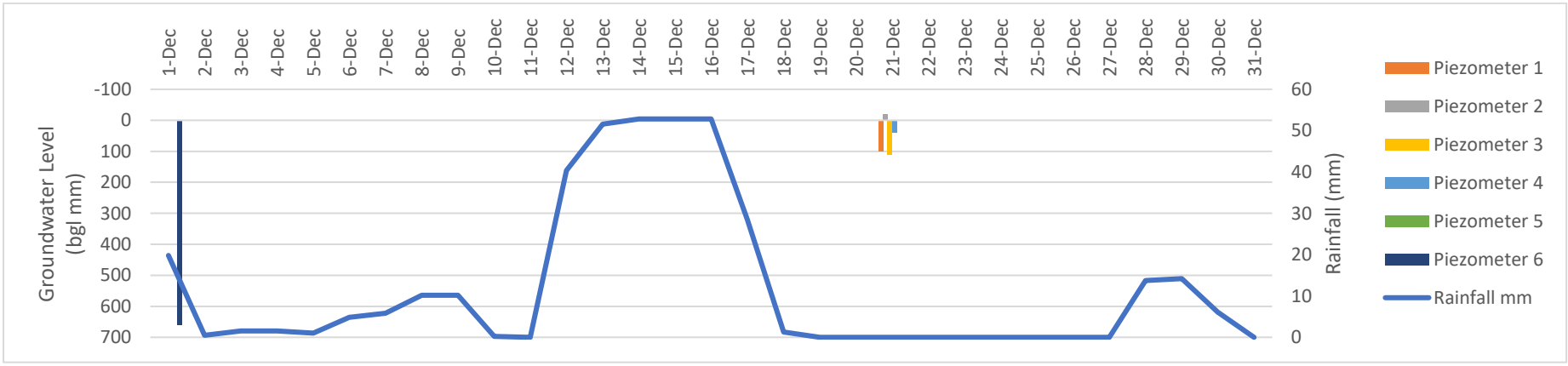


*Figure 60: Rainfall (blue line) vs piezometer groundwater levels (coloured bars) across the month of December 2021. The negative groundwater levels accounts for water being in the standpipe above ground level at the time of sampling*

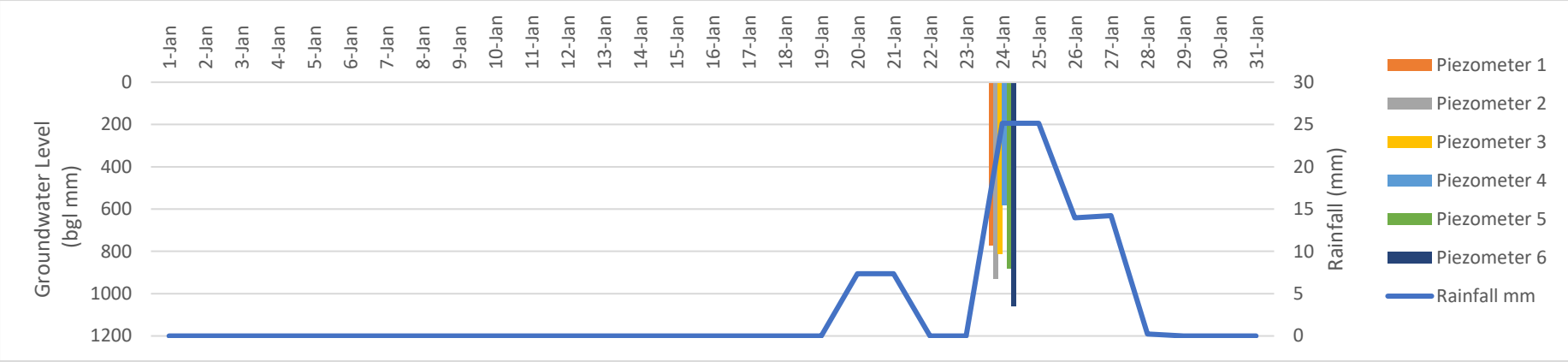


*Figure 61: Rainfall (blue line) vs piezometer groundwater levels (coloured bars) across the month of January 2022.*

### 5.1.3. Water Sensor Results

For the infield sensor sampling the first two months (June and July 2021) were disregarded for all piezometers due to incorrect sampling methods giving incorrect results. The samples that were collected were analysed in the field for RDO (readily dissolved oxygen), ORP (oxidation-reduction potential) and pH.

Piezometer 1 had 4 valid readings from the 7 months of sampling (Appendix 3 – table 20) with the sampling of January 2022 being incomplete due to the piezometer having low water levels insufficient enough for reliable sampling. The 4 valid samplings showed that the RDO results were all above 1mgL$^{-1}$ that range from 4.1mg$^{-1}$ to 1.2mgL$^{-1}$(Figure 62a). The results show a decreasing RDO trend throughout the months. The ORP results were all above 150mV with a range from 478mV to 222mV (Figure 62b). The results show no trends between the 4 months. The pH results range from 5.7 to 4.5 making them within the spectrum of being acidic (Figure 62c).

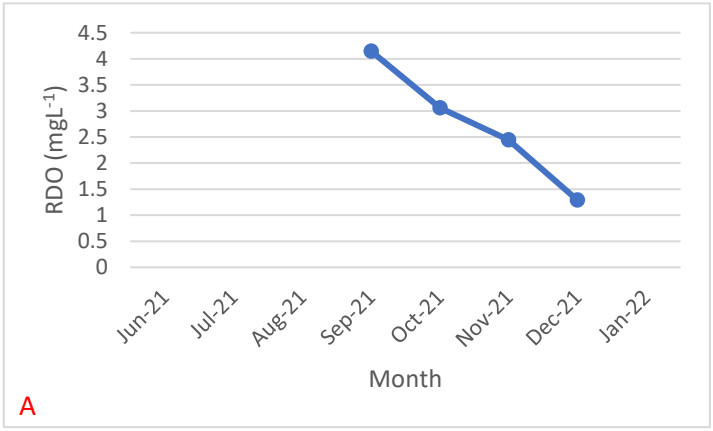


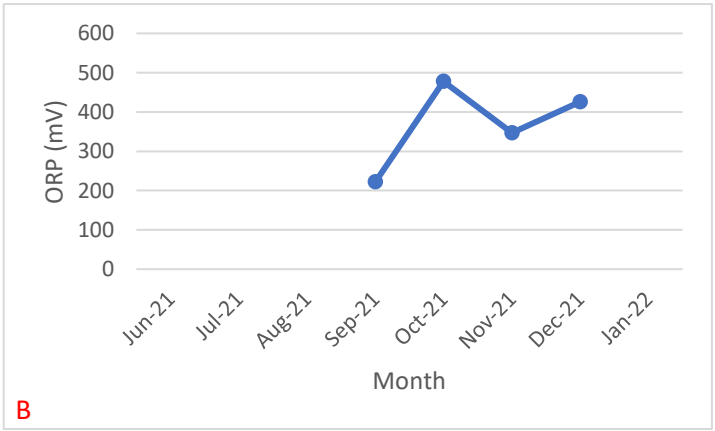


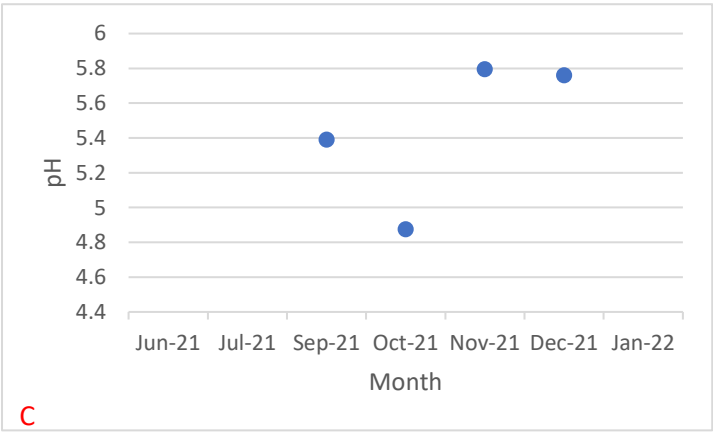


*Figure 62 : A) The readily dissolved oxygen (RDO – mgL$^{-1}$) results for piezometer 1. B) The oxidation-reduction potential (ORP – mV) results for piezometer 1. C) The pH results for piezometer 1.*

Piezometer 2 had 4 valid readings from the 7 months of sampling (Appendix 3 – table 21) with the sampling of January 20222 being incomplete due to there being a lack of water within the piezometer for reliable sampling. The 4 valid samplings showed that the RDO results were all below 1mg$^{-1}$ that range from 0.49mgL$^{-1}$ to 0.29 mgL$^{-1}$ (Figure 63a). The results show a decreasing RDO trend throughout the months. The ORP results were all above 150mV which range between 444.5mV to 402.2mV (Figure 63b). The same as piezometer 1, piezometer 2 shows no trend between the 4 months. The pH results are all within the spectrum of being acidic which range from 5.7 to 5.1 (Figure 63c).

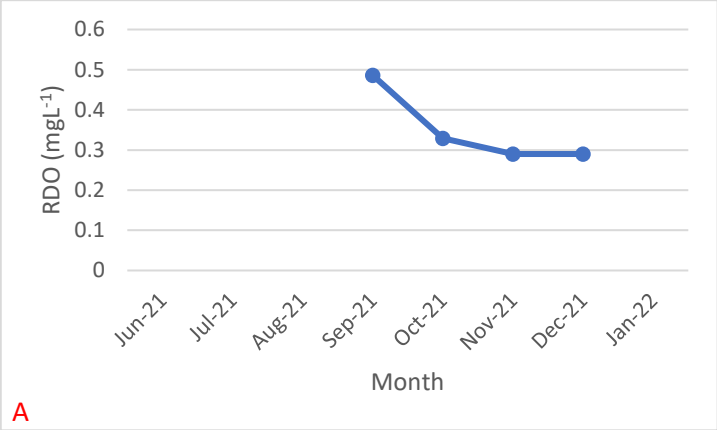


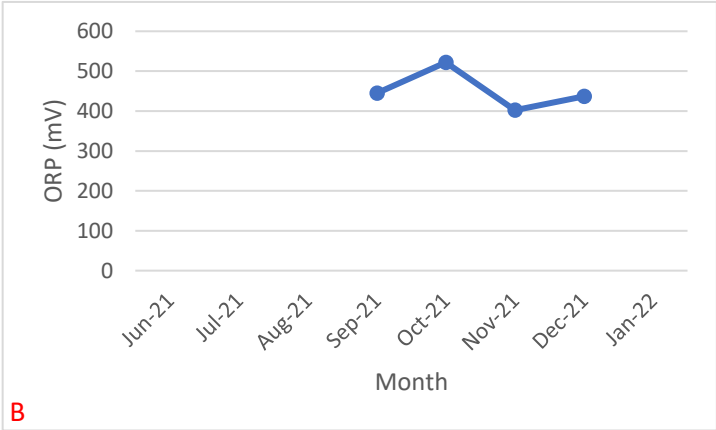


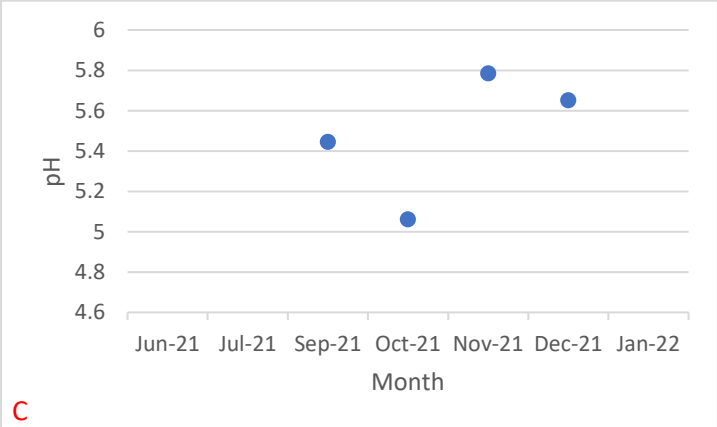


*Figure 63: A) The readily dissolved oxygen (RDO – mgL$^{-1}$) results for piezometer 2. B) The oxidation-reduction potential (ORP – mV) results for piezometer 2. C) The pH results for piezometer 2.*

Piezometer 3 from the 7 months of sampling had 4 valid readings (Appendix 3 – table 22) with the sampling for January 2022 not having enough water within the system to collect a reliable sample. The four valid samplings gave the following results for RDO. All 4 results were below 1mgL$^{-1}$ which ranged from 0.41mgL$^{-1}$ to 0.22mgL$^{-1}$ and showed no trend across the sampling months (Figure 64a). The ORP results showed a decreasing trend from 543mV to 427.1mV excluding September 2021 which is an outlier with 209.8mV (Figure 64b). The pH showed a decreasing trend from June 2021 to September 2021 which ranged from 4.998 to 2.998 excluding January 2022 which is an outlier at 5.22 with all results falling within the spectrum of being acidic (Figure 64c).

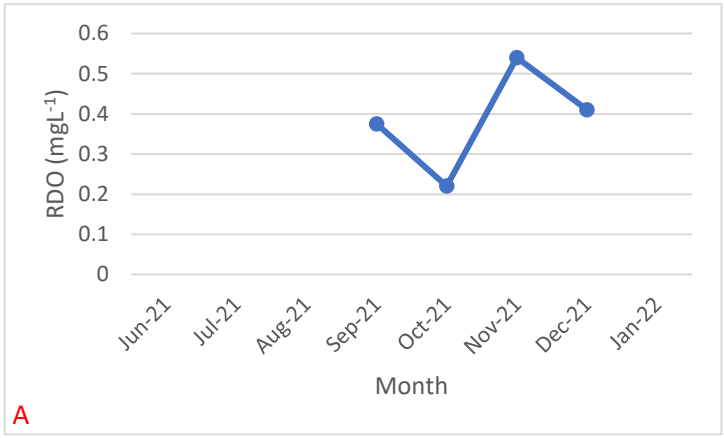


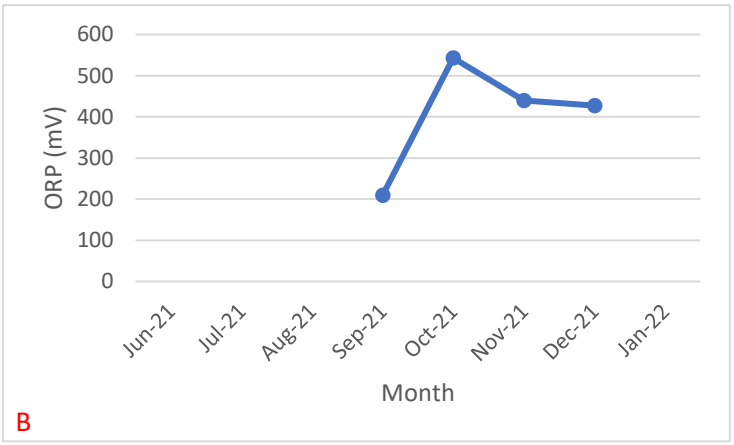


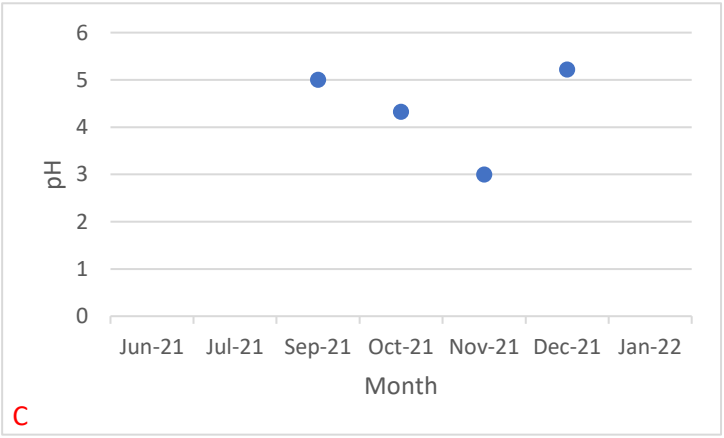


*Figure 64: A) The readily dissolved oxygen (RDO – mgL$^{-1}$) results for piezometer 3. B) The oxidation-reduction potential (ORP – mV) results for piezometer 3. C) The pH results for piezometer 3.*

Piezometer 4 from the 7 months of sampling had 4 valid readings (Appendix 3 – table 23). The sampling of January 2022 was incomplete due to lack of water within the piezometer for reliable sampling. The remaining 4 months of sampling showed that the RDO results were all below 1mgL$^{-1}$ and ranged between 0.26mgL$^{-1}$ to 0.43mgL$^{-1}$ presenting an increasing trend across the sampling months (Figure 65a). The ORP results showed no trend across the sampling months and all the results were above 150mV that ranged between 403.9mV and 747.3mV (Figure 65b). The pH readings were all within the spectrum of being acidic which ranged between 5.4 and 3.2 with no trend amongst the sampling months (Figure 65c).

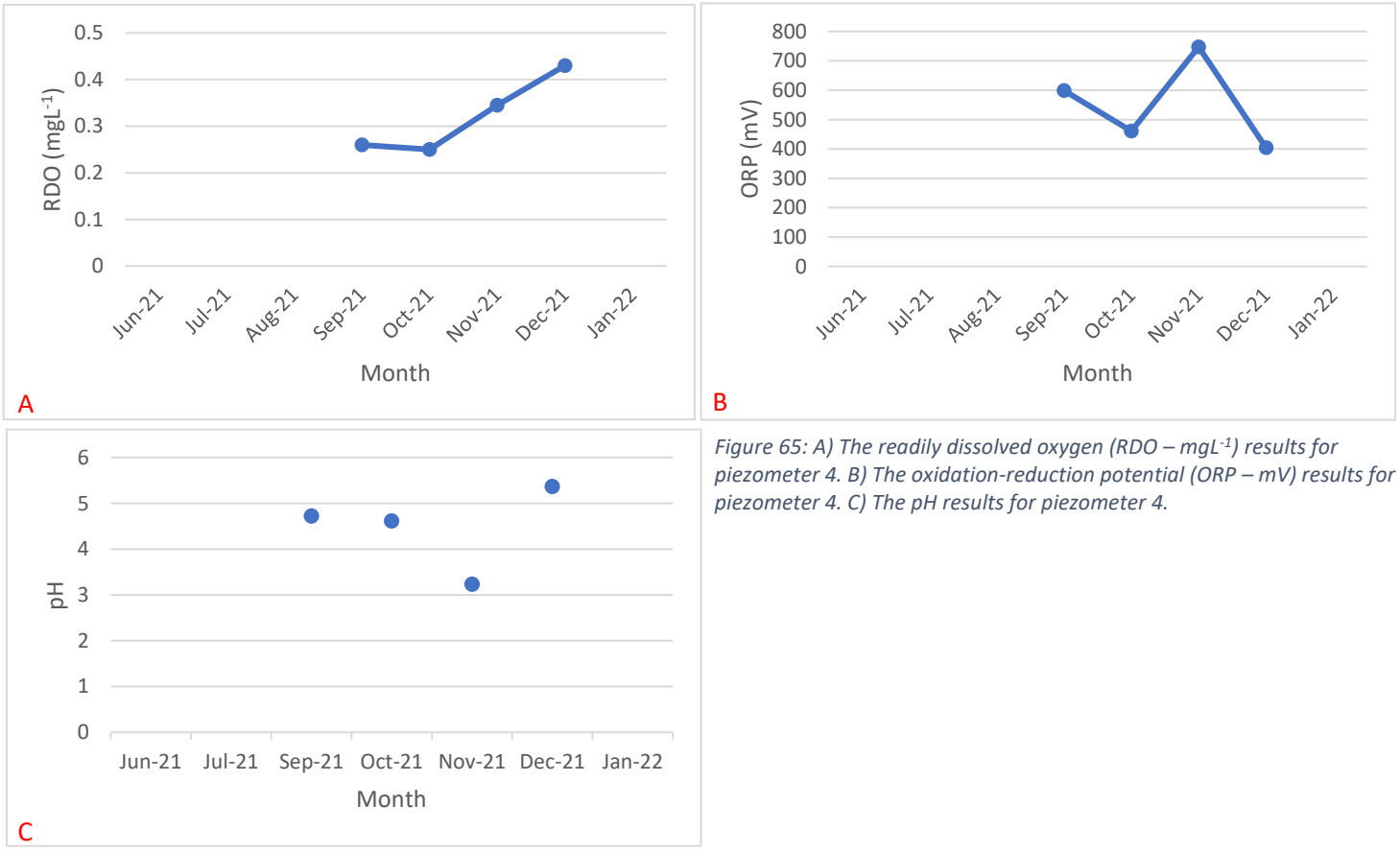


*Figure 65: A) The readily dissolved oxygen (RDO – mgL$^{-1}$) results for piezometer 4. B) The oxidation-reduction potential (ORP – mV) results for piezometer 4. C) The pH results for piezometer 4.*

Piezometer 5 had 5 valid readings from the 7 months of sampling (Appendix 3 – table 24). The RDO results had no trend across the sampling months, but all results were below 1mgL$^{-1}$ and ranged between 0.9mgL$^{-1}$ to 0.36mgL$^{-1}$ (Figure 66a). The ORP results were all above 150mV which ranged between 189.3mV and 711.9mV with no trend visible across the sampling months (Figure 66b). The pH results ranged between 4.6 and 5.58 showing that the results are within the spectrum of being acidic along with a weakly increasing trend across the sampling months (Figure 66c).

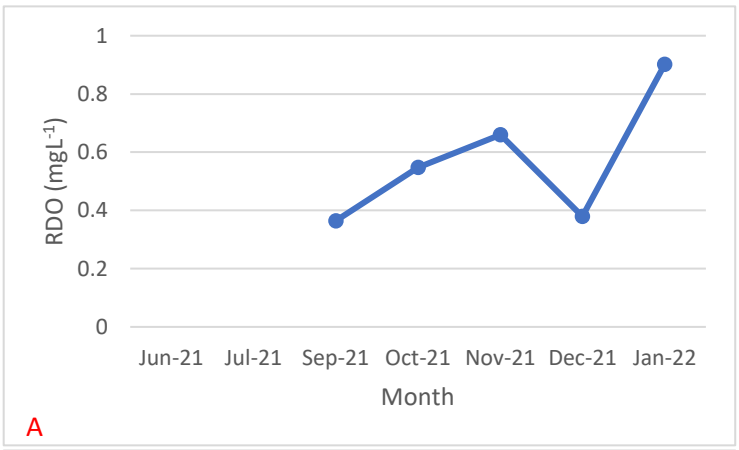


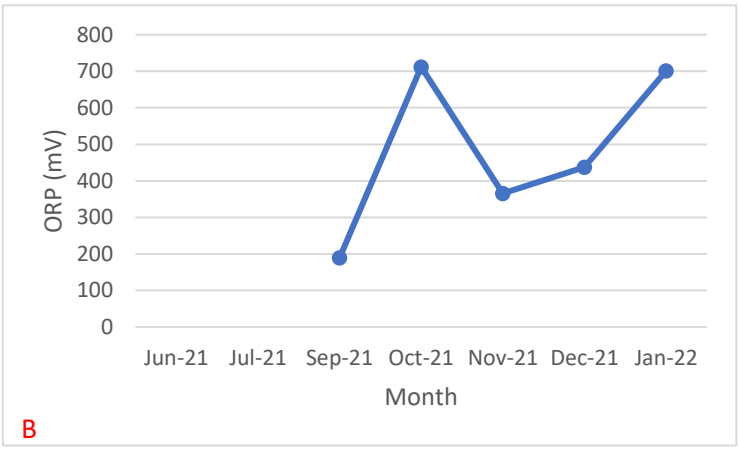


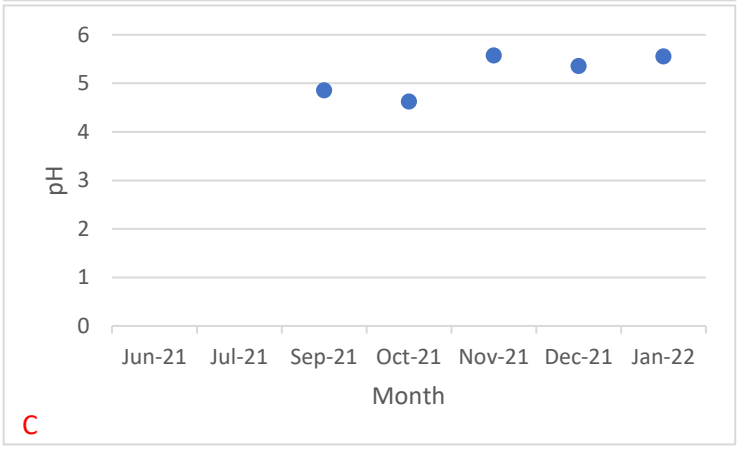


*Figure 66: A) The readily dissolved oxygen (RDO – mgL$^{-1}$) results for piezometer 5. B) The oxidation-reduction potential (ORP – mV) results for piezometer 5. C) The pH results for piezometer 5.*

Piezometer 6 had 3 valid readings from the 7 months of sampling (Appendix 3 – table 25) with the December 2021 and January 2022 samplings being incomplete due to the piezometer having low water levels insufficient enough for reliable sampling. The 3 RDO results showed that the September 2021 and October 2021 samplings were below 1mgL$^{-1}$ with 0.35mgL$^{-1}$ and 0.42mgL$^{-1}$ respectively while the November 2021 sampling was above 1mgL$^{-1}$ with 3.6mgL$^{-1}$ (Figure 67a). The ORP results showed that all the results were above 150mV apart from the September 2021 reading which was below 150mV. The results ranged from 138.2mV to 674.1mV with no visible trend across the sampling months (Figure 67b). The pH results were all within the spectrum of being acidic with a range between 5.5 and 4.2 (Figure 67c).

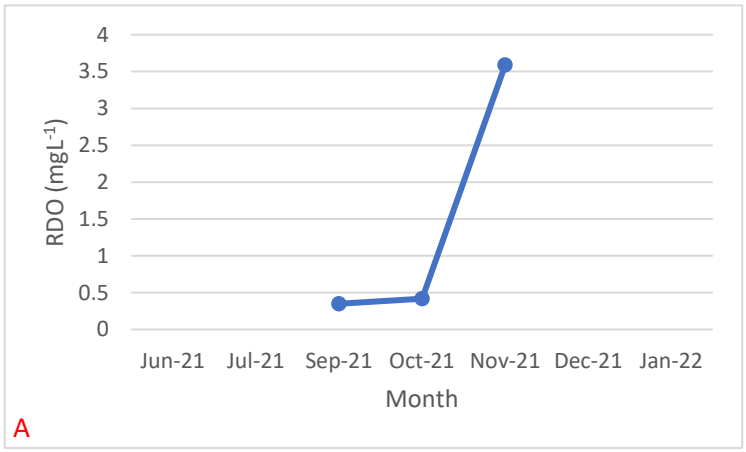



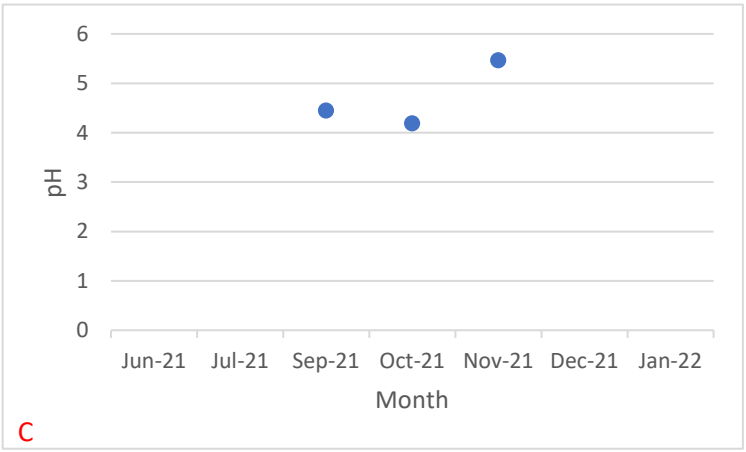


*Figure 67: A) The readily dissolved oxygen (RDO – mgL$^{-1}$) results for piezometer 6. B) The oxidation-reduction potential (ORP – mV) results for piezometer 6. C) The pH results for piezometer 6.*

## 5.2. Laboratory Results

### 5.2.1. Surface Water Results

The samplings for surface water 2 in June 2021, surface water 3 in June 2021 and July 2021, and surface water 4 in June 2021 and July 2021 were not completed due to these locations having yet to be identified and selected as sources of sampling of surface waters. The January 2022 samplings for surface water 2, 3 and 4 were not completed due to the water bodies at these locations were dried up at the time of sampling.

Surface Water 2 (Figure 33) had 5 valid sampling months and of the 5 valid sampling months the N-$NO_3$ results for September 2021 was below the detectable range resulting in no value being provided (Appendix 3 – table 26). The remaining N-$NO_3$ samples were all below 0.110mg$L^{-1}$ ranging from 0.025mg$L^{-1}$ to 0.143mg$L^{-1}$ except for the November 2021 with 1.291mg$L^{-1}$ (Figure 68a). The results show an increasing trend throughout the sampling months. The 5 valid DRP samples were above 0.010mg$L^{-1}$ ranging from 0.012mg$L^{-1}$ to 0.081mg$L^{-1}$ showing an increasing trend throughout the sampling months (Figure 68b).

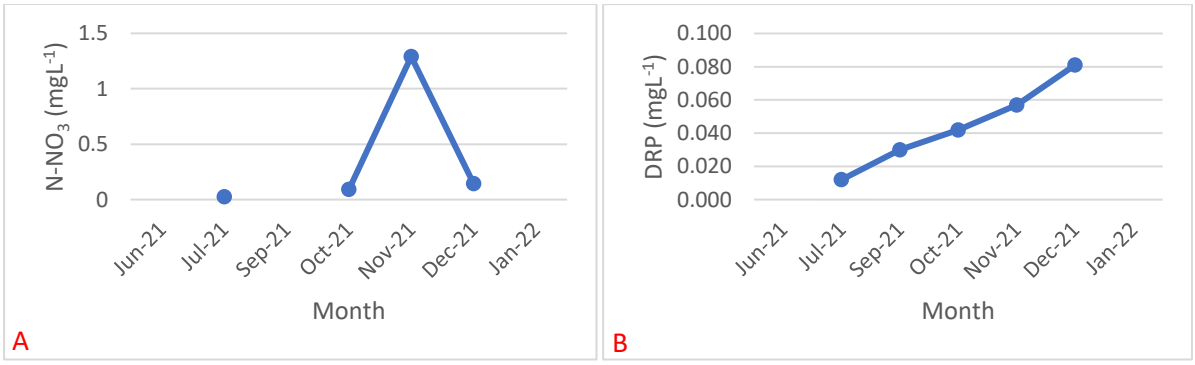


*Figure 68: A) The N-$NO_3$ (mg$L^{-1}$) results for Surface Water 2. B) The DRP (mg$L^{-1}$) results for Surface Water 2.*

Surface Water 3 (Figure 33) had 5 valid sampling months and of the 5 valid sampling months the N-$NO_3$ results for September 2021 was below detectable range resulting in no value being provided (Appendix 3 – table 27). The October 2021 and November 2021 samples were both above 0.110mg$L^{-1}$ with 3.44mg$L^{-1}$ and 0.33mg$L^{-1}$ respectively while the December 2021 sample was below 0.110mg$L^{-1}$. The results show a decreasing trend across the sampling months (Figure 69a). The 4 valid DRP samples were all above 0.010mg$L^{-1}$ ranging from 0.19mg$L^{-1}$ to 0.69mg$L^{-1}$ with a generalised increasing trend across the sampling months (Figure 69b).

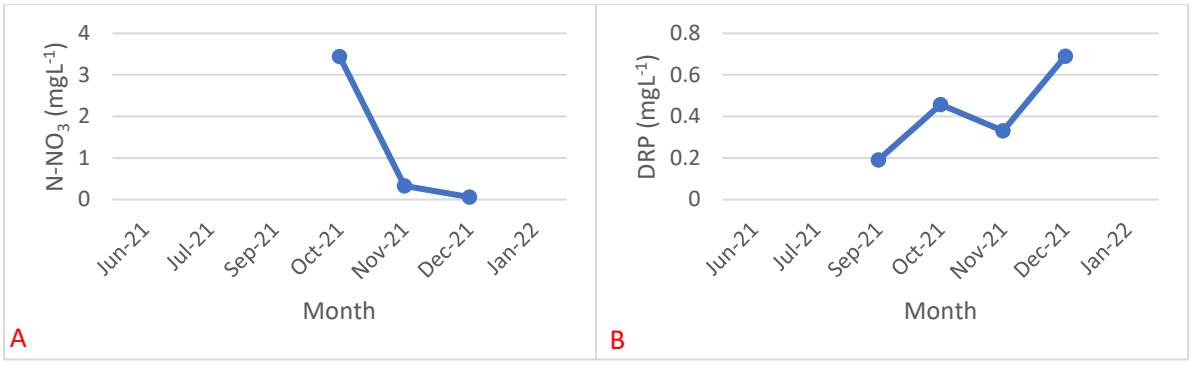


*Figure 69: A) The N-$NO_3$ ($mgL^{-1}$) results for Surface Water 3. B) The DRP ($mgL^{-1}$) results for Surface Water 3.*

Surface Water 4 (Figure 33) had 3 valid sampling months with the sampling in November 2021 was incomplete due to the water source having low levels insufficient enough for reliable sampling. (Appendix 3 – table 28). Of the 3 valid sampling months the N-$NO_3$ sample for December 2021 was above $0.110mgL^{-1}$ at $0.34mgL^{-1}$ while the September 2021 and October 2021 samples were below $0.110mgL^{-1}$ with $0.098mgL^{-1}$ and $0.083mgL^{-1,}$ respectively. There is no visible trend across the sampling months (Figure 70a). The 3 valid DRP samples were all above $0.010mgL^{-1}$ ranging from $0.083mgL^{-1}$ to $0.104mgL^{-1}$ with no visible trend across the sampling months (Figure 70b).

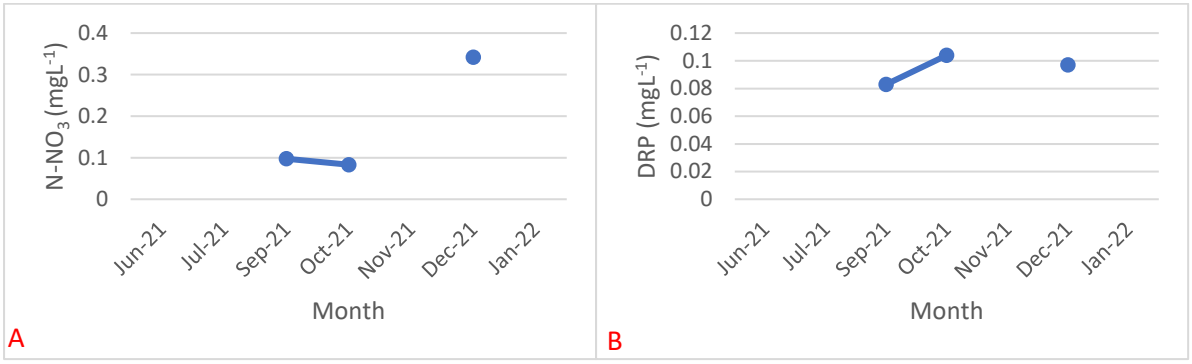


*Figure 70: A) The N-$NO_3$ ($mgL^{-1}$) results for Surface Water 4. B) The DRP ($mgL^{-1}$) results for Surface Water 4.*

Surface Water 5 (Figure 33) had 7 valid sampling months; however, the November 2021 showed the N-$NO_3$ results were below detectable range resulting in no value being provided (Appendix 3 – table 29). From the remaining sampling months, the samples from July 2021 and December 2021 were all below $0.110mgL^{-1}$ with $0.090mgL^{-1}$ and $0.019mgL^{-1}$ respectively. The samplings from June 2021, September 2021, October 2021, and January 2022 were all above $0.110mgL^{-1}$ ranging between $0.13mgL^{-1}$ to $5.61mgL^{-1}$. The results show a generalised increase in trend until the sudden increase in January 2022 (Figure 71a). The 7 valid DRP samples were all above $0.010mgL^{-1}$ ranging from $0.055mgL^{-1}$ to $0.591mgL^{-1}$ with no visible trend across the sampling months (Figure 71b).

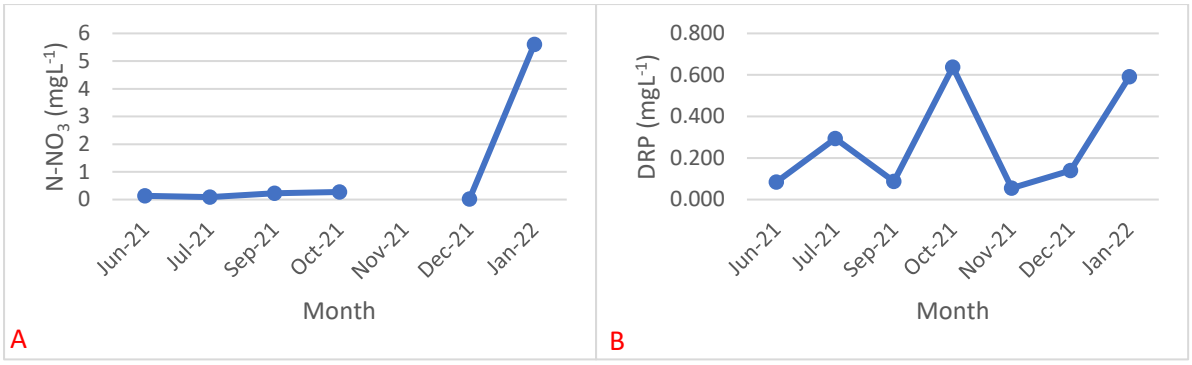


*Figure 71: A) The N-$NO_3$ ($mgL^{-1}$) results for Surface Water 5. B) The DRP ($mgL^{-1}$) results for Surface Water 5.*

### 5.2.2. Ground Water Results

Piezometer 1 had 6 valid sampling months with the sampling for January 2022 being incomplete due to the piezometer having low water levels insufficient enough for reliable sampling. The analysing for N-$NO_3$ from the June 2021, July 2021, October 2021, and November 2021 samples were below detectable range resulting in no value being provided (Appendix 3 – table 20). From the remaining sampling months, the sample from September 2021 was below $0.110mgL^{-1}$ with $0.017mgL^{-1}$ while the sample from December 2021 was above $0.110mgL^{-1}$ with $0.70mgL^{-1}$. There is no visible trend across the sampling months for N-$NO_3$ (Figure 72a). The 6 valid DRP samples were all above $0.010mgL^{-1}$ ranging from $0.040mgL^{-1}$ to $0.22mgL^{-1}$ with an increasing trend across the sampling months (Figure 72b).

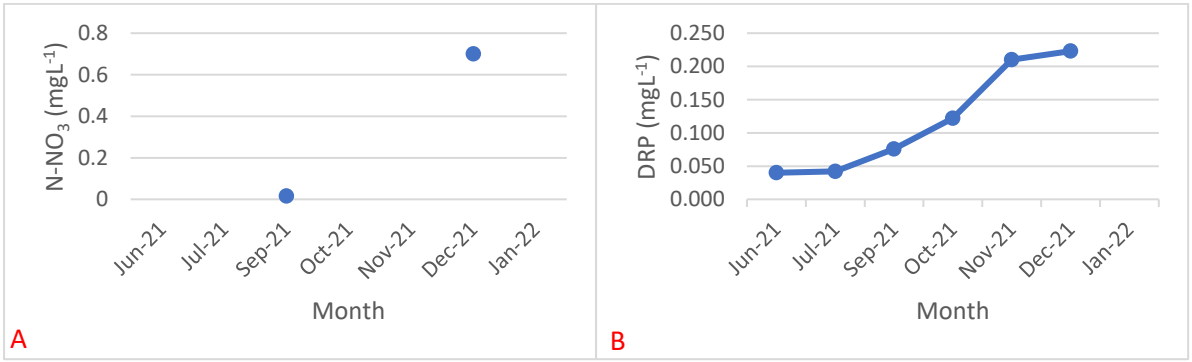


*Figure 72: A) The N-$NO_3$ ($mgL^{-1}$) results for Piezometer 1. B) The DRP ($mgL^{-1}$) results for Piezometer 1.*

Piezometer 2 had 6 valid sampling months due to the piezometer having low water levels insufficient enough for reliable sampling for January 2022. However, the analysing for N-$NO_3$ from the June 2021 and September 2021 samplings were below detectable range resulting in no values being provided (Appendix 3 – table 21). From the remaining sampling months, the samples for July 2021, October 2021, November 2021, and December 2021 were all below $0.110mgL^{-1}$ ranging from $0.032mgL^{-1}$ to $0.049mgL^{-1}$. The results show no trend across the sampling months (Figure 73a). The 6

valid sampling months for DRP were all above 0.010mgL$^{-1}$ ranging from 0.024mgL$^{-1}$ to 0.087mgL$^{-1}$ with the results showing a general increasing trend across the sampling months (Figure 73b).

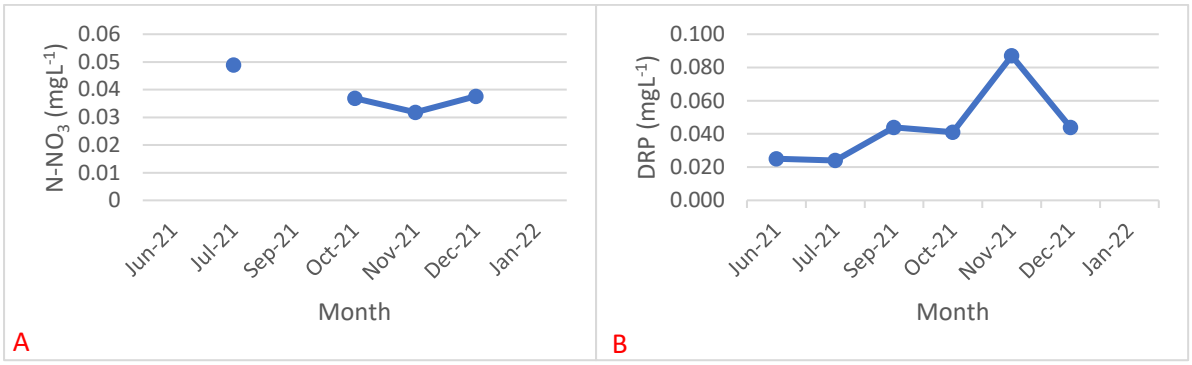


*Figure 73: A) The N-NO$_3$ (mgL$^{-1}$) results for Piezometer 2. B) The DRP (mgL$^{-1}$) results for Piezometer 2.*

Piezometer 3 had 6 valid sampling months due to the piezometer having low water levels insufficient enough for reliable sampling for January 2022 (Appendix 3 – table 22). The N-NO$_3$ analysing for the July 2021 sampling was above 0.110mgL$^{-1}$ with 0.24mgL$^{-1}$. The remaining sampling months were all below 0.110mgL$^{-1}$ ranging from 0.0084mgL$^{-1}$ to 0.105mgL$^{-1}$ with no visible trend across the sampling months (Figure 74a). The 6 valid sampling months for DRP were all above 0.010mgL$^{-1}$ ranging from 0.032mgL$^{-1}$ to 0.068mgL$^{-1}$ with a visible increase in the results across the sampling months (Figure 74b).

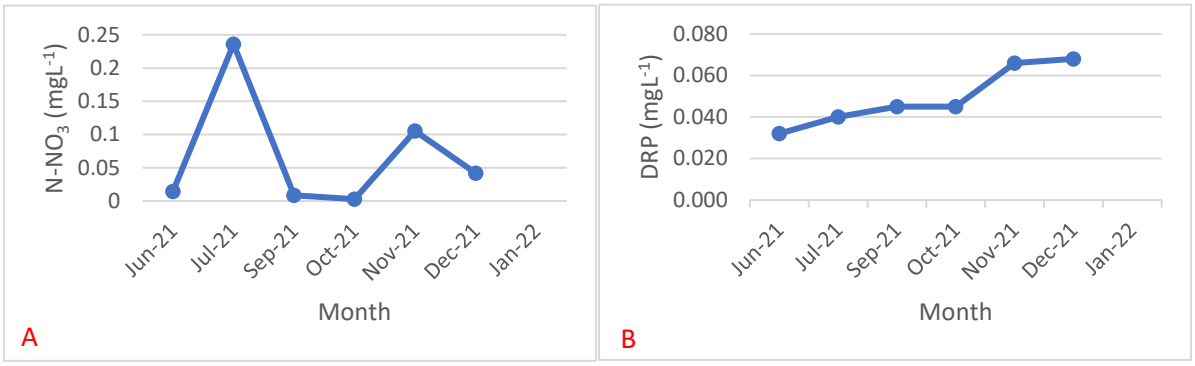


*Figure 74: A) The N-NO$_3$ (mgL-1) results for Piezometer 3. B) The DRP (mgL-1) results for Piezometer 3.*

Piezometer 4 had 5 valid sampling months due to the piezometer being dried up for the June 2021 and due to the piezometer having low water levels insufficient enough for reliable sampling for January 2022. However, the analysing for N-NO$_3$ for the November 2021 and December 2021 samplings were below detectable range resulting in no values being provided (Appendix 3 – table 23). From the remaining sampling months, the samples were all below 0.110mgL$^{-1}$ ranging from 0.15mgL$^{-1}$ to 0.29mgL$^{-1}$ with no visible trend across the sampling months (Figure 75a). The 5 valid

sampling months for DRP were all above 0.010mgL$^{-1}$ ranging from 0.041mgL$^{-1}$ to 0.19mgL$^{-1}$ with an increasing trend across the sampling months until December 2021 (Figure 75b).

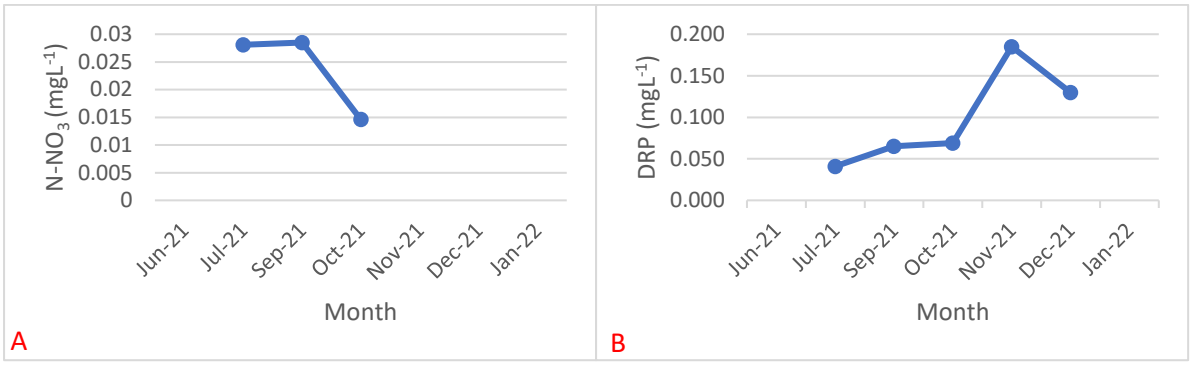


*Figure 75: A) The N-NO$_3$ (mgL$^{-1}$) results for Piezometer 4. B) The DRP (mgL$^{-1}$) results for Piezometer 4.*

Piezometer 5 had 7 valid sampling months, however, the analysing for N-NO$_3$ from the June 2021, July 2021 and January 2022 samplings were all below detectable range resulting in no values being provided (Appendix 3 – table 24). From the remaining sampling months, the samples for September 2021, October 2021, November 2021, and December 2021 were all below 0.110mgL$^{-1}$ ranging from 0.017mgL$^{-1}$ to 0.067mgL$^{-1}$ with a weak declining trend until December 2021 (Figure 76a). The 7 valid sampling months for DRP were all above 0.010mgL$^{-1}$ ranging from 0.039mgL$^{-1}$ to 0.45mgL$^{-1}$ with no visible trend across the sampling months other than a significant peak in October 2021 (Figure 76b).

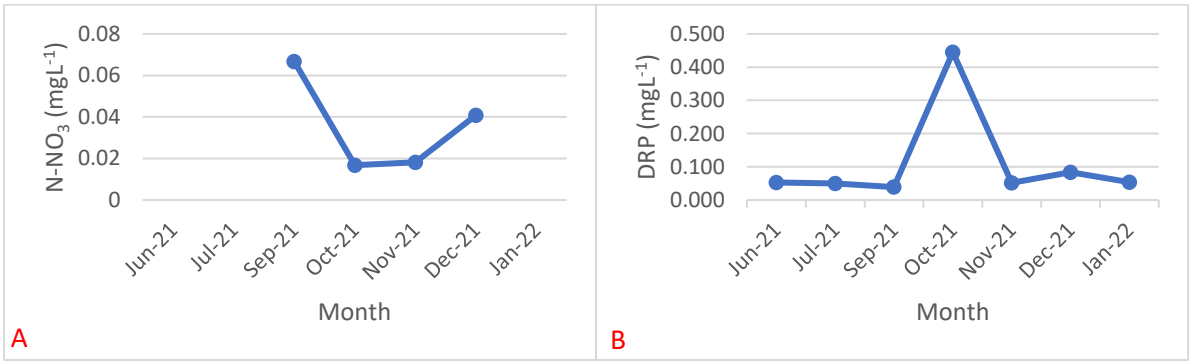


*Figure 76: A) The N-NO$_3$ (mgL$^{-1}$) results for Piezometer 5. B) The DRP (mgL$^{-1}$) results for Piezometer 5.*

Piezometer 6 had 5 valid sampling months due to being unable to sample the piezometer for December 2021 while the piezometer had low water levels insufficient enough for reliable sampling for January 2022 (Appendix 3 – table 25). However, the analysing for N-NO$_3$ from the July 2021 and December 2021 samplings were below detectable range resulting in no values being provided. From the remaining sampling months, the samples for September 2021, October 2021 and November 2021 were all below 0.110mgL$^{-1}$ ranging from 0.024mgL$^{-1}$ to 0.049mgL$^{-1}$ while the sampling from June 2021 was above 0.110mgL$^{-1}$ with 1.11mgL$^{-1}$. The results show no visible trend across the

sampling months (Figure 77a). The 5 valid sampling months for DRP were above 0.010mgL$^{-1}$ ranging from 0.040mgL$^{-1}$ to 0.13mgL$^{-1}$ with an increasing trend across the sampling months (Figure 77b).

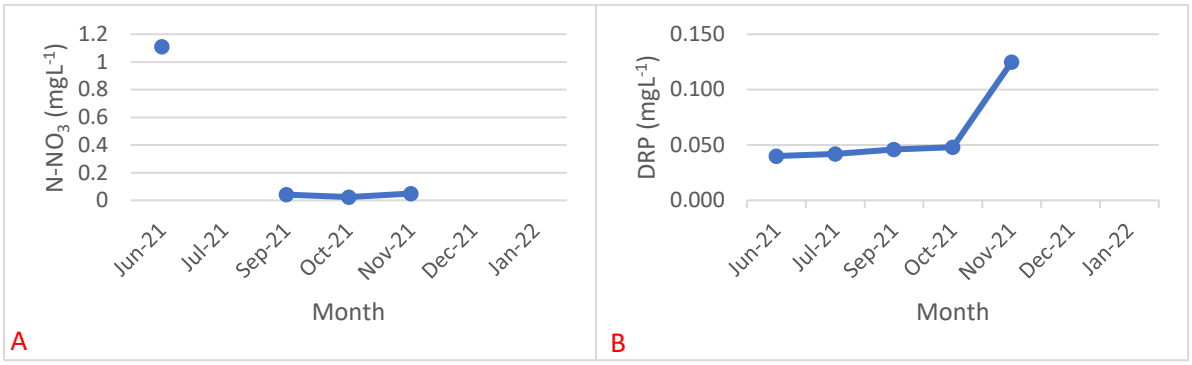


*Figure 77: A) The N-NO$_3$ (mgL$^{-1}$) results for Piezometer 6. B) The DRP (mgL$^{-1}$) results for Piezometer 6.*

### 5.2.3. Surface Water vs Ground Water (Sensor results vs lab results)

The July 2021 N-NO$_3$ sampling for piezometer 2 was the only month where the piezometer results were higher than the surface water results with 0.049mgL$^{-1}$ and 0.025mgL$^{-1}$ respectively. The October 2021, November 2021, and December 2021 samplings all had surface water N-NO$_3$ results higher than the results presented for piezometer 2. The October 2021, November 2021, and December surface water results were 0.09mgL$^{-1}$, 1.29mgL$^{-1}$, and 0.1425mgL$^{-1}$ respectively with the November 2021 surface water results being significantly higher than piezometer 2 results. The results for September 2021 surface water and piezometer 2 were both below detectable level with June 2021 piezometer 2 also being below detectable level. The results for January 2022 for both surface water 2 and piezometer 2 were not comparable due to both months not having enough sample for analysis (Figure 78a; Appendix 3).

The October 2021, November 2021, and December 2021 N-NO$_3$ surface water 3 results were all above the piezometer 3 results for the relevant months with the October 2021 surface water being significantly higher than the piezometer 3 results. The results for surface water 3 for the months stated were 3.44mgL$^{-1}$, 0.33mgL$^{-1}$, and 0.06mgL$^{-1}$ respectively and the results for piezometer 3 were 0.0028mgL$^{-1}$, 0.113mgL$^{-1}$, and 0.042mgL$^{-1}$. The July 2021 piezometer sample cannot be compared to the surface water results due to the surface water not being sampled for this month. The September 2021 surface water 3 results were below detectable level when compared with the piezometer 3 results. The results for January 2022 for both surface water 3 and piezometer 3 were not comparable due to both months not having enough sample for analysis (Figure 78b; Appendix 3).

The September 2021, October 2021, and December 2021 N-NO$_3$ surface water results are all higher than the piezometer 4 results for the associated months, with December 2021 being significantly

higher than the piezometer 4 results. The results for surface water 4 for the months stated were 0.098mgL$^{-1}$, 0.08mgL$^{-1}$, and 0.34mgL$^{-1}$ respectively with the results for piezometer 4 being 0.029mgL$^{-1}$ and 0.015mgL$^{-1}$ respectively for September 2021 and October 2021 while Piezometer 4 results for December 2021 were below detectable level. The July 2021 piezometer sample cannot be compared with the surface water results due to the surface water not being sampled for this month. Surface water 4 and piezometer 4 both had results that were below detectable level for November 2021. The results for January 2022 for both surface water 4 and piezometer 4 were not comparable due to both months not having enough sample for analysis (Figure 78c; Appendix 3).

The December 2021 piezometer 5 N-$NO_3$ result was the only month that had results higher than the surface water results. The piezometer 5 results were 0.041mgL$^{-1}$ compared to surface water 5 results of 0.019mgL$^{-1}$. June 2021, July 2021, September 2021, October 2021, and January 2022 all had surface water results higher than piezometer 5 results, with January 2021 surface water being significantly higher than the piezometer results. The surface water 5 results for the stated months were 0.13mgL$^{-1}$, 0.09mgL$^{-1}$, 0.23mgL$^{-1}$, 0.27mgL$^{-1}$, 0.019mgL$^{-1}$, and 5.61mgL$^{-1}$ respectively. The piezometer 5 results for September 2021, October 2021, and November 2021 were 0.067mgL$^{-1}$, 0.017mgL$^{-1}$, and 0.018mgL$^{-1}$ respectively. The piezometer 5 results for June and July were both below detectable level while the surface water 5 results for November 2021 was also below detectable level. The piezometer 5 results for January 2022 cannot be compared with the surface water 5 results for January 2022 due to there not being enough sample collected from the piezometer to analysed (Figure 78d; Appendix 3).

The October 2021 and December 2021 DRP results were the only months that had higher surface water 2 results when compared with piezometer 2, with December 2021 being significantly higher. The surface water 2 results for the stated months were 0.042mgL$^{-1}$ and 0.081mgL$^{-1}$ respectively while compared to piezometer 2 results of 0.041mgL$^{-1}$ and 0.044mgL$^{-1}$ respectively. July 2021, September 2021, and November 2021 all had higher piezometer 2 results when compared to surface water 2, with November 2021 being significantly higher. The July 2021, September 2021, and November 2021 piezometer 2 results were 0.024mgL$^{-1}$, 0.044mgL$^{-1}$, and 0.087mgL$^{-1}$ respectively with the surface water 2 results being 0.012mgL$^{-1}$, 0.030mgL$^{-1}$ and 0.057mgL$^{-1}$ respectively. The piezometer 2 results cannot be compared to the results for surface water 2 from July 2021 due to the surface water not being sampled. The results for January 2022 for both surface water 2 and piezometer 2 were not comparable due to both months not having enough sample for analysis (Figure 78e; Appendix 3).

The September 2021, October 2021, November 2021, and December 2021 DRP results for surface water 3 were all above the piezometer 3 results with December 2021 being significantly higher than the piezometer results. The DRP results for surface water were 0.19mgL$^{-1}$, 0.46mgL$^{-1}$, 0.33mgL$^{-1}$, and 0.69mgL$^{-1}$ respectively while the piezometer results were 0.045mgL$^{-1}$, 0.045mgL$^{-1}$, 0.066mgL$^{-1}$, and 0.068mgL$^{-1}$ respectively. The June 2021 and July 2021 results for piezometer 3 cannot be compared to surface water 3 results as surface water 3 was not sampled during these respective months. The results for January 2022 for both surface water 3 and piezometer 3 were not comparable due to both months not having enough sample for analysis (Figure 78f; Appendix 3).

The September 2021 and October 2021 DRP results for surface water 4 were all above the piezometer 4 results. The surface water results were 0.083mgL$^{-1}$ and 0.10mgL$^{-1}$ respectively while the piezometer results were 0.065mgL$^{-1}$ and 0.069mgL$^{-1}$. The July 2021 piezometer results cannot be compared with the surface water results due to the surface water not being sampled. The November 2021 piezometer results also cannot be compared to the surface water results due to there not being enough sample to analyse for DRP. The results for January 2022 for both surface water 4 and piezometer 4 were not comparable due to both months not having enough sample for analysis (Figure 784g; Appendix 3).

The surface water 5 results for all sample months from June 2021 to January 2022 were all above the results for piezometer 5 with January 2022 being significantly higher. The surface water 5 results for the months of June 2021, July 2021, September 2021, October 2021, November 2021, December 2021, and January 2022 were 0.085mgL$^{-1}$, 0.29mgL$^{-1}$, 0.087mgL$^{-1}$, 0.64mgL$^{-1}$, 0.055mgL$^{-1}$, 0.14mgL$^{-1}$, and 0.59mgL$^{-1}$ respectively. The results for piezometer 5 for the sampling months were 0.053mgL$^{-1}$, 0.05mgL$^{-1}$, 0.039mgL$^{-1}$, 0.45mgL$^{-1}$, 0.052mgL$^{-1}$, 0.084mgL$^{-1}$, and 0.054mgL$^{-1}$ respectively (Figure 78h; Appendix 3).

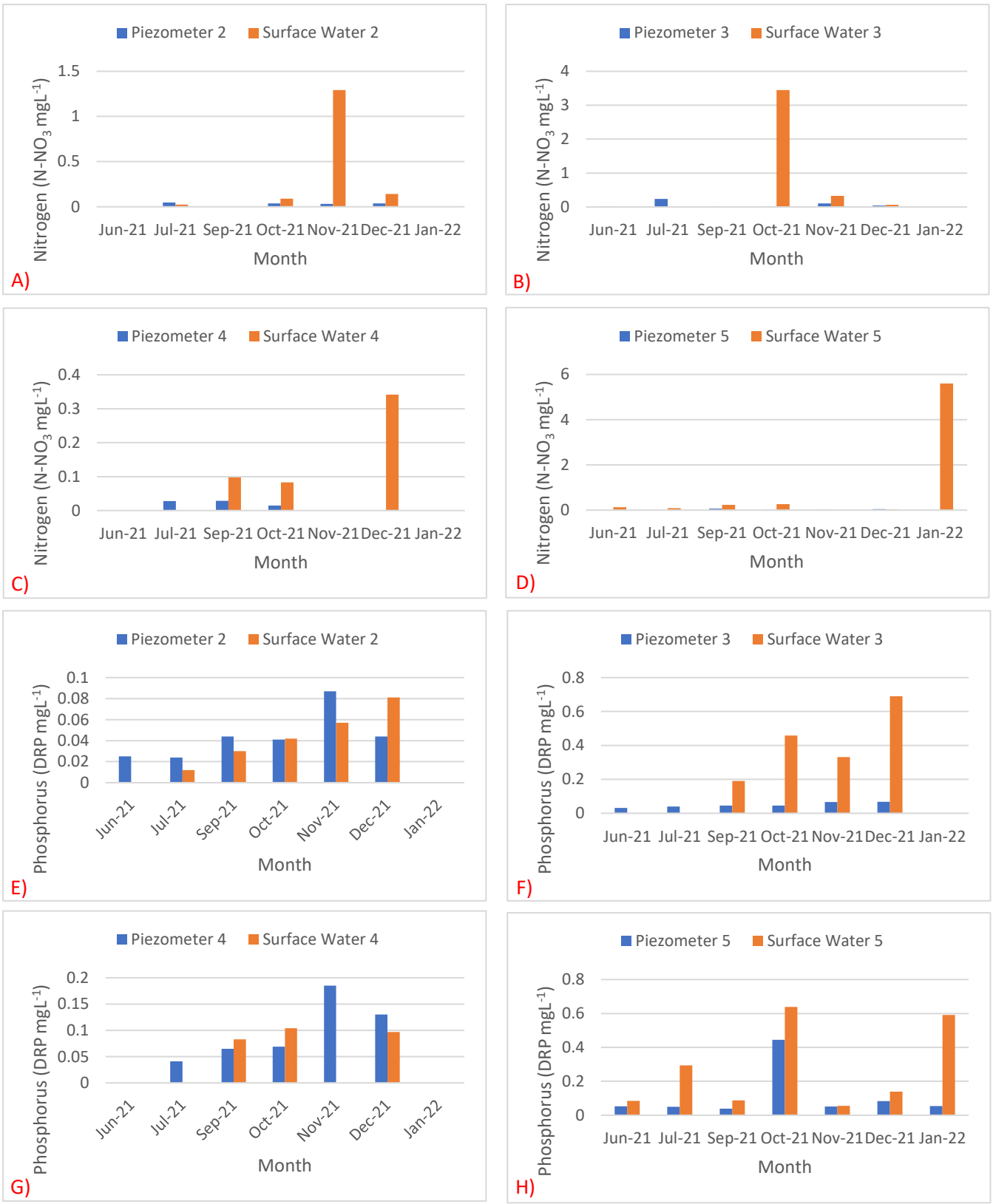


*Figure 78: A) Nitrogen (N-$NO_3$mgL$^{-1}$) of piezometer 2 vs surface water 2. B) Nitrogen (N-$NO_3$mgL$^{-1}$) of piezometer 3 vs surface water 3. C) Nitrogen (N-$NO_3$mgL$^{-1}$) of piezometer 4 vs surface water 4. D) Nitrogen (N-$NO_3$mgL$^{-1}$) of piezometer 5 vs surface water 5. E) Phosphorus (DRP mgL$^{-1}$) of piezometer 2 vs surface water 2. F) Phosphorus (DRP mgL$^{-1}$) of piezometer 3 vs surface water 3. G) Phosphorus (DRP mgL$^{-1}$) of piezometer 4 vs surface water 4. H) Phosphorus (DRP mgL$^{-1}$) of piezometer 5 vs surface water 5.*

## 5.3. Geographic Information Systems (GIS) Results

### 5.3.1. Slope, Aspect, & Landform Elements

The slope image (Figure 81) created from the 1m DEM retrieved (Figures 79 & 80) showed the result that the steep (26-35°) and very steep (>35°) classes dominated the study area with coverage of approximately 45% with steep being the dominant slope identified . Flat to gently undulating (0-3°) has the lowest area coverage with approximately 3% (Table 14).

The aspect results (Figure 82) derived from the 1m DEM (Figure 79 & 80) showed that South and West aspects are dominating approximately 61% coverage with South being the dominant class (Table 15).

The landform elements image (Figure 83) derived from the 1m DEM (Figure 79 & 80) showed that over half of the study area was unclassified with valleys occupying approximately 15% of the remaining area (Table 16).

The elevation profile utilised for the development of the soil landscape model was created from three profile lines (Figure 53). The resulting elevation profiles are presented in appendix 5 - figures 114, 115 and 116.

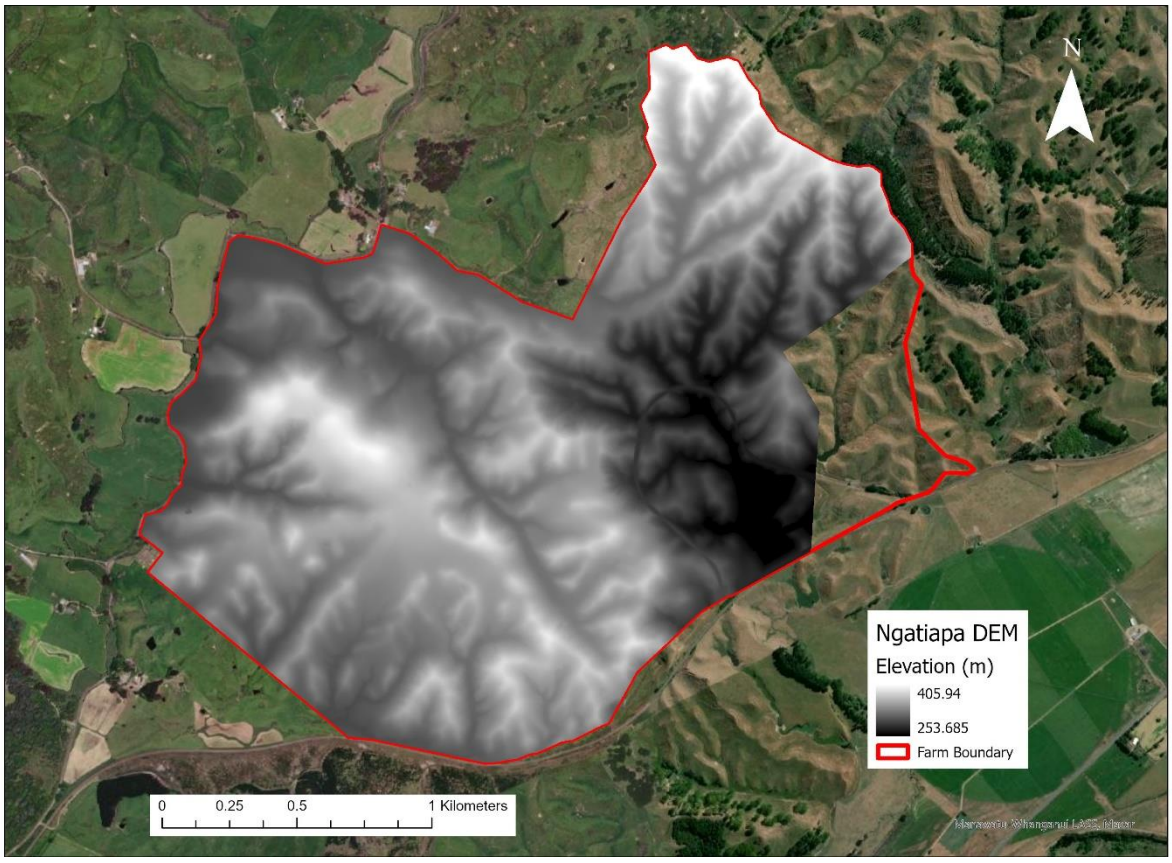


*Figure 79: The DEM retrieved for the base of GIS analysis after being clipped to the farm boundary extent (Red line).*

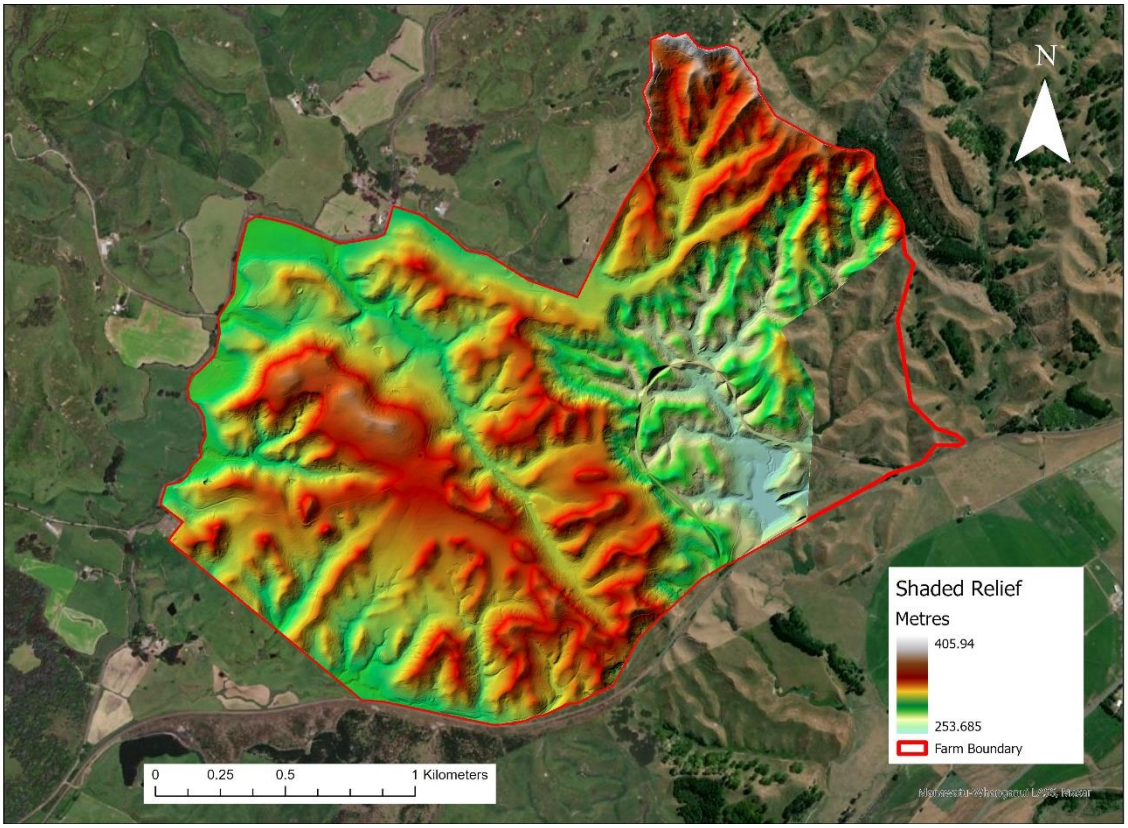


*Figure 80: Hill shade distribution across Ngatiapa based off a 1m DEM using GIS.*

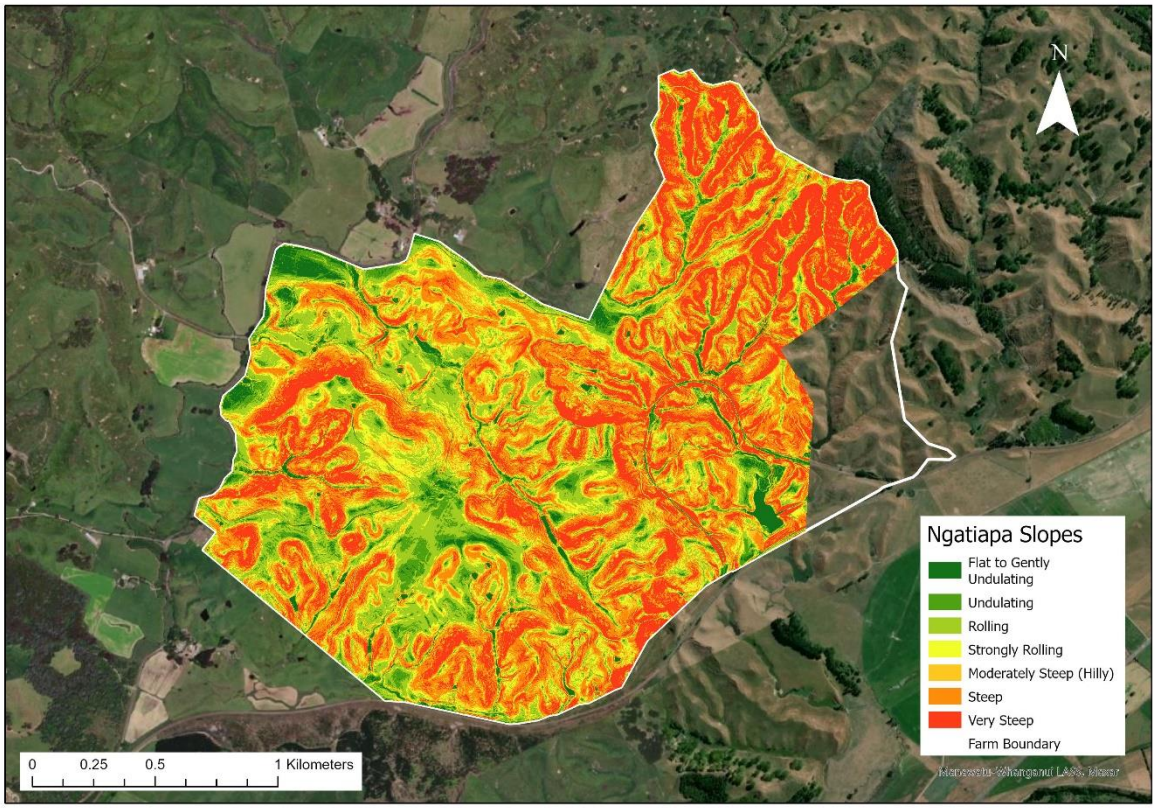


*Figure 81: Slope class distribution across the farm based off of a 1m DEM using GIS.*

| Slope | Area (Ha) | Area % |
|---|---|---|
| Steep (26-35°) | 110.9185 | 24.25 |
| Very Steep (>35) | 96.5219 | 21.10 |
| Rolling (8-15°) | 71.9905 | 15.74 |
| Moderately Steep – Hilly (21-25°) | 50.2463 | 10.99 |
| Strongly Rolling (16-20°) | 48.611 | 10.63 |
| No Coverage (No DEM coverage on farm) | 35.8196 | 7.83 |
| Undulating (4-7°) | 26.9968 | 5.90 |
| Flat to gently undulating (0-3°) | 13.8585 | 3.02 |

*Table 14: Slope class distribution across the farm in area ha and area %. Total farm area based off area provided by landowner (457.40ha).*

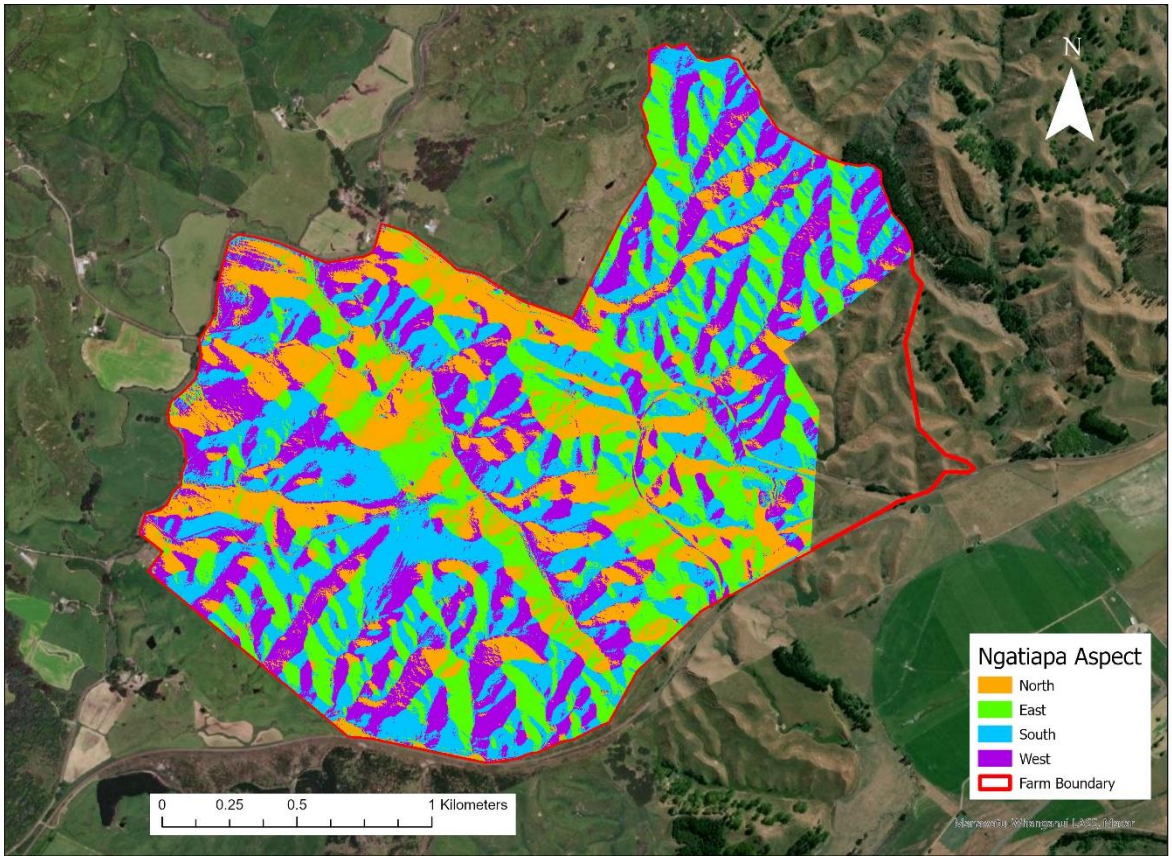


*Figure 82: Aspect class distribution across Ngatiapa based off of a 1m DEM using GIS.*

| Aspect | Area (Ha) | Area % |
|---|---|---|
| South | 124.4154 | 27.20 |
| West | 105.0235 | 22.96 |
| East | 97.2400 | 21.26 |
| North | 91.3126 | 19.96 |
| Flat | 1.1537 | 0.25 |
| No Coverage (No DEM coverage on farm) | 35.8179 | 7.83 |

*Table 15: Aspect class distribution across the study area in area ha and area %. Total farm area based off area provided by landowner (457.40ha).*

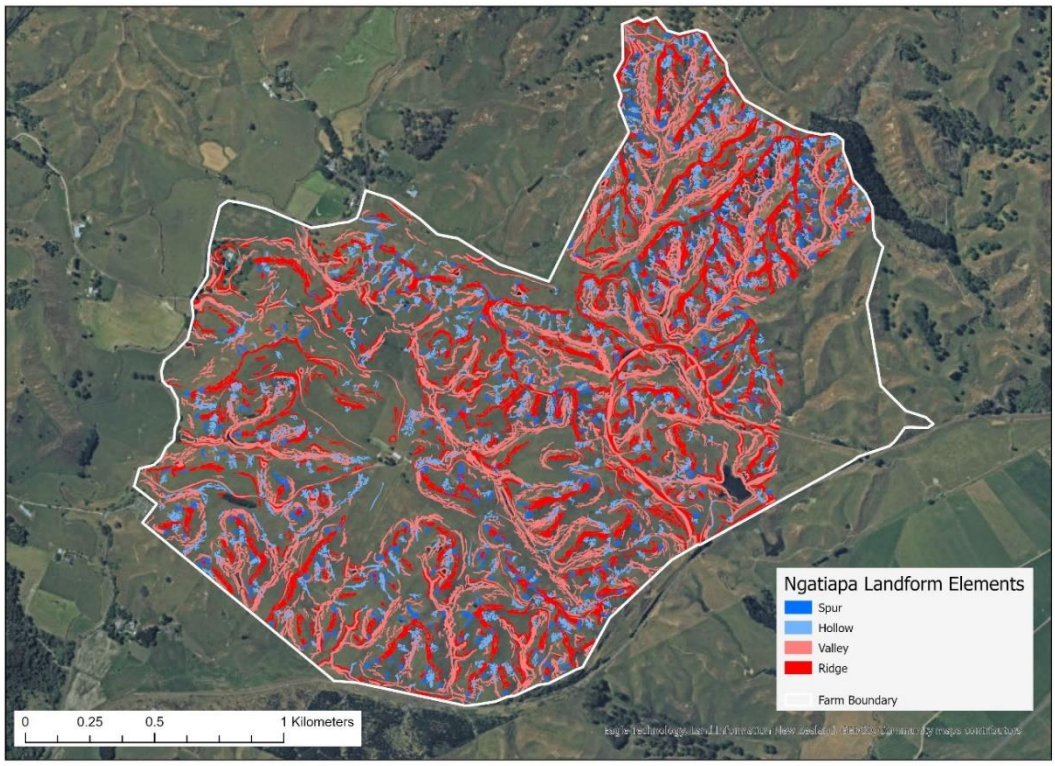


*Figure 83: Landform element class distribution across Ngatiapa based off of a 1m DEM using GIS.*

| Landform Element | Area (Ha) | Area % |
|---|---|---|
| Valley | 70.5340 | 15.42 |
| Ridge | 52.3260 | 11.44 |
| Hollow | 22.9614 | 5.02 |
| Spur | 10.1290 | 2.21 |
| Other | 265.6300 | 58.07 |
| No Coverage (No DEM coverage on farm) | 35.8196 | 7.83 |

*Table 16: Landform element class distribution across Ngatiapa (area ha and area %). Total farm area based off area provided by landowner (457.40ha).*

# Chapter 6 – Discussion

## 6.1. Fieldwork Discussion

### 6.1.1. Soil Mapping

During the beginning stage of field work, the presence of COVID-19 throughout New Zealand resulted in lockdowns and continued restrictions for travel, inhibiting the accessibility to the study area. Following the alleviation of restrictions access was limited due to the occurrence of the lambing and calving period on the farm. The north-western reaches of the study area was not accessed for safety reasons due to the steep terrain. This limited accessibility to the study area prevented the extent and quantity of soil descriptions and information collected for this thesis. The soil descriptions completed resulted in areas that required interpretation from areas of similarity (e.g., landscapes with related landforms, identical vegetation cover and distribution etc) to give a complete overview of the study area. Increased soil description numbers across the eastern reaches of the farm and on the border of the western reaches of the farm are needed to improve results. A wider distribution of soil descriptions will help differentiate the soils of the landscape (e.g., the soils between the steep land of the north-eastern reaches and the south-eastern reaches beneath the old main-line railway tracks) and further distinguish drainage status.

Existing soil mapping of the Rangitikei region (such as the Soil Map of Rangitikei County (Maanaki Whenua Landcare Research, 2010)) have pre-existing names that are associated to units with smaller scales (1:63 360). The larger scales used within this study results in units that are different to those that are described for the larger scaled units. Units with no pre-existing names required names to be created. The names that were used reflect the surrounding locations.

Soil type identifications were used to create soil orders. The Pallic Soils cover approximately 50% of the study area. This high proportion  is to be expected as conditions hypothesised for Pallic soil formation (including silica-sedimentary parent material and an annual rainfall levels by Hewitt, Balks, & Lowe (2021) and Molloy (1988)The environments of Ngatiapa have these supporting properties for the formation of these soils, specifcally the wetting/drying cycles of soils throughout summer and winter and conform to the following hypotheses set out by Hewitt, Balks & Lowe (2021) and Molloy (1988). These soils have been identified to be structurally unstable and erosion prone (determined by low porosity and dense subsoils) under cultivation, initiating a vulnerability to slip and sheet erosion on hill and steep slopesThe suseptability of Pallic Soils to summer drought and winter-spring wet is exagerated by slow subsoil permeability and restricted root depth.The limited root depth indicates limited water movement often forming perched water tables in winter and spring. The dry/wet cycles often form desiccation shrinkages consequently initiating cracking (often in

hexagonal patterns) limiting structural strength of the soil profile. The movement of Pallic Soils particularly on rolling surface and steeper slopes results in catena formations being predominant. The soils identified as Pallicare further conforming to the description that Pallic soils are predominanlty silt loam in texture with low clay content (Molloy, 1988).

Brown Soils were identified to cover the remaining 50% of the study area. The large allocation of Brown soils was to be expected with the geology of Ngatiapa conforming to the principal that Brown soils develop in locations that comonly have silica rich parent materials that are typically of sedimentary origin (Molloy, 1988). In addition to the geology conforming the annual rainfall received within the Rangitikei region is supplementing the theory for the formation of Brown Soils. Brown Soils have been shown to have predominantly silt loam textures but occasionally have sandy loam textures with moderate clay content (Molloy, 1988). These texutres are evident within the Brown Soils identified across Ngatiapa.

Brown and Pallic soils are often found alongside each other with the soil moisture of slopes influencing the occurance of these two soils. Brown Soils have been interpreted to developon more stable slopes that have higher soil moisture while Pallic Soils have been interpreted to develop on drier slopes and at lower altitudes (Hewitt, Balks, & Lowe, 2021). Hewitt, Balks & Lowe (2021) identified the interaction between aspect and slope provides an environment of high soil variability. Therefore the soils found conformed to the accepted information hypothesis

The smallest allocation of soils was identified as Gley Soils, with literature modeling their formation being dependent on impeded drainage that excludes oxygen from all or some horizons within the soil profile throughout formation (Molloy, 1988). Identified swamp deposits were located in areas of depressions across the study area, supporting the impedance on drainage, inhibiting oxidation of the profile further aiding the hypothesis of Gley soil formation. Gley Soils have been seen to be a feature of catena formation in association with Pallic Soils, linked to the movement of sediment and solutes and occur in shallow valleys (Hewitt, Balks, & Lowe, 2021). Sediment and material movements within a soil catena or within a K-cycle system, are deposited along valley floors and at the base of slopes forming colluvial deposits. Over time these deposits, depending on drainage status and position in the landscape, are liable to develop into swamp deposits and/or Gley Soils (Figure 84). The presence of peat (Figure 85 – Appendix 4) supports the hypothesis of Gley soil formation influenced by soil catena or being within a K-cycle. Drainage accumulation and the swamp deposit parent material all support the formation of these Gley Soils, with further supporting evidence of oxygen occlusion present within the soil profiles.

*Figure 84: A shallow valley floor identified on Ngatiapa with low drainage capability (identified by the ephemeral stream and surface ponding) with a potential for sediment and material movement off the steep slopes. Conforming to the conditions hypothesised for swamp deposit formation and/or Gley soil formation.*

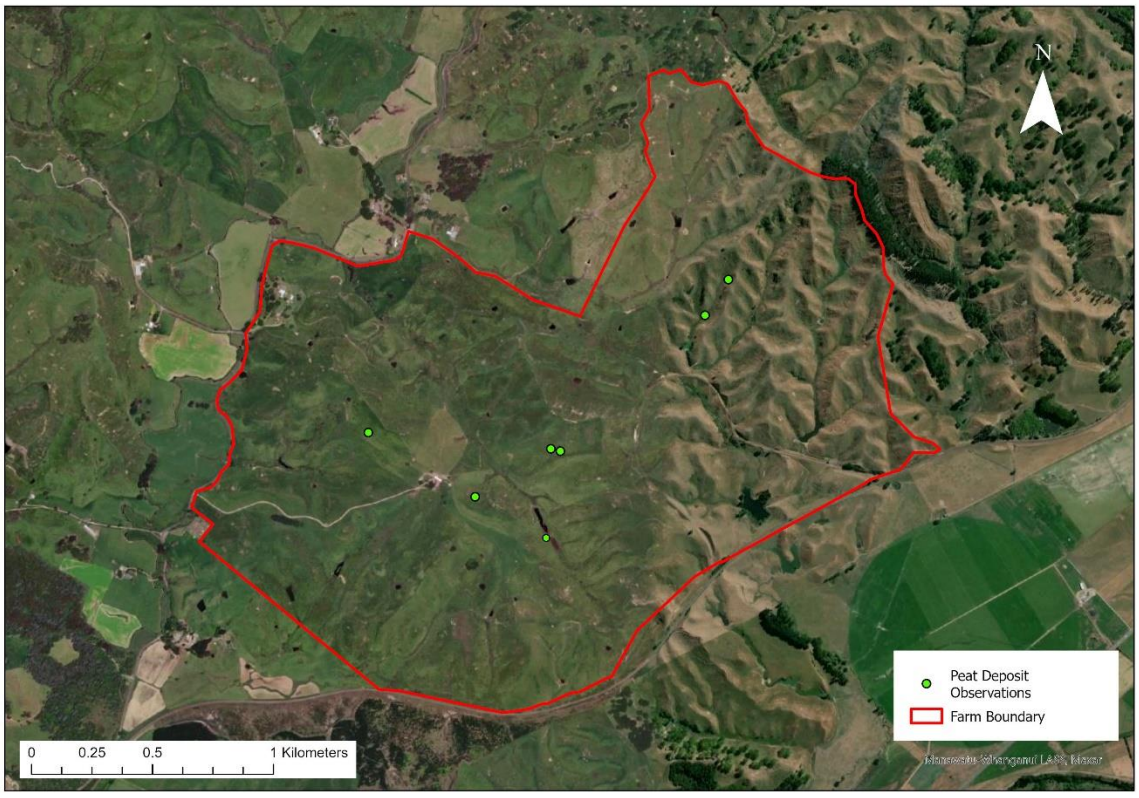


*Figure 85: The presence of peaty wood deposits within soil profiles across Ngatiapa, discovered during soil sampling.*

Drainage classes were assigned to each of the soils identified across Ngatiapa. Pallic Soils have been shown to have imperfectly to poorly drained soils, while Brown Soils have well to moderately well draining soils (Molloy, 1988), with Gley Soils having poor to very poor drainage. 50% of drainage identified across the study area conforms to the definition of being imperfectly and well drained (Figure 43), these high percentages when aligned with soil order (Figure 42) corroborates the relationship between soil drainage and soil order across Ngatiapa. The Gley Soils in valleys and depression, that have swamp deposit parent material, corroborates the drainage relationship to soil order by expresing poor drainage (Figure 43). These drainage factors all have different influences to the transport and removal of nitrogen ($N\text{-}NO_3$) throughout the soil profile. Roley et al (2012) concludes that the longer the residence time of $N\text{-}NO_3$ within the soil profile the more exposure there is for denitrification proccess to occur, with organic matter providing sources of electrons for denitrification. The evidence of peat within soils at locations across Ngatiapa (within valley floors, drainage pathways at base of slopes and within stabilised depressions on slopes) (Figure 85) coincides with the low $N\text{-}NO_3$ levels experienced across sampling sites (Chapter 5.2). Thus, demonstrating the theory stated by Roley (2012) where the poor drainage of the Gley Soils will result in an increased residence time and increased anoxic conditions, and theoretically increase the exposure of $N\text{-}NO_3$ to denitrifying factors. It can therefore be postulated that the high proportion of imperfectly drained soils will further increase the residence time of $N\text{-}NO_3$ within the soils, with contrasting affects with the larger proportion of well drained soils increasing the risks for $N\text{-}NO_3$ leaching through the soil profile from lower residence times.

The three soil landscape models (Figures 49-51) show strong relationships between soil formation and aspect, with Brown Soils being primarily found on south facing slopes and Pallic Soils being primarily found on north facing slopes. The formation of Brown and Pallic Soils can be reinforced by the annual rainfall for the study area (~1044mm) due to the annual rainfall straddling the hypothesised limits identified for both soil classification formation. The soil landscape model for location 1 clearly shows the relationship between aspect and soil formation. The soil PhS is developed on a south facing slope and is classified as a Brown Soil, while soil WhS is developed on a north facing slope and is classified as a Pallic Soil, this soil exhibiting evidence of wetting-drying cycles during formation supporting the hypothesis identified in literature. The Brown Soils for location 2 are located on south facing slopes with the Pallic Soils being located on north facing slopes again exhibiting waterlogging throughout the soil profile in support of demonstrated soil formation patterns. The soil landscape model at location 3 identifies the Brown Soils as being located on south facing slopes while the Pallic soil, is located on the north facing slopes, further conforming to the hypotheses identified in literature surrounding soil formation patterns (Chapter

2.2.1).

The three soil landscape models have all demonstrated strong relationships between the geology and the soil textures observed. The silt and clay sediments identified with the soil landscape model for location 2 showed that over time the locations that the locations saturated or filled with water for an extended period of time influenced the soils during formation to demonstrate characteristics of poor aeration throughout soil profiles and having high water tables or flooding throughout the year. The strong influence of the geology on soil formation allows for a more interpretable and essentially efficiently modelled landscape.

### 6.1.2. Water Level

A strong seasonal control on the water level in the piezometers is observed with lower levels in summer months and higher levels in winter. These observations are attributed to both rainfall and evapotranspiration. The decreasing water levels during the drier months (November 2021 to January 2022) and the higher water levels during the wetter months (June 2021 to October 2021) illustrates the seasonal influence on groundwater level.

Piezometer location is an additional factor that is impactful on water levels and is evident across piezometer samplings, specifically during the samplings of October 2021. During this sampling period 3 piezometers (1, 3 and 4) showed higher water levels while the other 3 piezometers (2, 5 and 6) had lower water levels when comparing them all. Piezometers 1, 3 and 4 are all aligned within the same drainage valley (Figure 30) therefore respond in comparable patterns according to the drainage direction down the valley system. Piezometers 2, 5 and 6 are all located in zones of drainage collection, with piezometer 2 being at the base of a small drainage valley and below a seepage zone, piezometer 5 being on the edge of a dam that collects drainage from the surrounding area and from the valley containing piezometers 1, 3 and 4, and piezometer 6 being directly along the drainage path in steep-sloped valley system with a pond system at the bottom of the valley, downstream of the piezometer location.

Piezometer 6 has shown a higher variability in piezometer water levels when compared to the other piezometers. The slopes of the surrounding landscape are considerably steeper and the valley narrower than those surroundings around the piezometers south-west of piezometer 6, demonstrating the response of increased water evacuation rates from the slopes during the drier months while channelling water movement throughout the wetter months.

Rainfall intensity and extent prior to sampling days have a large influence on water levels within the piezometers. The evidence presented conforms to these demonstrations with the rainfall event in June prior to the July samplings, along with the rainfall events throughout July presenting a significant response with the piezometer water levels increasing between samplings (Figures 55 and

56). Furthermore, the opposite can be demonstrated where delayed rainfall and lack of rainfall (from the beginning of July to the 16th of July) has shown to have the result of lower water levels within the piezometer (Figure 56). Additionally, it can be seen by the rainfall delay between December 2021 and January 2022, which had a significant response in water level change from the December sampling to the January sampling (Figures 60 and 61). The effect of a rainfall period intensity on piezometer water level response is seen in the sampling of December 2021 where water level increases. There will be an element of delay seen between rainfall events and the responding changes seen within a piezometer unit. These delays have not been assessed throughout this study but is a potential subject for future study.

### 6.1.3. Water Sensor

The first two months of sampling were disregarded from the results due to human error. The assembly of the YSI Flowcell sensor requires an inflow tube to be attached to the lower port, which is connected to the Solinst Peristaltic Pump, however, the inflow tube was connected to the upper port during the first two months of sampling, incorrectly filling the flow cell (allowing increased air flow within the sensor) and subsequently producing incorrect results. The incorrect sampling methods will give skewed and incorrect results therefore the removal of the data from these two sampling months will give a more accurate presentation of the results.

Groundwater under reducing conditions have RDO levels below 1 mg $L^{-1}$ with an ORP below 150mv, while groundwater under non-reducing conditions have RDO levels above 1 mg $L^{-1}$ with an ORP above 150mv (McMahon & Chappelle, 2008). It is shown in studies that denitrification is considerably slower in soils of pH 5.8 than soils with high pH values and that denitrification was very slow in the soil of pH 4.1 and almost undetectable in soils of pH 3.6 (Bremner & Shaw, 1958). The same response was seen throughout groundwater studies where at pH <7 denitrification was completely inhibited and that as pH rose the specific rate of nitrate reduction increased (Glass & Silverstein, 1998), however the state of denitrification cannot be determined primarily based on the pH.

The results for piezometer 1 indicate the soil conditions were not supporting N-$NO_3$ reduction evident from the RDO level, with ORP levels corroborating the conclusion presented by the RDO levels; the pH range indicates that denitrification rates reduced between September 2021 to October 2021 with an observed increase throughout November 2021. The piezometer 2 results for RDO indicate that the soil conditions were supporting N-$NO_3$ reduction, with ORP levels indicating that conditions were not supporting N-$NO_3$ reduction; the pH results indicate that denitrification rates reduced between September 2021 to October 2021 with an observed increase throughout

November 2021 and December 2021. The piezometer 3 results for RDO indicate that the soil conditions were supporting N-$NO_3$ reduction, with ORP levels indicating that the soil conditions were not supporting N-$NO_3$ reduction; the pH results indicate that denitrification rates experienced a decline between July 2021 and November 2021 with an observed increase in rate in December 2021. The piezometer 4 results for RDO indicates that the soil conditions were supporting N-$NO_3$ reduction, with ORP results indicating that conditions were not supporting N-$NO_3$ reduction; the pH results indicate that denitrification rates experienced a decline until November 2021 with an increase in rate in December 2021. The piezometer 5 results for RDO indicate that the soil conditions were supporting N-$NO_3$ reduction, with ORP results indicating that soil conditions were not supporting N-$NO_3$ reduction; the pH results indicate a gradual increase in denitrification rates across the sampling months. The piezometer 6 results for RDO indicate that for all sampling months that soil conditions were supporting N-$NO_3$ reduction until November 2021 where conditions converted to non-reducing conditions. The ORP results indicate that during the September 2021 sampling soil conditions were supporting N-$NO_3$ reduction, however, the conditions changed during the October 2021 and November 2021 samplings to non-reducing conditions. The pH results indicate a decreased denitrification rate from September 2021 to October 2021 but experienced an increase in denitrification in November 2021.

## 6.2. Laboratory Discussions

### 6.2.1. Surface Water

National standards on acceptable levels of N-$NO_3$ and DRP have been widely discussed within literature. The Horizons Regional Council have set out within OnePlan (a resource management planning document) water quality targets for different water management zones covering a variety of water quality parameters. The standards set for the Rangitikei region for N-$NO_3$ were 0.110 mg $L^{-1}$ and for DRP the standards were 0.010 mg $L^{-1}$ (Horizons Regional Council, 2014). These standards were specifically applied to rivers but within the OnePlan these standards additionally encompass most surface water bodies.

The presented laboratory results for surface water 2 have shown that the N-$NO_3$ levels were significantly low across the sampling months apart from the month of November 2021. The increase observed in November 2021 is likely attributed to the increased rainfall prior to sampling, illustrating the response of flushing more N-$NO_3$ out of the soil system into surface waters. The DRP levels presented were all above the accepted standards with an increasing trend visible. This increasing trend can be associated to the increased levels of rainfall across the sampling months mobilising phosphorus from the soil surface.

The presented results for surface water 3 shows that September 2021 was the only month to have $N\text{-}NO_3$ levels below the detectable level, along with December 2021 being below the accepted standards and the remaining sampling months being above accepted standards. A sudden increase in rainfall prior to sampling in October 2021, mobilising $N\text{-}NO_3$ within the soil profile is to all appearances the reason for the increased $N\text{-}NO_3$ levels at the October 2021 sampling. The DRP levels presented were all above the accepted standards set out in the OnePlan. The increasing DRP trend across the sampling months can be associated to the increased levels of rainfall across the sampling months, mobilising phosphorus from the soil surface.

Surface water 4 has presented results showing the sampling months of September 2021 and October 2021 have $N\text{-}NO_3$ levels below the accepted standards while the December 2021 sampling had levels above the accepted standards. The variation in results for December 2021 is most likely associated to the increased rainfall prior to sampling further mobilising $N\text{-}NO_3$ from the soil profile. As with the previous two surface water locations DRP levels were all above the accepted standards with an increasing trend across the sampling months associated again to the increased rainfall mobilising phosphorus prior to sampling.

The results presented for surface water 5 shows a vast difference when compared with the other 3 surface water locations. The lower $N\text{-}NO_3$ results are influenced by the location of the surface water samplings with them being collected on the edge of a dam that is exposed to dilution with rainfall and continued input of surface water into the system, therefore, presenting results that are below the accepted standards set. During the summer months drying of water bodies occurs and combined with limited rainfall has shown to have the effect of increasing $N\text{-}NO_3$ concentrations as seen during the sampling of January 2022. The DRP levels were seen to all be above the accepted standards with an increasing trend across the sampling months, which can be associated to increased rainfall across the sampling months. The sudden increase in DRP at the October 2021 sampling is consistent with increased rainfall prior to sampling washing higher concentrations of phosphorus into the surface water body.

The location of each of the surface water sampling sites have an influence on the responses and patterns seen across each of the sites. Surface water 3 and surface water 4 are located along the same drainage catchment, therefore, these surface waters will have very similar responses and patterns amongst the results. The slightly higher position (further into the drainage valley) of surface water 3 within the landscape results in surface water reaches this location prior to surface water 4, consequently any significant changes are most likely to be observed in surface water 3 first, nevertheless due to the extended time between sampling periods (1-month intervals) this is unlikely to have a significant effect in this study. Surface water 2 is located further down the landscape from

surface water 3 and surface water 4 but is associated to a drainage branch that feeds into the drainage catchment of surface waters 3 and 4 (not influencing the result of these two surface water bodies). The different drainage branch of surface water 2 will result in different responses observed across the sampling periods, however, due to the close proximity of the different surface water locations it is less likely that small scale influences will be displayed between the different surface water sampling sites (specifically for the observed sampling frequency). Surface water 5 location is further along the drainage catchment to the previous surface water locations and receives all drainage from the surrounding areas including the drainage from surface water locations 2, 3 and 4. This site is likely to show the largest variations in results due to receiving a larger area of drainage compared to the other surface water bodies and therefore will show a compounded response from the surrounding landscapes. The different design of this water body, an open system dam, is vastly different from the other surface water sample sites which are free flowing streams and will therefore have a differing response pattern to changes. The free-flowing streams will respond to changes more rapidly with shorter residence times while the open system dam will show slower response times to changes and have longer residence times, all effecting the results observed. Livestock exposure to all of the surface water bodies during the sampling periods will have an influence on the results presented, primarily the phosphorus levels, by cause of increased pugging damage and erosion releasing trapped phosphorus within the soil profile into surface waters.

### 6.2.2. Ground Water

The accepted standards for surface water $N\text{-}NO_3$ are what the groundwater results were being analysed against, as the standards for ground water are only set for drinking water standards. The ground water drinking water standards are set at 50 mg $L^{-1}$ for $N\text{-}NO_3$ with all groundwater results presented being below this standard. There are no standards set for ground water DRP (LAWA - Land Air Water Aotearoa, n.d. a) therefore the ground water results will be analysed against surface water acceptable standards for DRP.

The ground water results for piezometer 1 show very low levels of $N\text{-}NO_3$ within the system with levels coming back as below detectable level. When combined with the $N\text{-}NO_3$ reducing conditions identified the groundwater conditions do not conform with the theory presented by the ORP and RDO results that express non-reducing conditions. The lack of conformity between the observed low $N\text{-}NO_3$ levels in the ground water and the presented $N\text{-}NO_3$ reducing conditions can be recognised in piezometers 2, 4, 5 and 6. It is only within piezometer 3 that the low $N\text{-}NO_3$ levels conform to the theory demonstrated presented by the RDO and ORP results that indicate the $N\text{-}NO_3$ reducing conditions within the soil system.

The significantly low ground water N-$NO_3$ levels and the few samples with rapid peaks in N-$NO_3$ levels observed across the piezometers could be explained by ground water recharge rate but this topic is not investigated as it is out of the scope of this thesis and further research would be recommended. A fraction of the high ground water DRP levels observed across the piezometers, could be associated to the external input of sediment into the piezometer but for this thesis can be disregarded due to the 'cleaning' phase of the piezometer before sample collection. However, the continued lack of conformity between the theorised N-$NO_3$ reducing conditions and the observed low N-$NO_3$ groundwater levels warrants further analysis into the processes taken to remove N-$NO_3$ from the soil system, which is beyond the scope of this thesis.

### 6.2.3. Surface Water vs Ground Water (Sensor vs lab)

The low levels of ground water N-$NO_3$ from piezometer 2 have been shown to be lower than the N-$NO_3$ levels identified in the corresponding surface water except for the July 2021 sampling that have higher ground water N-$NO_3$ than surface water N-$NO_3$ levels. The lower levels of ground water N-$NO_3$ is evidence that supports the results seen from the RDO results that show conditions support N-$NO_3$ reduction. There are no uniform patterns visible between the surface water and ground water for the DRP results.

The low levels of ground water N-$NO_3$ from piezometer 3 have been shown to be considerably lower than the N-$NO_3$ levels identified in the corresponding surface waters. This supports the results seen for RDO that indicate that the conditions support N-$NO_3$ reducing conditions. All of the ground water DRP levels, when compared with the surface water, are considerably lower showing there is a degree of 'filtering' of the surface water throughout the soil profile. Total phosphorus is primarily transported via overland flow while DRP is more commonly transport via surface water through to the groundwater (Land Air Water Aotearoa, n.d.). The anoxic conditions presented for soil K (a) increased the residence time of phosphorus within the soil system influencing the low levels of phosphorus within the ground water and the indication of 'filtering' throughout the profile.

The low levels of ground water N-$NO_3$ from piezometer 4 have been shown to be lower than the N-$NO_3$ levels identified in the corresponding surface water. The lower levels of ground water N-$NO_3$ is evidence that supports the results seen from the RDO results that show conditions support N-$NO_3$ reduction. There are no uniform patterns visible between the surface water and ground water for the DRP results.

The low levels of ground water N-$NO_3$ from piezometer 5 have been shown to be lower than the N-$NO_3$ levels identified in the corresponding surface water except for the December 2021 sampling which have higher ground water N-$NO_3$ than surface water N-$NO_3$ levels. The lower levels of ground water N-$NO_3$ is evidence that supports the results seen from the RDO results that support N-$NO_3$

reducing conditions. All of the DRP levels were considerably lower when compared with the surface water showing there is a degree of 'filtering' of the surface water throughout the soil profile. The anoxic conditions presented for soil Oh (a) increased the residence time of phosphorus within the soil system influencing the low levels of phosphorus within the ground water and the indication of 'filtering' throughout the profile.

## 6.3. Geographic information Systems (GIS) Discussions

### 6.3.1. Slope, Aspect, & Landform Elements

The availability of DEM information that covered the study area was limited to two DEM files; the 1m resolution DEM and the 8m resolution DEM for the Manawatu-Wanganui Region. The preferred DEM for use was the Manawatu-Whanganui LiDAR 1m DEM (2015-2016) (Toitū Te Whenua - Land Information New Zealand, 2019) due to the higher clarity of the information presented, however, the 1m DEM did not have a complete coverage of the study area with a small section (7.83%) in the east of the study area not being covered (Figure 79). At the time when this thesis was completed the 1m DEM was the best available option, however, further research has shown that the use of a drone for collecting elevation data would have been an acceptable alternative. The results from the drone data would have given a point cloud density of 943 points/sqm (for a 100m flight elevation) (Irwin, 2023) compared to the 3.41 points/sqm for the Manawatu-Whanganui LiDAR 1m DEM (2015-2016) (OpenTopography, n.d.). The use of the drone was not available due to covid restrictions, time constraints and drone availability for use in this thesis. The 1m DEM data was presented as two differing maps: the greyscale elevation map (Figure 79) and the hill shade map (Figure 80). The use of the greyscale elevation map provides the values necessary for use in creating maps that rely on elevation data (e.g., slope and aspect) while the hill shade map provides a clearer image of the varying elevations present across the study area.

The digitising of the farm boundary resulted in a slight discrepancy between the total digitised area and the area provided by the landowner. This discrepancy could have been prevented by the use of survey information that would have given the correct area for the study area and an accurate placement of the boundary. However, at the time there was no survey information available to access, resulting in the methods utilised giving the less than accurate results seen across this thesis.

The slope map was classified into 7 classes. These groupings are based on the classes set out in the "Land Use Capability Survey Handbook" (Lynn, et al., 2009). The aspect data was classified into north, east, south, west, and flat. Limiting the classification of aspect to 5 classes prevents the

unnecessary need for additional, finer detail that is associated to increasing the number of aspect classes.

The results presented have varied across the study area from being able to strongly identify the difference amongst land elements to overestimating the land elements within the study area. Figure 86 is an example of where the landform element map strongly identifies the different land elements whereas, figure 87 is an example of where the landform element map overestimates the extent of the elements within the landscape and the patchiness of the identified elements. The areas of high gradient (e.g., the steep land of the north-east reach of the study area) had a stronger relationship between the landform element map and the landscape. The opposite can be seen where the areas of low gradient (e.g., the rolling land to the south-west reach of the study area) had a weaker relationship between the landform element map and the landscape.
The surface parameter tool in ArcGIS Pro was the best option available at the time of this thesis, however, other options have been presented within literature including the use of the TopHat algorithm. Barringer et al (2008) shows an example of the results produced using TopHat, which shows a significant increase in clarity amongst the landform elements. Access to TopHat would have increased the clarity of the results presented, reducing 'noise' pollution, and having a stronger relationship between the landform element map and the landscape particularly in areas of low gradients.

The elevation profile images were created using the 'exploratory 3D analysis' tool in ArcGIS Pro and was the preferred elevation profile image when compared with the other methods. The profile elevation images created using the 'profile' tool (under 'Ready to use tools') in ArcGIS Pro and the elevation profile in Google Earth Pro both provided generalised elevation profiles, however, smaller details were smoothed out across the profile (Figure 88). The 'Exploratory 3D Analysis' tool allows for interactive tracking which helped to identify areas of change when overlaid with either the geology layer or the soil layer. Each of these methods produced different versions of the same profiles but the exploratory 3D analysis tool provided the most accurate results for what was required for this thesis and allowed for interaction between the elevation profile and additional layers when required.

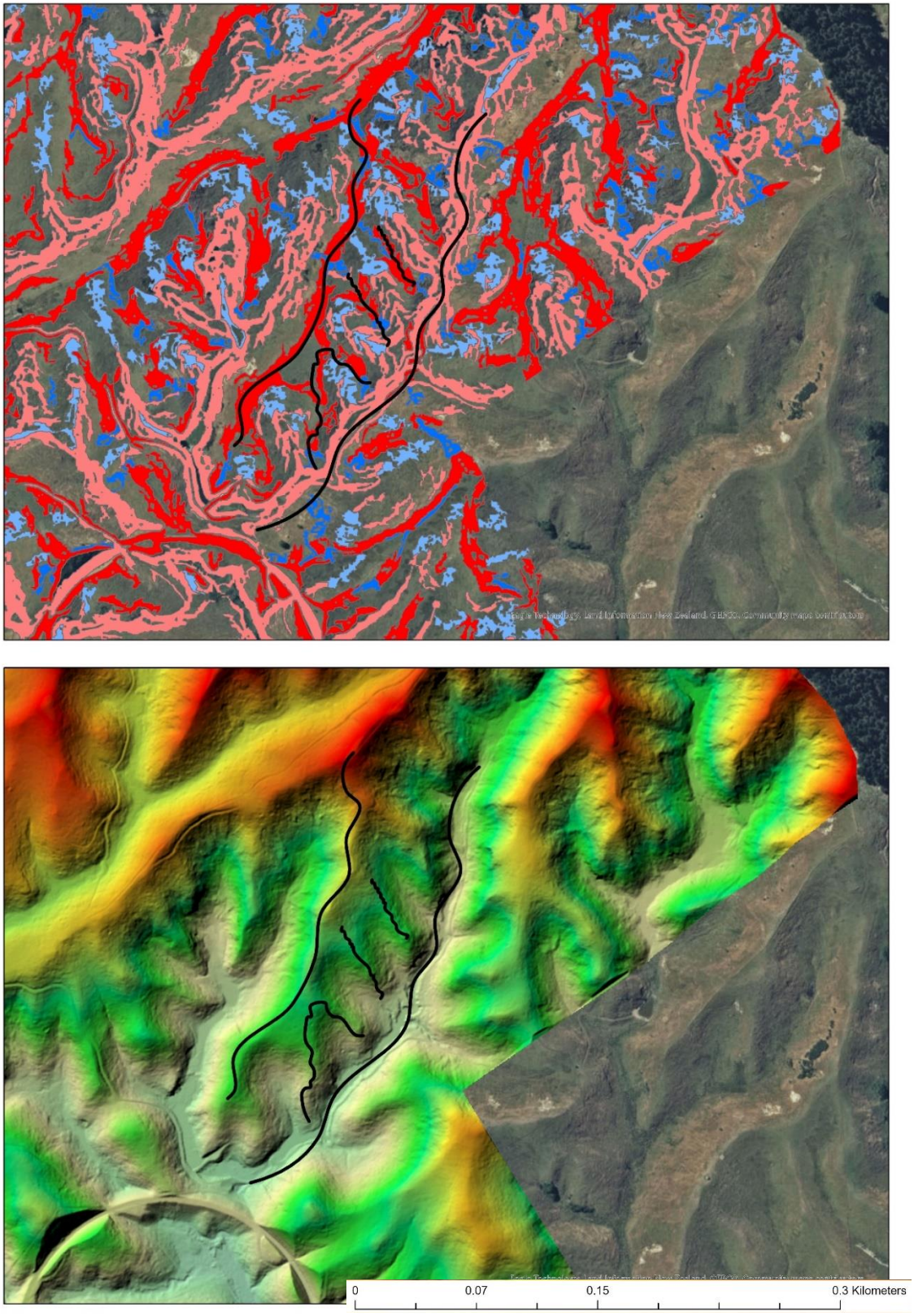


*Figure 86: An example from the landform element showing the stronger relationship between the landform element map and the landscape. This shows where the map clearly identified different land elements across the landscape. (Top image: Light blue – hollow; dark blue – spur; light red – valley; dark red – ridge. Black line – identifying the features being identified).*

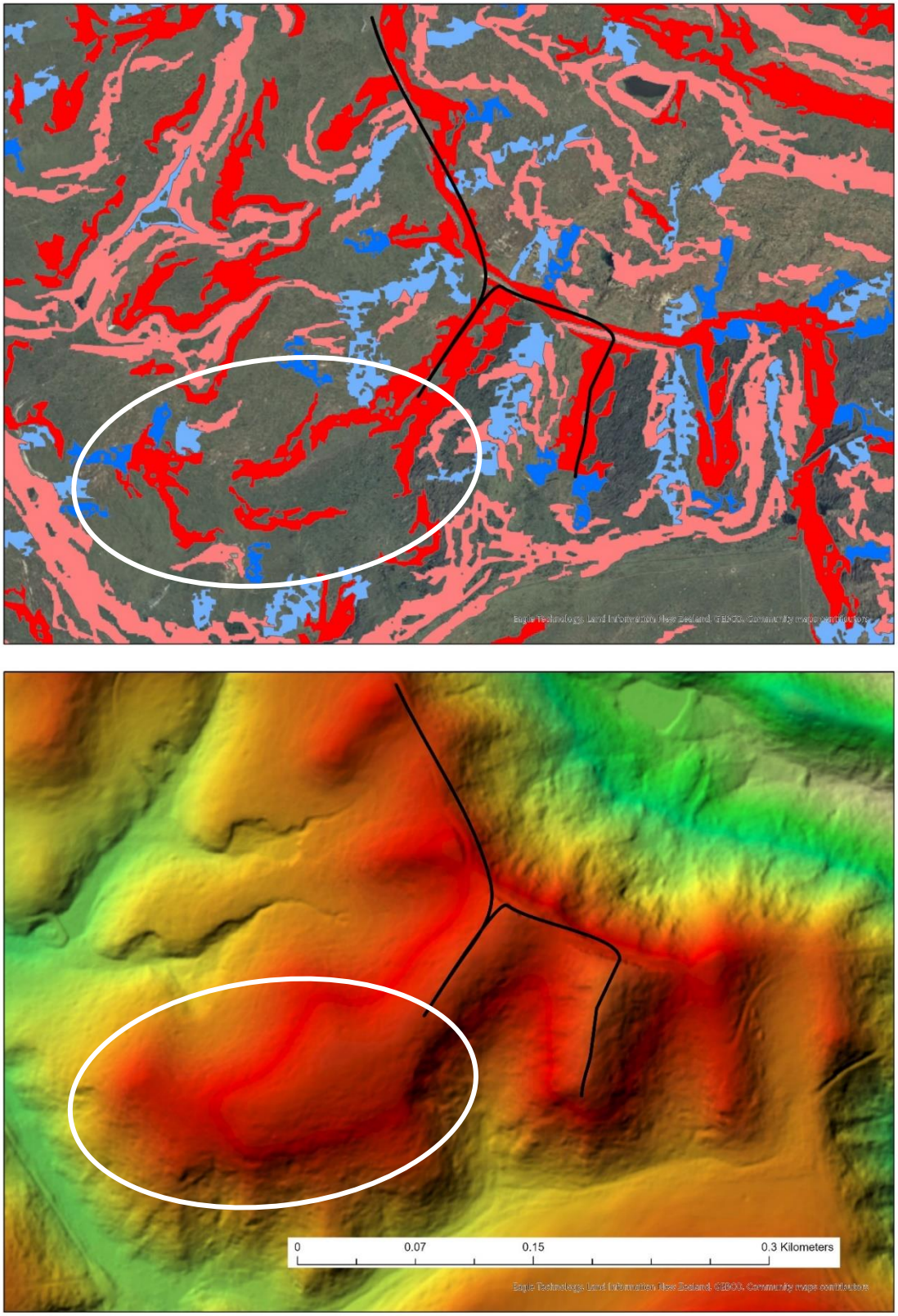


*Figure 87: An example from the landform element showing the weaker relationship between the landform element map and the landscape. This shows where the map overestimated the presence of landform element across the landscape. (Top image: Light blue – hollow; dark blue – spur; light red – valley; dark red – ridge. Both Images: Black line – identifying the features being identified; White oval – identifying an example of a zone of weaker relationship).*

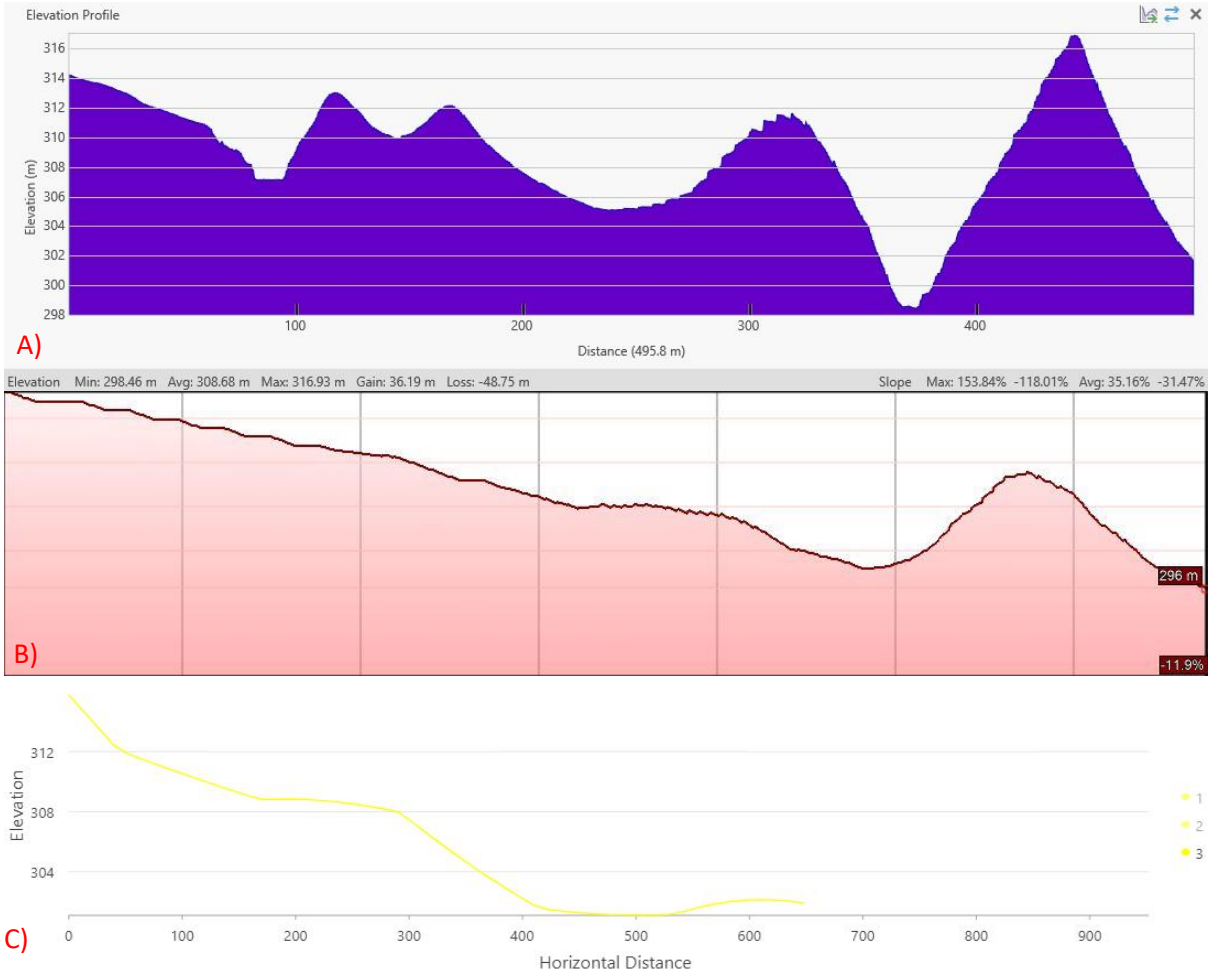


*Figure 88: A comparison of the three available elevation profiles for location 3 of the soil landscape model profiles, showing the smoothing of the profiles across B and C. A) The elevation profile produced using the 'exploratory 3D analysis' tool in ArcGIS Pro. B) The elevation profile produced using the 'profile' tool in ArcGIS Pro. C) The elevation profile produced using the elevation profile in Google Earth Pro.*

# Chapter 7 – Conclusion

The Rangitikei catchment is located in the Manawatu-Whanganui region of the lower North Island. The catchment accounts for 18% of the approximate 22,000 $km^2$ of the Manawatu-Wanganui (Singh, et al., 2017) with 58% of the Manawatu-Whanganui region being comprised of steep hill country and hilly steep lands (Rees, Palmer, & Palmer, 2020). The 450-hectare study area surrounding Hunterville, located within the Rangitikei catchment, has been found to have 6 geological units. The two dominant geologies are the Or and Mo formations which contain repeating siliciclastic sandstone and siliciclastic siltstone units. The alternating siliciclastic units within these geologies made the identification of the parent material texture for the soil descriptions more difficult i.e., a non-dominant texture was distinguishable, resulting in neither a sandstone nor siltstone parent material being classified easily. Swamp deposit lithology was identified to have a strong influence on the location of Gley soils across the study area. The Q1k1 and Q1k2 terrace deposits have shown to have an influence on the formation of the PkS soils, particularly seen at the location of SD McFadden Poplars (Appendix 4) where fine gravels are present throughout the soil profile and the seasonal surface flooding of these soils. A small portion of the geological map is classified as UQl at the scale of 1:25,000, however, at a larger scale the small scale landslides (landslide term is used loosely to include all forms of land movement across the study area) may be included within this geological unit, but depending on the density and spread of these small scale landslides they may not be classes as a single geological unit but may be referred to as a set of different K-cycles.
The geological map presented was adapted from a geological information (including a geological map) provided by Rees (2020) with the descriptions of the geological units being adapted from previous literature (Abbott, Naish, Carter, & Pillans, 2005; Boreham, 1963; Clement & Fuller, 2007; Naish & Kamp, 1995; Naish, et al., 1996; National Geographic Society, 2022; Palmer, 2023; Palmer, Begg, Townsend, & Wilson, 2006; Smith & McGrath, 2011). Time limitations prevented further infield data collection that could provide additional information or provide evidence for the information provided by Rees (2020).

26 soil descriptions were taken for the purpose of establishing a soil map and providing information to the identified soil types across the study area. In addition, a further 6 soil descriptions were provided for supplementary use, however, there was still a lack of soil descriptions distributed across the study area. The addition of further soil descriptions across the study area was identified to enhance the existing soil information and to provide information where information was lacking or inconsistent. For instance, the lack of information regarding soil drainage for a small portion of the study area would have been mitigated from additional soil descriptions being completed in these

areas. However, from the information collected ~94% of the soils identified across the study area were classified as Brown or Pallic soils, with 8 distinct drainage classes being associated to them. The soil information along with slope information (produced via ArcGIS data processing) and vegetation and erosion information (collected from infield analysis) allowed for the producing of an LRI and LUC map of the study area. The resulting LRI and LUC maps recognised 10 LRI classes and 6 LUC across the study area allowing for the identification of physical factors critical for long-term land use and management organisation.

Groundwater level was collected and analysed and was found to have a strong seasonal influence, in particular to rainfall occurring prior to sampling. The shallow nature of the piezometers have shown a more rapid response to rainfall events, influencing the degree of nutrients mobilised through and from the soil profile. During the sampling process of the piezometers for the first two months, incorrect instillation of the sampling equipment resulted in results having incorrect values. The human error influence in the sampling for these months resulted in this data being eliminated from the overall results. This could have been prevented via more thorough teaching of the equipment use prior to the beginning of field sampling. In-field readily dissolved oxygen (RDO) results showed an overall consensus across all piezometers installed that soil conditions supported nitrogen reduction conditions except for Piezometer 1 that indicated non-supporting nitrogen reduction conditions. The oxidation-reduction potential (ORP) results for all piezometers collectively showed non-reducing conditions within the soils excluding one sampling month for Piezometer 6. The months of September 2021 and October 2021 showed a decline in pH values across all piezometers. These declining pH values indicate a declining rate in nitrogen reduction within the soils. Following the declining pH values across these months, an increase in pH values and therefore an increase in nitrogen reduction rate is observed across all installed piezometers except for Piezometer 5 that continued to have declining pH values. Laboratory analysis of nitrogen ($N\text{-}NO_3$) and dissolved reactive phosphorus (DRP) for groundwater and surface water samples was completed with the surface water locations showing that one month of sampling across all locations was above the accepted standards for $N\text{-}NO_3$ in surface water bodies, except for surface water location 5 that indicated 2 sampling months were above the accepted $N\text{-}NO_3$ standards. In contrast, all surface water locations showed DRP well above accepted DRP standards for surface water bodies. The laboratory analysis for all piezometers indicated that all $N\text{-}NO_3$ results were below the accepted standards, except for Piezometers 1 and 6 that had one sampling month each above standards, when compared to surface water accepted standards and well below the standards set out for drinking water. The laboratory DRP analysis for the piezometers showed unanimously that all piezometers have values above accepted standards. The analysis of surface water in comparison to

groundwater showed the low nitrogen values for the surface waters are greater than those observed in the groundwater analysis. These responses coincide with the DO indications showing conditions support N-$NO_3$ reduction. The DRP analysis comparing both surface water and groundwater did not establish a clear pattern with Piezometers 2 and 4 showing no patterns when compared with the surface waters of the same locations, while in contrast to this, piezometers 3 and 5 show that groundwater DRP is lower than that of the surface waters of the same locations.

The primary data utilised for GIS analysis across this study was LiDAR DEM data with a resolution of 1m. Through the analysis process it was established that the resolution of the LiDAR DEM data was considerably lower than what would have been produced if drone work was completed to produce digital elevation model (DEM) data. The point cloud density of the LiDAR DEM data was established to be 3.41 points/sqm, when compared with the point cloud density of potential drone data that was established to be 943 points/sqm (for a 100m elevation flight path) the LiDAR DEM data was considerably lower, limiting the information presented in the data provided. The utilisation of drone data would have resulted in higher resolution data however, due to time constraints and limited access to drones prevented the use of drone data within this study. The landform element map developed for this study was created using ArcGIS processes. The results showed strong relationships between the map created and landform elements in the field in high gradient area (areas of high slope angles) but the map over estimated relationships between the map created and landform elements in the field in low gradient areas (areas of low slope angles). Examples of TopHat algorithm use within literature gives examples of where the relationships between maps and landforms in the field produce greater clarity and more accurate results. There was no access to the TopHat algorithm which prevent its use within this study.

Overall, the strong influence of the geology of the area on soil formation, has shaped the soil landscape and soil behaviours across Ngatiapa. Standard LRI/LUC and farm management plans have been shown to be negligent of nutrient inclusion when addressing water quality standards in the aim to improve freshwater quality of the region. Soil drainage understanding is only just starting to be recognised as an important feature in understanding nutrient movement between the soil surface and groundwater reservoirs. Drainage pattern importance was illustrated across Ngatiapa with the inclusion of nutrient level at a number of sample locations. It has been shown that despite drainage pattern variations across Ngatiapa, N-$NO_3$ levels in surface waters and groundwaters are below standards with RDO and ORP indicating that the dominating status supports nitrogen reduction. However, the high levels of DRP in both surface and groundwaters across the study area shows that further mitigation of DRP loss is required to meet the standards currently applied to the region. These soil conditions and the low levels of nitrogen within the surface and subsurface waters across

Ngatiapa contributes towards improved water quality across the Rangitikei region. Understanding the relationship and interactions between the geology of the area, soil types, soil drainage, and nutrient behaviour helps to improve freshwater plans, and on farm management across the Rangitikei with the intention of improving freshwater quality. By redesigning soil-landscape models to represent the relationship between soil types and nutrient levels status it is intended to help improve the understanding of the landscapes of the Rangitikei District with the intention to improve freshwater quality across the region.

# Chapter 8 – References

Abbott, S. T., Naish, T. R., Carter, R. M., & Pillans, B. J. (2005). Sequence stratigraphy of the Nukumaruan Stratotype (Pliocene-Pleistocene, c. 2.08-1.63 Ma), Wanganui Basin, New Zealand. *Journal of the Royal Society of New Zealand, 35*(1-2), 123-150.

AgResearch Grasslands. (2007). *Specifications of whole farm plans as a tool for affecting land use change to reduce risk to extreme climatic events.* AgResearch.

Annan, A. P. (2008). Electromagnetic Principles of ground penetrating radar. In H. M. Jol, *Ground penetrating radar theory and applications* (pp. 3-40). Elsevier.

Ausseil, A.-G. E., & Dymond, J. R. (2008). Estimating the spatial distribution of sediment concentration in the Manawatu River, New Zealand, under different land use scenarios. *325*, 502.

Ballance, P. (2009). New Zealand Geology: an illustrated guide. *2*. Geoscience Society of New Zealand.

Barringer, J. R., Hewitt, A. E., Lynn, I. H., & Schmidt, J. (2008). National mapping of landform elements in support of S-Map, a New Zealand soils database. In Q. Zhou, B. Lees, & G. Tang, *Advances in DIgital Terrain Analysis.* (pp. 443-458). Springer Science & Business Media.

Basher, L., Spiekermann, R., Dymond, J., Herzig, A., Hayman, E., & Ausseil, A.-G. (2020). Modelling the effect of land management interventions and climate change on sediment loads in the Manawatu-Whanganui region. *New Zealand Journal of Marine and Freshwater Research, 54*(3), 490-511.

Bathurst, J. C. (2011). Predicting impacts of land use and climate change on erosion and sediment yield in river basins using SHETRAN. In R. Morgan, & M. Nearing (Eds.), *Handbook of erosion modelling* (pp. 263-288). John Wiley & Sons, Ltd.

Beyer, M., Rissmann, C., Rodway, E., Killick, M., Pearson, L., Marapara, T. R., & Hodgetts, J. (2016). *Technical Chapter 6: Influence of soil and geological composition over redox conditions for Southland groundwater and surface waters.* Environment Southland. Retrieved from https://contentapi.datacomsphere.com.au/v1/h%3Aes/repository/libraries/id:1tkqd22dp17q9stkk8gh/hierarchy/Scientific%20reports/Physiographics%20of%20Southland%20-%20Part%201/TC%206%20-%20Influence%20of%20Soil%20and%20Geological%20Composition%20over%20Redox

Bleam, W. F. (2016). *Soil and environmental chemistry.* Academic Press.

Blume, T., & Van Meerveld, H. J. (2014). From hillslope to stream: methods to investigate subsurface connectivity. *Wiley Interdisciplinary Reviews: Water, 2*(3), pp. 177-198.

Boreham, A. U. (1963). Some problems concerning the application of the lower Nukumaruan (Hautawan) substage (Pleistocene, New Zealand). *New Zealand Journal of Geology and Geophysics, 6*(1), 3-27.

Bremner, J., & Shaw, K. (1958). Denitrification in soil. II. Factors affecting denitrification. *The Journal of Agricultural Science, 51*(1), 40-52.

Bretherton, M. R. (2012). An investigation into repellency-induced runoff and its consequences in a New Zealand hill country pasture system. *[Unpublished Doctorial Dissertation]*. Massey University.

Brevik, E. C., Calzolari, C., Miller, B. A., Pereira, P., Kabala, C., Baumgarten, A., & Jordán, A. (2016). Soil mapping, classification, and pedologic modeling: History and future directions. *Geoderma, 264*, 256-274.

Campbell, I. B. (1978). *Extended legend of soil map of Rangitikei County, North Island, New Zealand.* Department of Scientific and Industrial Research.

Carrick, S., Fraser, P. M., Dennis, S., Knight, T., & Tabley, F. (2013). *Challenges for leachate monitoring from alluvial sedimentary soils.* (Eds. L. D. Currie and C. L. Christensen), Occasional Report No. 26. Fertilizer and Lime Research Centre. Palmerston North, New Zealand: Massey University. Retrieved from http://flrc.massey.ac.nz/publications.html

Carrick, S., Hainsworth, S., Lilburne, L., & Fraser, S. (2014). *S-map @ the farm-scale? Towards a national protocol for soil mapping for farm nutrient budgets.* (Eds. L. D. Currie and C. L. Christensen), Occasional Report No. 27. Fertilizer and Limer Research Centre. Palmerston North, New Zealand: Massey University. Retrieved from http://flrc.massey.ac.nz/publications.html

Chappell, P. R. (2015). The climate and weather of Manawatu-Wanganui. NIWA, Taihoro Nukurangi. Retrieved from https://niwa.co.nz/sites/niwa.co.nz/files/NIWA_ManawatuWanganui_Climate_WEB.PDF

Clement, A. J., & Fuller, I. C. (2007). Fluvial responses to environmental change in the North Island, New Zealand, during the past c. 30 ka recorded in river terrace sequences: a review and model for river behaviour. *New Zealand Journal of Geology & Geophysics, 50*, 101-116.

Close, M. E., Abraham, P., Humphries, B., Lilburne, L., Cuthill, T., & Wilson, S. (2016). Predicting groundwater redox status on a regional scale using linear discriminant analysis. *Journal of Contaminant Hydrology, 191*, 19-32.

Cogle, A. L., Lane, L. J., & Basher, L. (2003). Testing the hillslope erosion model for application in India, New Zealand and Australia. *Environmental Modelling & Software, 18*, 825-830.

Collins, S., Singh, R., Rivas, A., Palmer, A., Horne, D., Manderson, A., . . . Matthews, A. (2017). Transport and potential attenuation of nitrogen in shallow groundwaters in the lower Rangitikei catchment, New Zealand. *Journal of Contaminant Hydrology, 206*, 55-66.

Conacher, A. J., & Dalrymple, J. B. (1977). The nine-unit landsurface model: an approach to pedogeomorphic research. *Geoderma, 18*(1-2), 1-154.

Cowie, J. D., & Rijkse, W. C. (1977). *Soils of the Manawatu County, North Island, New Zealand.* Wellington, New Zealand: New Zealand Soil Bureau.

Cumberland, K. B. (1941). A century's change: Natural to cultural vegetation in New Zealand. *Geographical Review, 31*(4), 529-554.

Dixon, J. C. (2015). Soil morphology in the critical zone: The role of climate, geology, and vegetation in soil formation in the critical zone. In *Developments in Earth surface processes* (Vol. 19, pp. 147-172). Elsevier.

Doolittle, J. A. (1987). Using ground-penetrating radar to increase the quality and efficiency of soil surveys. *Soil survey techniques, 20*, 11-32.

Dymond, J. R., & Vale, S. S. (2018). An event-based model of soil erosion and sediment transport at the catchment scale. *Geomorphology, 318*, 240-249.

Dymond, J. R., Betts, H. D., & Schierlitz, C. S. (2010). An erosion model for evaluating regional land-use scenarios. *Environmental Modelling & Software, 25*, 289-298.

Dymond, J. R., Herzig, A., Basher, L., Betts, H. D., Marden, M., Phillips, C. J., . . . Roygard, J. (2016). Development of a New Zealand SedNet model for assessment of catchment-wide soil-conservation works. *Geomorphology, 257*, 85-93.

Elwan, A., Singh, R., Horne, D., Roygard, J., & Clothier, B. (2015). *Nitrogen attenuation factor: can it tell a story about the journey of nutrients in different subsurface environments.* (Eds L. D. Currie and L. L. Burkitt), Occasional Report No. 28. Fertilizer and Lime Research Centre. Palmerston North, New Zealand: Massey University. Retrieved from http://flrc.massey.ac.nz/publications.html

Envirolink. (2012). *New Zealand Emprical Erosion Model (NZeem®)*. Retrieved from Envirolink Decision Support System (DSS) Directory: http://tools.envirolink.govt.nz/dsss/new-zealand-empirical-erosion-model/

ESRI. (n.d.). *How surface parameters works*. Retrieved from ArcGIS Pro: https://pro.arcgis.com/en/pro-app/latest/tool-reference/3d-analyst/how-surface-parameters-works.htm

Fernandez, M. A., & Daigneault, A. (2017). Erosion mitigation in the Waikato District, New Zealand: economic implications for agriculture. *Agricultural Economics, 48*(3), 341-361.

Food and Agriculture Organization. (2006). *Guidelines for soil description.* Retrieved from Food and Agriculture Organization: https://www.fao.org/3/a0541e/a0541e.pdf

*Fundamental Soil Layers*. (n.d.). Retrieved from Manaaki Whenua - Landcare Research: https://soils.landcareresearch.co.nz/soil-data/fundamental-soil-layers/

Gerrard, J. (1993). Soil geomorphology - Present dilemmas and future challenges. *Geomorphology, 7*, 61-84.

Gillingham, A. G. (1973). Influence of physical factors on pasture growth on hill country. *Proceedings of the New Zealand Grassland Association, 35*, 77-85.

Glass, C., & Silverstein, J. (1998). Denitrification kinetics of high nitrate concentration water: pH effect on inhibition and nitrite accumulation. *Water Research, 32*(3), 831-839.

Gradwell, M. W. (1979). Subsoil hydraulic conductivities of major New Zealand soil groups at water contents near field capacity. *New Zealand Journal of Agricultural Research, 22*(4), 603-614.

Hall, G. F. (1983). Pedogenesis and soil taxonomy. In *Developments in soil science* (Vol. 11, pp. 117-140). Elsevier.

Hammond, A. P. (1997). Late Quaternary landscape evolution of western Hawkes Bay, North Island, New Zealand. *[Unpublished Doctoral Thesis]*. Massey University.

Heuvelink, G. B., & Webster, R. (2001). Modelling soil variation: past, present, and future. *Geoderma, 100*(3-4), 269-301.

Hewitt, A. E., Balks, M. R., & Lowe, D. J. (2021). Pallic Soils. In A. E. Hewitt, M. R. Balks, & D. J. Lowe, *The soils of Aotearoa New Zealand* (pp. 145-162). Springer Cham.

Hewitt, A., & Dymond, J. (2013). Survey of New Zealand soil orders. *Ecosystem services in New Zealand, 1*(10), 121-131.

Hewitt, A., Lynn, I., Manderson, A., Wilde, H., & Willoughby, J. (2008). *Assessment of avaliable soil and land resource information for the Manawatu-Whanganui region.* Landcare Research.

Horizons Regional Council. (2014). *One Plan: The consolidated regional policy statement, regional plan and regional coastal plan for the Manawatu-Whanganui region.* Manawatu, New Zealand: Horizon Regional Council.

Horizons Regional Council. (2019). Rangitikei Catchment - State of environment summary 2019. Horizons Regional Council. Retrieved from Horizons: https://www.horizons.govt.nz/HRC/media/Media/Water/Catchment-Summary-Rangitikei.pdf

Huggett, R. J. (1975). Soil landscape systems: A model of soil genesis. *Geoderma, 13*, 1-22.

Jenny, H. (1941). *Factors of soil formation: A system of quantitative pedology.* New York: McGraw-Hill.

Jha, N., Singh, R., & McMillan, A. (2018). *Efficacy of subsurface denitrification to attenuate nitrate in shallow groundwaters.* (Eds L. D. Currie and C.L. Christensen), Occasional Report No. 31. Fertilizer and Lime Research Centre. Palmerston North, New Zealand: Massey University. Retrieved from http://flrc.massey.ac.nz/publications.html

Jol, H. M. (2008). *Ground penetrating radar theory and applications.* Elsevier.

Klute, A. (1982). Tillage effects on the hydraulic properties of soil: a review. *Predicting tillage effects on soil physical properties and process, 44*, pp. 29-43.

Korom, S. F. (1992). Natural denitrification in the saturated zone: a review. *Water resources research, 28*(6), 1657-1668.

Lambert, M. G., & Roberts, E. (1976). Aspect differences in an unimproved hill country pasture. *New Zealand Journal of Agricultural Research, 19*(4), 459-467.

Lambert, R. (2022, March 20). Personal Communication.

LandVision. (2017). *Whole Farm Plans*. Retrieved from LandVision: https://landvision.co.nz/whole-farm-plans/

LAWA - Land Air Water Aotearoa. ((n.d. b)). *Manawatu - Whanganui region - Rangitikei at Mangaweka*. Retrieved from Lawa - Land Air Water Aotearoa: https://www.lawa.org.nz/explore-data/manawat%C5%AB-whanganui-region/water-quantity/monitoring-sites/rangitikei-at-mangaweka/

LAWA - Land Air Water Aotearoa. (2022, November 14). *Manawatu-Whanganui Region - Pourewa Catchment at Tututotara*. Retrieved from LAWA-Land Air Water Aotearoa:

https://www.lawa.org.nz/explore-data/manawat%C5%AB-whanganui-region/water-quantity/monitoring-sites/porewa-catchment-at-tututotara/

LAWA - Land Air Water Aotearoa. (n.d.). *Land Cover*. Retrieved from LAWA: https://www.lawa.org.nz/explore-data/land-cover/

LAWA - Land Air Water Aotearoa. (n.d. a). *Factsheet: Phosphorus*. Retrieved from LAWA: Land Air Water Aotearoa: https://www.lawa.org.nz/learn/factsheets/phosphorus/

Lilburne, L. R., Hewitt, A. E., & Webb, T. W. (2012). Soil and informatics science combine to develop S-map: A new generation soil information system for New Zealand. *Geoderma, 170*, 232-238.

Lilburne, L. R., Lynn, I. H., & Webb, T. H. (2016). Issues in using Land Use Capability class to set nitrogen leaching limits in moisture-deficient areas - a South Island case study. *New Zealand Journal of Agricultural Research, 59*(1), 1-17.

Lilburne, L., Hewitt, A., Webb, T., & Carrick, S. (2004). S-map - a new soil database for New Zealand. *SuperSoil 2004: Proceediings of the 3rd Australian New Zealand Soils Conference, Sydney, Australia*, pp. 5-9.

Lynn, I., Manderson, A., Page, M., Harmsworth, G., Eyles, G., Douglas, G., . . . Newsome, P. (2009). *Land use capability survey handbook: A New Zealand handbook for the classification of land.* Hamilton: Landcare Research.

Maanaki Whenua Landcare Research. (2010). *Soil Map of Rangitikei County*. Retrieved from LRISPortal: https://lris.scinfo.org.nz/layer/48161-soil-map-of-rangitikei-county/

Maher, W., & Woo, L. (1998). Procedures for the storage and digestion of natural waters for the determination of filterable reactive phosphorus, total filterable phosphorus and total phosphorus. *Analytica Chimica Acta, 375*(1-2), 5-47.

Manaaki Whenua - Landcare Research. (2020, August). LINKOnline Webinar: digging deeper improved soil water retention information in S-map [Video]. Retrieved from https://www.youtube.com/watch?v=XJtSwat1jDY

Manaaki Whenua - Landcare Research. (2023). *S-Map Online - The digital soil map for New Zealand*. Retrieved from S-Map Online - Manaaki Whenua: https://smap.landcareresearch.co.nz/

Manaaki Whenua - Landcare Research. (n.d.). *Glossary*. Retrieved from S-Map Online: https://smap.landcareresearch.co.nz/support/glossary/

Manderson, A., & Palmer, A. (2006). Soil information for agricultural decision making: A New Zealand perspective. *Soil Use and Management, 22*, 393-400.

Manderson, A., Mackay, A., Lambie, J., & Roygard, J. (2013). Sustainable land use initative by Horizons. *NZ Journal of Forestry, 57*(4), 4-8.

Maynard, J. J., & Johnson, M. G. (2014). Scale-dependency of LiDAR derived terrain attributes in quantitative soil-landscape modelling: Effects of grid resolution vs. neighbourhood extent. *Geoderma, 230*, 29-40.

McIntosh, P. D., Lynn, I. H., & Johnstone, P. D. (2000). Creating and testing a geometric soil-landscape model in dry steeplands using a very low sampling density. *Australian Journal of Soil Research, 38*(1), 101-112.

McLeod, M., Rijikse, W. C., & Dymond, J. R. (1995). A soil-landscape model for close-jointed mudstone, Gisborne-East Cape, North Island, New Zealand. *Soil Research, 33*(3), 381-396.

McMahon, P. B., & Chapelle, F. (2008). Redox processes and water quality of selected principal aquifer systems. *Groundwater, 46*(2), 259-271.

McMillan, H. K., & Srinivasan, M. S. (2015). Characteristics and controls of variablility in soil moisture and groundwater in a headwater catchment. *Hydrology and Earth Systems Sciences, 19*(4), 1767-1786.

McNeill, S. J., Lilburne, L. R., Carrick, S., Webb, T. H., & Cuthill, T. (2018). Pedotransfer functions for the soil water characteristics of New Zealand soils using S-map information. *Geoderma, 326*, 96-110.

Milne, J. D. (1972). River terraces in the Rangitikei basin, North Island, New Zealand. Scale 1:50,000. New Zealand Soil Bureau Maps 142/1, 142/2, 142/3, 142/4, to accompany New Zealand Soil Survey Report 34.

Milne, J. D., Claydon, B., Singleton, P. L., & Wilson, A. D. (1995). *Soil description handbook - Revised edition.* Lincoln, Canterbury, New Zealand: Manaaki Whenua Press.

Ministry for the Environment and Ministry for Primary Industries. (2021). *Freshwater farm plan regulations: Discussion document.* Wellington, New Zealand: Ministry for the Environment.

Molloy, L. (1988). *Soils in the New Zealand landscape: the living mantle* (2 ed.). New Zealand Society of Soil Science.

Munsell Color. (2009). *Munsell soil-colour charts - with genuine Munsell® colour chips.* Munsell Color.

Naish, T., & Kamp, P. J. (1995). Pliocene-Pleistocene marine cyclothems, Wanganui Basin, New Zealand: A lithostratigraphic framework. *New Zealand Journal of Geology and Geophysics, 38*(2), 223-243.

Naish, T., Kamp, P. J., Alloway, B. V., Pillans, B., Wilson, G. S., & Westgate, J. A. (1996). Integrated tephrochronology and magnetostratigraphy for cyclothemic marine strata, Wanganui Basin: implications for the Pliocene-Pleistocene boundary in New Zealand. *Quaternary International, 34-36*, 29-48.

National Geographic Society. (2022). *Swamp*. Retrieved from National Geographic: https://education.nationalgeographic.org/resource/swamp/

*New Zealand Land Resource Inventory - Soil*. (n.d.). Retrieved from Manaaki Whenua - Landcare Research: https://soils.landcareresearch.co.nz/soil-data/nzlri-soils/

OpenTopography. (n.d.). *Manawatu-Whanganui, New Zealand 2015-2016*. Retrieved from OpenTopography - High-Resolution Topography Data and Tools: https://portal.opentopography.org/datasetMetadata?otCollectionID=OT.052019.2193.1

Palmer, A. (2023). Personal Communication.

Palmer, A., Begg, J., Townsend, D., & Wilson, K. (2006). The late Castlecliffian and early Haweran stratigraphy of the Manawatu and Rangitikei districts. GSNZ Conference.

Pennock, D., Yates, T., & Braidek, J. (2008). Chapter 1: Soil Sampling Designs. In M. R. Carter, & E. G. Gregorich (Eds.), *Soil sampling and methods of analysis* (2nd ed., pp. 26-39). Canadia Society of Soil Science.

Phillips, C., Marden, M., & Basher, L. R. (2018). Geomorphology and forest management in New Zealand's erodible steeplands: An overview. *Geomorpholgy, 307*, 107-121.

Radcliffe, J. E. (1968). Soil conditions on tracked hillside pastures. *New Zealand Journal of Agricultural Research, 11*(2), 359-370.

Radcliffe, J. E. (1976). X. Rangitikei district. *New Zealand Journal of Experimental Agriculture, 4*(2), 163-170.

Rees, C. (2020, October). Personal Communication.

Rees, C., Palmer, A., & Palmer, J. (2020). Litho-structural controls on Quaternary landslide distribution in the Rangitikei hill counrty, North Island, New Zealand. *New Zealand Journal of Geology and Geophysics, 63*(1), 90-109.

Rees, C., Palmer, A., Palmer, J., & Singh, R. (2020). Variation in saturated hydraulic conductivity at the outcrop scale, the Whanganui Basin, New Zealand. *Groundwater, 58*(4), 622-637.

Rees, C., Palmer, J., Palmer, A., & Singh, R. (2019). Landscape evolution and hydrogeochemical characteristics of the Pourewa Stream catchment, lower North Island, New Zealand. *New Zealand Journal of Geology and Geophysics, 62*(2), 147-170.

Reid, J. (2014). Achieving improved soil management on-farm - insights from a New Zealand case study. *11th European IFSA Symposium, Farming Systems Facing Global Challenges: Capacities and Strategies, Proceedings, Berlin, Germany 1- 4 April* (pp. 1920-1928). International Farming Systems Association (IFSA) Europe.

Richter, J. L., & Burras, C. L. (2017). Human-impacted catenas in North-Central Iowa, United States. In P. Pereira, E. Brevik, M. Munoz-Rojas, & B. Miller (Eds.), *Soil mapping and process modeling for sustainable land use management* (pp. 335-363). Elsevier.

Rissmann, C. (2011). *Regional mapping of groundwater denitrification potential and aquifer sensitivity.* Environment Southland - Te Taiao Tonga.

Ristau, J. (2008). Implementation of routine regional moment tensor analysis in New Zealand. *Seismological Research Letters, 79*(3), 400-415.

Rivas, A., Singh, R., Horne, D., Roygard, J., Matthews, A., & Hedley, M. J. (2017). Denitrification potential in the subsurface environment in the Manawatu River catchment, New Zealand: Indications from oxidation-reduction conditions, hydrogeological factors, and implications for nutrient management. *Journal of Environmental Management, 197*, 476-489.

Roley, S. S., Tank, J. L., Stephen, M. L., Johnson, L. T., Beaulieu, J. J., & Witter, J. D. (2012). Floodplain restoration enhances denitrification and reach-scale nitrogen removal in an agricultural stream. *Ecological Applications, 22*(1), 281-297.

Roygard, C., & Clark, M. (2012). Supplementary statement by Jon Roygard and Maree Clark on nutrient load scenarios and methodology. Palmerston North. Retrieved from https://www.horizons.govt.nz/HRC/media/Media/One%20Plan/New-Approach-to-evidence-Jon-and-Maree-20120224.pdf?ext=.pdf

Schaetzl, R. J. (2013). Catenas and soils. In *Treatise on Geomorphology* (Vol. 4, pp. 145-158). Elsevier.

Schierlitz, C., Dymond, J., & Shepherd, J. (2006). *Erosion/sedimentation in the Manawatu catchment associated with scenarios of Whole Farm Plans.* Report (0607/028). Palmerston North, New Zealand: Landcare Research.

Schmidt, J., & Hewitt, A. (2004). Fuzzy land element classification from DTMs based on geometry and terrain position. *Geoderma, 121*(3-4), 243-256.

Schmidt, J., Tonkin, P., & Hewitt, A. (2005). Quantitative soil-landscape models for the Haldon and Hurunui soil sets, New Zealand. *Australian Journal of Soil Research, 43*, 127-137.

Selbie, D. R., Watkins, N. L., Wheeler, D. M., & Shepherd, M. A. (2013). Understanding the distribution and fate of nitrogen and phosphorus in OVERSEER®. *Proceedings of the New Zealand Grassland Association*, 113-118.

Sherlock, M. D., & McDonnell, J. J. (2003). A new tool for hillslope hydrologists: Spatially distributed groundwater level and soilwater content measured using electromagnetic induction. *Hydrological Processes, 17*(10), 1965-1977.

Singh, R., Elwan, A., Horne, D., Manderson, A., Patterson, M., & Roygard, J. (2017). *Predicting land-based nitrogen loads and attenuation in the Rangitikei river catchment - The model development.* (Eds. L. D. Currie and M. J. Hedley), Occasional Report No. 30. Fertilizer and Lime Research Centre. Palmerston North, New Zealand: Massey University. Retrieved from http://flrc.massey.ac.nz/publications.html

Smith, K. C., & McGrath, D. A. (2011). The alteration of soil chemistry through shell deposition on a Georgia (U.S.A) barrier island. *Journal of Coastal Research, 27*(1), 103-109.

Snelder, T. H., Whitehead, A. L., Fraser, C., Larned, S. T., & Schallenberg, M. (2020). Nitrogen loads to New Zealand aquatic receiving environments: comparison with regulatory criteria. *New Zealand Journal of Marine and Freshwater Research, 54*(3), 527-550.

Stenger, R., Clague, J., Woodward, S., Moorhead, B., Burbery, L., & Canard, H. (2012). *Groundwater assimilative capacity - An untapped opportunity for catchment-scale nitrogen management?* (Eds L. D. Currie and C. L. Christensen), Occasional Report No. 25. Fertilizer and Lime Research Centre. Palmerston North, New Zealand: Massey University. Retrieved from http://flrc.massey.ac.nz/publications.html

Stieglitz, M., Shaman, J., McNamara, J., Engle, V., Shanley, J., & Kling, G. W. (2003). An approach to understanding hydrologic connectivity on the hillslope and the implications for nutrient transport. *Global Biogeochemical Cycles, 17*(4).

Sutherland, R. (1999). Basement geology and tectonic development of the greater New Zealand region: An interpretation from regional magnetic data. *Tectonophysics, 308*, 341-362.

Taylor, N. H., & Pohlen, I. J. (1962). *Soil survey methods: A New Zealand handbook for the field study of soils* (Vol. 25). Department of Scientific and Industrial Research.

Todd, M. (2018). *Learnings from ten years of hill country farm plan mapping.* (Eds L. D. Currie and C. L. Christensen), Occasional Report No. 31. Fertilizer and Lime Research Centre. Palmerston North, New Zealand: Massey University. Retrieved from https://www.massey.ac.nz/~flrc/publications.html

Toitū Te Whenua - Land Information New Zealand. (2019, May). *LINZ Data Service - Manawatu-Whanganui LiDAR 1m DEM (2015-2016)*. Retrieved from LINZ Data Service: https://data.linz.govt.nz/layer/102475-manawatu-whanganui-lidar-1m-dem-2015-2016/

Toitū Te Whenua - New Zealand Land Information. (2013). *New Zealand Gazetteer*. Retrieved from Toitū Te Whenua - New Zealand Land Information: https://gazetteer.linz.govt.nz/place/36537

Tommaso, C. (2015). Analysis of rainfall trend in New Zealand. *Environmental Earth Sciences, 73*(10), 6297-6310.

Tonkin, P. J. (1994). Principles of soil-landscape modeling and their application in the study of soil-landform relationships within drainage basins. In T. H. Webb (Ed.), *Soil-landscape modelling in New Zealand* (pp. 20-37). Manaaki Whenua Press.

Trudell, M. R., Gillham, R. W., & Cherry, J. A. (1986). An in-situ study of the occurrence and rate of denitrification in a shallow unconfined sand aquifer. *Journal of Hydrology, 83*(3-4), 251-268.

Vogeler, I., Carrick, S., Cichota, R., & Lilburne, L. (2019). Estimation of soil subsurface hydraulic conductiviy based on inverse modelling and soil morphology. *Journal of Hydrology, 574*, 373-382.

Vogeler, I., Cichota, R., & Beautrais, J. (2016). Linking Land Use Capability classes and APSIM to estimate pasture growth for regional land use planning. *Soil Research, 54*, 94-110.

Waterclean. (2011). *Hunterville Wastewater Treatment Plant*. Retrieved from Waterclean Technologies: http://waterclean.co.nz/case-studies/hunterville-wastewater-treatment-plant/

Weihermüller, L., Huisman, J. A., Lambot, S., Herbst, M., & Vereecken, H. (2007). Mapping the spatial variation of soil water content at the field scale with different ground penetrating radar techniques. *Journal of Hydrology, 340*(3), 205-216.

Westerhoff, R. S., Tschritter, C., & Rawlinson, Z. J. (2019). *New Zealand groundwater atlas: Depth to hydrogeological basement.* GNS Science.

Wilkinson, S. N., Prosser, I. P., Rustomji, P., & Read, A. M. (2009). Modelling and testing spatially distributed sediment budgets to relate erosion processes to sediment yields. *Enviromental Modelling & Software, 24*, 489-501.

Wilson, S., Close, M., & Abraham, P. (2016). *Predicting groundwater redox status in the Southland region.* (Report No. 1026-2-R1). Christchurch: Lincoln AgriTech.

Wuddivira, M. N., & Camps-Roach, G. (2007). Effects of organic matter and calcium on soil structural stability. *European Journal of Soil Science, 58*(3), 722-727.

Zajícová, K., & Chuman, T. (2019). Application of ground penetrating radar methods in soil studies: A review. *Geoderma, 343*, 116-129.

Zarour, H. I. (2018). Characterisaton and numerical simulation of the lower Manawatu catchment hydrogeological system. *[Unpublished doctorial dissertation]*. Massey University. Retrieved from https://mro.massey.ac.nz/handle/10179/14791

# Chapter 9 – Appendix

## Appendix 1 – LRI Extended Codes

| LRI Code | Geology | Soil Name | Slope | Erosion (Type & Severity) | Vegetation Cover |
|---|---|---|---|---|---|
| **Class1** | Or | WhS + PhS | D + G | SS,s1 | gIgT* |
| **Class 2** | Mo + Mm | RgS | C + F/G | SS,sϴ + Shϴ | gI |
| **Class 3** | Mm + Mo | RaH-T | C/D + F/G | Sh1 + SS,s1 | gIgT* |
| **Class 4** | Mo | MmS + KkS | D + F/G | SS,s1 | gIgT* |
| **Class 5** | Q1k1/Q1k2 + Or | PkS | C + F | Shϴ | gI |
| **Class 6** | Or | SpS + RaH-H | C + F | SS,s1 + Shϴ | gIgT* |
| **Class 7** | Or + Mo | MoS | D + F | Shϴ | gIgT* |
| **Class 8** | Or + Q1a | K + Oh | A | Sb2 | hRhW* |
| **Class 9** | Mm | MmS | D + G | Trϴ + SS,s1 | gIgT* |
| **Class 10** | Mm + Or | HvH | C + F | SS,s1 | gI |

*Table 17: The extended LRI codes for Ngatiapa, displaying the individual classes involved in LRI classification. K - includes the soils of K (a) and K (b); Oh - includes the soils of Oh (a) and Oh(b); RaH-T - includes the soils of RaH -T, RaH-T (a), RaH-T (b) and RaH-T (c); MmS – includes the soils of MmS, MmS (a) and MmS (b).*

## Appendix 2 – Rainfall Data for July 2021 to January 2022.

| June Rainfall (mm) | | July Rainfall (mm) | | August Rainfall (mm) | | September Rainfall (mm) | |
|---|---|---|---|---|---|---|---|
| 01/06/2021 | 2.54 | 01/07/2021 | 0 | 01/08/2021 | 0 | 01/09/2021 | 0 |
| 02/06/2021 | 0 | 02/07/2021 | 0.25 | 02/08/2021 | 0 | 02/09/2021 | 0 |
| 03/06/2021 | 0 | 03/07/2021 | 0.25 | 03/08/2021 | 13.72 | 03/09/2021 | 0 |
| 04/06/2021 | 0 | 04/07/2021 | 0.25 | 04/08/2021 | 0 | 04/09/2021 | 0 |
| 05/06/2021 | 0 | 05/07/2021 | 0 | 05/08/2021 | 2.54 | 05/09/2021 | 0 |
| 06/06/2021 | 0 | 06/07/2021 | 0 | 06/08/2021 | 2.79 | 06/09/2021 | 0 |
| 07/06/2021 | 0 | 07/07/2021 | 8.38 | 07/08/02021 | 0.51 | 07/09/2021 | 2.45 |
| 08/06/2021 | 0 | 08/07/2021 | 2.29 | 08/08/2021 | 33.27 | 08/09/2021 | 19.56 |
| 09/06/2021 | 0 | 09/07/2021 | 1.78 | 09/08/2021 | 7.37 | 09/09/2021 | 4.06 |
| 10/06/2021 | 0 | 10/07/2021 | 0.76 | 10/08/2021 | 0 | 10/09/2021 | 9.4 |
| 11/06/2021 | 0 | 11/07/2021 | 0.76 | 11/08/2021 | 0 | 11/09/2021 | 3.05 |
| 12/06/2021 | 0 | 12/07/2021 | 0 | 12/08/2021 | 0 | 12/09/2021 | 0 |
| 13/06/2021 | 0 | 13/07/2021 | 0 | 13/08/2021 | 7.62 | 13/90/2021 | 25.15 |
| 14/06/2021 | 0 | 14/07/2021 | 0 | 14/08/2021 | 1.52 | 14/09/2021 | 14.48 |
| 15/06/2021 | 10.67 | 15/07/2021 | 0 | 15/08/2021 | 0 | 15/09/2021 | 3.81 |
| 16/06/2021 | 2.03 | 16/07/2021 | 0 | 16/08/2021 | 0 | 16/09/2021 | 11.94 |
| 17/06/2021 | 1.52 | 17/07/2021 | 11.18 | 17/08/2021 | 23.88 | 17/09/2021 | 0.51 |
| 18/06/2021 | 2.29 | 18/07/2021 | 8.64 | 18/08/2021 | 17.02 | 18/09/2021 | 0 |
| 19/06/2021 | 0 | 19/07/2021 | 32.26 | 19/08/2021 | 0.25 | 19/09/2021 | 0 |
| 20/06/2021 | 5.84 | 20/07/2021 | 0 | 20/08/2021 | 3.3 | 20/09/2021 | 0.25 |
| 21/06/2021 | 1.52 | 21/07/2021 | 0 | 21/08/2021 | 0 | 21/09/2021 | 0 |
| 22/06/2021 | 1.27 | 22/07/2021 | 7.87 | 22/08/2021 | 0 | 22/09/2021 | 5.84 |
| 23/06/2021 | 0 | 23/07/2021 | 1.52 | 23/08/2021 | 0 | 23/09/2021 | 1.27 |
| 24/06/2021 | 0 | 24/07/2021 | 0 | 24/08/2021 | 0 | 24/09/2021 | 0 |
| 25/06/2021 | 0.25 | 25/07/2021 | 0 | 25/08/2021 | 0 | 25/09/2021 | 0.2 |
| 26/06/2021 | 0.25 | 26/07/2021 | 0.51 | 26/08/2021 | 0 | 26/09/2021 | 2.29 |
| 27/06/2021 | 5.33 | 27/07/2021 | 16 | 27/08/2021 | 9.4 | 27/09/2021 | 2.29 |
| 28/06/2021 | 28.45 | 28/07/2021 | 0.25 | 28/08/2021 | 6.86 | 28/09/2021 | 31.5 |
| 29/06/2021 | 6.35 | 29/07/2021 | 1.27 | 29/08/2021 | 17.53 | 29/09/2021 | 31.5 |
| 30/06/2021 | 10.92 | 30/07/2021 | 0.25 | 30/08/2021 | 1.27 | 30/09/2021 | 2.79 |
| | | 31/07/2021 | 0 | 31/08/2021 | 0 | | |

*Table 18: Rainfall data for June to September 2021 from weather station in Mangaonoho retrieved from Weather Underground.*

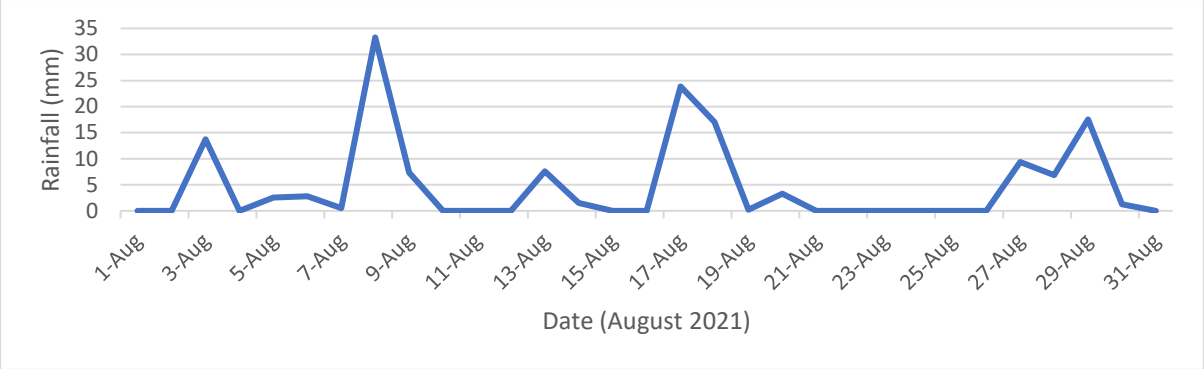


*Figure 89: Rainfall across the month of August 2021.*

| October Rainfall (mm) | | November Rainfall (mm) | | December Rainfall (mm) | | January Rainfall (mm) | |
|---|---|---|---|---|---|---|---|
| 01/10/2021 | 2.79 | 01/11/2021 | 3.56 | 01/12/2021 | 19.81 | 01/01/2022 | 0 |
| 02/10/2021 | 0.25 | 02/11/2021 | 0.25 | 02/12/2021 | 0.51 | 02/01/2022 | 0 |
| 03/10/2021 | 0 | 03/11/2021 | 0 | 03/12/2021 | 1.52 | 03/01/2022 | 0 |
| 04/10/2021 | 20.32 | 04/11/2021 | 0 | 04/12/2021 | 1.52 | 04/01/2022 | 0 |
| 05/10/2021 | 20.32 | 05/11/2021 | 1.27 | 05/12/2021 | 1.02 | 05/01/2022 | 0 |
| 06/10/2021 | 0 | 06/11/2021 | 1.27 | 06/12/2021 | 4.83 | 06/01/2022 | 0 |
| 07/10/2021 | 1.02 | 07/11/2021 | 0.25 | 07/12/2021 | 5.84 | 07/01/2022 | 0 |
| 08/10/2021 | 4.32 | 08/11/2021 | 0 | 08/12/2021 | 10.16 | 08/01/2022 | 0 |
| 09/10/2021 | 4.32 | 09/11/2021 | 0 | 09/12/2021 | 10.16 | 09/01/2022 | 0 |
| 10/10/2021 | 4.06 | 10/11/2021 | 0 | 10/12/2021 | 0.25 | 10/01/2022 | 0 |
| 11/10/2021 | 4.06 | 11/11/2021 | 0 | 11/12/2021 | 0 | 11/01/2022 | 0 |
| 12/10/2021 | 25.65 | 12/11/2021 | 0.25 | 12/12/2021 | 40.39 | 12/01/2022 | 0 |
| 13/10/2021 | 25.65 | 13/11/2021 | 9.91 | 13/12/2021 | 51.56 | 13/01/2022 | 0 |
| 14/10/2021 | 17.78 | 14/11/2021 | 9.91 | 14/12/2021 | 52.83 | 14/01/2022 | 0 |
| 15/10/2021 | 0 | 15/11/2021 | 7.87 | 15/12/2021 | 52.83 | 15/01/2022 | 0 |
| 16/10/2021 | 0 | 16/11/2021 | 8.89 | 16/12/2021 | 52.83 | 16/01/2022 | 0 |
| 17/10/2021 | 0 | 17/11/2021 | 39.37 | 17/12/2021 | 28.45 | 17/01/2022 | 0 |
| 18/10/2021 | 4.83 | 18/11/2021 | 39.37 | 18/12/2021 | 1.27 | 18/01/2022 | 0 |
| 19/10/2021 | 4.83 | 19/11/2021 | 0.25 | 19/12/2021 | 0 | 19/01/2022 | 0 |
| 20/10/2021 | 0 | 20/11/2021 | 0 | 20/12/2021 | 0 | 20/01/2022 | 7.37 |
| 21/10/2021 | 0 | 21/11/2021 | 0 | 21/12/2021 | 0 | 21/01/2022 | 7.37 |
| 22/10/2021 | 0 | 22/11/2021 | 5.84 | 22/12/2021 | 0 | 22/01/2022 | 0 |
| 23/10/2021 | 0 | 23/11/2021 | 5.84 | 23/12/2021 | 0 | 23/01/2022 | 0 |
| 24/10/2021 | 0 | 24/11/2021 | 0 | 24/12/2021 | 0 | 24/01/2022 | 25.12 |
| 25/10/2021 | 1.78 | 25/11/2021 | 0 | 25/12/2021 | 0 | 25/01/2022 | 25.15 |
| 26/10/2021 | 1.78 | 26/11/2021 | 0 | 26/12/2021 | 0 | 26/01/2022 | 13.97 |
| 27/10/2021 | 2.03 | 27/11/2021 | 0 | 27/12/2021 | 0 | 27/01/2022 | 14.22 |
| 28/10/2021 | 25.65 | 28/11/2021 | 0 | 28/12/2021 | 13.72 | 28/01/2022 | 0.25 |
| 29/10/2021 | 25.91 | 29/11/2021 | 1.78 | 29/12/2021 | 14.22 | 29/01/2022 | 0 |
| 30/10/2021 | 4.06 | 30/11/2021 | 19.81 | 30/12/2021 | 6.1 | 30/01/2022 | 0 |
| 31/10/2021 | 3.56 | | | 31/12/2021 | 0 | 31/01/2022 | 0 |

*Table 19: Rainfall data for October 2021 to January 2022 from weather station in Mangaonoho retrieved from Weather Underground.*

## Appendix 3 – Infield and Laboratory Data for Piezometers and Surface Waters.

| Piezometer 1 | | | | | | | | |
|---|---|---|---|---|---|---|---|---|
| **Date (Month/Year)** | Water Level (bgl, cm) | Water Level (masl) | RDO ($mgL^{-1}$) – Average | ORP (mV) – Average | pH – Average | Nitrogen ($N\text{-}NO_3$, $mgL^{-1}$) | Phosphorus (DRP – $mgL^{-1}$) | Phosphorus (DRP – Abs) |
| **June 2021** | 23 | 306.271 | ~~6.875~~ | ~~N/A~~ | ~~5.027~~ | BDL | 0.040 | 0.039 |
| **July 2021** | 13 | 306.371 | ~~6.838~~ | ~~N/A~~ | ~~4.582~~ | BDL | 0.042 | 0.041 |
| **September 2021** | 13.00 | 306.371 | 4.148 | 221.995 | 2.39 | 0.0165 | 0.076 | 0.073 |
| **October 2021** | 12.50 | 306.376 | 3.058 | 477.718 | 4.875 | BDL | 0.122 | 0.116 |
| **November 2021** | 6.00 | 306.441 | 2.445 | 346.973 | 5.795 | BDL | 0.210 | 0.199 |
| **December 2021** | 10.00 | 306.401 | 1.289 | 425.963 | 5.760 | 0.7009 | 0.223 | 0.211 |
| **January 2022** | 77.00 | 306.731 | N/A** | N/A** | N/A** | N/A** | N/A** | N/A** |

*Table 20: Piezometer 1 groundwater sampling data (infield and lab analysis). N/A – Attribute not collected during sampling, ~~Strike through~~ – data omitted due to incorrect sampling procedures, BDL – below detectable level, N/A** - Not enough in piezometer to collect sample.*

| Piezometer 2 | | | | | | | | |
|---|---|---|---|---|---|---|---|---|
| **Date (Month/Year)** | Water Level (bgl, cm) | Water Level (masl) | RDO ($mgL^{-1}$) – Average | ORP (mV) – Average | pH – Average | Nitrogen ($N\text{-}NO_3$, $mgL^{-1}$) | Phosphorus (DRP – $mgL^{-1}$) | Phosphorus (DRP – Abs) |
| **June 2021** | 32.00 | 312.791 | ~~9.111~~ | ~~N/A~~ | ~~5.376~~ | BDL | 0.025 | 0.025 |
| **July 2021** | 3.00 | 313.081 | ~~7.442~~ | ~~N/A~~ | ~~4.053~~ | 0.0489 | 0.024 | 0.024 |
| **September 2021** | -3.00 | 313.081 | 0.486 | 444.515 | 5.446 | BDL | 0.044 | 0.042 |
| **October 2021** | -5.00 | 313.061 | 0.329 | 522.006 | 5.062 | 0.0369 | 0.041 | 0.043 |
| **November 2021** | 16.00 | 312.951 | 0.290 | 402.227 | 5.786 | 0.0318 | 0.087 | 0.083 |
| **December 2021** | -2.00 | 313.091 | 0.290 | 437.200 | 5.652 | 0.0376 | 0.044 | 0.042 |
| **January 2022** | 93.00 | 312.181 | N/A** | N/A** | N/A** | N/A** | N/A** | N/A** |

*Table 21: Piezometer 2 groundwater sampling data (infield and lab analysis). N/A – Attribute not collected during sampling, ~~Strike through~~ – data omitted due to incorrect sampling procedures, BDL – below detectable level, N/A** - Not enough in piezometer to collect sample.*

| Piezometer 3 | | | | | | | | |
|---|---|---|---|---|---|---|---|---|
| **Date (Month/Year)** | Water Level (bgl, cm) | Water Level (masl) | RDO ($mgL^{-1}$) – Average | ORP (mV) – Average | pH – Average | Nitrogen ($N\text{-}NO_3$, $mgL^{-1}$) | Phosphorus (DRP – $mgL^{-1}$) | Phosphorus (DRP – Abs) |
| **June 2021** | 23.00 | 317.513 | ~~3.455~~ | ~~N/A~~ | ~~5.072~~ | 0.0143 | 0.032 | 0.031 |
| **July 2021** | 15.00 | 317.493 | ~~5.096~~ | ~~N/A~~ | ~~4.582~~ | 0.236 | 0.040 | 0.039 |
| **September 2021** | 11.00 | 317.633 | 0.375 | 209.800 | 4.998 | 0.0084 | 0.045 | 0.043 |
| **October 2021** | 11.00 | 317.633 | 0.22 | 543.023 | 4.326 | 0.0028 | 0.045 | 0.043 |
| **November 2021** | 15.50 | 317.588 | 0.54 | 439.508 | 2.998 | 0.1053 | 0.066 | 0.063 |
| **December 2021** | 11.00 | 317.633 | 0.41 | 427.073 | 5.220 | 0.0419 | 0.068 | 0.065 |
| **January 2022** | 81.00 | 316.933 | N/A** | N/A** | N/A** | N/A** | N/A** | N/A** |

*Table 22: Piezometer 3 groundwater sampling data (infield and lab analysis). N/A – Attribute not collected during sampling, ~~Strike through~~ – data omitted due to incorrect sampling procedures, BDL – below detectable level, N/A** - Not enough in piezometer to collect sample.*

| Piezometer 4 | | | | | | | | |
|---|---|---|---|---|---|---|---|---|
| **Date (Month/Year)** | Water Level (bgl, cm) | Water Level (masl) | RDO ($mgL^{-1}$) – Average | ORP (mV) – Average | pH – Average | Nitrogen ($N\text{-}NO_3$, $mgL^{-1}$) | Phosphorus (DRP – $mgL^{-1}$) | Phosphorus (DRP – Abs) |
| **June 2021** | DRY | DRY | DRY | ~~N/A~~ | DRY | DRY | DRY | DRY |
| **July 2021** | 8.40 | 311.745 | ~~5..998~~ | ~~N/A~~ | ~~3.66~~ | 0.0281 | 0.041 | 0.040 |
| **September 2021** | 7.40 | 311.755 | 0.26 | 598.313 | 4.727 | 0.0285 | 0.065 | 0.062 |
| **October 2021** | 8.40 | 311.745 | 0.25 | 460.866 | 4.620 | 0.0146 | 0.069 | 0.066 |
| **November 2021** | 34.40 | 311.485 | 0.35 | 747.300 | 3.234 | BDL | 0.185 | 0.175 |
| **December 2021** | 3.90 | 311.790 | 0.43 | 403.909 | 5.365 | BDL | 0.130 | 0.123 |
| **January 2022** | 57.90 | 311.250 | N/A** | N/A** | N/A** | N/A** | N/A** | N/A** |

*Table 23: Piezometer 4 groundwater sampling data (infield and lab analysis). DRY – The piezometer was dry at the time of sampling, N/A – Attribute not collected during sampling, ~~Strike through~~ – data omitted due to incorrect sampling procedures, BDL – below detectable level, N/A** - Not enough in piezometer to collect sample.*

| Piezometer 5 | | | | | | | | |
|---|---|---|---|---|---|---|---|---|
| **Date (Month/Year)** | Water Level (bgl, cm) | Water Level (masl) | RDO ($mgL^{-1}$) – Average | ORP (mV) – Average | pH – Average | Nitrogen ($N\text{-}NO_3$, $mgL^{-1}$) | Phosphorus (DRP – $mgL^{-1}$) | Phosphorus (DRP – Abs) |
| **June 2021** | 68.70 | 294.111 | ~~4.495~~ | ~~N/A~~ | ~~4.144~~ | BDL | 0.053 | 0.051 |
| **July 2021** | -1.20 | 294.810 | ~~7.336~~ | ~~N/A~~ | ~~4.829~~ | BDL | 0.050 | 0.048 |
| **September 2021** | -0.20 | 294.800 | 0.3644 | 189.254 | 4.856 | 0.0668 | 0.039 | 0.038 |
| **October 2021** | -4.70 | 294.845 | 0.548 | 711.889 | 4.625 | 0.0168 | 0.445 | 0.42 |
| **November 2021** | 28.30 | 294.515 | 0.660 | 365.381 | 5.575 | 0.0181 | 0.052 | 0.05 |
| **December 2021** | -0.20 | 294.800 | 0.380 | 437.768 | 5.360 | 0.0409 | 0.084 | 0.08 |
| **January 2022** | 87.80 | 293.920 | 0.902 | 701.010 | 5.560 | BDL | 0.054 | 0.052 |

*Table 24: Piezometer 5 groundwater sampling data (infield and lab analysis). N/A – Attribute not collected during sampling, ~~Strike through~~ – data omitted due to incorrect sampling procedures, BDL – below detectable level, N/A** - Not enough in piezometer to collect sample.*

| Piezometer 6 | | | | | | | | |
|---|---|---|---|---|---|---|---|---|
| **Date (Month/Year)** | Water Level (bgl, cm) | Water Level (masl) | RDO ($mgL^{-1}$) – Average | ORP (mV) – Average | pH – Average | Nitrogen ($N\text{-}NO_3$, $mgL^{-1}$) | Phosphorus (DRP – $mgL^{-1}$) | Phosphorus (DRP – Abs) |
| **June 2021** | 16.50 | 283.096 | ~~6.054~~ | ~~N/A~~ | ~~4.53~~ | 1.11 | 0.040 | 0.039 |
| **July 2021** | -29.00 | 283.551 | ~~3.755~~ | ~~N/A~~ | ~~4.657~~ | BDL | 0.042 | 0.041 |
| **September 2021** | 5.00 | 28.211 | 0.349 | 138.197 | 4.447 | 0.0407 | 0.046 | 0.044 |
| **October 2021** | -22.00 | 28.481 | 0.416 | 674.067 | 4.19 | 0.0237 | 0.048 | 0.046 |
| **November 2021** | 66.00 | 283.601 | 3.588 | 651.870 | 5.463 | 0.0494 | 0.125 | 0.119 |
| **December 2021** | DNS | DNS | DNS | DNS | DNS | DNS | DNS | DNS |
| **January 2022** | 105.80 | 282.206 | N/A** | N/A** | N/A** | N/A** | N/A** | N/A** |

*Table 25: Piezometer 6 groundwater sampling data (infield and lab analysis). N/A – Attribute not collected during sampling, ~~Strike through~~ – data omitted due to incorrect sampling procedures, BDL – below detectable level, N/A** - Not enough in piezometer to collect sample, DNS – Did not sample the piezometer.*

| Surface Water 2 | | | |
|---|---|---|---|
| **Date (Month/Year)** | Nitrogen ($N\text{-}NO_3$, $mgL^{-1}$) | Phosphorus (DRP – $mgL^{-1}$) | Phosphorus (DRP – Abs) |
| **June 2021** | DNS | DNS | DNS |
| **July 2021** | 0.025 | 0.012 | 0.012 |
| **September 2021** | BDL | 0.030 | 0.029 |
| **October 2021** | 0.0902 | 0.042 | 0.041 |
| **November 2021** | 1.2906 | 0.057 | 0.055 |
| **December 2021** | 0.1425 | 0.081 | 0.077 |
| **January 2022** | DRY | DRY | DRY |

*Table 26: Surface water 2 data. DNS – Did not sample location, BDL – below detectable level, DRY – surface water location was dried up at sampling.*

| Surface Water 3 | | | |
|---|---|---|---|
| **Date (Month/Year)** | Nitrogen ($N\text{-}NO_3$, $mgL^{-1}$) | Phosphorus (DRP – $mgL^{-1}$) | Phosphorus (DRP – Abs) |
| **June 2021** | DNS | DNS | DNS |
| **July 2021** | DNS | DNS | DNS |
| **September 2021** | BDL | 0.191 | 0.181 |
| **October 2021** | 3.4442 | 0.458 | 0.432 |
| **November 2021** | 0.3288 | 0.331 | 0.313 |
| **December 2021** | 0.0602 | 0.690 | 0.651 |
| **January 2022** | DRY | DRY | DRY |

*Table 27: Surface water 3 data. DNS – Did not sample location, BDL – below detectable level, underlined – the sample was diluted 1:1 with water with results presented accounting for dilution factor, DRY – surface water location was dried up at sampling.*

| Surface Water 4 | | | |
|---|---|---|---|
| **Date (Month/Year)** | Nitrogen ($N\text{-}NO_3$, $mgL^{-1}$) | Phosphorus (DRP – $mgL^{-1}$) | Phosphorus (DRP – Abs) |
| **June 2021** | DNS | DNS | DNS |
| **July 2021** | DNS | DNS | DNS |
| **September 2021** | 0.0975 | 0.083 | 0.079 |
| **October 2021** | 0.0832 | 0.104 | 0.099 |
| **November 2021** | BDL | N/A* | N/A* |
| **December 2021** | 0.342 | 0.097 | 0.092 |
| **January 2022** | DRY | DRY | DRY |

*Table 28: Surface water 4 data. DNS – Did not sample location, BDL – below detectable level, N/A* - not enough sample was collected for analysing, underlined – the sample was diluted 1:1 with water with results presented accounting for dilution factor, DRY – surface water location was dried up at sampling.*

| Surface Water 5 | | | |
|---|---|---|---|
| **Date (Month/Year)** | Nitrogen ($N\text{-}NO_3$, $mgL^{-1}$) | Phosphorus (DRP – $mgL^{-1}$) | Phosphorus (DRP – Abs) |
| **June 2021** | 0.132 | 0.085 | 0.081 |
| **July 2021** | 0.0902 | 0.294 | 0.278 |
| **September 2021** | 0.229 | 0.087 | 0.083 |
| **October 2021** | 0.269 | 0.638 | 0.602 |
| **November 2021** | BDL | 0.055 | 0.053 (RT) |
| **December 2021** | 0.0192 | 0.139 | 0.132 |
| **January 2022** | 5.605 | 0.591 | 0.557 |

*Table 29: Surface water 5 data. DNS – Did not sample location, BDL – below detectable level, RT – Sample was retested using 5ml sample to 10ml Murphy-Riley Reagent, underlined – the sample was diluted 1:1 with water with results presented accounting for dilution factor.*

# Appendix 4 – Soil Descriptions: Soil Map Locations, Soil Description Test Sites and Oa,S Descriptions.

## Soil Map Locations

**LOC SD 1** (Figure 90)

**Location:** Loc SD1

175.6223160°E 39.8939770°S

**Parent Materials**: Mudstone (Orangipongo formation)

**Slope:** F (Steep at 26.5°)

**Aspect:** South

**Drainage:** Moderate over slow; depth to slow below 1040mm

**Erosion:** Sheet/ Runoff; present 0/5, potential 2/5

**Vegetation**: ***Present****:* Pasture and thistles

**Classification:** Hunterville hill soil - HvH

**Profile:**

| | | |
|---|---|---|
| Ap | 0 – 320mm | Silt loam; 7.5YR 3/2 (dark brown); moderately to weakly small blocky; very slightly sticky; fine roots (to 200mm) and few worms present; non plastic; diffuse contact (colour change) |
| Bw | 320 – 755mm | Silt loam; 10YR 4/4 (dark yellowish brown); moderate to weakly fine blocky; slightly sticky; slightly plastic; diffuse contact (colour change) |
| Cg | 755 – 1040mm+ | Silt loam; 10YR 4/6 (dark yellowish brown); weak crumb; 10% HC mottles (between 2.5YR 3/6 (dark red) and 2.5YR 4/8 (red)); slightly sticky; peaty wood fragments located; weakly, slightly plastic (30mm) |


*Figure 90: A) A photo of a section of the soil profile for soil description Loc 1. B) The location and surrounding area for soil description Loc 1.*

**LOC SD2**

**Location:** Loc SD2

175.6175733°E 39.8952965°S

**Parent Materials**: Mudstone (Mangamako shell bed formation)

**Slope:** D (Strongly rolling at 16°)

**Aspect:** East

**Drainage:** Well drained; depth to slow below 1105mm

**Erosion:** Sheet/ Runoff; present 0/5, potential 2/5

**Vegetation**: ***Present****:* Pasture, grasses, and few thistles

**Classification:** Murimotu silt loam – MmS

**Profile:**

| | | |
|---|---|---|
| Ap | 0 – 330mm | Silt loam; 7.5YR 3/4 (dark brown); moderately blocky; very weak stickiness; fine roots present; distinct contact (colour change) |
| Bw | 330 – 780mm | Silt loam; between 10YR 3/4 & 3/6 (dark yellowish brown & dark yellowish brown); fine weakly blocky; slightly sticky; few fine roots; non plastic; diffuse contact (colour change) |
| C | 780 – 1105mm+ | Silty clay loam; 10YR 5/4 (yellowish brown); no structure; strongly sticky; strong slightly plastic (40mm) |

**LOC SD3** (Figure 91)

**Location:** Loc SD3

175.6218575°E 39.8939043°S

**Parent Materials**: Mudstone (Orangipongo formation)

**Slope:** A (Flat to gently undulating at 3°)

**Aspect:** Southeast

**Drainage:** Moderate; depth to slow below 1111mm

**Erosion:** Sheet/ Runoff; present 0/5, potential 2/5

**Vegetation**: ***Present:*** Pasture, thistles, and few grasses

**Classification:** Ohakea heavy silt loam – Oh (a)

**Profile:**

| | | |
|---|---|---|
| Ap | 0 – 205mm | Silt clay loam; 7.5YR 3/2 (dark brown); moderately blocky; sticky; 1-2% fine HC mottle; fine roots present; non plastic; indistinct contact |
| Bw | 205 – 625mm | Silt loam; 7.5YR/ 4/3 (brown); weak crumb; 5% HC mottles (between 2.5YR 3/6 & 4/8 (dark red & red)); slightly sticky; non plastic; indistinct contact |
| Cg1 | 625 – 645mm | Silty clay loam; 7.5YR/ 4/4 (brown); no structure; 1% fine HC mottles; fine peaty wood fragments present; sticky; weakly slightly plastic (30mm); distinct contact |
| Cg2 | 645 – 1111mm | Silty clay; 10YR/ 4/3 (brown); no structure; 1-2% fine HC mottles; fine peaty wood fragments present; slightly sticky; weakly slightly plastic (30mm) |


*Figure 91: A) A photo of a section of the soil profile for soil description Loc 3. B) The different soils exposed during the excavation for soil description Loc 3.*

*Figure 92: A photo of a section of the soil profile for soil description Loc 4.*

**LOC SD4** (Figure 92)

**Location:** Loc SD4

175.6220222°E 39.8932507°S

**Parent Materials**: Mudstone (Mangamako shell bed member)

**Slope:** C (Rolling at 13°)

**Aspect:** South

**Drainage:** Well drained; depth to slow below 1120mm

**Erosion:** Sheet/ Runoff; present 0/5, potential 2/5

**Vegetation**: ***Present****:* Pasture, thistles, and few grasses

**Classification:** Hunterville hill soil - HvH

**Profile:**

| | | |
|---|---|---|
| Ap | 0 – 265mm | Silt loam; 7.5YR 3/3 (dark brown); moderately small nutty; fine roots and worms present; non sticky; strongly non plastic (20mm); diffuse contact (colour change) |
| Bw | 265 – 615mm | Silt loam; 10YR/ 3/4 (dark yellowish brown); weak, medium crumb; non sticky; non plastic; diffuse contact |
| C | 615 – 1120+mm | Sandy clay loam; between 10YR 5/6 (yellowish brown) & 2.5Y 5/4 (reddish brown); very weak nutty to no structure; slightly sticky; strongly non plastic (20mm) |

**LOC SD5** (Figure 93)

**Location:** Loc SD5

175.6182648°E 39.8957660°S

**Parent Materials**: Mudstone (Mangamako shell bed member)

**Slope:** D (Strongly rolling at 17°)

**Aspect:** North

**Drainage:** Slow; depth to slow 535mm

**Erosion:** Soil slip; present 1/5, potential 2/5

**Vegetation**: ***Present:*** Pasture and grasses

**Classification:** Murimotu silt loam - MmS

**Profile:**

| | | |
|---|---|---|
| Ap | 0 – 230mm | Silt loam; 7.5YR 3/2 (dark brown); moderately nutty; 1% fine HC mottles; fine roots and worms present; peaty wood fragments present at 140mm; slightly sticky; strongly non plastic (15-20mm); distinct contact |
| Bg | 230 – 535mm | Fine sandy clay; 5Y 7/1 (light gray); no structure; 25% coarse HC mottles (between 5YR 4/6 & 5/6(yellowish red & yellowish red)); non sticky; strongly slightly plastic (50mm); distinct wavy contact |
| Cg | 535 – 1080+mm | Fine sand; 5YR 4/6 (yellowish red); no structure; 50% HC mottles (5YR 4/6); slightly sticky; non plastic; water seepage occurred |


*Figure 93: A) A photo of the soil excavated for soil description Loc 5. B) The surrounding area for soil description Loc 5.*

**LOC SD6** (Figure 94)

**Location:** Loc SD6

175.6181642°E 39.8950160°S

**Parent Materials**: Mudstone (Mangamako shell bed member)

**Slope:** C (Rolling at 13°)

**Aspect:** East-Southeast

**Drainage:** Well drained; depth to slow below 1045mm

**Erosion:** Sheet/ Runoff; present 0/5, potential 2/5

**Vegetation**: ***Present****:* Pasture

**Classification:** Murimotu silt loam – MmS

**Profile:**

| | | |
|---|---|---|
| Ap | 0 – 280mm | Silt loam; 7.5YR 3/2 (dark brown); moderately fine crumb; fine roots and worms present; non sticky; strongly non plastic (20mm); convolute indistinct contact |
| Bw | 280 – 805mm | Fine sandy loam; 2.5Y 5/4 (light olive brown); weak nutty; slightly sticky; strongly non plastic (20mm); indistinct contact |
| C | 805 – 1045+mm | Fine sand; 2.5Y 5/4 (light olive brown); no structure; non sticky; non plastic |


*Figure 94: A) A photo of an upper section of the soil profile for soil description Loc 6. B) A photo of a lower section of the soil profile for soil description Loc 6.*


*Figure 95: A) A photo of an upper section of the soil profile for soil description Loc 7. B) A photo of a lower section of the soil profile for soil description Loc 7.*

**LOC SD7** (Figure 95)

**Location:** Loc SD7

175.6214857°E 39.8936130°S

**Parent Materials**: Mudstone (Mangaonoho formation)

**Slope:** F (Steep at 27°)

**Aspect:** East

**Drainage:** Moderate over slow; depth to slow 720mm

**Erosion:** Sheet/ Runoff; present 0/5, potential 2/5

**Vegetation**: ***Present:*** Pasture, grasses, and few thistles

**Classification:** Hunterville hill soil - HvH

**Profile:**

| | | |
|---|---|---|
| Ap | 0 – 190mm | Silt loam; 7.5YR 3/2 (dark brown); moderately fine crumb/weakly nutty; 2% fine HC mottles in lower 100mm; few fine roots and worms present; very slightly sticky; strongly non plastic (20mm); diffuse contact (colour/mottle change) |
| Bg | 190 – 320mm | Fine sandy loam; 2.5Y 5/4 (light olive brown); weakly crumb; 15% HC mottles (5YR 4/6 (yellowish red)); very few fine roots; non sticky; non plastic; distinct contact (colour change) |
| Cg1 | 320 – 595mm | Sandy clay loam; 10YR 5/2 (grayish brown); no structure; 6% fine HC mottles (2.5YR 4/8 (colour)); sticky; weakly slightly plastic (35mm); indistinct contact |
| Cg2 | 595 – 720mm | Fine sandy clay; 5YR 5/1 (gray); no structure; 30% coarse HC mottes (between 7.5 YR 5/6 & 4/6 (strong brown & strong brown)); sticky; strongly slightly plastic (50mm); abrupt contact |
| C | 720 – 920mm | Silty clay; 10YR 5/6 (yellowish brown); no structure; very sticky; water seepage occurred |

**LOC SD8** (Figure 96)

**Location:** Loc SD8

175.6222165°E 39.8934293°S

**Parent Materials**: Mudstone (Mangaonoho formation)

**Slope:** C (Rolling at 14°)

**Aspect:** Southwest

**Drainage:** Moderate; depth to slow 680mm

**Erosion:** Sheet/ Runoff; present 0/5, potential 2/5

**Vegetation**: ***Present****:* Pasture and grasses

**Classification:** Hunterville hill soil - HvH

**Profile:**

| | | |
|---|---|---|
| Ap | 0 – 150mm | Silty clay loam; 7.5YR 4/3 (brown); moderately nutty; fine roots and worms present; sticky; weakly slightly plastic (30mm); diffuse contact (colour change) |
| Bw | 150 – 425mm | Fine sandy loam; 2.5Y 5/4 (light olive brown); weakly nutty; 1% fine HC mottles; non sticky; non plastic; abrupt contact |
| C1 | 425 – 680mm | Silty loam; between 10YR 5/4 & 5/6 (yellowish brown & yellowish brown); weakly crumb; slightly sticky; strongly non plastic (20mm) indistinct contact |
| C2 | 680 – 1073+mm | Fine sandy clay loam; 2.5Y 5/4 (light olive brown); weakly crumb; sticky; strongly non plastic (25mm) |

*Figure 96: A photo of the soil profile for soil description Loc 8.*

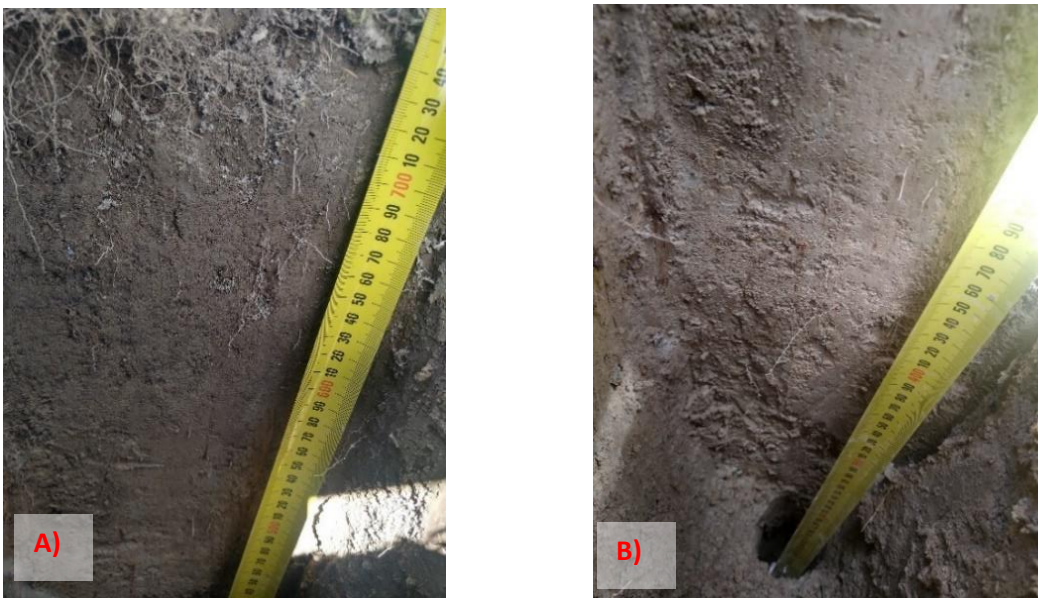


*Figure 97: A) A photo of an upper section of the soil profile for soil description Loc 9. B) A photo of a lower section of the soil profile for soil description Loc 9.*

**LOC SD9** (Figure 97)

**Location:** Loc SD9

175.6232785°E 39.8991985°S

**Parent Materials**: Mudstone (Mangaonoho formation)

**Slope:** D (Strongly rolling at 18°)

**Aspect:** North Northwest

**Drainage:** Moderate over slow; depth to slow below 1055mm

**Erosion:** Sheet/ Runoff; present 0/5, potential 2/5

**Vegetation**: ***Present:*** Pasture and grasses

**Classification:** Murimotu silt loam - MmS

**Profile:**

| | | |
|---|---|---|
| Ap | 0 – 240mm | Silty loam; 7.5YR 4/3 (brown); moderately blocky; few fine roots present; weakly sticky; strongly non plastic (25mm); distinct contact (mottle change) |
| Bw | 240 – 320mm | Silty clay loam; between 10YR 5/3 & 5/4 (brown & yellowish brown); weakly blocky; 2% fine HC mottles; sticky; weakly slightly plastic (30mm); distinct contact |
| Bg | 320 – 690mm | Fine sandy clay loam; 2.5Y 5/3 (light olive brown); weakly crumb; 10% HC (combination of 5YR 4/6 & 5/8 (yellowish red & yellowish red)) & 5% LC mottles (Gley1 6/10Y (greenish gray)); sticky; slightly plastic; indistinct contact |
| Cg | 690 – 1055+mm | Fine sandy clay; 2.5Y 5/3 (light olive brown); no structure; 30% coarse HC mottles (5YR 4/6 (yellowish red)) and 5% fine LC mottles; slightly sticky; weakly plastic (50mm) |

**LOC SD10** (Figure 98)

**Location:** Loc SD10

175.6248203°E 39.8992745°S

**Parent Materials**: Mudstone (Mangamako shell bed member)

**Slope:** E (Moderately steep (hilly) at 25°)

**Aspect:** Southwest

**Drainage:** Slow; depth to slow 625mm

**Erosion:** Sheet/ Runoff; present 0/5, potential 2/5

**Vegetation**: ***Present:*** Pasture, grasses, and few thistles

**Classification:** Raumai hill soil (Tidal_5a.1) – RaH-T (c)

**Profile:**

| | | |
|---|---|---|
| Ap | 0 – 220mm | Silty clay loam; 10YR 4/3 (brown); moderately fine nutty; few fine roots and worms present; slightly sticky; weakly slightly plastic (30mm); indistinct contact |
| Cg1 | 220 – 625mm | Clay; 10YR 5/4 (yellowish brown); no structure; 10% fine HC mottles (5YR 4/6 (yellowish red)); non sticky; weakly plastic (50mm); distinct contact |
| Cg2 | 625 – 855+mm | Fine sandy clay; 2.5Y 5/4 (light olive brown); no structure; 50% coarse HC mottles (between 7.5YR 5/8 & 4/6 (strong brown & strong brown)) and 40% fine LC mottles (Gley 1 6/10Y (greenish gray)); non sticky; weakly plastic (50mm) |


*Figure 98: A) A photo of an upper section of the soil profile for soil description Loc 10. B) A photo of a lower section of the soil profile for soil description Loc 10.*


*Figure 99: A) A photo of an upper section of the soil profile for soil description Loc 11. B) A photo of a lower section of the soil profile for soil description 11. C) The surrounding area for soil description Loc 11.*

**LOC SD11** (Figure 99)

**Location:** Loc SD11

175.6251162°E 39.9002432°S

**Parent Materials**: Mudstone (Mangamako formation)

**Slope:** C (Rolling at 8°)

**Aspect:** West-Northwest

**Drainage:** Moderate over Slow; depth to slow below 1020mm

**Erosion:** Sheet/ Runoff; present 0/5, potential 2/5

**Vegetation**: ***Present****:* Pasture and few thistles

**Classification:** Murimotu hill soil - MmS

**Profile:**

| | | |
|---|---|---|
| Ap | 0 – 220mm | Silty clay loam; 7.5YR 4/2 (brown); moderately nutty; few fine roots and worms present; slightly sticky; slightly plastic; indistinct contact |
| Bw | 220 – 655mm | Silty clay loam; 10YR 5/4 (yellowish brown); weakly crumb; 5% fine HC mottles (2.5YR 5/4 (reddish brown)); slightly sticky; slightly plastic; indistinct contact |
| Cg | 655 – 1020+mm | Fine sandy clay; 2.5Y 5/4 (light olive brown); no structure; 40% HC mottles (combination of 5YR 5/8 & 4/6 (colour & colour)); slightly sticky; weakly plastic (45-50mm) |

**LOC SD12** (Figure 100)

**Location:** Loc SD12

175.6216292°E 39.8960093°S

**Parent Materials**: Mudstone (Mangamako shell bed member)

**Slope:** A (Flat to gently undulating at 3°)

**Aspect:** Flat

**Drainage:** Well drained; depth to slow below 1035mm

**Erosion:** Sheet/ Runoff; present 0/5, potential 2/5

**Vegetation**: ***Present****:* Pasture and few grasses

**Classification:** Raumai hill soil (Tidal_5a.1) – RaH-T

**Profile:**

| | | |
|---|---|---|
| Ap | 0 – 213mm | Fine sandy loam; between 10YR 5/3 & 5/4 (brown & yellowish brown); fine nutty; few fine roots and worms present; non sticky; non plastic distinct contact |
| Bw | 213 – 460mm | Fine sandy silt; between 10YR 3/4 & 4/6 (dark yellowish brown & dark yellowish brown); moderately crumb; non sticky; non plastic; indistinct contact |
| C1 | 460 – 660mm | Fine sand; between 10YR 5/4 & 6/4 (yellowish brown & light yellowish brown); no structure; non sticky; non plastic; diffuse contact |
| C2 | 660 – 1035+mm | Fine sand; between 10YR 5/4 & 6/4 (yellowish brown & light yellowish brown); no structure; 1% fine HC mottles; non sticky |

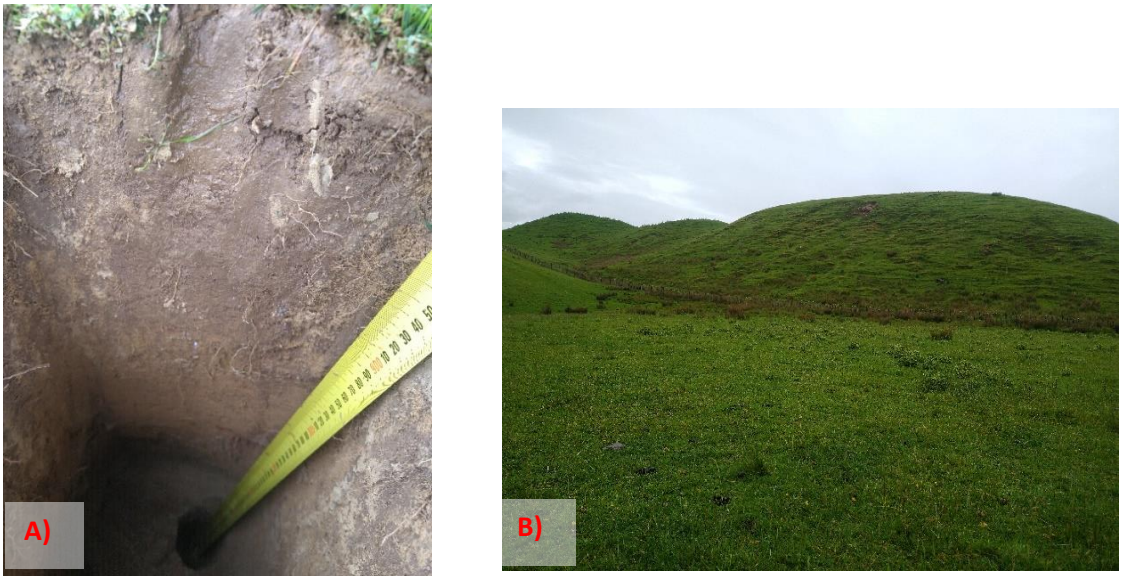


*Figure 100: A) Photo of the soil profile for soil description Loc 12. B) The surrounding area for soil description Loc 12.*


*Figure 101: A) The surrounding area for soil description Loc 13. B) A photo of the soil profile for soil description 13. C) A photo of the lower section of the soil profile for soil description Loc 13.*

**LOC SD13** (Figure 101)

**Location:** Loc SD13

175.6212008°E 39.8957707°S

**Parent Materials**: Mudstone (Fine grained fluvial deposits)

**Slope:** D (Strongly rolling at 17°)

**Aspect:** Northwest

**Drainage:** Slow; depth to slow 505mm

**Erosion:** Sheet/ Runoff; present 0/5, potential 2/5

**Vegetation**: ***Present****:* Grasses and thistles

**Classification:** Ohakea heavy silt loam – Oh (a)

**Profile:**

| | | |
|---|---|---|
| Ap | 0 – 92mm | Silty clay; 2.5YR 3/2 (dusky red); weakly nutty; 1% fine HC mottles; few fine roots and worms present; slightly sticky; weakly plastic (50mm); distinct contact |
| Bg | 92 – 505mm | Silty clay loam; 2.5YR 4/3 (reddish brown); moderately nutty; 10% HC fine mottles; few fine roots to 165mm; sticky; slightly plastic; indistinct contact |
| Cg | 505 – 1000+mm | Fine sandy clay; no structure; non sticky; 50% coarse HC (7.5YR 5/8 (strong brown)) & 50% LC (gley 1 6/10Y (greenish gray)) mottles; weakly slightly plastic (35mm) |

**LOC SD14** (Figure 102)

**Location:** Loc SD14

175.6244947°E 39.8947792°S

**Parent Materials**: Mudstone (Mangamako shell bed member)

**Slope:** C (Rolling at 11°)

**Aspect:** North

**Drainage:** Slow; depth to slow 665mm

**Erosion:** Sheet/ Runoff; present 0/5, potential 2/5

**Vegetation**: ***Present:*** Pasture and grasses

**Classification:** Raumai hill soil (Tidal_5a.1) – RaH-T

**Profile:**

| | | |
|---|---|---|
| Ap | 0 – 160mm | Fine sandy loam; between 7.5YR 3/1 & 3/2(very dark gray & dark brown); fine blocky; 1% fine HC mottles; few fine roots and worms present; sticky; strongly non plastic (20mm); distinct contact |
| Bw | 160 – 500mm | Fine sandy loam; 2.5Y 5/2 (grayish brown); weakly nutty; 30% HC mottles (5YR 4/6 (yellowish red)); non sticky; strongly non plastic; indistinct contact |
| Cg1 | 500 – 665mm | Fine sandy clay; 5Y 6/2 (light olive brown); no structure; 30% coarse HC mottles (combination of 7.5YR 4/6 & 5YR 4/6 (strong brown & yellowish red)); non sticky; non plastic; distinct contact |
| Cg2 | 665 – 1115+mm | Fine sand; no structure; 50% coarse HC (between 7.5YR 5/8 & 4/6 (strong brown & strong brown)) & 50% coarse LC (gley 1 6/10Y (greenish gray)) mottles; non sticky; non plastic |

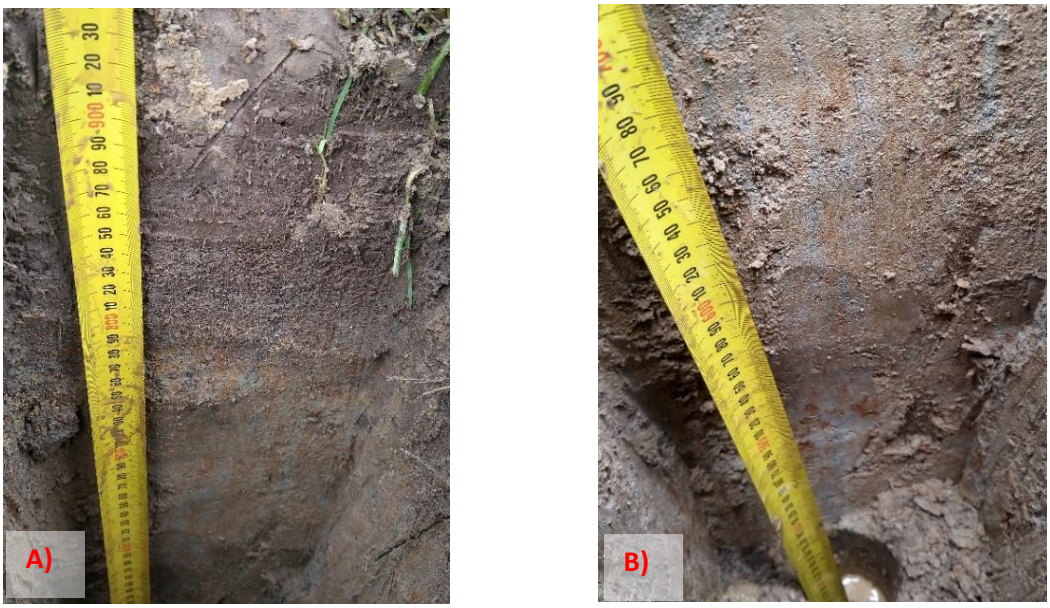


*Figure 102: A) A photo of an upper section of the soil profile for soil description Loc 14. B) A photo of a lower section of the soil profile for soil description Loc 14.*


*Figure 103: Photos of the soil profile for soil description Loc 15.*

**LOC SD15** (Figure 103)

**Location:** Loc SD15

175.6235338°E 39.8948952°S

**Parent Materials**: Mudstone (Mangaonoho formation)

**Slope:** E (Moderately steep (hilly) at 22°)

**Aspect:** Northeast

**Drainage:** Moderate; depth to slow below 1070mm

**Erosion:** Sheet/ Runoff; present 0/5, potential 2/5

**Vegetation**: ***Present****:* Pasture and thistles

**Classification:** Raumai hill soil (Tidal_5a.1) – RaH-T

**Profile:**

| | | |
|---|---|---|
| Ap | 0 – 210mm | Fine sandy loam; 10YR 3/2(very dark grayish brown); moderately nutty; few fine roots present; non sticky; weakly slightly plastic (30mm); indistinct contact |
| Bw | 210 – 500mm | Fine sandy loam; combination of 10YR 6/4 & 4/3 (light yellowish brown & brown); moderately nutty; few fine roots to 375mm; 1% fine HC mottles; slightly sticky; weakly slightly plastic (30mm); indistinct contact |
| Cg | 500 – 765mm | Fine sandy clay; 2.5Y 5/3 (light olive brown); no structure; 15% HC mottles (5YR 4/6 (yellowish red)); non sticky; non plastic; distinct contact |
| C | 765 – 1070+mm | Fine sand; 2.5Y 5/4 (light olive brown); no structure; non sticky; non plastic |

**LOC SD16** (Figure 104)

**Location:** Loc SD16

175.6130248°E 39.8935020°S

**Parent Materials**: Mudstone (Manamako shell bed member)

**Slope:** C (Rolling at 13°)

**Aspect:** South-south-west

**Drainage:** Moderate; depth to slow below 1040mm

**Erosion:** Sheet/ Runoff; present 0/5, potential 2/5

**Vegetation**: ***Present:*** Pasture

**Classification:** Raumai hill soil (Tidal_5a.1) – RaH-T

**Profile:**

| | | |
|---|---|---|
| Ap | 0 – 280mm | Silt loam; 10YR 3/4 (dark yellowish brown); moderately small blocky; few fine roots present; few worms present; non sticky; weakly slightly plastic (30mm); irregular, diffuse contact |
| Bw | 280 – 570mm | Fine sandy silt loam; between 10YR 4/6 & 5/6 (dark yellowish brown & yellowish brown); weakly small blocky; very few fine roots to 298mm; slightly sticky; strongly non plastic (20mm); slightly firm strength; occluded indistinct contact |
| Bw | 570 – 920mm | Fine sandy loam; 10YR 5/6 (yellowish brown); weakly fine nutty; 5% fine HC mottles (2.5YR 4/8 (red)); non sticky; non plastic; weak strength; wavy, distinct contact |
| C | 920 – 1040+mm | Medium to fine sand; between 10YR 5/4 &5/6 (yellowish brown & yellowish brown); no structure;15% HC coarse mottles (between 5YR 4/6 & 5/8 (yellowish red & yellowish red)) non sticky; non plastic; fine peaty wood fragments present |


*Figure 104: A) A photo of an upper section of the soil profile for soil description Loc 16. B) The soil profile for soil description Loc 16.*

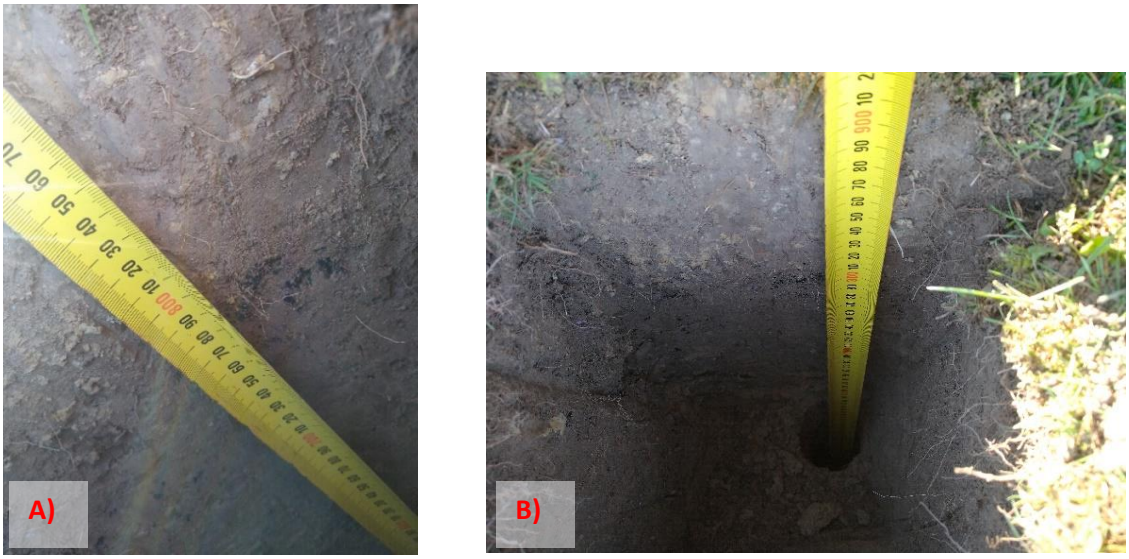


*Figure 105: A) A photo of an upper section of the soil profile for soil description Loc 17. B) A photo of a section of the soil profile for soil description Loc 17.*

**LOC SD17** (Figure 105)

**Location:** Loc SD17

175.6301858°E 39.8874142°S

**Parent Materials**: Sandstone (Orangipongo formation)

**Slope:** E (Moderately steep (hilly) at 22°)

**Aspect:** South-south-west

**Drainage:** Moderate; depth to slow below 930mm

**Erosion:** Earthflow; present 0/5, potential 2/5

**Vegetation**: ***Present****:* Grasses and pasture with few trees and few thistle

**Classification:** Whangehu steepland soil – WhS

**Profile:**

| | | |
|---|---|---|
| Ap | 0 – 240mm | Silty clay loam; 10YR 3/2 (very dark grayish brown); moderately small blocky; few fine roots present; wood fragments of 1cm length at 140 & 210mm; slightly sticky; weakly slightly plastic (30mm); slightly firm strength; occluded, diffuse contact |
| Bw | 240 – 480mm | Fine sandy clay loam; between 2.5Y 5/3 (light olive brown); very weakly medium blocky; 2% fine HC mottles; very few fine roots to 298mm; sticky; weakly slightly plastic (30mm); very firm strength; wavy, indistinct contact |
| C | 480 – 930mm+ | Fine sandy clay; 10YR 5/6 (yellowish brown); weakly fine nutty; 50% coarse HC (between 7.5YR 4/6 & 5/8(strong brown & strong brown)) & 50% coarse LC (Gley 1 6/10Y (greenish gray)) mottles; slightly sticky; weakly plastic (50mm) plastic; very firm strength |

**LOC SD18** (Figure 106)

**Location:** Loc SD18

175.6291080°E 39.8887650°S

**Parent Materials**: Sandstone (Orangipongo formation)

**Slope:** B (Undulating at 6°)

**Aspect:** South

**Drainage:** Slow; depth to slow below 365mm

**Erosion:** Sheet/ Runoff; present 0/5, potential 2/5

**Vegetation**: ***Present:*** Grasses and pasture

**Classification:** Ohakea silt loam – Oh (b)

**Profile:**

| | | |
|---|---|---|
| Ap | 0 – 205mm | Sandy clay loam; 2.5Y 4/2 (dark grayish brown); weakly medium crumb; 2% fine HC mottes; few fine roots present; worms present near surface; weakly, slightly sticky; strong slightly plastic (40mm); slightly firm strength; occluded, diffuse contact |
| Bw | 205 – 365mm | Fine sandy loam; between 2.5Y 5/1 & 4/1 (gray & dark gray); no structure; 8% fine HC mottles (5YR 4/6 (yellowish red)); band of wood at 305mm in wedge shape (thickest end 20mm); slightly sticky; non plastic; firm strength; wavy, distinct contact |
| Cg | 365 – 540mm | Fine sandy loam; 10YR 5/6 (yellowish brown); no structure; 50% HC (both 5YR 4/6 & 5/8 (yellowish red & yellowish red)) & 50% LC (Gley 1 5/10Y (greenish gray)) mottles; slightly sticky; weakly plastic (50mm) plastic; firm strength; smooth, distinct contact; thin (10mm) layer of 5YR 3/3 (dark reddish brown) at contact |
| C | 540 – 610mm+ | Fine sand; 2.5Y 4/4 (olive brown); no structure; non sticky; non plastic; very weak strength |


*Figure 106: A) A photo of the lower section of the soil profile for soil description Loc 18. B) A photo of the soil profile for soil description Loc 18.*


*Figure 107: A) Small stones found within the soil profile for soil description Loc McFadden Poplars. B) A photo of the soil profile for soil description Loc McFadden Poplars.*

**LOC McFadden Poplars** (Figure 107)

**Location:** Loc Poplar

175.6167788°E 39.8873063°S

**Parent Materials**: Degradational river terraces (Lower Kakariki river terrace subset)

**Slope:** C (Rolling at 15°)

**Aspect:** North

**Drainage:** Moderate/slow; depth to slow below 420mm

**Erosion:** Sheet/ Runoff; present 0/5, potential 2/5

**Vegetation**: ***Present****:* Grasses and pasture with few trees

**Classification:** Pukiore soil – PkS

**Profile:**

| | | |
|---|---|---|
| Ap | 0 – 235mm | Silty clay, stone chips present throughout (approx. 3-6mm length); 5YR 4/2 dark reddish gray); moderately fine nutty; few fine roots present; 1% fine HC mottles sticky; strongly slightly plastic (50mm); slightly firm strength; smooth, indistinct contact |
| Bw | 235 – 420mm | Silty clay; between 5Y 5/2 (olive gray); medium weak nutty; 5% fine HC mottles; sticky; strongly slightly plastic (50mm); firm strength; smooth, distinct contact |
| Cg | 420 – 635mm | Clay; no structure; 50% HC (7.5YR 4/6 (strong brown)) & 50% LC (Gley 1 6/10Y (greenish gray)) mottles; non sticky; strongly slightly plastic (50+mm); very firm strength; smooth, distinct contact |
| C | 635– 740mm+ | Silty clay; 10YR 5/3 (brown); no structure; sticky; strongly slightly plastic (50mm); weak strength |

## Soil Description Test Sites

**LOC 1T** (Figure 108)

**Location:** Loc 1T – Bottom of Burn Hill along fence line.

175.619163°E 39.894984°S

**Parent Materials**: Siltstone (Fine grained fluvial deposits)

**Slope:** B (Undulating at 5$^{o}$)

**Aspect:** North – North Northeast

**Drainage:** Moderate over slow; Depth to slow 31cm

**Erosion:** Sheet/ Runoff; present 0/5, potential 2/5

**Vegetation**: ***Present****:* Pasture and grasses

**Classification:** Ohakea heavy silt loam – Oh (a)

**Profile:**

| | | |
|---|---|---|
| Ap | 0 – 160mm | Silty loam; 2.5YR 3/1 (dark reddish brown); moderately blocky; friable; slightly sticky; slightly plastic; 10% HC mottles (between 2.5YR 4/6 (red) and 4/8 (red)); faded contact; fine roots and few worms present |
| Bw | 160 – 260mm | Silty clay loam; 5YR 4/2 (dark reddish brown); weakly blocky; friable; non-sticky; slightly plastic; 10% HC mottles (5YR 5/8 (yellowish red)) and 10% LC mottles (gley 1 7/N (light gray)); sharp contact |
| Bw | 260 – 317mm | Silty loam; 5YR 3/3 (dark reddish brown); moderately blocky; friable; non-sticky; slightly plastic; 5% HC and LC mottles; wavy contact |
| Cg | 317 – 573mm | Silty clay; 10YR 4/2 (dark grayish brown); weakly blocky; friable; slightly sticky; plastic; 30% HC mottles (7.5YR 5/8 (strong brown)) and 40% LC mottles (2.5Y 7/2 (pale red)); faded contact |
| C | 57.3 – 1150mm+ | Silty clay; 10YR 5/2 (grayish brown); weakly blocky; friable; non-sticky; plastic; 10% HC and 10% LC mottles; water table reached |


*Figure 108: A) A photo of the soil profile for soil description Loc 1T. B) The surrounding area for soil description Loc 1T.*


*Figure 109: A) A photo of the soil profile for soil description Loc 2T. B) The different soils excavated from the profile of soil description Loc 2T.*

**LOC 2T** (Figure 109)

**Location:** Loc 2T – Along the northern fence line of Burn Flat paddock.

175.6227262°E 39.894224°S

**Parent Materials**: Siltstone (Orangipongo formation)

**Slope:** D (Strongly rolling at 18$^{o}$)

**Aspect:** Northwest

**Drainage:** Rapid; below 1.14m

**Erosion:** Sheet/ Runoff; present 0/5, potential 2/5

**Vegetation**: ***Present****:* Pasture and grasses

**Classification:** Raumai hill soil (Tidal_5a.1) – RaH-T

**Profile:**

| | | |
|---|---|---|
| Ap | 0 – 331mm | Silty loam; 5YR 3/3 (dark reddish brown); strong blocky; friable; non-sticky; slightly plastic; faint wavy contact; fine roots present to 18.1cm and few worms present |
| Bw | 331 – 861mm | Silty; 7.5YR 4/4 (brown); moderate blocky; friable; slightly sticky; plastic; abrupt, smooth (density change) contact |
| C | 861 – 1114mm+ | Fine sand; 10YR 5/4 (yellowish brown); no structure; very friable; non-sticky; non-plastic; 5% HC mottles (colour unachievable due to fine mottling); water table reached |

**LOC 3T** (Figure 110)

**Location:** Loc 3T – Near swampy area – (potential winter stream, feeding dams) against edge of valley in Back Paddock.

175.624122°E 39.899523°S

**Parent Materials**: Siltstone (Fine grained fluvial deposits)

**Slope:** A (Flat to gently undulating at 3$^{o}$)

**Aspect:** North

**Drainage:** Slow; 13.3cm

**Erosion:** Sheet/ Runoff; present 0/5, potential 2/5

**Vegetation**: ***Present****:* Pasture and grasses

**Classification:** Kairanga deep silt loam on clay – K (a)

**Profile:**

| | | |
|---|---|---|
| Ap | 0 – 331mm | Silty; 7.5YR 4/3 (brown); weak blocky; friable; slightly sticky; plastic; faint, wavy contact; low fine roots present |
| Bg | 331 – 861mm | Silty; 7.5YR 4/4 (brown); moderate blocky; friable; slightly sticky; plastic; 50% HC mottles (7.5YR 4/6 (strong brown)) and 50% LC mottles (Gley 1 6/N (gray)); water table reached |


*Figure 110: A) The surrounding area for soil description Loc 3T. B) A photo of the top section of the soil profile for soil description Loc 3T. C) A photo of the soil excavated from the soil profile for soil description Loc 3T.*


*Figure 111: A) A photo of the soil excavated from the soil profile for soil description Loc Dams. B) A photo of the soil profile for soil description Loc Dams.*

**LOC DamsT** (Figure 111)

**Location:** Loc DamsT – Land bridge between two dams in Millennium Paddock

175.621762°E 39.897230°S

**Parent Materials**: Siltstone (Fine grained fluvial deposits)

**Slope:** C (rolling at 13$^{o}$)

**Aspect:** North

**Drainage:** Moderate over slow

**Erosion:** Sheet/ Runoff; present 0/5, potential 2/5

**Vegetation**: ***Present****:* Pasture

**Classification:** Ohakea heavy silt loam – Oh (a)

**Profile:**

| | | |
|---|---|---|
| Ap | 0 – 112mm | Silty; 7.5YR 4/3 (brown); moderately blocky; friable; slightly sticky; plastic; diffuse contact; fine roots present to base of horizon |
| Cg | 112 – 423mm | Silty clay; between 7.5YR 3/4 (dark brown) and 4/4 (brown); no structure; friable; slightly sticky; plastic; 5% HC mottles (5YR 4/6 (yellowish red)); abrupt, smooth (density change) contact; presence of wood piece amongst mottling |
| C | 423 – 909mm | Silty clay; 10YR 4/4 (dark yellowish brown); no structure; friable; slightly sticky; plastic; water table reached |

**LOC 5T** (Figure 112)

**Location:** Loc 5T – Within Burn Paddock, presence of stream near by

175.617484°E 39.891953°S

**Parent Materials**: Siltstone (Orangipongo formation)

**Slope:** C (rolling at 8$^{o}$)

**Aspect:** Southwest (towards stream)

**Drainage:** Moderate over slow; 25.7cm

**Erosion:** Sheet/ Runoff; present 0/5, potential 2/5

**Vegetation**: ***Present****:* Pasture

**Classification:** Ohakea heavy silt loam – Oh (a)

**Profile:**

| | | |
|---|---|---|
| Ap | 0 – 162mm | Silty clay; 7.5YR 4/3 (brown); weakly blocky; friable; sticky; plastic; 2% HC and 1% LC mottling; faint, wavy contact; fine roots and worms present |
| Bw | 162 – 257mm | Silty clay; 7.5YR 4/3 (brown); weakly crumb; friable; sticky; plastic; 5% HC mottles (5YR 4/6 (yellowish red)) 5% LC; diffuse contact |
| Cg | 257 – 658mm | Silty clay; 7.5YR 3/4 (brown); no structure; friable; sticky; plastic; 40% HC mottles (2.5YR 4/8(red)) and 50% LC mottles (Gley 1 5/N (gray)); water table reached |

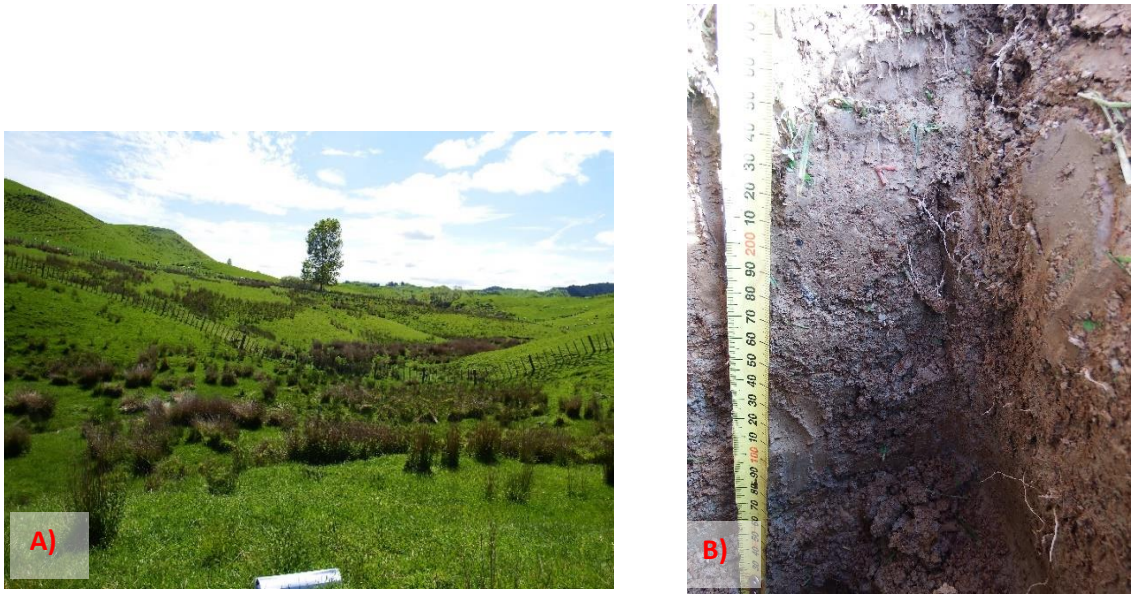


*Figure 112: A) The surrounding area for soil description Loc 5T. B) A photo of a section of the soil profile for soil description Loc 5T.*


*Figure 113: A&B) The surrounding area for soil description Loc 6T. C) A photo of the upper section of the soil profile for soil description Loc 6T.*

**LOC 6T** (Figure 113)

**Location:** Loc 6T – Within Greens Paddock near potential stream (in winter)

175.618635°E 39.889870°S

**Parent Materials**: Siltstone (Orangipongo formation)

**Slope:** C (rolling at 10$^{o}$)

**Aspect:** Southeast

**Drainage:** Rapid over slow

**Erosion:** Sheet/ Runoff; present 0/5, potential 2/5

**Vegetation**: ***Present****:* Pasture and grasses

**Classification:** Raumai hill soil (Heretaunga_28a.1) – RaH-H

**Profile:**

| | | |
|---|---|---|
| Ap | 0 – 241mm | Silty; 7.5YR 4/3 (brown); weakly blocky; friable; slightly sticky; plastic; diffuse contact; fine roots present |
| Bw | 241 – 395mm | Silty clay; 7.5YR 5/2 (brown); very fine, weakly blocky; friable; sticky; plastic; 5% HC mottles; water table reached |

**LOC 9T** (Figure 114)

**Location:** Loc 9T – Within Tunnel Paddock down in valley

175.629388°E 39.88815°S

**Parent Materials**: Siltstone (Orangipongo formation)

**Slope:** C (rolling at 13$^{o}$)

**Aspect:** East

**Drainage:** Rapid over slow

**Erosion:** Sheet/ Runoff; present 0/5, potential 2/5

**Vegetation**: ***Present****:* Pasture and grasses

**Classification:** Pohangina steepland soil – PhS

**Profile:**

| | | |
|---|---|---|
| Ap | 0 – 177mm | Fine sandy loam; 10YR 3/2 (very dark greyish brown); moderately blocky; friable; non-sticky; non-plastic; indistinct contact; fine roots present |
| Bw | 177 – 517mm | Fine sandy clay loam; 2.5YR 5/4 (light olive brown); moderately blocky; friable; slightly sticky; slightly plastic; worms present; diffuse contact |
| Bw | 517 – 800mm | Fine sandy loam; between 10YR 5/4 and 5/6 (yellowish brown); weakly nutty; friable; non-sticky; non-plastic; 5% HC (5 YR 4/6(yellowish red)), 2% LC mottles; abrupt, wavy contact |
| Cg | 80 – 1120mm+ (Top) | Fine sand; between 10YR 5/4 and 5/6 (yellowish brown); no structure; friable; compact; non-sticky; non-plastic; 10% HC (7.5YR 5/6 (strong brown)), 2% LC (Gley 1 6/5GY (greenish grey)) |
| | 80 – 1120mm+ (Bottom) | Fine sand; between 10YR 5/4 (yellowish brown); no structure; friable; compact; non-sticky; non-plastic; 50% HC (5YR 4/6 (yellowish red)), 15% LC (Gley 2 6/5PB (bluish grey)); gradational throughout profile lower contact unclear within sample location |


*Figure 114: A) The surrounding area for soil description Loc 9T. B) A photo of a section of the soil profile for soil description Loc 9T.*

## Stanley Oa Soil Descriptions - 2019

**Location:** AS 1

175.616440731954°E 39.8984546897321°S

**Parent Materials**: Colluvium/Siltstone/Mudstone (Mangaonoho Formation)

**Slope:** E (Moderately steep at 24°)

**Aspect:** South (192°)

**Drainage:** Imperfectly drained

**Erosion:** Soil slip; present – none; potential – likely

**Vegetation**: ***Present:*** Pasture and leguminous species

**Classification:** Kumeroa soil series – 4E1

**Profile:**

| | | |
|---|---|---|
| Ap | 0 – 180mm | Moist greyish yellow brown (10YR 4/2); silty clay loam; friable, slightly sticky and slightly plastic; many very fine and fine roots (mostly pasture); diffuse smooth boundary to; |
| AB | 180 – 370mm | Moist greyish yellow brown (10YR 4/2); silty clay loam; inclusions of charcoal fragments between 210-270mm; friable, slightly sticky and slightly plastic; many very fine and fine roots (mostly pasture); clear smooth boundary to; |
| ABg | 370 – 460mm | Moist greyish yellow brown (10YR 5/2); very few, very fine and faint yellowish brown (10YR 5/8) mottles; silty clay; slightly firm, sticky and plastic; diffuse smoot boundary to; |
| Bg1 | 460– 670mm | Moist dull yellowish brown (10YR 5/4); very few, very fine and faint yellowish brown (10YR5/8) mottles; clay; slightly firm, sticky and plastic; diffuse smooth boundary to; |
| Bg2 | 670– 1000mm | Moist greyish yellow brown (10YR 6/2); many, coarse and prominent yellowish brown (10YR 5/8) mottles; clay; slightly firm, sticky and plastic; diffuse clear smooth boundary to; |
| C | 1000mm+ | Moist greyish yellow brown (10YR 5/2); many, coarse and distinct yellowish brown (10YR 5/6) mottles; fine sandy clay; slightly firm, sticky and plastic. |

**Location:** AS 2

175.614241584682°E 39.9018283740801°S

**Parent Materials**: Sandstone (Swamp Deposits)

**Slope:** A (Flat to gently undulating at 0-1°)

**Aspect:** South (175°)

**Drainage:** Well drained

**Erosion:** Negligible; present – none; potential – none

**Vegetation**: ***Present****:* Pasture and leguminous species

**Classification:** Ohakea soil series – 6W1

**Profile:**

| | | |
|---|---|---|
| A1 | 0 – 180mm | Very moist greyish olive (2.5Y 4/2); common fine roots (mostly pasture); soft, sticky and slightly plastic; silty loam; diffuse smooth boundary to; |
| A2g | 180 – 280mm | Very moist olive black (2.5Y 3/2); common fine distinct brown (10YR 4/6) mottles; silt loam; soft, slightly sticky and slightly plastic; clear smooth boundary to; |
| Brg1 | 280 – 460mm | Very moist grey olive (5YR 6/2); many coarse and prominent orange (7.5YR 6/8) mottles; silt clay; soft, sticky and plastic; diffuse smooth boundary to; |
| Brg2 | 460– 1200mm | Very moist grey olive (5YR 6/2); many coarse and prominent orange (7.5YR 6/8) mottles; light silt clay; soft, sticky and plastic. |
| | | Note: At below 1060mm the water table was reached. |

**Location:** AS 3

175.619597031278°E 39.9005633912874°S

**Parent Materials**: Sandstone (Mangaonoho Formation)

**Slope:** G (Very steep at 35°)

**Aspect:** West (260°)

**Drainage:** Imperfectly drained

**Erosion:** Soil slip; present – severe; potential – highly likely

**Vegetation**: ***Present****:* Pasture and leguminous species

**Classification:** Ohakea soil series – 6E14

**Profile:**

| | | |
|---|---|---|
| Ah1 | 0 – 120mm | Dry brown (10YR 4/4); silty clay loam; weakly developed fine granular and crumbly structures; friable, slightly sticky and slightly plastic; many very fine and fine roots (mostly pasture); diffuse smooth boundary to; |
| Ah2 | 120 – 350mm | Dry brown (10YR 5/3); silty clay loam; weakly developed fine granular and crumbly structures; friable, slightly sticky and slightly plastic; many very fine and fine roots (mostly pasture); diffuse smooth boundary to; |
| B1 | 350 – 560mm | Moist bright yellowish brown (2.5Y 6/6); light silty clay; moderately developed medium sub-angular blocky structures; slightly sticky and slightly plastic; clear smooth boundary to; |
| B2 | 560 – 840mm | Moist bright yellowish brown (2.5Y 7/6); fine sandy loam; weakly developed to structureless; non-sticky and non-plastic; clear smooth boundary to; |
| BC | 840 – 1020mm | Moist yellowish grey (2.5Y 5/6); fine sandy clay loam; compacted; non-sticky and non-plastic; diffuse smooth boundary to; |
| C | 1020mm+ | Moist yellowish grey (2.5Y 5/4); common, medium reddish-brown mottles (5YR 4/8); fine sandy clay loam; compacted; non-sticky and non-plastic. |

**Location:** AS 4

175.636868326812°E 39.8897941860528°S

**Parent Materials**: Sandstone (Orangipongo Formation)

**Slope:** F (Steep at 34°)

**Aspect:** South (170°)

**Drainage:** Well drained

**Erosion:** Soil slip; present – severe; potential – very highly likely

**Vegetation**: ***Present****:* Pasture and leguminous species

**Classification:** Whangehu soil series – 7E5

**Profile:**

| | | |
|---|---|---|
| Ap1 | 0 – 160mm | Moist dark drown (10YR 3/3); fine sandy loam; friable, slightly sticky, and slightly plastic; many fine roots (mostly pasture); clear smooth boundary to; |
| Bg | 160 – 300mm | Moist brown (10YR 4/4); fine sandy loam; friable, slightly sticky, and slightly plastic; many fine roots (mostly pasture); diffuse smooth boundary to; |
| Cg | 300 – 460mm | Moist dull yellow brown (10YR 5/4); common, medium, and faint bright yellowish brown (10YR 6/6) mottles; fine sandy clay loam; slightly firm, non-sticky and non-plastic; diffuse smooth boundary to; |
| Cgr | 460 – 600mm | Moist dull yellowish orange (10YR 6/3); sandy clay diffuse smooth boundary to; |
| C | 600mm+ | Moist dull yellowish orange (10YR 6/3); sandy clay diffuse smooth boundary to; |
| | | Compacted layer |

**Location:** AS 5

175.608783838403°E 39.8970616623658°S

**Parent Materials**: Sandstone (Mangaonoho Formation)

**Slope:** B (Undulating at 4°)

**Aspect:** South (189°)

**Drainage:** Well drained

**Erosion:** Surface; present – none; potential – not likely

**Vegetation**: ***Present****:* Pasture and leguminous species

**Classification:** Ohakune soil series – 3W1

**Profile:**

| | | |
|---|---|---|
| Ap | 0 – 220mm | Moist dark reddish brown (5YR 3/6); fine sandy loam; friable, non-sticky and non-plastic; many very fine and fine roots (mostly pasture); clear smooth boundary to; |
| B | 220 – 560mm | Moist yellowish brown (10YR 5/6); fine sandy loam; friable, non-sticky and non-plastic; few fine roots (mostly pasture); clear smooth boundary to; |
| BC | 560 – 880mm | Moist dull yellow orange (10YR 6/3); sandy loam; friable to very friable, non-sticky and non-plastic; clear smooth boundary to; |
| C | 880 – 1200mm+ | Moist greyish olive (5Y 5/3); very few, very fine and faint greyish yellow brown (10YR 4/2) mottles; loamy sand; very friable, non-sticky and non-plastic. |
| | | Note: The soils were suspected to have allophanic material in the A and B horizons because of the friable dark reddish brown loamy textures typical of ash soils. This needs to be tested for allophanic clay minerals. Classed arbitrary as Ohakune soil series. |

**Location:** AS 6

175.615882517364°E 39.8963863785285°S

**Parent Materials**: Colluvium/Uplifted Sandstones/Siltstones (Mangaonoho Formation)

**Slope:** C (Rolling at 13°)

**Aspect:** East (125°)

**Drainage:** Well drained

**Erosion:** Negligible; present – none; potential – likely

**Vegetation**: ***Present****:* Pasture (legumes and grasses) and few thistles

**Classification:** Kumeroa soil series – 3W

**Profile:**

| | | |
|---|---|---|
| Ap | 0 – 180mm | Moist olive brown (2.5Y 4/4); fine sandy loam; friable, non-sticky and non-plastic; many very fine and fine roots (mostly pasture); clear smooth boundary to; |
| BA | 180 – 280mm | Moist yellowish grey (2.5Y 5/4); fine sandy loam; friable, non-sticky and non-plastic; many very fine and fine roots (mostly pasture); diffuse smooth boundary to; |
| Bw1 | 280 – 580mm | Moist yellowish grey (2.5Y 5/6); fine sandy loam; friable, non-sticky and non-plastic; diffuse smooth boundary to; |
| Bw2g | 580 – 900mm | Moist yellowish grey (2.5Y 5/4); very few, fine and faint yellowish brown (10YR 6/8) mottles; loamy fine sand; friable, non-sticky and non-plastic; diffuse smooth boundary to; |
| C | 900 – 1200mm+ | Moist yellowish grey (2.5Y 5/4); loamy fine sand to very fine sandy textures; very friable to loose, non-sticky and non-plastic.<br><br>Note: A lot of earth worms were found in the first 300mm of the soil surface (A horizon). Fine roots were observed to be extending as far as 350mm depth. |

## Appendix 5 – Elevation Profiles Utilised for the Development of Soil Landscape Models

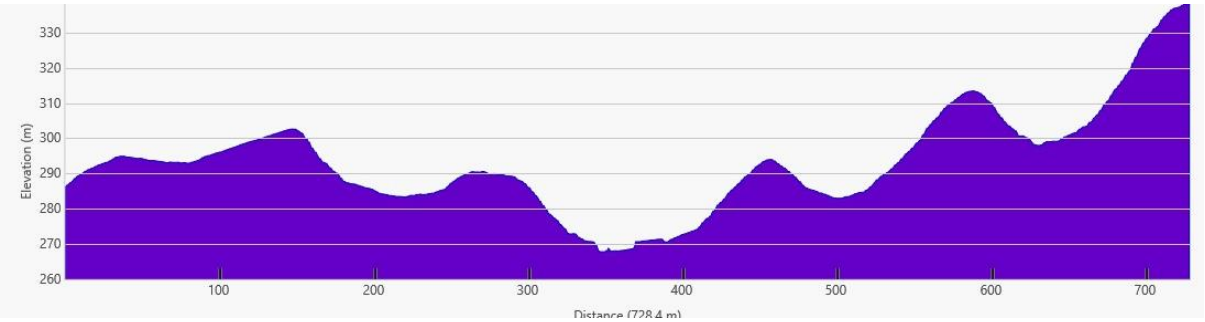


*Figure 115: The elevation profile for profile 1 for the development of the soil landscape model.*

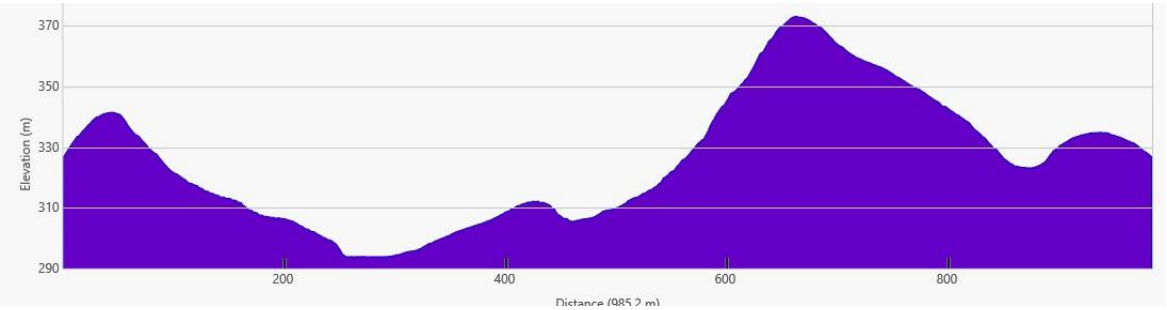


*Figure 116: The elevation profile for profile 2 utilised for the development of the soil landscape model.*

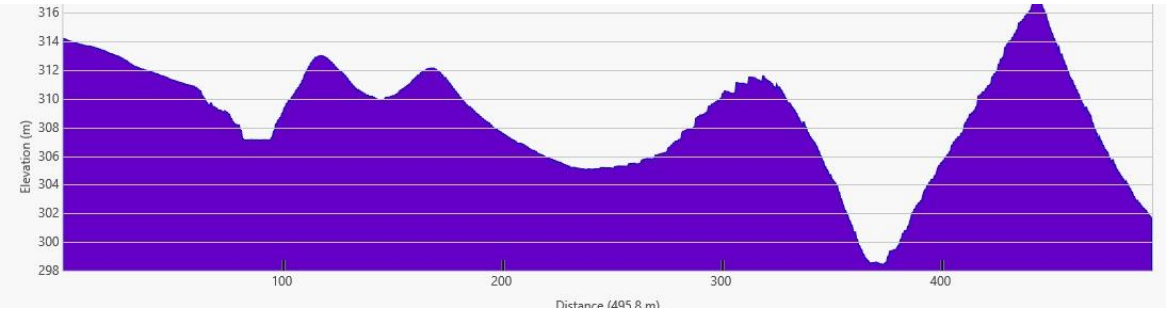


*Figure 117: The elevation profile for profile 3 utilised for the development of the soil landscape model.*